SUSTAINABLE VALORIZATION OF BIOMASS WASTE: PROCESS DEVELOPMENT, ARTIFICIAL INTELLIGENCE BASED OPTIMIZATION, AND DECISION-MAKING

YOUSAF AYUB

PhD

The Hong Kong Polytechnic University

2025

The Hong Kong Polytechnic University

Department of Industrial and Systems Engineering

Sustainable Valorization of Biomass Waste: Process Development, Artificial Intelligence Based Optimization, and Decision-Making

Yousaf AYUB

A thesis submitted in partial fulfilment of the requirements for the degree of Doctor of Philosophy

September 2024

Certificate of originality

I hereby declare that this thesis is my own work and that, to the best of my knowledge and belief, it reproduces no material previously published or written, nor material that has been accepted for the award of any other degree or diploma, except where due acknowledgement has been made in the text.

_____ (Signed)

Yousaf Ayub

_____ (Name of student)

In the memory of my **LOVE** – **PAKIZA**

who left this world but transformed my life

Abstract

The primary objectives of this study are to develop, optimize, and decision-making for the sustainable valorization of biomass waste. It includes a Strengths, Weaknesses, Opportunities, and Threats (SWOT) analysis of thermal and biological valorization processes, and a sustainability analysis considering environmental, economic, energy, exergy, and safety (4E, 1S) parameters. Environmental performance was reviewed from existing literature, and also from the models developed in this study. Life Cycle Assessment (LCA) reflects thermal processes more sustainable than direct land disposal of biomass. Economic analysis includes payback period (PBP), and internal rate of return (IRR) results indicate that thermal processes, specifically gasification and pyrolysis, outperform land disposal in both economic and environmental aspects. Although anaerobic digestion (AD) is technically and environmentally feasible at domestic level, it has a longer payback period. Hence, thermal processes are considered better for biomass valorization compared to biological methods when there is large quantity of biomass waste.

Sustainability evaluation of different thermal valorization processes have been performed. Hydrothermal gasification (HTG) is one of the thermal processes to convert biomass waste into valuable products. HTG process simulation model for syngas production was developed and artificial intelligence (AI) algorithms were applied to predict high-quality syngas production. Comparative analysis of Convolutional Neural Network (CNN), Artificial Neural Network (ANN), Gradient Boosting Regression (GBR), Extreme Gradient Boosting (XGB), and Random Forest Regression (RFR) models identified XGB as the best predictor, with coefficient of determination (R^2) values between 0.85-0.95 and mean square errors (MSE) between 0.008-0.01. Optimization based on process parameters such as temperature, pressure, and biomass concentration were analyzed which predict optimal hydrogen and methane yields around 540°C, 25 MPa, and 20% feedstock concentration. Energy analysis indicated a 61% efficiency, and economic analysis showed HTG to be at least 10% more cost-effective than coal, natural gas, or distillate oil for steam

production. LCA confirmed HTG's advantage over direct land disposal of biomass in terms of economy, environmental impact, and energy efficiency. The analysis highlighted that process temperature and resident time significantly affect hydrogen and methane yields.

This study also examines the different gasification routes for sustainable valorization of biomass waste through a novel tri-generation process involving gasification, solid oxide fuel cells (SOFC), and combined heat and power systems (CHP). Using Aspen Plus simulations and XGB, the optimal parameters were identified, with biomass to air ratio (BMR) being the most significant factor, achieving a R^2 greater than 0.97. The process demonstrated an exergy efficiency 34.6% higher than gasification. The tri-generation process, which includes torrefaction and SOFC, showed economic feasibility only above 90% efficiency. Particle Swarm Optimization (PSO) resulted in an energy efficiency of 57%, yielding 242.6 kg/ton of dimethyl ether (DME) at 667°C and 2 bar. The HDMR method predicted gasification outcomes with high accuracy, showing the efficient operation at 765°C, 0.59 BMR, and 1 bar. This integrated approach enhanced economic viability and environmental sustainability compared to traditional methods.

Plasma gasification (PG) tri-generation process for biomass waste valorization and DME production has been developed, considering 4E sustainability. Process optimization performed by the application of a radial basis function surrogate algorithm. Optimized process enhanced the DME yield by 6%, with energy efficiencies of 44% and 48% for the base (without optimization) process. It produces 1271 kW of electricity from 10 t/h feedstock processing and has a sustainability index of 2.509. The PBP for the optimized process is 7.2 years at 70% efficiency, while the base process is not feasible below 90% efficiency. A co-gasification process for biomass and plastic waste to produce blue and green hydrogen was proposed. This model, with a 20 t/h capacity, can generate approximately 1079 kW of electric power and surplus electricity for producing around 213.5 kg/d of hydrogen through alkaline electrolysis. Economic analysis shows an IRR of 8% at 70% efficiency. Exergy analysis highlights the gasifier component's lowest

efficiency, resulting in a 40% exergy loss, with exergoeconomics costs of approximately $6,561.3 and $6,541.9 per hour for the steam turbine and gasifier, respectively, suggesting potential improvements in these areas for enhanced sustainability.

Finally, a comprehensive evaluation of biological and thermal waste valorization methods was conducted using the Interval Valued Fermatean Fuzzy Set (IVFFS) with the Dombi Operator (DO) integrated with the Analytical Hierarchy Process (AHP). The analysis assessed four waste valorization processes—anaerobic digestion, gasification, pyrolysis, and HTG—based on economic, environmental, technological, and social-governance criteria. The Advanced Combinative Distance-Based Assessment (CODAS) ranked these processes with gasification as the most sustainable with an assessment score (A_s) of 0.063, followed by pyrolysis (0.009) and HTG (-0.033). Threefold validation confirmed gasification's sustainability. Furthermore, the process safety of biomass thermal valorization technologies, evaluated using the Numerical Descriptive Logistics Equation (NuD), found HTG to be the safest among HTG, pyrolysis, and gasification, with the lowest Process Safety Total Score (PSTS) of 210.2. HTG's lower temperature operations contribute to its safety profile. The findings align with the Inherent Safety Index (ISI), and risk mitigation strategies have been proposed based on these results. But overall evaluation based on economic, environmental, technological, and social-governance criteria recommend gasification process as a sustainable solution for biomass waste valorization due to process maturity and its wide application. Policymakers can propose short-term, mid-term, and long-term action plans for waste valorization based on the findings of this research. These plans include training and awareness programs, the installation of pilot plants, and the provision of subsidies and loans, among other initiatives, to optimize the waste valorization process, specifically the gasification process.

Publications

First author journal publications

1. **Ayub, Y.**, Hu, Y., & Ren, J. (2023). Estimation of syngas yield in hydrothermal gasification process by application of artificial intelligence models. **Renewable Energy**, 215, 118953. https://doi.org/10.1016/j.renene.2023.118953 **(JCR Q1, IF=9.0)**
2. **Ayub, Y.,** Hu, Y., Ren, J., Shen, W., & Lee, C. K. M. (2023). Hydrogen prediction in poultry litter gasification process based on hybrid data-driven deep learning with multilevel factorial design and process simulation: A surrogate model. **Engineering Applications of Artificial Intelligence**, 126, 107018. https://doi.org/10.1016/j.engappai.2023.107018 **(JCR Q1, IF=7.5)**
3. **Ayub, Y.**, Mehmood, A., Ren, J., & Lee, C. K. M. (2022). Sustainable recycling of poultry litter to value-added products in developing countries of South Asia. **Journal of Cleaner Production**, 357. https://doi.org/10.1016/j.jclepro.2022.132029 **(JCR Q1, IF=9.7)**
4. **Ayub, Y.**, Moktadir, Md. A., & Ren, J. (2024). Sustainable waste valorization process selection through AHP and advanced Interval Valued Fermatean Fuzzy with integrated CODAS. **Process Safety and Environmental Protection**, 185, 408–422. https://doi.org/10.1016/j.psep.2024.03.019 **(JCR Q1, IF=6.9)**
5. **Ayub, Y.**, & Ren, J. (2024a). Co-Pyrolysis of biomass and plastic waste: Process prediction and optimization based on Artificial Intelligence and response optimizer surrogate model. **Process Safety and Environmental Protection**, 186, 612–624. https://doi.org/10.1016/J.PSEP.2024.04.049 **(JCR Q1, IF=6.9)**
6. **Ayub, Y.,** & Ren, J. (2024b). Revealing the synergistic effect of feedstock compositions and process parameters in co-pyrolysis: A review based on bibliometric analysis and experimental studies. **Journal of Cleaner Production** (Vol. 459). https://doi.org/10.1016/j.jclepro.2024.142540 **(JCR Q1, IF=9.7)**

7. **Ayub, Y.,** Ren, J., & He, C. (2024). Unlocking waste potential: A neural network approach to forecasting sustainable acetaldehyde production from ethanol upcycling in biomass waste gasification. **Energy**, 299, 131482. https://doi.org/10.1016/J.ENERGY.2024.131482 **(JCR Q1, IF=9.0)**
8. **Ayub, Y.,** Ren, J., He, C., & Azzaro-Pantel, C. (2024). Co-gasification of biomass and plastic waste for green and blue hydrogen Production: Novel process development, economic, exergy, advanced exergy, and exergoeconomics analysis. **Chemical Engineering Journal**, 480, 148080. https://doi.org/10.1016/J.CEJ.2023.148080 **(JCR Q1, IF=13.3)**
9. **Ayub, Y.,** Ren, J., & Shi, T. (2024). Exploring gasification process and technology for biomass-waste utilization: A comprehensive review on the path to sustainable energy. **Process Safety and Environmental Protection,** 188, 1489–1501. https://doi.org/10.1016/J.PSEP.2024.06.056 **(JCR Q1, IF=6.9)**
10. **Ayub, Y.,** Ren, J., Shi, T., Shen, W., & He, C. (2023). Poultry litter valorization: Development and optimization of an electro-chemical and thermal tri-generation process using an extreme gradient boosting algorithm. **Energy**, 263. https://doi.org/10.1016/j.energy.2022.125839 **(JCR Q1, IF=9.0)**
11. **Ayub, Y.,** Tao, S., Ren, J., Lee, C. K. M., He, C., & Manzardo, A. (2022). Poultry litter valorization by application of hydrothermal gasification: Process simulation, Economic, Energic, and Environmental analysis. **International Journal of Energy Research,** 46(15), 23095–23109. https://doi.org/10.1002/er.8610 **(JCR Q1, IF=4.3)**
12. **Ayub, Y.,** Zhou, J., & Ren, J. (2023). Critical reviews of hydrothermal gasification for poultry litter valorization: Process yield, economic viability, environmental sustainability and safety. In **Journal of Cleaner Production** (Vol. 415). Elsevier Ltd. https://doi.org/10.1016/j.jclepro.2023.137876 **(JCR Q1, IF=9.7)**

13. **Ayub, Y.,** Zhou, J., Ren, J., & He, C. (2023). An innovative integration of torrefaction, gasification, and solid oxide fuel cell for carbon–neutral utilization of biomass waste: Process development, economic, exergy, advanced exergy, and exergoeconomics analysis. **Energy Conversion and Management,** 292. https://doi.org/10.1016/j.enconman.2023.117426 **(JCR Q1, IF=9.9)**
14. **Ayub, Y.,** Zhou, J., Ren, J., Shen, W., He, C., & Toniolo, S. (2023). Tri-generation for sustainable poultry litter valorization: Process design, simulation, optimization, and sustainability assessment for waste-to-wealth. **Journal of Cleaner Production**, 418. https://doi.org/10.1016/j.jclepro.2023.138139 **(JCR Q1, IF=9.7)**
15. **Ayub, Y.,** Zhou, J., Ren, J., Shi, T., Shen, W., & He, C. (2023). High-Dimensional Model Representation-Based Surrogate Model for Optimization and Prediction of Biomass Gasification Process. **International Journal of Energy Research,** 2023, 1–14. https://doi.org/10.1155/2023/7787947 **(JCR Q1, IF=4.3)**
16. **Ayub, Y.,** Zhou, J., Ren, J., Wang, Y., Shen, W., He, C., Dong, L., & Toniolo, S. (2023). Plasma gasification based monetization of poultry litter: System optimization and comprehensive 5E (Energy, Exergy, Emergy, Economic, and Environmental) analysis. **Energy Conversion and Management,** 282. https://doi.org/10.1016/j.enconman.2023.116878 **(JCR Q1, IF=9.9)**
17. **Ayub, Y.,** Zhou, J., Shen, W., & Ren, J. (2023). Innovative valorization of biomass waste through integration of pyrolysis and gasification: Process design, optimization, and multi-scenario sustainability analysis. **Energy**, 282. https://doi.org/10.1016/j.energy.2023.128417 **(JCR Q1, IF=9.0)**
18. **Ayub, Y.,** Zhou, J., Shi, T., & Ren, J. (2023). Process safety assessment of thermal technologies for biomass valorization by numerical descriptive approach. **Process Safety and**

Environmental Protection, 171, 803–811. https://doi.org/10.1016/j.psep.2023.01.075 **(JCR Q1, IF=6.9)**

19. **Ayub, Y.,** Zhou, J., Shi, T., Toniolo, S., & Ren, J. (2025). Sustainability assessment of blue hydrogen production through biomass gasification: A comparative analysis of thermal, solar, and wind energy sources. **Bioresource Technology**, *418*, 131798. https://doi.org/10.1016/J.BIORTECH.2024.131798 **(JCR Q1, IF=9.7)**
20. **Ayub, Y.,** Ren, J., & He, C. (2023). Biomass Waste Upcycling by Synergistic Integration of Gasification, Wind Energy, and Power-to-Fuel Production for Sustainable Cities (Energy Journal, **second minor review submitted**)

Other collaborative work during Ph.D.

21. Moktadir, M. A., Shi, T., **Ayub, Y**., Ren, J., & He, C. (2024). Upcycling potential of hazardous tannery sludge to value-added products: Process modelling, simulation, and 3E analysis. **Journal of Environmental Chemical Engineering**, 12(5), 113710. https://doi.org/10.1016/J.JECE.2024.113710 **(JCR Q1, IF=7.4)**
22. Moktadir, Md. A., Ren, J., **Ayub, Y.,** & Shi, T. (2024). Monetizing and selection of sustainable tannery sludge-to-energy technology using a simulation-based novel integrated MCDM model along with life cycle Techno-Economic-ESG analysis. **Chemical Engineering Journal**, 155428. https://doi.org/10.1016/J.CEJ.2024.155428 **(JCR Q1, IF=13.3)**
23. Shi, T., Zhou, J., **Ayub, Y**., Toniolo, S., & Ren, J. (2024). Novel process optimization based on machine learning: A study on biohydrogen production from waste resources. Biomass and Bioenergy, 185, 107222. https://doi.org/10.1016/J.BIOMBIOE.2024.107222 **(JCR Q1, IF=5.8)**
24. Shi, T., Zhou, J., Ren, J., **Ayub, Y.,** Yu, H., Shen, W., Li, Q., & Yang, A. (2023). Co-valorisation of sewage sludge and poultry litter waste for hydrogen production: Gasification process design, sustainability-oriented optimization, and systematic assessment. **Energy**, 272, 127131. https://doi.org/10.1016/J.ENERGY.2023.127131 **(JCR Q1, IF=9.0)**

25. Zhou, J., **Ayub, Y.,** Shi, T., Ren, J., & He, C. (2024). Sustainable co-valorization of medical waste and biomass waste: Innovative process design, optimization and assessment. **Energy**, 288, 129803. https://doi.org/10.1016/J.ENERGY.2023.129803 **(JCR Q1, IF=9.0)**

Conference presentations

1. **Ayub, Y.,** and Ren, J., (2024). Co-Gasification Process for Green and Blue Hydrogen Production: Innovative Process Development, Economic Analysis, and Exergy Assessment. 14th International Conference on Renewable and Clean Energy.

Acknowledgements

First of all, I am grateful to Allah Almighty who gave me sound physical and mental health. Thanks to my chief supervisor, Dr. Jingzheng Ren, co-supervisor Dr. Carman Lee, and my research group colleagues who assisted me in this work. Special thanks to my chief supervisor, Dr. Ren, who shortlisted me for this prestigious PhD scholarship and guided me from day one. Without his guidance, I was a raw gem with no research background, but he knows, how to utilize and polish the potential of his students to make them valuable gems. That's the same strategy he applied to me. It's the result of Dr. Ren guidance and his lead due to which I am able to perform well in my research work. Special thanks to Dr. Xiao Lin, University of York who provided me with an opportunity to work as an Associate during my study exchange program.

Thanks to my parents especially, my mother who loves me more than I love her, she gave me permission to travel thousand miles distance from her to start this PhD in Hong Kong, SAR, China. I believe it's the prayer and efforts of my parents due to which I am here, otherwise, I am nothing. Thanks to my lovely niece 'Ayesha' who always missed me and makes me happy whenever I depressed or exhaust from my work. Many thanks to my beloved sisters, 'Aqsa' and 'Ayesha' who are taking care of my parents in my absence.

I would like to thank all of my group colleagues, especially Dr. Aamir, Mr. Abdul Moktadir, Dr. Tao Shi, Mr. Jianzhao, Dr. Shengfang Lu, Dr. Huijuan Xiao, Dr. Yusha Hu, Ms. Kathy, Ms, Qiming, and my community friends Dr. Saddam Aziz, and Mr. Zahid Anwar who helped in this milestone achievement. I would also like to thanks to the Research Committee of The Hong Kong Polytechnic University to support me financially for the project through a PhD studentship (project account code: RHWR).

Table of Contents

List of Figures

List of Tables

List of Appendix

Abbreviations

Sustainability assessment score	A_s	Hydrothermal Gasification	HTG
Anaerobic digestion	AND	Hydrothermal liquification	HTL
Anaerobic digestion	AD	Lower heating value	LHV
Artificial Intelligence	AI	Machine Learning	ML
Artificial Neural Network	ANN	Megapascal	MPa
Biochar production	P_b	Municipal Solid Waste	MSW
Biomass	BM	Plasma gasification	PG
Biomass to Air Ratio	BMR	Poultry Litter	PL
Carbon gasification efficiency	CGE	Pressure	P_p
Circular economy	CE	Process inventory	I_p
Dry Poultry Litter	DPL	Process safety index	PSI
Economic gain maximization	E_{max}	Process temperature	T_p
Economics Analysis	EA	Residence Time	RT
Electric power maximization	P_{max}	Rice Straw	RS
Energy Information Administration	EIA	Root means square error	RMSE
Equivalence Ratio	ER	Slow pyrolysis	SP
Extreme Gradient Booster	XGB	Solid Concentration	SC
Fast pyrolysis	FP	Solid Oxide Fuel Cell	SOFC
Fuel utilization factor	U_f	Strengths, Weaknesses, Opportunities, and Threats	SWOT
Greenhouse gases	GHG	Sugar Bagasse	SB
Heat of reaction	H_p	Supercritical Water Gasification	SCWG
Higher heating value	HHV	Sustainability Index	SI

1 Introduction

The increasing trend of waste generation, specifically solid waste including both organic and inorganic constituents, raises formidable challenges in the form of greenhouse gas (GHGs) emissions into the atmosphere, land contamination and subterranean water sources. According to estimates provided by the World Bank, the global generation of municipal solid waste (MSW) reached 2.01 billion tons in 2018, with a significant portion 33% of this waste lacking environmentally friendly disposal. Projections indicate that the global MSW will reach 3.40 billion tons by the year 2050 [1]. Traditional methodologies such as landfills and incineration, globally employed for waste management, exhibit an unsustainable characteristic in terms of economic, environmental, and social dimensions due to the substantial emissions produced during decomposition processes [2,3]. Furthermore, sustainability challenges are arising from the entire waste management life cycle, from collection, transportation, handling, disposal, and the generation of by-products [4,5]. Therefore, the selection of an appropriate and sustainable waste decomposition process assumes significant importance in mitigating the aforementioned challenges and ensuring the enduring sustainability of the waste management process.

Biomass waste is available in different forms, but the most common are woody, biogenic, agriculture, and manure waste etc. [6]. Thermal and biological processes can be applied to valorize these biomasses into various forms of energy. Thermal processes primarily comprise on pyrolysis, hydrotreating, and gasification, while biological processes are categorized as aerobic or anaerobic [7]. But each technique has its own benefits and drawbacks. For example, pyrolysis and gasification provides a better economic return at commercial level, whereas anaerobic digestion is also viable at the domestic level [8]. According to the United States Energy Information Administration (EIA), biomass energy fulfilled approximately 5 quadrillion British thermal units (Btu), or 5% of the overall energy needs of the United States in 2021 [9]. Furthermore, electricity generation potential only from poultry litter is around 8893,

8745, and 4803 megawatts per day, in Pakistan, India, and Bangladesh, respectively, with 60% of the poultry litter utilization through anaerobic digestion process [8]. Therefore, biomass waste has a high energy potential if it is being converted by utilizing any suitable valorization process which can solve the biomass waste disposal problem but also helps satisfy energy demands using renewable energy resources.

1.1 Research background

Biomass waste valorization is one of the potential approaches for reducing GHG emissions while meeting energy demands. Globally, various methods are used to manage MSW, primarily categorized into thermal and biological approaches. A higher amount of hydrogen and less tar in the syngas is a key indicator of quality syngas produces in gasification process. While higher bio-gas production with less contaminants in term of sulphate, nitrates compounds etc. are the primary objective of anaerobic digestion (biological process). Poultry litter (PL) is one of the biomass types, along with poultry beads, water droplets, feathers, poultry feed, and rice husk straws, that may be used to create renewable energy [10]. PL can be transformed into several value-added products that may be utilized as bioenergy in developed countries. But currently, developing countries are not utilizing this waste potential appropriately due to which some unsettling issues in term of GHGs emission, surface, and underground waters contaminations have been increased. Therefore, proper waste disposal mechanism needs to be developed which can incorporate emissions related and waste disposal issues.

Incineration is the simplest thermal conversion process adopted in different regions of the world for biomass waste valorization. However, the high moisture content of biomass waste, along with the enormous amount of ash makes incineration a less eco-friendly and energy-intensive process [11]. The pyrolysis of biomass waste for biochar and biofuel production is also a sustainable option with respect to its energy, economic, and environmental performance,

but it is a complex process due to the stringent parameter requirements and high initial investment cost. The gasification valorization process, which is a techno-economic, environment, and energy feasible solution for thermal power generation using the final product, has also been examined in different research [12]. Gasification is the primary process for most co-generation and poly-generation technologies. However, the high moisture content in biomass is a major concern, which affects the energy yield of the process [13]. Similarly, plasma gasification valorises biomass waste at extremely high temperature which ultimately produce better quality syngas, but the process is highly energy intensive. The hydrothermal gasification (HTG) valorization process is a solution to the problem caused by high moisture which can be used for liquid or slurry biomass valorization. However, maintaining a high pressure of 25–30 MPa at 375–500 °C makes this process less energy-efficient and not economically viable when compared to other thermal processes. Therefore, every primary valorization process has its own limitations, but the final product generated by the gasification process can be used in poly-generation to make the respective process economic and energy efficient.

The poly-generation process is one of the viable ways to increase the sustainability of the process performance (i.e., energy, economic, and environmental). Different secondary processes, such as solid oxide fuel cells (SOFCs), hydrogen, gasoline, diesel, ethanol, methanol, dimethyl ether (DME), and combined heating power systems (CHP), can be integrated with primary valorization processes (i.e., gasification and pyrolysis) [14]. Ebrahimi and Ziabasharhagh (2020) developed a tri-generation process used for biomass valorization by generating heat, power, and liquefied natural gas. The exergy efficiency of the total process was increased to 74% and the CHP efficiency increased from 38.95 to 48.0% [15]. Zhou *et al.* (2023) have proposed a co-combustion and SOFC based tri-generation process, and the thermal energy efficiency of the process was reported to be ~69% with an electrical efficiency of 27.4%

[16]. Similarly, the plasma gasification-based CHP and DME production process energy and exergy efficiencies were 48% and 42%, respectively, with a significant impact on the economic performance [17]. Therefore, poly-generation processes can improve the energy efficiency, which ultimately affects the economic output of the process.

Biomass waste secondary conversion processes have been analysed in different studies. Syazaidah *et al.* (2021) conducted research on the conversion of PL biomass into bio-oil based on a fast pyrolysis process, and the bio-oil yield increased by adding a catalyst in the reaction. However, the higher heating value (HHV) of the resulting fuel was only 16.01 MJ/kg, which is lower when compared with that of normal fuel used in vehicles. Therefore, additional processes are required for further refining bio-oil [18]. DME is an alternative high-energy fuel with a high HHV and combustion properties like liquefied petroleum gas (LPG). It can be used in vehicles and as a raw material for different industrial chemicals [19]. DME can be produced from syngas generated via biomass valorization if it contains a major portion of H_2, CH_4, and CO. However, the significant H_2 content in syngas is an important factor, which significantly contributes to the synthesis of DME [20]. The quality of syngas can be improved by altering the process parameters, including temperature, pressure, resident time, and gasifying agent. Zhang *et al.* (2016) analysed the techno-economic suitability of CO_2 utilisation as a gasifying agent for steam reforming to produce methanol, which can be converted into DME. However, energy analysis and life cycle assessment of the process was not considered [21]. Nakyai *et al.* (2020) developed a simulation model for rubberwood conversion into methanol and DME. The results of their exergoeconomics analysis showed that the DME unit cost was 1.66 $/kg from the direct system synthesis which was lower when compared with the indirect synthesis (2.26 $/kg) [22]. However, the DME production costs are not market competitive (0.65 $/kg) [23]. Therefore, a sustainable biomass waste valorization process is required to produce DME in terms of its environmental, economic, and energy aspects.

Comixing of biomass waste with plastic waste in a co-gasification process also presents a favorable synergistic approach to enhance the production of hydrogen within the syngas. Various studies have demonstrated that co-gasification of biomass and plastic waste can result in a higher rate of H_2 production in the syngas, along with an improved HHV. In a study conducted by Maninderjit Singh et al. (2022), a co-gasification model based on biomass and plastic waste has been developed. Research findings suggested that a higher proportion of plastic waste, particularly in the range of 30-70% plastic to biomass ratio at a temperature of 750°C, yielded the highest concentration of H_2, ranging between 63-65% [24]. This study focused solely on kinetic modeling, analyzing the impact of process parameters such as temperature, pressure, and gasification on the final product. However, economic, energy, and exergy feasibility aspects of the process were not considered. Similarly, Kaydouh and Hassan (2022) developed a thermodynamic model to study the co-gasification of plastic and biomass waste, which were further analyzed by applying different gasifying agents, including CO_2, O_2, air, and steam. Their analysis revealed that an increased proportion of plastic waste in the feedstock led to an overall rise in H_2 production. However, using CO_2 as a gasifying agent had an adverse impact on H_2 production due to the reversed water gas shift reaction. Using air as a gasifying agent decreased the HHV of the syngas in comparison to using O_2, primarily due to the higher concentration of N_2 in the resulting syngas. While steam demonstrated high efficiency as a gasifying agent, significantly promoting H_2 production [25]. However, this study focuses on simulating the co-gasification process's thermodynamic equilibrium, specifically targeting the optimization of H_2 using various gasifying agents and process parameters. Li et al. (2021) also supported the research finding of enhanced syngas production through co-gasification compared to utilization of biomass feedstock alone. According to their findings, a synergistic solution resulting in a 69% energy yield was achieved through the gasification of high-density polyethylene (HDPE) and acid-treated pine wood at a 27% fraction

[26]. Therefore, the co-gasification of biomass and plastic waste offers a synergistic approach to yield higher-quality syngas, with a higher concentration of H_2. To ensure sustainable performance, other process performance indicators such as economic, energy, and exergy efficiencies are an aspect that seems to be overlooked in current studies.

Optimization of the process parameters is another way to obtain good quality product with higher hydrogen content, which ultimately produces a higher yield of methanol, H_2, DME etc. in the secondary process. The optimization process can be performed using two different techniques: simulation software such as Aspen Plus, which is based on mechanistic models, and data-driven modelling through machine learning (ML) algorithms. Li *et al.* (2021) applied a gradient boost regressor (GBR) for hydrogen prediction in the gasification process. The model performance was good in terms of the coefficient of determinant (R^2 >0.90) [27]. Similarly, Shahbeik *et al.* (2023) applied a Gaussian-based ML regression model to predict the pyrolysis process output with a model performance of R^2 >0.90, which is quite good with respect to the applied model [28]. But there are always some errors in these ML models that depend on the R^2, and the higher the R^2 value, the lower the prediction error. These errors, along with dataset availability, are limitations for black-box models because ML-based prediction models rely on the data available. Therefore, if the dataset is not refined, model has a misleading result. The optimization process can also be effectively performed by integrating a mechanism-based model and efficient optimization algorithms (particle swarm optimization and genetic algorithm). The optimization accuracy of this method is higher than that determined using ML-based models because these models are integrated with the first-principal simulation model and there are also no errors derived from the data fitness in the optimization results [29,30]. A pre-collected dataset is also not required because data refinement issues are not created for such models. Therefore, considering the economic, environmental, energy, and process optimization limitations, the Biomass-to-*X* (where *X* could be DME, methanol, electric

power, CO_2, H_2 etc.) production process needs to be developed, which may be sustainable in terms of its economic, environmental, and energy aspects.

1.2 Problem statement

Substantial landfilling activities through biomass waste and social consequences are key obstacles to the development of the circular economy (CE) and bioenergy [31]. South Asian countries like Pakistan, India, and Bangladesh, the majority of biomass waste (PL, livestock excretion) is disposed of landfills or spread directly on agricultural land to boost the fertility. However, this method has some drawbacks, including eutrophication of land water, untreated exposure to the environment generating foul odor, pathogen growth, GHG emissions, and phytotoxin compound generation [32,33]. Some studies indicates that PL biomass may contain pathogens such as salmonella spp., enterococci, staphylococci, and lactobacilli bacteria, making underground or surface water vulnerable if utilized directly on land as a fertilizer [34]. Furthermore, Class 1 Integron, which promotes the transmission of antibiotic resistance genes in bacteria is identified in more than 90% of PL samples [35]. Therefore, an efficient safe disposal of biomass waste without damaging the environment could be a viable solution to these problems.

Different biomass valorization processes including thermal and biological which have their own limitations. Biological valorization methods are time taking while thermal valorization processes involve lot of capital investment. The thermal incineration process is a well-established and extensively utilized method for the valorization of waste in different regions. However, this approach is hindered by its significant GHG emissions. According to estimates, each ton of MSW emits approximately 134±17 kg of CO_2, 88±36 g of CH_4, and 69±16 g of N_2O during the incineration treatment process, which represents a considerable environmental impact [36]. Consequently, there is a need for process improvements or alternative methods to manage MSW in a more sustainable manner. Nakatsuka et al. (2020)

presented an innovative approach that integrates MSW incineration with wastewater treatment. The thermal energy generated during the incineration process is utilized for electrical energy production, which is subsequently employed in wastewater treatment. Implementation of this model yielded significant results with a reduction of around 35% of total annual costs and a commendable 1% decrease in CO_2 emissions [37]. Niu et al. (2019) integrated a torrefaction-based pre-treatment to address biomass inherent limitations such as low energy and mass density, as well as hydrophilicity in biomass waste at an optimum torrefaction temperature of 250°C to enhances biomass quality which ultimately increases carbon content with decreases H/C and O/C ratios. Therefore, the final fuel production exhibits a better combustion efficiency, mitigating issues related to downstream ash content [38]. Hence, integrating various methods such as combining thermal processes with biological approaches or incorporating pre-treatment steps can enhance the quality of the final product in waste valorization. However, further exploration of the sustainability perspective of these processes is necessary to mitigate emissions and achieve carbon neutrality.

Biomass waste valorization process sustainability in terms of energy, exergy, economic, environment, and social perspective need to be further optimized by application of different algorithms integration with simulation model. Biomass waste valorization process output is dependent on feedstock characteristics and process input parameters. Therefore, appropriate process parameters selection and feedstock composition is challenging for the researchers to get the optimum output. Similarly, selection of the appropriate valorization processes among different available thermal (pyrolysis, gasification, plasma gasification, hydrothermal gasification, incineration) and biological (anaerobic digestion, aerobic digestion) is quite challenging for the decision makers considering sustainability perspectives. Hence, appropriate decision-making is required which can address these challenges and research gaps for the selection of sustainable valorization process.

Merely relying on conventional valorization methods such as gasification, incineration, and pyrolysis is often unsustainable, particularly when dealing with biomass containing high levels of moisture. Hence, secondary process integration is required to make the process more sustainable. The synergistic integration of these processes serves to optimize yield, ultimately improvement in techno-economic, environmental, energy, and exergy sustainability aspects. Primary processes have been integrated with the secondary processes by researchers which include CHP system, methanol, dimethyl ether, CO_2, and H_2, etc. production. Safari and Dincer had developed an integrated multigeneration process for hydrogen, power, fresh water, and heat production through AND. Overall process is energy and exergy efficiencies were 63.6% and 40%, respectively [39]. Similarly, Prestipino et al. (2022) have devised a bio-hydrogen production method utilizing biomass waste as the primary feedstock. The highest hydrogen yield was obtained at a steam-to-biomass ratio of 1.25, achieving an exergy efficiency of 33% and exhibiting a carbon footprint of -1.9 $kg_{CO_2\text{-}eq}/kg_{H_2}$ [40]. Therefore, process sustainability can be improved by application of different pre-treatment and secondary processes integration which needs to be explored further in terms of techno-economic, energy, exergy, and environmental aspects.

Although different research studies have explored sustainable methods for the disposal of biomass waste, including primary, secondary, and tertiary processes. However, in developing countries such as Pakistan, India, and Bangladesh, traditional methods like combustion and land disposal frequently adopted for managing biomass waste. This reliance on outdated practices can be attributed to several factors, including inadequate infrastructure, limited technical expertise in valorization process selection, insufficient investor interest, and the absence of concrete policies and regulatory frameworks. Despite these challenges, these countries possess significant biomass waste potential that could be transformed into valuable products, contributing to GHGs reduction efforts. Estimates suggest that valorizing poultry

litter through gasification could enable Pakistan, India, and Bangladesh to reduce CO_2 emissions by 10.1, 9.9, and 5.4 million tons per annum, respectively [41]. However, to achieve these reductions, there is a need for concrete policies, improved infrastructure, optimal process development, techno-economic sustainability analyses, and decision-making models to facilitate effective process selection and attract investors. Accordingly, several research objectives have been given in Section 2.5 to address these critical aspects.

2 Literature review

For this study, literature review has been conducted to calculate the biomass waste potential along with the waste valorization techniques. Different waste valorization optimization and prediction methods have been summarized. Finally, decision making techniques have been concise from the literature.

2.1 Biomass waste potential and current scenario

In 2020, European nations will have reached a milestone of 20% renewable energy, with biomass energy accounting for the largest share [42,43] and these nations have set a target of producing 30% of total power from renewable sources by 2030 [44]. Since, biomass waste contains nitrogen, potassium, and phosphorus compounds, therefore, majority of biomass waste is being used as a (compost) fertilizer for agricultural land in developing countries [45] In current work, biomass waste is the main focus for assessment purpose. According to Economic Survey of Pakistan assessment, only commercial poultry (broilers and layers) population has reached over 1340 million [46]. Similarly, the commercial poultry populations in India and Bangladesh are 852 million [47] and 599 million [48], respectively which produces significant amount of poultry waste. In these South Asian countries, landfill disposal or composting is now the most prevalent method of dealing with poultry waste. Therefore, this

potential of poultry waste biomass energy can also be used as a source of energy by valorization into biofuel or biogas, which is common practice in most of the developed countries.

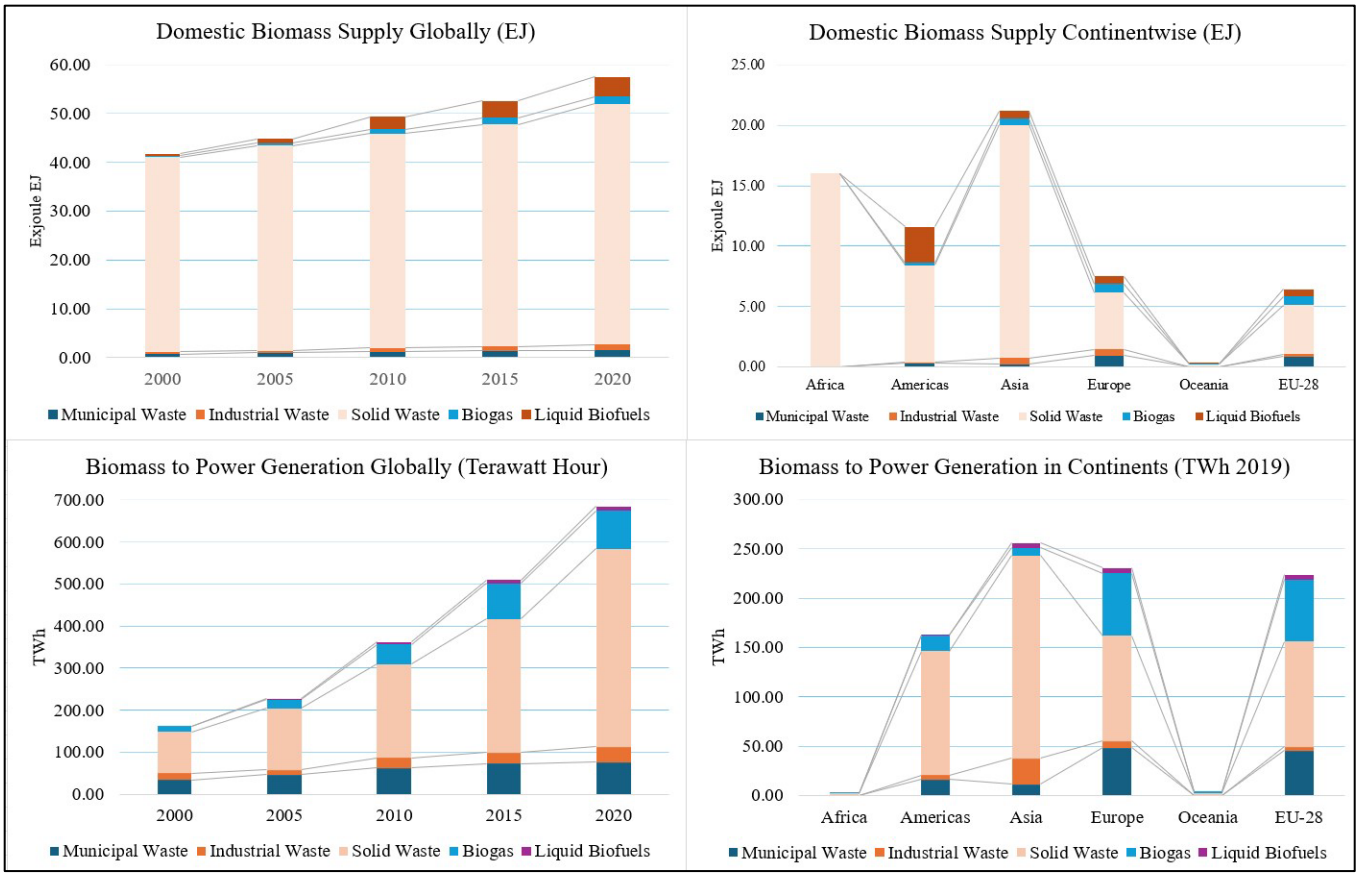

Fig. 2.A Global and continental biomass waste to energy trends

According to 2018 World Bank statistics, the global production of municipal solid waste (MSW) reached approximately 2.01 billion tons, with a projected increase to 3.40 billion tons by 2050 [1]. Out of this waste, at least 33% are not managed in an environmentally friendly manner. Despite regional initiatives to convert BM waste into various energy sources which is consist of around two-thirds of the total MSW waste had been utilized to meet the domestic energy need of 60 exajoules (EJ) in 2020 which primarily comprises of BM solid waste. The major contributors to this waste generation are Asian countries, followed by African nations, as depicted in Fig. 2.A [49]. While efforts have been made to convert some of this waste into electric power, with global generation escalating from 162 to 684 terawatt-hours over the past two decades, the distribution of utilization varies. Asian countries dominate BM waste-based

power generation, with Europe following suit. Specifically, African countries, despite being the second-largest contributors to BM waste production, exhibit the lowest utilization for power generation. Therefore, there exists substantial potential for BM waste to address both waste disposal concerns and energy production requirements.

2.2 Biomass waste valorization processes

There are different biomass waste valorization processes which have been described in sections 2.2.1 to 2.2.3.

2.2.1 Thermal processes

In thermal valorization processes, heat is applied to convert biomass waste into value added products. It has been mainly categorized into pyrolysis, gasification, hydrothermal gasification, and incineration. For this study, scope is limited to the pyrolysis, gasification, and co-generation processes which are summarized in the section below. Fig. 2.B has the process flow of thermal and biological valorization processes while SWOT from different studies has been summarized in Table 2.3. Thermal processes are the faster way to convert biomass waste as compared to biological processes for biomass waste valorization, but initial capital investment is high while biological valorization processes are also feasible at domestic level. Therefore, both thermal and biological processes have some limitations, but it depends on the decision makers which process they prefer as per regional needs.

2.2.1.1 Pyrolysis

Pyrolysis is a thermal conversion process that uses heat to convert biowaste into bio-oil or biochar. It is further subdivided into slow, intermediate, and fast pyrolysis based on conversion time and process parameters. If the feedstock is a mixture of different biomasses or polymers then such process also known as co-pyrolysis [50]. Final products of these processes are summarized in Table 2.2. Fast pyrolysis is the faster route to convert biomass into bio-oil,

biochar, and low molecular mass gases. Fast pyrolysis valorization process produces up to 78% of the bio-oil yield (dry biomass basis) at 400-650 ^{o}C [51] with a maximum particle size of 2 mm for better efficiency. Bio-oil is a mixture of organic molecules including alkane, aromatic compounds, phenols, ketones, esters, amines etc. Output yield of pyrolysis is dependent on the types of biomass and process parameters including biomass residence time, temperature, heating rate. But for better yield of bio-oil, residence time should be less than 3 seconds [52]. While slow pyrolysis promotes the production of biochar at slower rate which takes several hours [53]. According to experimental results, 350-450 ^{o}C with 1 hour residence time are the optimum parameters for biomass waste to biochar production. Increasing temperature reduce the biochar production rate [54]. Therefore, if the objective is to produce biochar, then lower temperature and higher residence time is more suitable for this while higher temperature and lower residence time promotes the production of bio-oil.

2.2.1.2 Gasification

Gasification is the thermochemical process of converting carbonaceous materials by reacting with air and moisture to form a syngas that contains CO_2, CO, H_2, and CH_4 [55]. Based on the process parameters and biomass characteristics, the gasification process is primarily separated into HTG, plasma gasification, and conventional gasification (CG) [56]. HTG process is primarily used for moist or liquid biomass without the involvement of drying process, which is being carried out at high pressure of 20-25 MPa and temperature ranges from 370-500 ^{o}C [57,58], whereas conventional gasification process is carried out at high temperature of around 700 ^{o}C, producing mainly H_2, CO, CO_2, and CH_4 gases with fractions of some other higher hydrocarbon [41]. Conventional gasification processes involve pre-treatment of biomass in the form of a drying process, whereas HTG requires biomass to be in liquid or slurry condition [59]. Therefore, conventional gasification is only appropriate for the solid biomass

at higher temperatures, whereas HTG is acceptable for both solid (producing slurry) and liquid biomasses.

HTG converts biomass waste into syngas, including hydrogen, at lower temperature compared to conventional gasification process. Water is a universal solvent with distinct properties such as great diffusivity and solubility in its supercritical state, which allows it to behave as both a liquid and a gas. Under high temperatures and pressures, the reaction between biomass and water can effectively disrupt the chemical bonds, resulting in the gasification of biomass [60]. HTG is a similar process to hydrothermal liquification (HTL), however there is temperature and pressure variation. The temperature of the reactor in the HTG process is 400-700 ^{o}C at 22-35 MPa pressure, whereas the temperature in the HTL process is 250-400 ^{o}C at 5-35 MPa pressure. HTG also known as supercritical water gasification [61,62]. Elemental compounds of the biomass such as carbon, hydrogen, and oxygen can be converted into gases such as carbon dioxide, hydrogen, and methane if the temperature and pressure in HTG remain above the super critical point (400-600 ^{o}C and 22-25 MPa) [63]. By adjusting the HTG process operating parameters, high efficiency syngas with more hydrogen gas concentrations can be produced [64]. Process parameters and biomass concentration are mainly contributed to the HTG output as some literature-based studies summarized in Table 2.1. Hence, the HTG process could be a viable option for turning hydrated biomass waste into energy in the form of high-quality, high-pressure syngas without prior drying.

Table 2.1 Summaries of gasification studies with biomass types

Feedstock	Applied Process	Summary of key findings	Ref.
Sewage sludge	HTG Simulation Model	Temperature, and biomass concentrations have a direct impact on the composition and quality of syngas.	[65]
Poultry manure	Lab Scale Experimentation of HTG	High temperature (580 °C) with a residence time of 10 min at 25 MPa pressure is an optimal for promoting hydrogen gas production.	[66]
Microalgae Spirulina	HTG Simulation Model	Biochar is produced at equilibrium condition of the model, and it is dependent on biomass composition.	[67]
Glycerol	SCWG Simulation Model	Biomass pre-heating and reforming temperatures have a substantial impact on the final gas quality and efficiency.	[68]
Glycerol, sewage sludge, microalgae, grape, phenol	SCWG Simulation Model	SCWG process is sustainable if biomass concentration of 15-25% is adopted. At the feed rate of 1000 kg/h 150 kWh of net energy power produces.	[69]
Pine Pallets, Eucalyptus	Gasification Simulation and Lab Model	ER from 0.17 to 0.35 and 709-859 °C temperature has the significant effect on syngas output.	[70]
Straws	Integrated Gasification Simulation Model	Effect of oxygen, air, temperature, and pressure has been studied. Findings concluded that increasing oxygen with air ratio less than 3.5 is the more suitable for better biomass efficiency.	[71]

2.2.1.3 Plasma gasification

Plasma gasification (PG) which is relatively advanced form of the conventional gasification process and can convert biomass waste at extremely high temperatures (1000-5000 °C) with the help of plasma torch. Accordingly, biomass waste can be converted into syngas and aggregate by application of high plasma state thermal process [72]. Syngas can be further processed for value-added use in various upgraded processes, whereas aggregate can be utilized as a building material. PG process can be mainly divided into two types: (1)

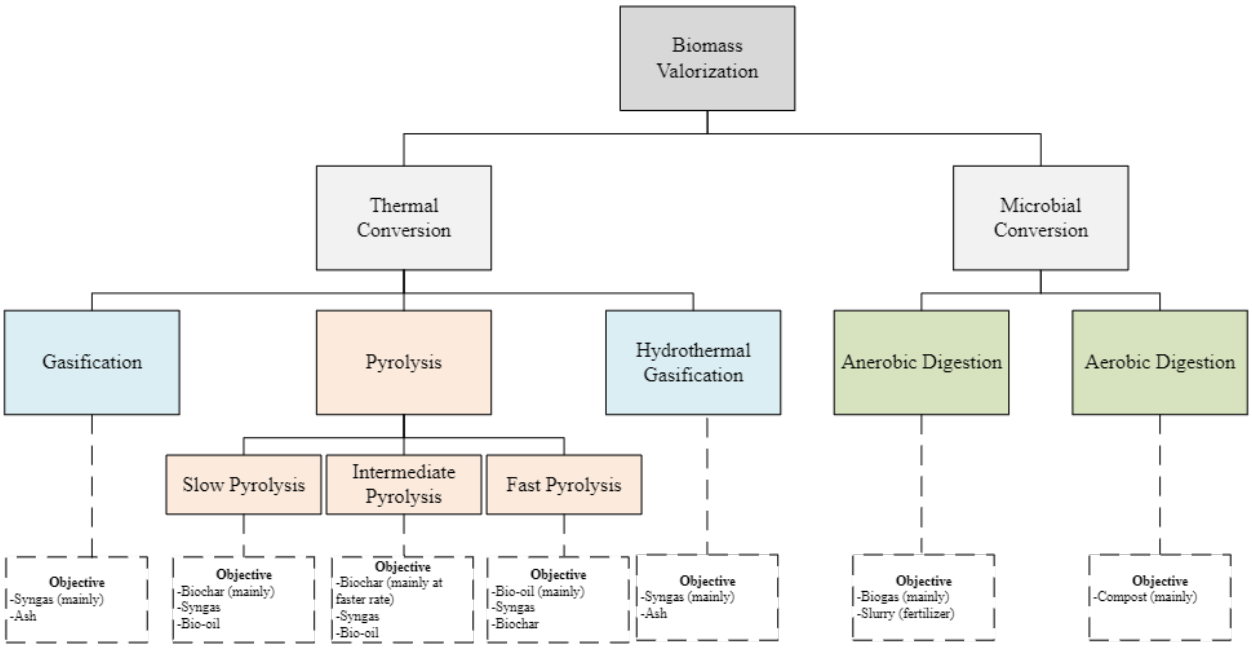

Fig. 2.B Thermal and biological valorization processes for biomass waste

conventional gasification (CG) coupled with PG and (2) plasma torch assisted gasification process [72]. PG is more preferable comparing with the conventional and the HTG because of less space requirement compared with conventional one and tar-free syngas can be produced in this process which can be directly used in upgraded process [73,74]. Furthermore, waste flexibility is high with lower levels of CO, NO_x, SO_x, and tars pollutants. The waste to energy (WTE) efficiency is also higher (29-33%) in PG as compared with that in conventional gasification (15-30%) and incineration (16%) [75,76]. Minutillo *et. al* 2009 concluded that system efficiency (31% LHV) of PG which is higher than that of incineration (20% LHV) [77]. Therefore, PG has been recognized as a promising option for biomass valorization compared to the conventional and the HTG process because of better quality output and higher efficiency of the process. Syngas generated in the PG process can be used in poly-generation for converting it into different high-value-added products including methanol and DME, etc.

2.2.2 Microbial processes

Microbes are also used to valorize the biomass waste into different products in the presence or absence of air. Microorganisms are used in the anaerobic process to produce the

methane-rich biogas and slurry [78]. Anaerobic process (AND) takes around 12 to 27 days, whereas composting or aerobic digestion (AD) takes approximately 28 to 42 days to convert the biomass waste into compost which can be used as an organic fertilizer [79]. Final products of the thermal and biological processes are summarized in Table 2.2. SWOT-PEST analysis of the thermal and microbial valorization processes is summarized in Table 2.3. Hence, by application of various conversion processes, biomass waste can be converted into a variety of value-added goods. Fig. 2.B illustrates the thermal and microbial methods for biomass waste valorization.

Table 2.2 Biomass pyrolysis, gasification, and biological valorization processes output

Pyrolysis conversions		**Gasification**	**Biological conversions**	
SP	**FP**		**AND**	**AD**
[80] Biochar (**mainly**) Bio-oil Syngas	[81] Bio-oil (**mainly**) Biochar Pyrolytic Gases	Syngas (**mainly**) (H_2, CO, CO_2, CH_4) Biochar	Rich **methane** (60-65%) biogas [82] CO_2 (30-35%) Organic (slurry) Ammonia, H_2S	Low moisture odorless product use as fertilizer [83]

Table 2.3 SWOT-PEST analysis of FP, SP, AND, and AD

		Strengths	**Weakness**
P			• Taxes on supporting equipment
E	**FP**	• Highest investment return and shorter payback period	• High capital investment requires, and it is feasible at commercial level [84]
S		• No need for land disposal of by-product [85]	• Heat emissions effects nearby [86]

T		• Continuous process with step-up conversion rate [87]	• Yield is temperature, flow time dependent [88]
P	**SP**		• Taxes on supporting equipment
E		• Low capital investment as compared to FP [84]	• Lower rate of return as compared to FP
S		• Final product free from volatile compounds [89]	• Heat emissions effects nearby [86]
T		• Simpler process as compared to FP	• Yield is temperature dependent [86]
P	**AND**	• Process is subsidized by government	• Limited scope of subsidies
E		• Economical process as compared to pyrolysis [86,90]	• Rate of investment return is time taking as compared to the pyrolysis process
S		• Less technical expertise requires as compared to thermal process [79,90]	• Biogas leakage issue; it can affect surroundings [82]
T		• Simpler process as compared to pyrolysis and suitable at the domestic level	• Temperature, flowtime, and organic load to be maintained [80]
P	**AD**		• No subsidy in South Asian countries
E		• Cheapest way for biomass conversion	• Low-value final product
S		• Simpler and less expertise is required	• High land area requires
T		• Simple hand tools require	• Conversion process takes 4-6 weeks[79]

		Opportunities	**Threats**
P	**AD**	• Better economical results after policymaking	• Neglected process by policymaker
E		• Earthworm utilization is a mutualistic approach and a source of protein for poultry	• Comparative cheaper product and only land application

S		• Process possible at domestic level	• Bad odor and large land space is required
T		• Vertical multiple level infrastructure can be used to tackle the space issue	• Carbon to nitrogen ratio effect in the product which is not effective [79]
P		• Government subsidies for larger plant	• Taxes on supplementary equipment
E		• CO_2, H_2S, and NH_3 gases produced can be recovered	• Lower yield and high investment return period
S	**AND**	• Safety features can be added to detect leakage	• Digestor leakage is damaging for surrounding [78]
T		• Temperature, organic load, and retention time, can be automated for better efficiency	• Periodic plant tanks maintenance requires [79]
P		• Government subsidies and carbon credit gain	• High taxes on equipment and no existing policies
E		• Phenol, nitrogen compounds, sterols, and water products can be converted into liquid fuel [86]	• Traditional technique and low rate of return
S	**SP**	• Biochar can be used as a bio-fertilizer and fuel to warm the houses	• High temperature of reactor causing nearby safety issues
T		• Self-sustain process	• Slower process as compared to FP.
P		• Government subsidies and carbon credit gain	• High taxes on equipment and no existing policies
E		• Commercial value compounds toluene, benzene, xylene, ethylbenzene produced at 719 ^oC [85]	• Higher capital investment as compared to the SP [84]
S	**FP**	• Clean process and limited plant space required	• Shifting to other processes due to pyrolytic gases and high-temperature safety issues
T		• Self-sustain process utilizing the product [91]	• Due to high temperature, periodic maintenance requires

2.2.3 Poly-generation processes

There are various combined cycle systems that can be used to enhance the net energy or exergy performance of biomass valorization specifically with thermal processes. SOFC co-generation is one of the methods which can be employed in a combined cycle with gasification due to its operational capability at higher temperatures and greater fuel contamination tolerance. Therefore, it has been considered an excellent fit for the gasification process. Processed syngas from the gasification process could be utilized in SOFC with air/oxygen input from the SOFC's anode and cathode, respectively [92]. Similarly, another tri-generation process includes the primary gasification process which can be extended to secondary methanol and DME production along with electrical energy from CHP [93,94]. These processes can also be integrated with renewable energy sources to make process allothermal [95]. Pyrolysis process can also be integrated with secondary thermal valorization processes of gasification and CHP along with CO_2. This process has been developed in chapter 7. But the primary objective of these processes is to improve sustainability in terms of energy, economic, environment, and social perspectives. There are different poly-generation processes that have been developed in this work and the sustainability analysis has been performed. These processes are summarized in chapter 5-7.

2.2.4 Research gaps

According to different studies, the circular economy is a potential business model, but it is still unclear whether it is economically viable for saving the environment and increasing social fairness at the same time [96]. Although some studies on biomass waste like cow, wood, and pig manures have been done, but there are limited research focusing on PL biomass valorization for South Asian developing countries. Consequently, one of the objectives of this research to develop a method for valorizing PL in an eco-friendly, economically feasible, and sustainable for South Asian developing countries. It will also help to accomplish United

Nations Sustainable Development Goal number 7, which is 'affordable, reliable, sustainable, and modern energy' [97] by creating policies for biomass waste valorization technologies based on the findings of this research.

Process parameters such as temperature, air ratio, and feedstock significantly influence the final quality of syngas produced through gasification. However, existing research has predominantly concentrated on enhancing the valorized production yield of sewage sludge and other agricultural biomasses, with PL biomasses receiving comparatively less attention. Wen Cao et al. (2022) conducted an experimental study focusing on poultry manure biomass, utilizing a lab-scale model restricted to analyzing the parametric aspects of the HTG process [66]. But for the optimum yield and other sustainability indicators analysis including economic, environment, energy, and process safety aspects are not feasible with lab scale experimental model. Therefore, a comprehensive research study needs to be conducted on the economic, energy, environmental, and process safety aspects of the HTG process with parametric analysis.

Simulation based model can be used to estimate the end product yield based on the input parameters, which is time intensive and costly in experimental setup. Furthermore, these models can be used for energy analysis and adjustment of input parameters to improve syngas quality which is quite and costly in an experimental setup. The final product quantity and quality of the valorization process can also be utilized to calculate the process's economic viewpoint. Therefore, the goal of this study is to develop a process simulation model for the conversion of biomass waste specifically for PL into syngas or steam using Aspen plus simulation. Different thermal valorization processes integration has been evaluated to find out the optimum sustainable process. Simulation model of these processes will aid in the prediction of final product parametric yield. These validated simulation models can also be utilized to adjust parameters for higher syngas yield without wasting time and money on experimental investigations. Hence, simulation of the valorization process can assist in the calculation of

some aspects like economic, energy, environment etc. which are not easily feasible with experimental setups.

Similarly for gasification-based co-generation processes are mostly dependent on the process parameters, particularly temperature and (biomass to air ratio) BMR, while in the HTG process, residence time, and solid contents have a major effect on the syngas quality. However, if syngas is used in SOFC based integrated process or in the production of DME, methanol, H_2, CO_2 etc. then process sustainability can be improved. Process parameters temperature, pressure, syngas fuel quality, and the use of concentrated O_2 as a gasifying agent significantly affect the process output. In the case of SOFC, the use of concentrated O_2 at the cathode has a substantial impact on SOFC efficiency. The overall exergy efficiencies of the gasification and SOFC models have been found to range between 50 and 61% which can be improved by controlling the process parameters [98,99]. Similarly, the use of different gasifying agents like air, the use of concentrated O_2, steam etc. plays a significant role in gasification process output which needs to be explored further with an integration of secondary or tertiary processes.

Current studies indicate the circular economy is a promising business model, its economic viability for environmental sustainability and social equity need to be explored, particularly in South Asian developing countries. Existing research has predominantly enhanced the yield of sewage sludge and agricultural biomasses, neglecting the comprehensive analysis of PL. Furthermore, lab-scale models have shown limitations in optimizing process parameters for syngas quality and sustainability indicators. Therefore, there is a need for a simulation-based model to evaluate the economic, energy, environmental, and safety aspects of PL valorization though an integration of multi-generation processes, utilizing advanced simulation tools like Aspen Plus to predict yields and improve process efficiency, thereby contributing to the United Nations Sustainable Development Goal 7.

2.3 Optimization of biomass waste valorization

2.3.1 Integration of the prediction and optimization models

Hydrogen is the most important element of the thermal valorization process like gasification process since it influences fuel quality in terms of HHV and LHV. Furthermore, it is a critical component in the hydrogenation process as well as the synthesis of other industrial chemicals such as ammonia, methanol, and SOFC efficiency [57,100]. However, current gasification process productivity is insufficient to make hydrogen synthesis an economically viable process because additional processes such as drying and separation of hydrogen from other gases are necessary which increase the process cost. Some studies use catalysts in the gasification process to boost the yield of hydrogen and methane gas and make the process more cost competitive, but yield is mostly determined by process parameters such as temperature, pressure, solid content etc. [101,102]. Therefore, biomass type and process input parameters such as temperature, solid content, biomass resident time, and pressure need to be altered for improved yield, which can be anticipated using various algorithms.

The underlying objective of the gasification process to produce syngas with a higher percentage of hydrogen and less carbon dioxide [103,104]. Hence, there are two-way outs to improve the quality of syngas, either a real-time experimental method or estimates based on simulation models. But both approaches have time, financial, and higher field skill constraints. This constraint can be overcome by developing artificial intelligence-based prediction models based on process inputs. Based on process input characteristics, machine learning is one type of computational AI technique that may be used to estimate syngas quality in terms of hydrogen, methane, carbon monoxide, and carbon dioxide production. The ML model learns and predicts the output depending on the input data trend that is presented to it. Therefore, input data collection and refining are crucial for ML models because it predicts based on the data provided. In the context of the prediction study for HTG, a comprehensive data collection framework for

the development of the prediction model is given in Section 3.2.1.1, as illustrated in Figure 3.A. This framework encompasses several key steps, including database selection, keyword shortlisting, and the screening and inclusion of relevant data for the prediction model.

Appropriate selection and development of the prediction model which can predict all elements in syngas is a challenging process, but researchers are trying for the best AI-based prediction model that can estimate all gas species with the least error. Different researchers have applied the ML model to predict waste-to-energy output via pyrolysis, hydrothermal carbonization, and gasification. Liang Li et al. (2015) used multiple linear regression and a regression tree to forecast the output of organic hydrothermal carbonization. The model results fit the product feature. However, the R^2 was slightly lower, ranging between 0.63-0.73 [105]. Jie Li et al. 2020 applied a deep neural network (DNN) model to predict the hydrochar fuel, carbon capture, and storage stability. The model R^2 was 0.88-0.91, which is pretty good for prediction, however the MAPE was up to 20% [106]. Xinzhe Zhu et al. 2019 estimated biochar yield and carbon content in biomass under pyrolysis conditions using the random forest regressor (RFR). R^2 values ranged from 0.75 to 0.85 for various simulated outcomes [107]. When compared to the random forest regressor, the artificial neural network (ANN) produces somewhat superior model results in terms of co-efficient of determinant for waste valorization output prediction [108]. Mutlu and Yucel (2018) predicted the gas composition and calorific value of biomass using multi-class random forests classifiers and binary least squares support vector machine with prediction accuracy of 96% and 89%, respectively [109]. Elmaz et al., 2020 used regression approaches to forecast HHV, H_2, CO_2, CO, and CH_4 in the pinecone and wood pellets gasification process. R^2 was in between 0.85-0.92. This model was developed based on woody biomass (pinecones and wood pellets) [110]. Irrespective of dataset quality, every AI-based method has its own limitations in terms of overfitting, bias, generalization, and computational resources etc. Therefore, selection of an appropriate model along with the data

selection and refining is an important aspect for the development of robust prediction model otherwise the accuracy of the model is questionable.

The gasification process can also be predicted and optimized by integration of the process simulation and mathematical modeling [111,112]. The fundamental parts of biomass gasification modeling and simulation are thermodynamic equilibrium and kinetic models. In thermodynamics modeling, Gibbs free energy minimization is used to get the thermodynamic properties of chemical processes, but kinetic modeling is more accurate than thermodynamic models in predicting the gasification process [113,114]. Application of kinetic modeling in simulation model development has more stringent criteria as compared to the thermodynamics model. Although, high-performance computing simulation programs have made it possible to simulate [115]. Researchers applied different optimization and prediction models for biomass waste valorization processes. Vascellari et al. (2014) suggested a method for validating and using kinetic parameters to predict and optimize process output [116]. Dang et al. (2021) used the Aspen Plus to anticipate and optimize the biomass gasification process [117]. Hashimoto et al. (2012) proposed another method for prediction purpose which is related to detailed data extraction from biomass valorization experimental or simulation studies for database construction, however, it does not allow for interpolation of intermediate values [118]. Ascher et al. (2022) developed ANN based model to predict the gasification process output based on input characteristics such as syngas quality, feedstock, and reactor type, with an R^2 of 0.9310 [119]. For predicting process output, machine learning and neural network models provide superior results, however, these models use a backbox approach that overlooks variable interactions. Kinetic modeling, on the other hand, has its own set of limits in terms of complexity and knowledge. Hence, a better prediction and optimization strategy for gasification is required, one with greater computational capacity, processing flexibility, and efficiency in terms of gasification prediction and optimization.

2.3.2 Research gaps

Different studies have applied regression, machine learning, or neural network-based prediction models for the biomass gasification process as discussed in section 2.3.1. But these models' applications are limited to either a specific type of biomass or individual output prediction such as H_2 gas in syngas. Therefore, a generic model for biomass syngas prediction that can compare regressor and neural network models to select the better prediction model for H_2, CO_2, CO, and CH_4 based on biomass types and process input parameters is required. In the current study, an AI-based model for syngas prediction was established by a comparative analysis of neural network and regressor models. Ultimate analysis and process input factors such as temperature, pressure, solid content, and resident duration were chosen as input parameters for predicting syngas quality based on Fig. 3.C analysis in section 3.2.1. The final yield varies due to dependence on the biomass type. Different biomass datasets can be used to construct a generic prediction model which can predict output regardless of biomass type. Similarly, for HTG process prediction; biomass solid content ratio in the water can be selected since HTG is a better valorization process for high moisture content biomass. Whereas resident time refers to the average time biomass-water mixture remains in the reactor. According to the analysis given in section 3.2.1, biomass type (final analysis), temperature, pressure, solid content, and resident time all have a substantial impact on syngas. Hence, these values were used as an input parameter to forecast syngas output (H_2, CO_2, CO, and CH_4) in the HTG.

In co-generation processes, some studies applied AI-based models for predicting the output of the gasification process and SOFC. ANN is one of the AI techniques that researchers typically apply for syngas prediction [92]. Pandey et al. 2016 [120] developed ANN model to estimate the LHV in the gasification of process municipal solid waste, whereas Milewski et al. 2009 used ANN to estimate SOFC output [121]. However, these neural network algorithms have various limitations, including over-fitting concerns, low generalization capability, and

instability issues, whereby slight changes in the input result in significant changes in the predicted output [122,123]. Therefore, better AI models require which can overcome these difficulties while estimating the output of gasification and SOFC. XGB could be the possible solution for this.

Aspen Plus is a process-based simulation software that has been widely used for thermodynamic and kinetic modeling in chemical process simulation [124]. Process modeling is possible using simulation software, but model input parameters must be altered for yield prediction, which is restricted by the availability of the corresponding model, simulation program, and significant expertise. Therefore, a high-accuracy process yields prediction model that can anticipate output without considering the aforementioned limits is required. The pattern search algorithm is one of the methods which can be integrated with the simulation model to get the optimum results by reducing the computational time. Wetter *et.al* 2003, applied a pattern search algorithm for building energy-saving optimization. Resultantly, 7% and 32% energy savings had been achieved depending upon the building location [125]. Duan *et.al* 2020 applied pattern search in the kinetic modeling of torrefaction process, resultantly, the model worked well for optimization calculation [126]. Therefore, model optimization can be achieved through a pattern search algorithm.

The high-dimensional model representation (HDMR) is another method to represent high-dimensional system input-output relationships. It is a mathematically proven and efficient processing paradigm since it moves from exponential scaling to polynomic complexity, reducing computational effort dramatically [127]. HDMR model can be utilized to characterize the relationships between variables more simply than 'black box' models such as ANN due to the explicit model coding. Furthermore, its basic mathematical structure and algorithms have flexibility as an objective function, which gives it advantages in algorithm selectivity for process optimization. Rabitz and Brownbridge et al. has developed this which is commonly

used to cope with complex problems in a chemical process such as predictive model creation, global uncertain analysis, and economic assessment [127]. Pan et al. (2016) applied HDMR to optimize chemical processes in eco-industrial parks [128]. Azadi et al. (2015) used HDMR to assess the worldwide sensitivity of LHV, cold gas efficiency (CGE), and gas output from algae biomass [129]. Wang et al. 2021 concluded that HDMR has a relatively low dependence on training data size and a strong capacity to assess output sensitivity to input variable for predicting dual-fuel ignition delay duration [130]. Hence, these HDMR-based surrogate models have been classified as data-driven, which employs data collected from complicated simulation models or experiments to make predictions [131]. Considering the advantages of HDMR over neural networks and databases, a data-driven model based on HDMR is being developed for gasification output prediction.

Existing research has utilized machine learning and neural network models for biomass gasification are often limited to specific biomass types or single output predictions, such as hydrogen in syngas. This highlights the need for a generic prediction model that can evaluate and compare different regression and neural network approaches for predicting multiple syngas components (H_2, CO_2, CO, and CH_4) based on different biomass types and process parameters. While some studies have utilized artificial intelligence for gasification output prediction, issues such as overfitting and low generalization capabilities persist. Therefore, there is a significant gap for developing a robust AI model, potentially incorporating techniques like XGB or HDMR, to accurately predict syngas output across diverse biomass inputs. This model should also integrate process simulation tools to optimize yield predictions efficiently, addressing the limitations of current methodologies.

2.4 Application of decision making for process selection

Biomass waste is a low value raw material which is abundantly produced from natural and human activities. Safe disposal of this waste is problematic, which also does not seem

economically feasible, if proper disposal mechanism is not applied. This waste can be disposed of through different valorization processes given in section 2.2. But appropriate selection of the disposal process along with the plant location design is an important factor to make this process economically sustainable. Therefore, one of this decision-making aspect has been analyzed in this study.

2.4.1 Decision making techniques

There are different decision-making methods which have been applied by the researchers for decision making in different aspects. TOPSIS, AHP, fuzzy, MCDM, ELECTRE etc. are most frequently applied methods for the selection of plant installation and location selection etc. based on different criteria's [132]. Yücenur *et al.* (2020) applied MCDM for the appropriate location selection in three big cities of the Turkey for biogas plant installation. Different criteria's have been included for decision making [133]. Curto and Martín (2019) have used ACC IP for multi-functional optimization method for the selection of technology among renewable and hydrogen production [134]. Lee *et. al* (2018) studies different renewable resources in Taiwan by application of TOPSIS, ELECTRE, and fuzzy [135]. Sakthivel *et. al* (2017) applied integration of fuzzy, TOPSIS, VIKOR to get the best biofuel combination for better efficiency in an engine [136] . Klein *et. al* (2015) used MCDM technique to investigate the renewable energy resources based on cost, land, water usage, greenhouse gases emission etc. [137]. Cobuloglu *et al.* (2015) studied sustainable biomass product for biofuel production though AHP method [138]. Amer *et al.* (2011) evaluated the renewable energy resources for electricity generation from political, economic, social, and technological perspectives by application of AHP [139]. Therefore, TOPSIS, AHP, fuzzy, MCDM, and ELECTRE are proven techniques which can be applied for decision making purposes in the field of renewable energy generation.

2.4.2 Research gaps

Appropriate decision making in the selection of valorization technique plays an important role in making biomass low value product monetization. Decision-making techniques which have been applied in this energy sector are mostly subjective, in which the input of the experts is involved. Therefore, a chance of biasness always exists while making decision. Similarly, criteria selection along with suitable decision-making technique is the most important aspect because the output results are dependent on the input criteria, irrespective of decision-making technique selection. Most of the studies are focused on the macro level political, economic, social, environment, and technology aspects for the appropriate decision making regarding renewable energy or biomass waste valorization process installation which helps to fulfill this research gap in biomass valorization domain [137–139]. There are several areas and cross-functional applications of appropriate techniques that require further exploration within the domain of biomass valorization. These areas include but are not limited to the sustainability of valorization processes as assessed through energy, exergy, economic, environmental, and safety considerations. Furthermore, the selection of process optimization techniques should account for these parameters. Subjective techniques may be replaced or integrated with objective methodologies through the application of quantitative data relevant to this field. Furthermore, artificial intelligence and mathematical algorithms, such as Particle Swarm Optimization (PSO), pattern search methods, and High-Dimensional Model Representation (HDMR)-based surrogate models, can be utilized to support the selection of optimal valorization processes.

MSW management study has been conducted by different researchers. Specifically, Rahimi et al. (2020) employed an integrated approach, combining Fuzzy MCDM with Geographic Information System (GIS) techniques to identify suitable landfill sites for MSW in Iran. Fuzzy Best-Worst Method (BWM), an advanced version of the traditional best-worst

method that addresses uncertainty had been applied to determine the weights of these criteria [140]. Although the integration of Fuzzy MCDM has addressed some challenges related to uncertainty in subjective decision-making, it is still sensitive to dynamic factors, non-linearity, computational intensity, and transparency issues. Makan et al. (2013) applied another technique Preference Ranking Organization Method for Enrichment Evaluation (PROMETHEE) for MSW management selection based on financial, social, and technical aspects [141]. However, the applied method is sensitive towards addition of new alternatives, rank reversal, and difficult to handle qualitative data etc. Tseng (2018) utilized Analytic Network Process (ANP) and Decision-Making Trial and Evaluation Laboratory (DEMATEL) to determine effective waste management solutions based on environment, economic, technological, and social aspect [142]. These methods have drawbacks, such as reliance on specialized software and sensitivity to non-linear relationships. Chaudhary et al. (2017) employed Fuzzy MCDM for MSW landfill selection in India based on eco-logical and socio-economic aspects [143], but this technique also faced challenges with non-linear relationships. Hence, there is a need for an updated decision-making model capable of handling non-linear relationships with respect to the economic, social, environmental, technological, and governance aspects to select the optimal waste management solution.

The Analytical Hierarchy Process (AHP) assesses various criteria independently, offering advantages like a structured decision-making approach, adaptability to diverse problems, and the ability to handle both quantitative and qualitative aspects. It also includes features such as consistency analysis [144]. However, AHP heavily relies on subjective opinions and demands substantial data [145]. But these constraints can be mitigated by implementing fair selection criteria for expert inclusion, ensuring suitable data collection procedures, and incorporating Fermatean Fuzzy set (FFS) theory. FFS is designed to address ambiguous human thoughts and perceptions by incorporating membership degree, non-

membership degree, and hesitancy degree—elements [146]. This integration offers flexibility in managing uncertainty, accommodates experts' hesitancy, enhances sensitivity, provides versatility in integration with other models, and demonstrates improved adaptability to real-world decision-making scenarios. Furthermore, integration of the Dombi operator (0.1-1) which address the intersection (close to 0) minimum operation and union (close to 1) maximum operations through which the final decision can be fine-tuned based on the desired level of the minimum-maximum operation can provide more robustness towards non-linearity and ambiguity which is being encountered in the real-world scenario [147,148]. Therefore, integration of these methods can overcome the limitations of the different decision-making models by acting synergically providing an economic, technological, environment, and social governance based optimum solution for the selection of suitable thermal or biological MSW processes.

2.5 Research objectives and thesis framework

Considering the problem statement in section 1.2 and research gaps summarized in the section 2.2.4, 2.3.2, and 2.4.2, this study has following objectives:

i. Sustainable processes development for biomass waste valorization based on pyrolysis, conventional gasification, hydrothermal gasification, and plasma gasification, considering economic, energy, exergy, environmental, and safety (4E, 1S) perspectives.
ii. Process sustainability improvement in terms of economics, energy, exergy, environment, and safety through the application of multi-generation processes, integrating artificial intelligence (AI) models and mathematical algorithms.
iii. Sustainability assessment and strategic decision-making model development for the sustainable valorization process selection in developing countries.

To meet these objectives, this study has been mainly categorized into four different phases as illustrated in Fig. 2.C.

Phase 1: It is related to the review and biomass valorization process selection in which different thermal and biological valorization processes have been analyzed to identify the research gaps and weak areas which need to be targeted for sustainability improvement purpose.

Phase 2: Considering the research gap, biomass valorization processes have been developed. Valorization process sustainability has been further improved in term of 4E, 1S perspective by application of co-generation or tri-generation processes for CHP, SOFC, DME, H_2, CH_4 etc. production.

Phase 3: Base process developed using experimental work has been optimized by application of AI or mathematical algorithms to make the process more sustainable in terms of economic, energy, exergy, environment, and safety (4E, 1S) perspectives. Then economic, environment, energy, exergy, and safety sustainability comparative analysis of the base and optimized process has been performed.

Phase 4: Finally, decision making models have been developed to select the optimum valorization process using pollical, economic, environmental, social, and technological aspects. Considering the decision making and process sustainability analysis, some policy implications have been recommended along with summarized conclusion.

To achieve the research objectives, the current thesis structure has been illustrated in Fig. 2.D which has an interlink of the three research objectives with the relevant sections of the current thesis. The process methodology for these research objectives is given in chapter 3. This includes the development of process simulation model in Section 3.1, process sustainability improvement through an AI-based prediction model in Section 3.2.1, surrogate model optimization in Section 3.2.2, and simulation process validation in Section 3.3.1. Further

analysis encompasses process energy, exergy, advanced exergy, and exergoeconomics assessments detailed in Sections 3.3.2, 3.3.3, 3.3.4, and 3.3.5, respectively. The methodology for calculating the potential of converting process thermal energy to electric power is described in Section 3.3.6. While methodology for economic, environmental, process safety, and strategic decision-making models are provided in Sections 3.3.7, 3.3.8, 3.3.9, and 3.12, respectively. The characteristics of Aspen Plus simulation model is different for each chapter, the unique characteristics of the simulation model development are presented in the corresponding chapter sections 4-7 while brief simulation methodology has been given in section 3.1. Finally, decision making sustainability assessment findings for the optimum process selection are given in chapter 8. Considering this whole study, some policy and managerial implications have been proposed in the section 9 along with study limitations and future directions in section 10.

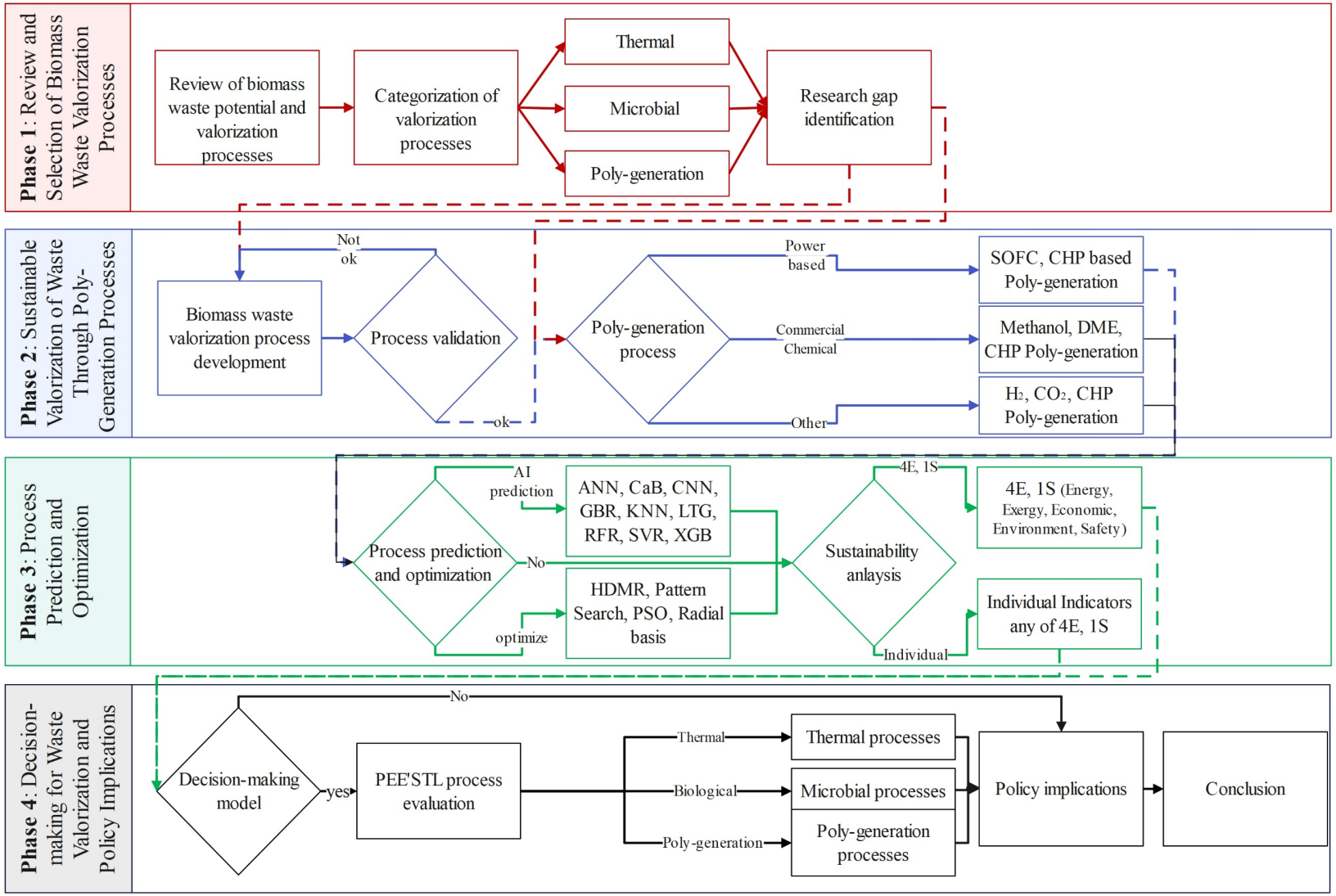

Fig. 2.C. Current research framework

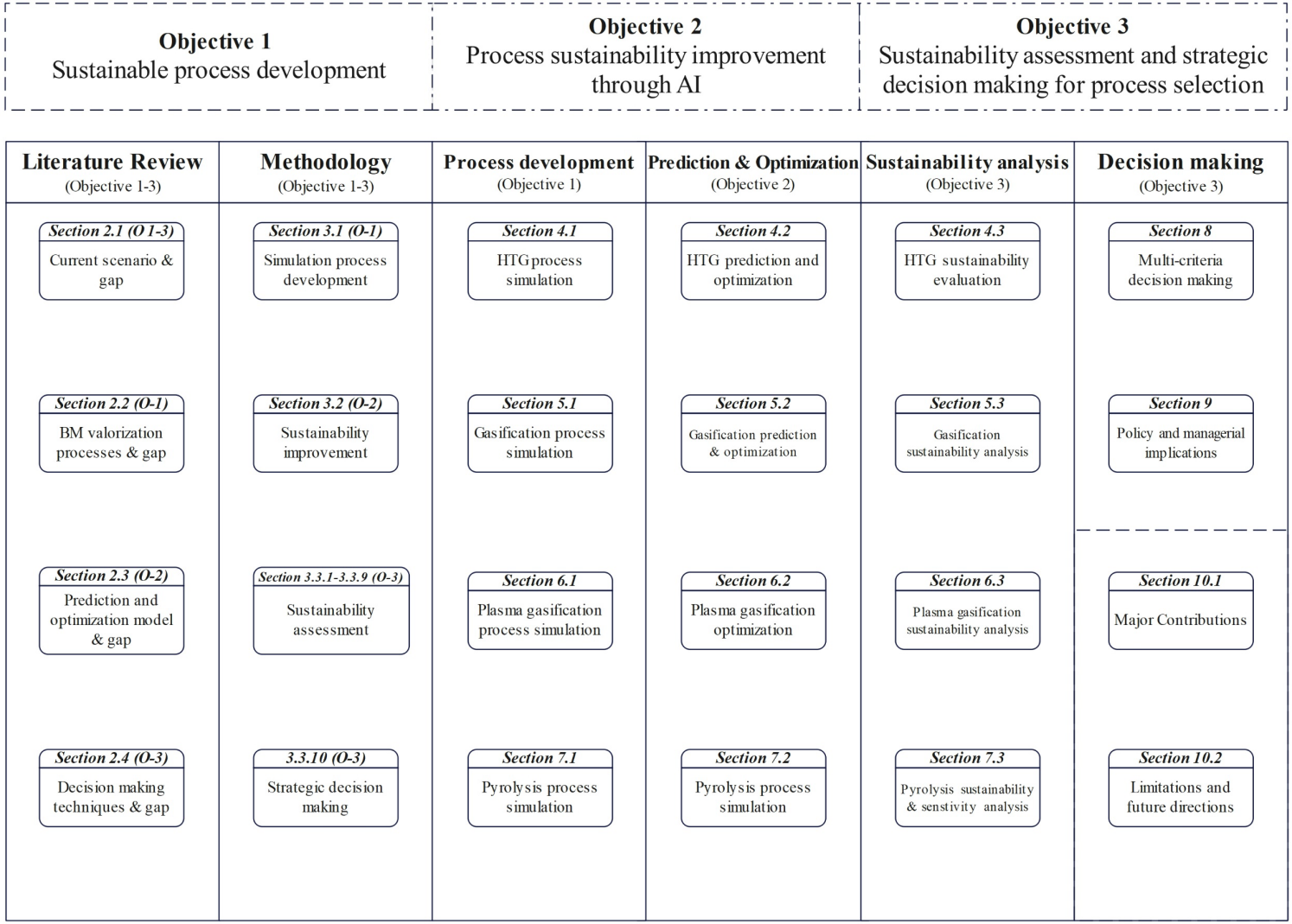

Fig. 2.D. Thesis structure

3 Methodology for the process development to decision-making

Biomass valorization processes have been developed in this study considering the research objectives in section 2.5. Mainly, this research methodology has been categorized into four different aspects including; valorization simulation process development, optimization, output prediction, sustainability evaluation, and finally, decision making. Valorization process development is a diversified subject which varies with respect to process, therefore, detail valorization process (gasification, HTG, plasma gasification, poly-generation, pyrolysis) development methodology has been defined in the respective chapter 4-7 while general methodology has been given in section 3.1. Process sustainability improvement in terms of prediction and optimization considering artificial intelligence-based model has been given in section 3.2. While process sustainability assessment and decision-making technique described in section 3.3. Sustainability evaluation has been done based on process energy, exergy, economic, environment, and safety analysis. Finally, multi-criteria decision-making technique has been adopted for decision making purposes given in section 3.3.

3.1 Simulation processes development for biomass waste

Process simulation modeling has been established through the use of experimental studies and every process is validated with the respective experimental study. In this context, Aspen Plus simulation software has been employed to develop steady-state simulation models for various valorization processes given in chapter 4-7. These models are either kinetic or equilibrium studies, which are summarized in chapter 4-7. Kinetics studies applied when the rate of reactants to products conversion is crucial, and process involves fast reactions while equilibrium studies applied when the focus is the final chemical state to get an equilibrium state in chemical reaction. The simulation model's development includes several valorization processes, including traditional gasification, hydrothermal gasification, and multi-generation gasification processes, aimed at producing products such as DME, methanol, CHP, and

hydrogen. Detailed descriptions of these models including proximate ultimate analysis, process parameters, and stoichiometric data are provided in the corresponding case studies where process boundaries have been clearly defined.

The simulation of thermal valorization processes involving lignocellulose biomass types or plastic waste for co-gasification was developed using Aspen Plus. However, the software lacks the inclusion of non-conventional (NC) compounds like biomass. To address this limitation, these compounds were defined using the proximate and ultimate analyses of the feedstock. The enthalpy and density of the NC compounds were determined using HCOALGEN and DCOALIGT setups as specified in the material properties. The model was developed based on the principles of Gibbs free energy minimization and reaction kinetics [149]. For handling the complex gas-liquid equilibrium and small molecular weight compounds, the Peng-Robinson equation of state with the Boston Mathias function was applied [124,150]. This equation of state has been employed in similar research by various researchers. These process characteristics vary with respect to simulation model. Therefore, chapter 4-7 respective studies have the complete details of these characteristics.

3.2 Process sustainability improvement

Simulation process sustainability improvement has been done with the application of AI and surrogate model-based optimization. AI-based models have been applied on the simulation process dataset for prediction purposes while surrogate model-based optimization has been done by integration of respective model with simulation process.

3.2.1 AI-based prediction models application

AI-based prediction models given in section 3.2.1.2 have been applied on the dataset which have been collected based on the methodology given in section 3.2.1.1.

3.2.1.1 Data collection

AI models predict the output based on input data. This data collection for prediction model development has been done through two sources; (1) published experimental studies, (2) simulation model development. For experimental data collection, a thorough assessment of the literature on the HTG process has been conducted. Google Scholar, Scopus, and Web of Science databases were explored for research-related keywords such as biomass gasification, supercritical water gasification, HTG, machine learning in biomass, pyrolysis etc. The primary goal of the literature review effort is to obtain experimental data for each valorization technique. There are various biomass-related publications in these databases; however, the required papers were selected based on the study objectives. A sample data collection methodology has been given in Fig. 3.A. A total of 511 experiments of 98 different types of biomasses with 6643 data points have been included in the final dataset for AI model development for the gasification process. Outliers have been excluded to avoid bias in the shortlisted data.

The model collected dataset was divided into three different types of training and testing sets with percentages of 70:30, 80:20, and 90:10 to achieve the best results based on R^2, MSE, MAE, and mean absolute percentage error (MAPE). To eliminate bias in training and testing data selection, AI models generated with the command "random" were utilized, due to which training and testing data was chosen randomly. Convolutional Neural Network (CNN), Artificial Neural Network (ANN), Gradient Boost Regressor (GBR), Extreme Boost Regressor (XGB), and Random Forest Regressor (RFR) methods were used on three distinct training and testing dataset ratios with the goal of improving R^2, MAE, MSE, and MAPE.

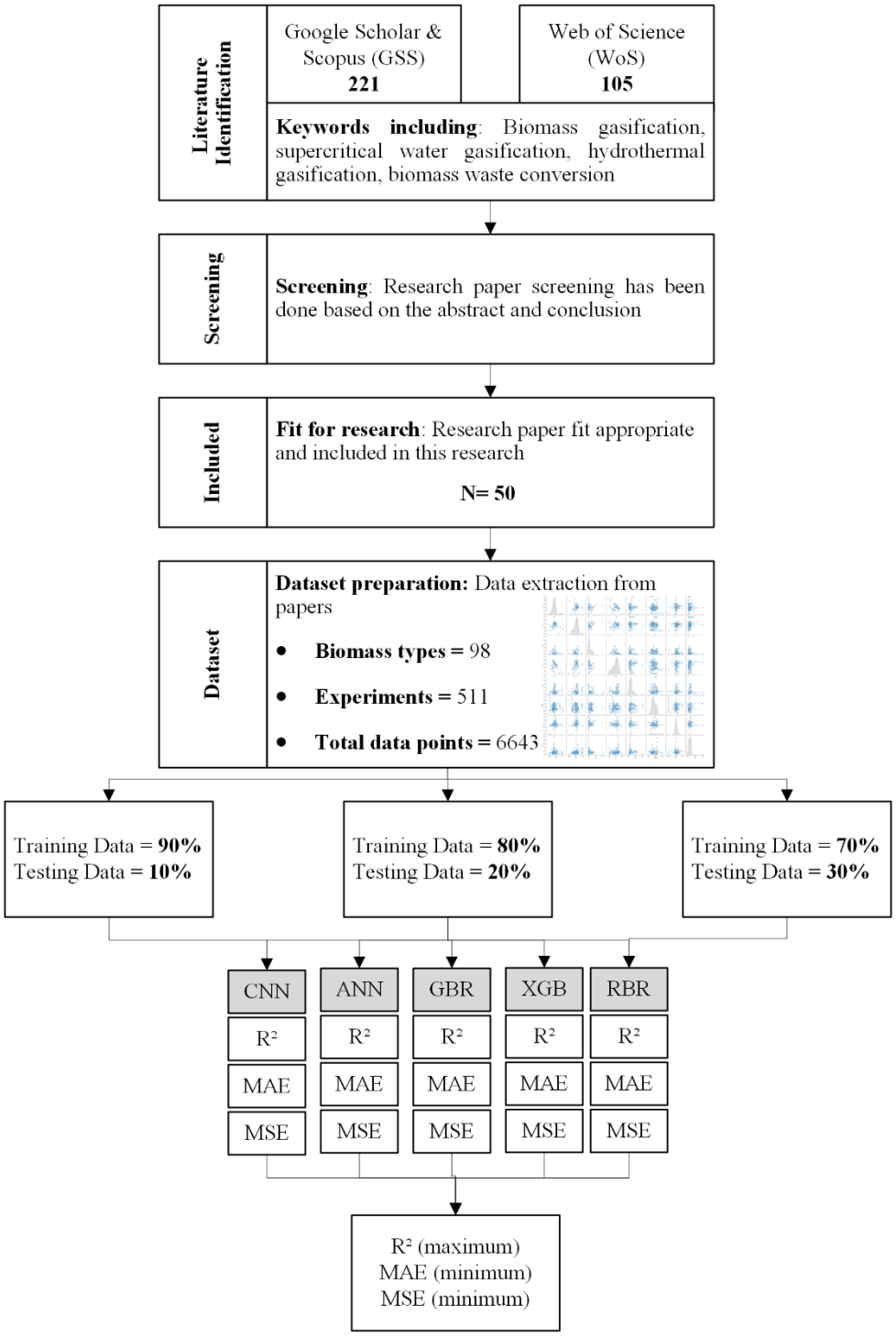

Fig. 3.A Methodology for HTG model data collection and evaluation

3.2.1.2 Machine learning models' development

Deep and machine learning algorithms such as CNN, ANN, GBR, XGB and RFR were applied in this study due to their better predictability performance for similar problems [151]. These models were applied to the gasification data by importing Python libraries on Jupyter

notebook web-based portal. Each of these models has their own set of advantages and disadvantages. For example, neural network models can handle both linear and nonlinear data [152], whereas CNN is more suited for complex problems than ANN [153] while regression mostly suitable for linear data. Therefore, the goal of the current model comparison is to find the best fit model for syngas prediction regardless of biomass type. XGB is the advanced form of GBR and it is being compared with most frequently applied regressors (gradient and random boost) for biomass predictions. XGB overcome the deficiency of single tree by ensemble multiple trees under tree boosting framework due to which it is more efficient and high flexibility[154]. Therefore, XGB along with random forest and gradient boost regressor model has been selected for this study. CNN is a more advanced type of ANN that is utilized for complicated applications, particularly massive data processing. It is not just confined to two-dimensional image processing, but it also has applications in one-dimensional (time series, signal analysis) and multi-dimensional (human action detection) settings. However, it is largely appropriate for classification difficulties [155]. Kathirgamanathan et al. (2022) compared the performance of ANN and CNN in estimating short-term electricity load [156]. The model input factors that can affect the syngas (H_2, CH_4, CO, and CO_2) have been selected based on literature data based on their correlation analysis Fig. 3B [157]. The *x*-axis in Fig. 3B has the shortlisted input parameters, while the *y*-axis represents the correlation coefficient (*r*). A positive value on the y-axis indicates direct correlation, whereas a negative value indicates inverse correlation on the output parameters. These model input parameters have been classified as feed composition, which is based on the final analysis of the biomass, and operating parameters. The percentages of carbon (C), hydrogen (H), oxygen (O), and nitrogen (N) in the final parameters vary depending on the type of biomass. Therefore, this is a universal model for various forms of biomasses based on the ultimate analysis. Similarly, operating process factors such as temperature (T), pressure (P), solid biomass content (SC), and resident time (RT) that

can affect syngas output have been added as input parameters. Hence, the amount of H_2, CO_2, CO, and CH_4 has been predicted based on both the ultimate analysis and process parameters as an independent factor.

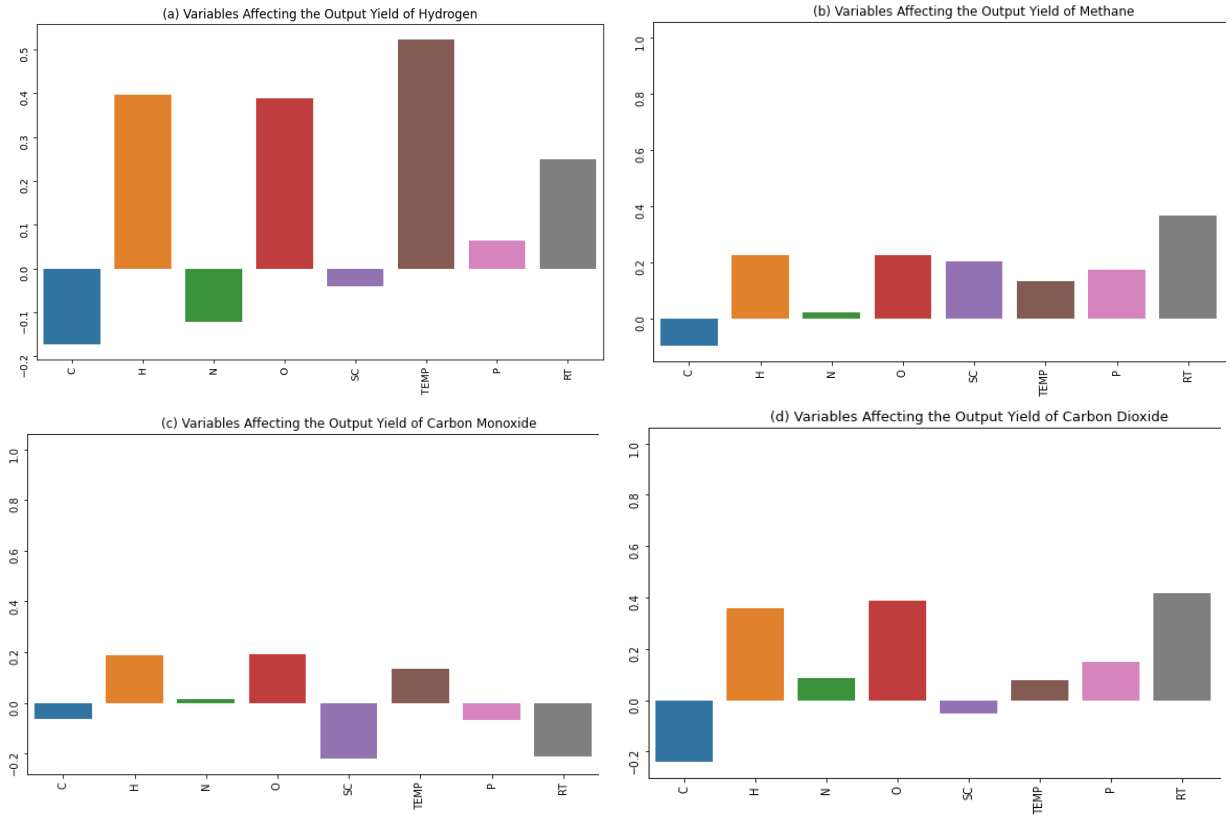

Fig. 3.B: Input variables affecting the syngas output

A total of four layers have been built for the CNN model which included the initial input layer of eight neurons and the last output layer, followed by two hidden levels of 16 neurons each which have been defined based on Eq. 3.1-3.3. The CNN model was developed using a web-based Python programming environment which is based on the algorithm function as shown in Eq. 3.4 [158]. In ANN, the first input layer includes eight neurons, followed by 16 and 32 neurons in the first and second hidden layers, respectively. Several studies have used various ways to select the number of neurons, but the number of input neurons is closely related to the input parameters, and the number of hidden layers should be less than the number of

$$\text{Input Neuron, X(n)} = \sum_i^j fN \tag{3.1}$$

where n is the number of input layers neurons, fN is the total number of input variables [159]

$$\text{Hidden Layers Neuron, H(n)} = X(n).\ I \tag{3.2}$$

$$\text{and H(n)} < \text{X(n)} \tag{159}$$

$$\text{Hidden Layers Neuron, H(n)} = L(n_j).W_n$$

where X(n) is the number of hidden layers neurons, I is the integer multiplier of the input neurons, $L(n_j)$ is the hidden layer neuron and W_n is the weightage of each neuron

$$\text{Output Neuron, Y(n)} = W_n.Y_n \tag{3.3}$$

where Y(n) is the number of output variables [159]

Convolutional Neural Network (CNN)

$$\hat{f}(x) = sign\ (2\delta_{sigmoid}(W_3\delta_{relu}(W_2\delta_{relu}(W_1x + b_1) + b_2) + b_3) - 1) \tag{3.4}$$

Where W_3, W_2, W_1 are the first, second and third neurons layers, δ_{relu} is the ReLu activation function [160]

input parameters [159]. Eq. 3.1-3.3 were used to select the number of neurons in each layer of CNN and ANN that are interconnected with significant weights and biases. Weights and biases connected with each neuron help to minimize loss of function. The ReLu activation function and Eq. 3.5 based algorithm were used to validate hyper-parameters such as the number of neurons, layers of neurons, and model learning rate for ANN using Python programming. The gradient boost regressor is an ensemble technique that can fit boosted decision trees by integrating multiple weak learning models into a powerful predicting model [161]. In this study, GBR is imported from the Python library to anticipate the output of the specified HTG syngas-based function given in Eq. 3.6. Similarly, the RFR regressors and XGB boost programs have been directly imported from the Python library, as shown in Eq. 3.7 and Eq. 3.8-3.9, respectively. Fig. 3.C shows a summarized schematic view of the applied models.

Artificial Neural Network (ANN)

$$\hat{y}_{=}\ \delta_2(\sum_{i=1}^{m}\left(w_i^{(2)}\delta_1(X)_{.}\right)+b^{(2)});\ X=\sum_{j=1}^{n}\left(x_j w_{xj}\right)+b^{(1)} \tag{3.5}$$

[110]

where $\hat{y}$ is the prediction vector, m is number of samples, n is the number of features in dataset, x_j is the jth vector, $w_i^{(2)}$ weight output and hidden layers, $w_i^{(1)}$ is weight of hidden layer connected to input, δ_2 output layer activation function, δ_1 neuron in hidden layer activation function, $b^{(1)}$ hidden layer bias vector, $b^{(2)}$ output layer bias vector

Gradient Boosting Regressor (GBR)

$$\hat{y}_{i\,=}\,\hat{F}_m\,(x_i)=\ \hat{\mu}+\sum_{m=1}^{M}\vartheta h_k\,(x_i) \tag{3.6}$$

[162]

Where $\hat{y}_i$ is the vector of observed phenotype, x_i is the matrix of respective genotype, h_k predictor model, $\hat{\mu}$ is population mean, ϑ shrinkage factor

Random Forest Regressor (RFR)

$$\hat{F}_m\,(x_i)=\hat{F}_{m-1}\,(x_i)+\ \vartheta h(y_i\,;x_i\,,mtry_m\,) \tag{3.7}$$

Where $\hat{F}_m\,(x_i)$ is the prediction function, m is tuning set iteration, x_i is the matrix of respective genotype, h coefficient, ϑ shrinkage factor, $mtry_m$ covariates sample out of random [162]

Extreme Gradient Boosting (XGB)

$$\hat{y}_{FS,i\,=}\ \sum_{k=1}^{k}f_k\,(\emptyset_i),\ \ f_k\in\ F \tag{3.8}$$

[154]

where $\emptyset_i$ is the random variable, $\hat{y}_{FS,i}$ is the predicted value by XGB, F is the ensemble model contains total K trees (f_k)

$$\hat{T}_{obj\,=}\ \sum_{i=1}^{n}l\left(y_{FS,i}\ ,\hat{y}_{FS,i}\ \right)+\sum_{k=1}^{k}\Omega(f_k) \tag{3.9}$$

where $\hat{T}_{obj}$ is the XGB objective function, $l(y_{FS,i}, \hat{y}_{FS,i})$ loss function fit with training data, n is the total training data, $\Omega(f_k)$ regularization term to avoid overfitting

In SOFC based trigeneration process, AI model applied for predicting syngas, current, and current density based on simulation data collected from factorial design runs. Neural network restrictions such as over-fitting problems, insufficient generalization capability, and instability issues highlighted by researchers were considered in the selection of a better AI model [163,164]. Hence, a unique tree-based approach called extreme gradient boosting (XGB) was used to forecast the H_2, SOFC current, and current density. This is the advanced version of gradient boosting (GB) and has more computational capacity to combat overfitting and instability issues with a faster execution algorithm when compared to another neural network [165]. Fig. 3.D shows a schematic design of the XGB prediction model. In terms of

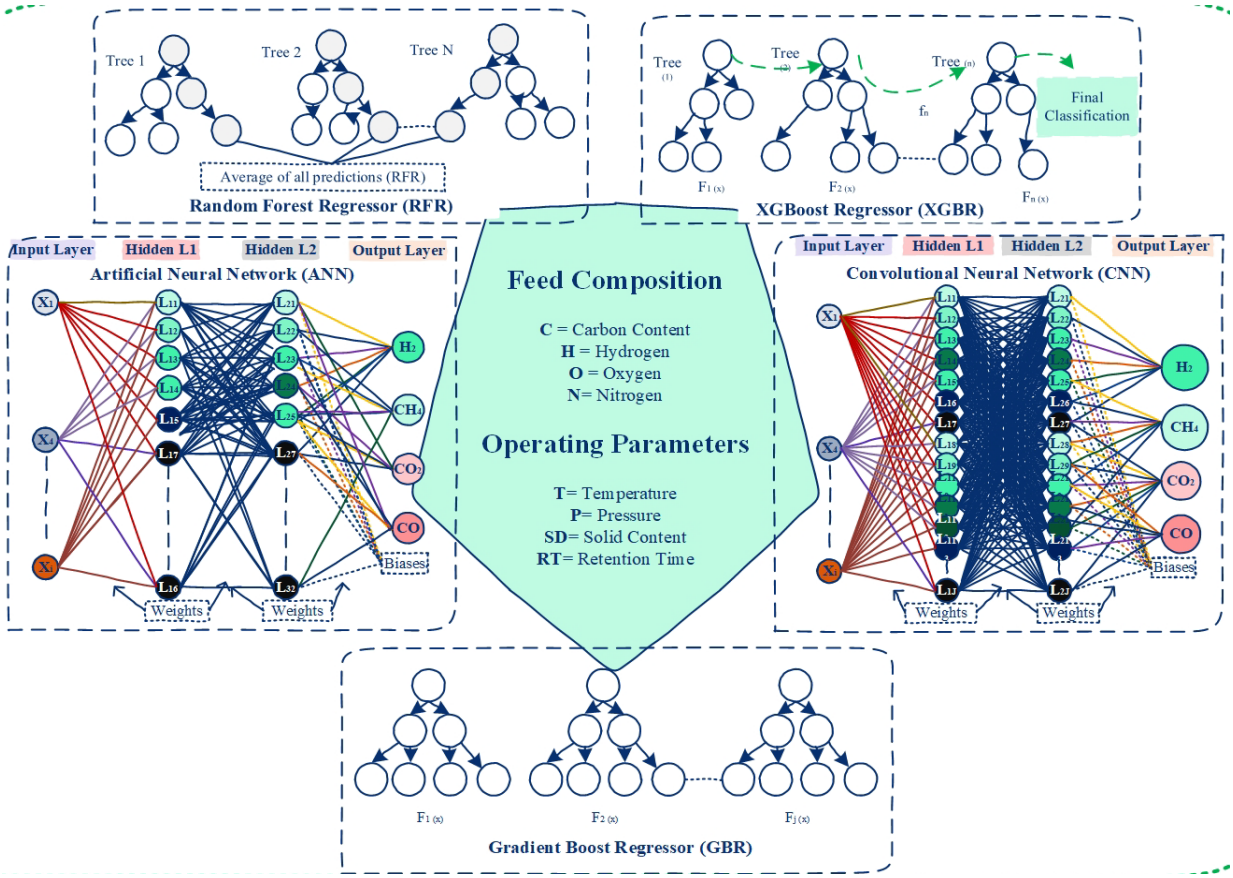

Fig. 3.C Deep learning and machine learning applied models for HTG

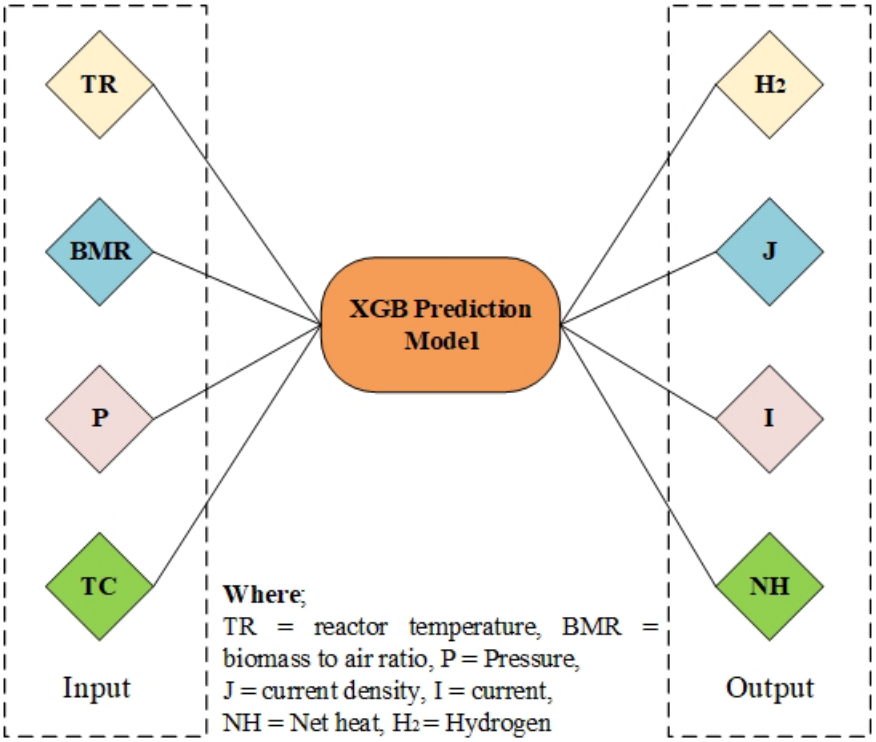

Fig. 3.D: XGB prediction model gasification process

performance, Kumari (2020) and Sheridan et al. (2016) claimed that XGB outperforms random forest, smart persistence, support vector regression (SVR), and deep neural networks but with a faster approach [165,166]. Therefore, XGB applied for the prediction of output in tri-generation. The performance of the XGB model was evaluated using the R^2 and MSE given in Eq. 3.14-3.16 [167].

3.2.2 Surrogate model-based optimization

Valorization processes optimization has been done through different optimization algorithms to make the process more sustainable. This optimization has been done by application of different surrogate models. Some of them are summarized in section 3.2.2.1 to 3.2.2.4.

3.2.2.1 High dimensional model representation

The HDMR model was developed to predict and optimize the gasification process [168]. In HDMR, the output variable is stated as a sum of functions that depend on subsets of the input variables, as shown in Fig. 3.E, and mathematically in Eq. 3.10 [169]. The inputs for HDMR are temperature, pressure, and gasifying agent (air) ratio, while the objective is to increase the outputs in terms of H_2, CO_2, HHV, LHV, and NH values [170].

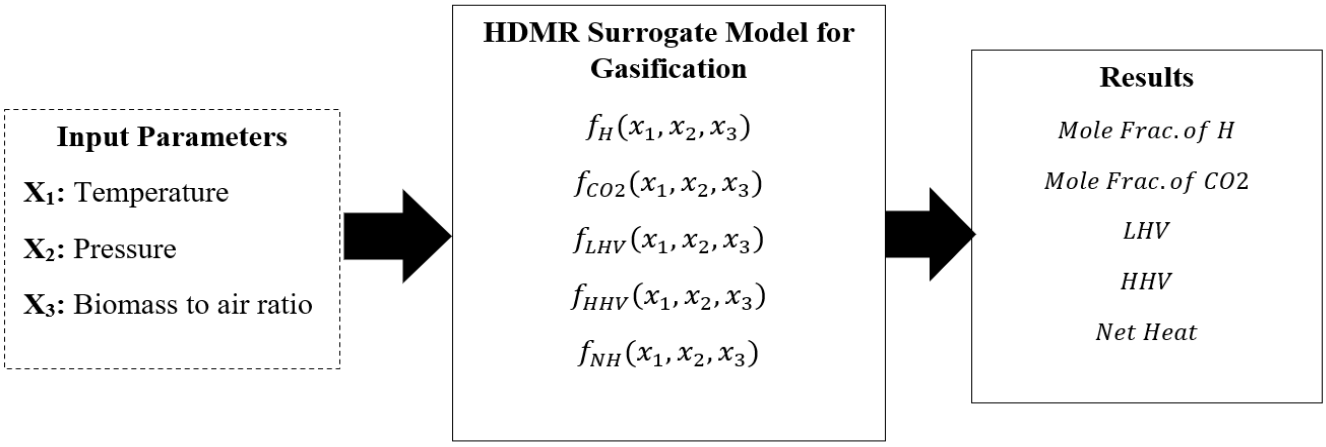

Fig. 3.E HDMR surrogate model illustration

$$y = f_0 + \sum_{i=1}^{N} f_i(x_i) + \sum_{i=1}^{N}\sum_{j=i+1}^{N} f_{ij}(x_i x_j) + \cdots + f_{12\cdots N}(x_1 x_2 \cdots x_N) \tag{3.10}$$

where f_0 denotes the zeroth order effect which is a constant; N is the number of input parameters; i and j index the input parameters; $f_i(x_i)$ represents the effect of the ith input variable to the output y and $f_{ij}(x_i x_j)$, $f_{12\cdots N}(x_1 x_2 \cdots x_N)$ indicates the correlated effect contributed by two input variables (x_i, x_j) and all the input variables (x_i, $x_j \cdots x_N$) to output, respectively.

Higher-order polynomial terms are necessary to produce correct findings due to some nonlinear aspects of the gasification process. A better model expression was used to build surrogate models for characterizing the biomass gasification process, as shown in Eq. 3.10 and 3.11. [171]

$$y = C + \sum_{i=1}^{N}\sum_{k=1}^{K} A_{i,k} \times x_i^k + \sum_{i=1}^{N}\sum_{j=i+1}^{N}\sum_{k=1}^{K}\sum_{n=1}^{K} B_{i,j,k,n} \times x_i^k \times x_j^n \qquad (3.11)$$

where C is a constant term, $A_{i,k}$ and $B_{i,j,k,n}$ are the first and second order coefficients, K is the highest degree of input variables, subscript i and j denote the input parameters, and y is the function value.

For better training efficiency, K has been parameterized in this study and then the training dataset of the HDMR model has been converted into polynomial regression problem. The coefficients including C, $A_{i,k}$, and $B_{i,j,k,n}$ were obtained by least squares method. For HDMR performance evaluation, R^2, MSE, MAE, and MRE in test dataset are calculated by Eq. 3.12-3.17 [172]. Data has been normalized before using the algorithms for effective analysis and processing.

$$SS_{res} = \sum_{i}^{n} (y_i^{pre} - y_i)^2 \qquad (3.12)$$

$$SS_{tot} = \sum_{i}^{n} (y_i^{pre} - y_i^{mean})^2 \qquad (3.13)$$

$$R^2 = 1 - \frac{SS_{res}}{SS_{tot}} \qquad (3.14)$$

$$MAE = \sum_{i}^{n} \frac{|y_i^{pre} - y_i|}{n} \qquad (3.15)$$

$$MSE = \frac{SS_{res}}{n} \qquad (3.16)$$

$$MRE = \sum_{i}^{n} \frac{|y_i^{pre} - y_i|}{y_i \times n} \times 100\% \qquad (3.17)$$

where y_i^{pre} is the ith predicted output value, y_i is the ith output value in dataset, n is the amount of data in dataset, SS_{res} represents explained sum of squares while SS_{tot} represents total sum of squares.

The HDMR data-driven models for different outputs have been named based on the element such as H_2 model for predicting the mole fraction of hydrogen in the products, similarly, CO_2, HHV, LHV, and NH models. The training process obtains parameter A, B and C with minimum error between model results and the training data which has been programmed in MATLAB. For this, data generated from the Aspen Plus model are divided into 75% training set and 25% testing set. Training data is employed to determine the best hyperparameter *K* based on 10-folds method which is based on the *K* results [169,173], then model can be generated. Finally, 25% testing data is used to test the model for assessing the predictability of the established model by calculating the MSE, MAE, and MRE.

3.2.2.2 Particle swarm optimization

PSO is a type of derivative-free optimization method that is commonly utilized in the optimization of chemical processes. PSO's operating premise is learning and communication between individuals (particles) and populations (swarms) to achieve the best solution with each iteration [29,30,174]. It was identified as an efficient algorithm using a mix of local and global searches, as well as the sharing of evolutionary information among individual particles. The PSO process flow is depicted in Fig. 3F. [175].

The particles will search the x_i for optimal objective value in each individual particle, and then determine the values of x_i (Eq. 3.18) for the global optimal objective value among all particles. Searching iterations is needed for this procedure. The position and velocity vector of each particle is randomly selected in the first iteration. In the rest of the iterations, particle swarm updates the position vector (x_i) Eq. 3.18 and velocity vector (v_i) Eq. 3.19. According to the inertia, individual optimal value (p_i) and global optimal value (p_g) can be calculated using Eq. 3.20 and 3.21 [176].

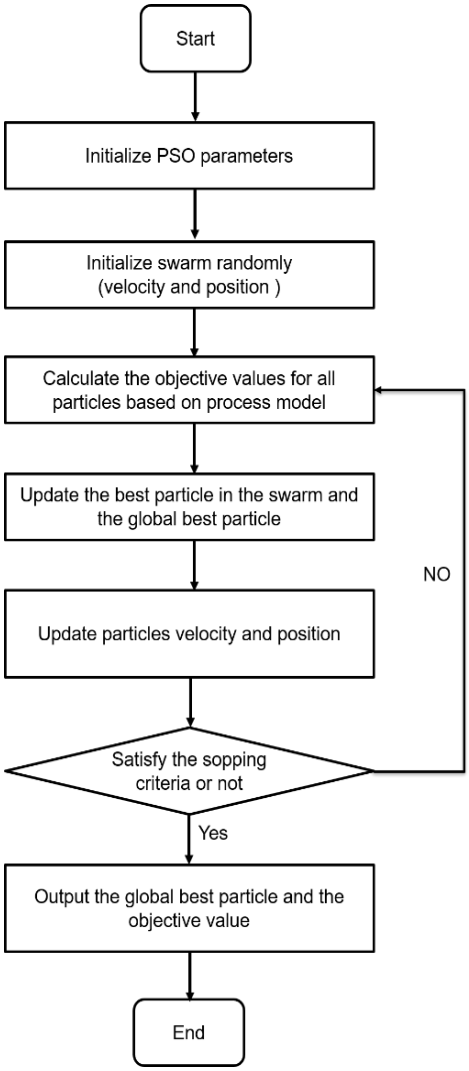

Fig. 3.F PSO process methodology

$$x_i = (x_i^1, x_i^2, I, x_i^N) \tag{3.18}$$

where 'N' represents the N-dimensional position vector of PSO system with the *i*-th particle.

$$v_i = (v_i^1, v_i^2, \dots, v_i^N), v_i \in (-vmax_{max}) \tag{3.19}$$

where v_i represents the velocity vector for the N-dimensional position vector

$$v_i^{k+1} = \omega v_i^k + c_1 r_1 (p_i - x_i^k) + c_2 r_2 (p_g - x_i^k) \tag{3.20}$$

$$x_i^{k+1} = x_i^k + v_i^{k+1} \tag{3.21}$$

where x_i^k and v_i^k are the position and the instantaneous velocity of the i-th particle in iteration k, ω is the inertia coefficient, c_1 and c_2 are the acceleration factor, and r_1 and r_2 are the random number ranging from 0 to 1.

Hence, the model objective value found by the r-th particle in iteration k (obj_i^k) is calculated based on its updated position vector (x_i^k). If obj_i^k is better than the previous optimal value (obj_i^{k-1}), x_i^k is set to p_i; otherwise, p_i is retained. Consequently, comparison of the obj_i^k particles have been done to select the best obj_i^k as the global optimal value. If this global optimal value is better than the p_g found in the previous iteration, p_g can be replaced with x_i^k; otherwise, p_g is retained. The procedure will stop as soon as the maximum iteration number is reached. Hence, PSO is applied to get the optimum output of the simulation model by integration of Aspen Plus and MATLAB. The objective and constrains are shown in the following optimization model [177,178].

$$max \ F_r^P \tag{3.22}$$

$$s.t. \begin{cases} 400 < T_G < 800 \\ 1 < P_G < 4 \\ 0.25 < G_A < 2 \\ 400 < T_{P1} < 800 \\ 100 < T_{P2} < 300 \end{cases} \tag{3.23}$$

where F_r^P is the flowrate of dimethyl ether, methanol or X product (kg/h), T_G is the primary gasification process temperature (°C), P_G is the primary gasification process pressure (bar), G_A is the air gasifying agent to biomass ration, T_{P1} and T_{P2} are reaction temperatures (°C) of reactor 1 and 2 (Appendix A6)

3.2.2.3 Radial basis surrogate optimization

Surrogate model-based optimization has been used for several chemical processes, resulting in good process efficiency [179,180]. The radial basis surrogate optimization function is used to optimize the gasification process with DME [181]. The PG based tri-generation process is exceedingly complex and typically contains a significant number of nonlinearities,

making optimization problematic; hence, surrogate-assisted optimization has been used for objective function evaluation. Although the radial function-based surrogate model reinforced by a linear polynomial is advised for time-consuming model optimization or when the objective functions are in the form of black boxes [181]. Hence, radial basis function-based surrogate optimization is used, which is fast and customizable. Following is a description for applying optimization process [182]:

i. Creating a set of trial points by sampling random points within the given bounds and evaluating the objective function at the trial points. The flowrate of DME would multiply by minus one so that the problem for maximizing the flowrate of DME can be converted into a minimization problem.

ii. Creating a surrogate model for the objective function by interpolating a radial basis function through random trial points.

iii. Using the merit function f_{merit} as shown in Eq. 3.24-3.26, locate a small value of the function by random sampling some points (x) in a region around the incumbent point (the best point can be found since the last surrogate reset). Then to use this point, called the adaptive point, as a new trial point.

$$f_{merit}(x) = \omega S(x) + (1 - \omega)D(x) \tag{3.24}$$

where ω is a weigh of parameter between 0 to 1. The $S(x)$ and $D(x)$ are scaled surrogate and scaled distance.

$$S(x) = \frac{s(x) - s_{min}}{s_{max} - s_{min}} \tag{3.25}$$

$$D(x) = \frac{d_{max} - d(x)}{d_{max} - d_{min}} \tag{3.26}$$

where s_{min} and s_{max} are the minimum and the maximum surrogate values among the sample points, $s(x)$ is the surrogate value at the point x, d_{max} and d_{min} represent the maximum and minimum distances from all sample points to all evaluated points, and $d(x)$ is the minimum distance of the point x to all evaluated points

iv. Evaluating the adaptive point using objective function, and updating the surrogate based on these points and their values. Counting a "success" if the objective function value is sufficiently lower than the previous best (lowest) value, otherwise counting it as "failure".

v. Updating the dispersion of the sample distribution upwards, if three successes occur before max (n_{var},5) failures, where n_{var} is the dimension of the inputs. Updating the dispersion downwards if max (n_{var},5) failures occur before three successes.

vi. Continuing from step 3 until all trial points are within a setting minimum distance of all evaluated points. At that time, resetting the surrogate by discarding all adaptive points from the surrogate, resetting the scale, and going back to step 1 to create new random trial points for evaluation.

3.2.2.4 Pattern search algorithm optimization

The pattern search algorithms were used due to the computational difficulty of the process simulation model, which is a black-box model, and gradient-based optimization algorithm. The pattern search technique, being one of the direct search methods, does not require information on the gradient or higher derivatives, making it ideal for optimization problems involving non-differentiable or even non-continuous functions [183]. And it is less susceptible to turning parameters than stochastic algorithms like genetic algorithms and particle swarm optimization [184]. The pattern search approach also includes a versatile and well-balanced operator for enhancing and fine-tuning the global search [185]. Because of its deterministic and robust performance for process optimization, it has been employed in dealing

with problems in chemistry or chemical engineering such as surface structure determination [186]. Therefore, the pattern search method was used in this study to optimize the basic procedure.

Pattern search is carried out by calculating a succession of points that approach an optimal point incrementally. The method investigates a mesh of points surrounding the current point, which was obtained in the previous stage, during each iteration. The mesh is constructed by multiplying the current point by a scalar multiple of a pattern of vectors. If the pattern search algorithm finds a position within the mesh that improves the objective function at the current point, that point is selected as the new current point for the process's next phase [187]. Therefore, this iteration will continue until the termination criteria are met. Ref. [187] contains more detailed information.

The multi-objective pattern search, also known as Pareto search, has used pattern search to discover a set of non-dominated (not inferior) answers. It can be stated as follows; detailed results are provided in chapter 6 [188]:

- The generation of an initial set of points, which is subsequently utilized to generate a mesh of points surrounding each beginning point.
- Evaluate the fitness of each point in the mesh and then poll to find better points by scoring against many objectives.
- If new points are collected, they are graded in order to select the current non-dominated points for updating the frontier. If this is not the case, the pareto search doubles the mesh sizes in iterations by 1/2.
- If the terminating criteria are met, output is acceptable. Alternatively, choosing points to generate a fresh set of points for the next iteration. This loop is repeated until convergence is reached.

- During each iteration, the algorithm searches for a better vector pattern that can be utilized to construct the point mesh. This is accomplished by evaluating the performance of various patterns and picking the one that produces the greatest results.

3.3 Process sustainability assessment and decision making

Simulation process sustainability assessment has been performed in terms of energy, exergy, economic, environmental, and safety basis. But all of these processes have been validated with relevant experimental works whose methodology is given in below sections.

3.3.1 Process validation

Biomass valorization processes validation have been performed by comparing the results determined in the experimental studies either by direct comparison with the output yield or by calculating root mean square error (RMSE) in Eq. 3.27. Valorization simulation processes have been verified through different types of biomasses to check the process robustness. In poly-generation processes, validations have also been done in terms of syngas and final product yield (%) with respect to biomass input. The RMSE between simulation model and reference model output for syngas has been calculated by using Eq. 3.27 [189]. Process with lower error or RMSE has utilized for further investigation.

$$\mathrm{RMSE} = \sqrt{\sum_{i=1}^{n} \frac{(S_i - E_i)^2}{n}} \tag{3.27}$$

where RMSE represents the root mean square error, E_i is the experimental value of element, S_i is simulation model value, i is the respective element, and n represents the total number of elements in comparison

3.3.2 Energy analysis

The energy efficiency of the biomass process may be determined using Eq. 3.28-3.31 [190,191] which is one of the indications for the process economic feasibility analysis. The material loss, enthalpy value, and unconverted material in the separate processes can all be

calculated. The output energy loss from direct material and biomass transformation into tar/biochar can be separated in the gasifier and cyclone separator. The sum of these losses equals the input energy, which may be computed using Eq. 3.29 [190,191]. The tar/biochar can be removed from the process stream by using a cyclone. Therefore, the internal energy in terms of material loss has been evaluated using the Aspen simulation model for energy analysis. There are some assumptions that have been considered when calculating the energy efficiency: (1) enthalpy energy of biomass, water, electricity (power to run equipment), and gasifying agent have been considered as an input; (2) the enthalpy energy of output product, unconverted product, ash, and steam generated have been considered as an output; (3) the process electricity consumption has been estimated based on vendor or literature data of the synthesis processes; and (4) the steam to power generation efficiency is being assumed in different processes.

$$\sum_{i=1}^{n} XE_{ij}\ (input) = \sum_{i=1}^{n} YE_{ij}\ \ (output) \tag{3.28}$$

where $\sum_{i=1}^{n} XE_{ij}$ is total input energy in the process, and $\sum_{i=1}^{n} YE_{ij}$ is the total output energy in term of enthalpy of the process

$$\sum_{i=1}^{n} XE_{ij} = XE_n^{BM} + XE_n^{GA} + XE_n^{water} + XW_n^{electricity} \tag{3.29}$$

where $\sum_{i=1}^{n} XE_{ij}$ is the total input energy in term of enthalpy, XE_n^{BM} enthalpy energy of biomass, XE_n^{GA} enthalpy energy of unconverted syngas, XE_n^{water} enthalpy energy of water, and W_n is the electricity utilization

$$\sum_{i=1}^{n} YE_{ij} = YE_n^{PD} + YE_n^{UC} + YE_n^{Steam} + YE_n^{Ash} \tag{3.30}$$

where $\sum_{i=1}^{n} YE_{ij}$ is the total output energy in term of enthalpy, YE_n^{PD} enthalpy energy of product, YE_n^{UC} enthalpy energy of unconverted product, XE_n^{steam} enthalpy energy of steam generated, and YE_n^{Ash} enthalpy energy of ash

$$\eta = \frac{\sum_{i=1}^{n} YE_{ij}}{\sum_{i=1}^{n} XE_{ij}} \tag{3.31}$$

where η is the energy efficiency of the process

3.3.3 Exergy analysis

Exergy analysis applies the first and second laws of thermodynamics to determine the quality of energy and efficiency at each action. Exergy analysis determines the quality of energy and process efficiency, whereas energy analysis quantifies energy. Exergy analysis can be performed to determine which areas have the highest energy deficit. Therefore, exergy analysis was performed using Eq. 3.32-3.38 [99] considering heat transfer, heating value, electricity/heat production, and material flow.

Exergy efficiency can help to determine the maximum possible work from a process while eliminating possible losses. It highlights the possible weakest area where energy deficiency exists. It is based on the first and the second law of thermodynamics to estimate the quality of available energy in a process. Exergy analysis of the newly developed process has been carried out based on Eq. 3.32-3.38 [192]. While the exergy of the biomass can be calculated based on Eq. 3.35 and 3.36 [192]. For overall exergy efficiency calculation of the process, the energy of the product has been divided by the exergy of the process input in term of exergy of reactants, gasifying agent, and heat, as presented in Eq. 3.37. The enthalpy, heat, temperature, entropy, and LHV have been taken from the Aspen Plus simulation model. The results of the exergy efficiency have been presented in chapter 5 and 6.

$$E_{i,total}=E_{i,chem}+E_{i,phy} \tag{3.32}$$

$$E_{i,chem}=x_i(s_i^{chem}+RT_o\ln[n_i]) \tag{3.33}$$

$$E_{i,phy}=x_i((H-H_o)-T_o(e-e_o)) \tag{3.34}$$

where $E_{i,total}$, $E_{i,chem}$, $E_{i,phy}$ are the total, chemical, and physical exergies of species *i*, e is the entropy, H is the enthalpy, s_i^{chem} is the chemical energy, n_i is the molar fraction of specie *i,* and 0 signifies the reference condition.

$$E_{biomass}=\varphi LHV_{biomass} \tag{3.35}$$

$$\varphi = \frac{1.0414 + 0.0177\frac{H}{C} - 0.3328(1 + 0.0537\frac{H}{C} + 0.0493\frac{N}{C})}{1 - 0.4021\frac{O}{C}} \quad (3.36)$$

$$\eta = \frac{E_{prod}}{E_{react} + E_{gas} + E_{heat} + E_{elec.}} \quad (3.37)$$

$$E_{prod} = E_n^{CHE} + E_n^{FG} + E_n^{Steam} + E_n^{Ash} \quad (3.38)$$

where E_{prod} is the product exergy, E_{react} is the reactant exergy, E_{gas} is the gas exergy, $E_{heat}$is the heat exergy, $E_{elec.}$is the power exergy, E_n^{CHE} exergy of chemical produce (targeted product like DME, methanol, H_2), E_n^{steam} exergy of steam generated, and $E_n^{Ash}$is exergy of ash.

3.3.4 Advanced exergy analysis of model

Conventional exergy analysis exhibits limitations in terms of identifying inefficiencies and losses, and it lacks a comprehensive treatment of irreversible relationships. Consequently, advanced exergy analysis not only adheres to the second law of thermodynamics but also incorporates economic dimensions. By integrating economic factors, this advanced analysis becomes more pertinent for decision-makers. This approach enables decision-makers to determine targeted components within a process for comprehensive sustainability improvements. Advanced exergy analysis has been applied to a gasification-based tri-generation process [193], which was originally taken from various studies [194–196]. Considering these studies, an advanced exergy analysis has been calculated [194–196]. Fig. 3.G provides an overview of the main parameters involved in the advanced exergy analysis, which can be broadly categorized into the following:

- Endogenous exergy destruction $E_{D,k}^{En}$ (Eq. 3.39) which is inherent or internal exergy loss due to component self-working condition and various irreversibility in the system.
- Exogenous exergy destruction $E_{D,k}^{Ex}$ (Eq. 3.39) refers to the exergy destruction due external factors or interaction with other components.

- Exergy destruction can be avoided $E_{D,k}^{av}$ (Eq. 3.41) by the application of appropriate technology introduction and improvement in process operations.
- Some exergy destruction cannot be avoided $E_{D,k}^{un}$ (Eq. 3.40) through any way out that is inherent within the system.
- Avoided and unavoidable exergy destructions have been categorized into endogenous and exogenous irreversibility rates which have been given in Fig. 3.G while it has been calculated through Eq. 3.39-3.45 [194–196].

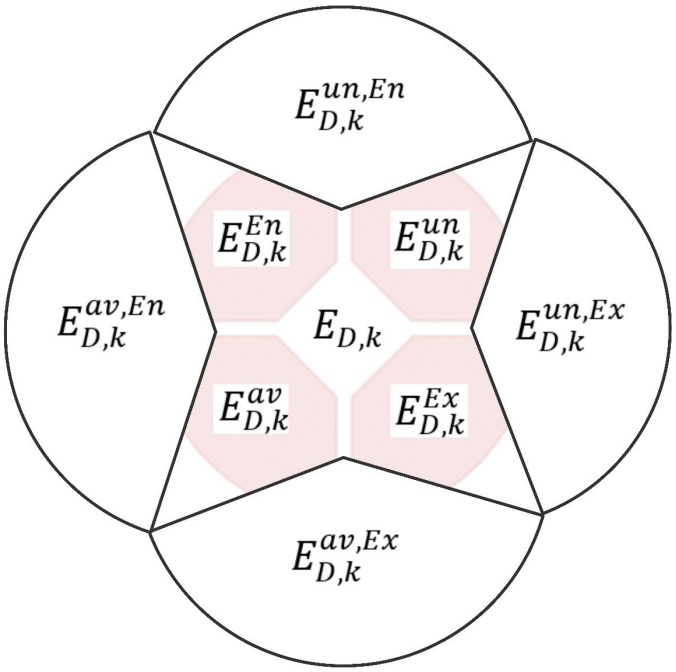

Fig. 3.G Indicators of advanced exergy analysis

To compute the endogenous exergy destruction of a particular component, the difference between its actual efficiency in real-time conditions and its maximum theoretical efficiency under ideal conditions have been considered.

$$E_{D,k} = E_{D,k}^{En} + E_{D,k}^{Ex} \tag{3.39}$$

where $E_{D,k}$ is irreversibility at real condition, $E_{D,k}^{En}$ is endogenous irreversibility, $E_{D,k}^{Ex}$ is exogenous irreversibility

$$E_{D,k}^{un} = E_{prod}\left(\frac{E_{D,k}}{E_{prod}}\right)^{un} \tag{3.40}$$

where $E_{D,k}^{un}$ is irreversibility unavoidable exergy, E_{prod} is exergy rate of product

$$E_{D,k}^{av}=E_D - E_{D,k}^{un} \tag{3.41}$$

where E_D^{av} is irreversibility avoidable exergy, E_D is destructive exergy

$$E_{D,k}^{un,En} = E_{prod}^{EN}(\frac{E_{D,k}}{E_{prod}^{EN}})^{un} \tag{3.42}$$

where $E_{D,k}^{un,En}$ is unavoidable endogenous irreversibility exergy

$$E_{D,k}^{un,Ex} = E_{D,k}^{un} - E_{D,k}^{un,En} \tag{3.43}$$

where $E_{D,k}^{un,Ex}$ is unavoidable exogenous irreversibility exergy

$$E_{D,k}^{av,En} = E_{D,k}^{En} - E_{D,k}^{un,En} \tag{3.44}$$

where $E_{D,k}^{av,En}$ is avoidable endogenous irreversibility exergy, $E_{D,k}^{un}$ irreversibility unavoidable exergy

$$E_{D,k}^{av,Ex} = E_{D,k}^{av} - E_{D,k}^{av,En} \tag{3.45}$$

where $E_{D,k}^{av,Ex}$ is avoidable exogenous irreversibility exergy

3.3.5 Exergoeconomics analysis of model

Exergoeconomics analysis is an integrated approach that combines the principles of exergy and economic analysis within a process. This approach utilizes both exergy and economic principles to assess the cost-effectiveness and thermodynamic efficiency. Primarily, the cost of exergy destruction has been divided into exogenous and endogenous components, which have been further categorized as avoidable and unavoidable elements. To assess cost-effectiveness, advanced exergy analysis has been conducted within the system [197,198]. Hence, exergoeconomics analysis was conducted by estimating the exergoeconomics indicators as given in Fig. 3.H based on Eq. 3.46-3.61 [197–200].

$$C_{D,k}^{En} = c_{F,k}E_{D,k}^{En} \tag{3.46}$$

where $C_{D,k}^{En}$ represents the endogenous exergy destruction cost

$$C_{D,k}^{Ex} = c_{F,k}E_{D,k}^{Ex} \tag{3.47}$$

where $C_{D,k}^{Ex}$ represents the exogenous exergy destruction cost

$$I_k^{En} = E_{prod}^{EN}(\frac{I}{E_{prod}}) \tag{3.48}$$

where I_k^{En} represents the endogenous exergy investment cost

$$I_k^{Ex} = I - I_k^{En} \tag{3.49}$$

Where I_k^{Ex} represents the exogenous exergy investment cost flow

$$C_{D,k}^{av} = c_{F,k}E_{D,k}^{av} \tag{3.50}$$

where $C_{D,k}^{av}$ represents the cost of exergy for avoidable destruction

$$C_{D,k}^{un} = c_{F,k}E_{D,k}^{un} \tag{3.51}$$

Where $C_{D,k}^{un}$ represents the cost of exergy for unavoidable destruction

$$I_k^{un} = E_{prod}(\frac{I}{E_{prod}})^{un} \tag{3.52}$$

where I_k^{un} represents the unavoidable investment cost

$$I_k^{av} = I - I_k^{un} \tag{3.53}$$

where I_k^{av} represents the avoidable investment cost

$$C_{D,k}^{un,En} = c_{F,k}E_{D,k}^{un,En} \tag{3.54}$$

where $C_{D,k}^{un,En}$ represents the unavoidable endogenous cost

$$C_{D,k}^{av,En} = c_{F,k}E_{D,k}^{av,En} \tag{3.55}$$

Where $C_{D,k}^{av,En}$ represents the avoidable endogenous cost

$$C_{D,k}^{un,Ex} = c_{F,k}E_{D,k}^{un,Ex} \tag{3.56}$$

where $C_{D,k}^{un,Ex}$ represents the unavoidable exogenous cost

$$C_{D,k}^{av,Ex} = c_{F,k}E_{D,k}^{av,Ex} \tag{3.57}$$

Where $C_{D,k}^{av,Ex}$ represents the avoidable exogenous cost

$$I_k^{un,En} = E_{prod}^{EN}(\frac{I}{E_{prod}})^{un} \tag{3.58}$$

where $I_{D,k}^{un,En}$ represents the unavoidable endogenous investment

$$I_k^{un,Ex} = I_k^{un} - I_k^{un,En} \tag{3.59}$$

where $I_{D,k}^{un,Ex}$ represents the unavoidable exogenous investment

$$I_k^{av,En} = I_k^{En} - I_k^{un,En} \tag{3.60}$$

where $I_{D,k}^{av,En}$ represents the avoidable endogenous investment

$$I_k^{av,Ex} = I_k^{Ex} - I_k^{un,Ex} \tag{3.61}$$

where $I_{D,k}^{av,Ex}$ represents the avoidable exogenous investment

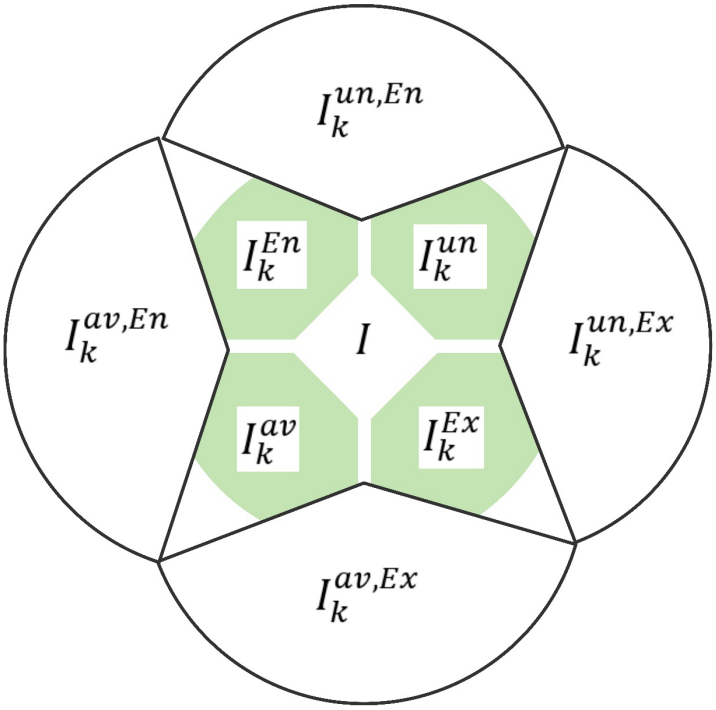

Fig. 3.H. Exergoeconomics indicator

3.3.6 Thermal energy to electric power potential

The thermal energy of the process was transformed into electrical energy by converting the thermal energy of the process into steam, which was then used in the steam turbine to generate electricity. To convert thermal into electrical energy, heat exchangers were utilized, which transferred process syngas energy (heat) into water and eventually produced high pressure and temperature steam. These steam properties, as well as the turbine and generation efficiency, will be utilized to compute the potential output energy using Eq. 3.62-3.65, as recommended by the United States Department of Energy [201]. For the calculation of electric power output, the following assumptions have been considered:

- Mass inlet flow (steam) is equal to the mass outlet flow [202]
- Isentropic efficiency of the turbine is around 60% [203]
- Generator efficiency is around 90% [204]

$$E_{if} = E_{iE} \times M_{Fr} \quad (3.62)$$

where E_{if} is the inlet energy flow, E_{iE} is the Inlet Specific Enthalpy, and M_{Fr} is the inlet mass flow

$$E_{OS} = E_{iE} - \eta_i \times (E_{iE} - E_{ios}) \quad (3.63)$$

where E_{OS} is the outlet specific enthalpy, E_{iE} is the Inlet Specific Enthalpy, η_i is the Isentropic Efficiency, and E_{ios} is the Ideal Outlet Specific Enthalpy

$$E_o = M_{Fr} \times (E_{iE} - E_{OS}) \quad (3.64)$$

where E_o is the energy out, and M_{Fr} is the mass flow

$$\text{Power Out} = E_o \times \eta_G \quad (3.65)$$

where η_G is the generator efficiency

3.3.7 Process economic analysis

The economic assessment of this process involves the application of two distinct economic methodologies: the Internal Rate of Return (IRR) and the Payback Period (PBP). The IRR represents the discount rate at which the net present value of future cash flows reaches zero. On the other hand, the PBP signifies the duration required for the original capital investment to be fully recovered [205,206]. A higher IRR or a shorter PBP indicates better economic performance for the project. For this purpose, two types of costs have been considered; plant capital and operational costs. Only plant installation costs, such as equipment and civil construction, have been included in the capital cost, which were obtained through literature or directly from vendors. The cost of land, legal duties, administrative or consultancy charges are not addressed because they vary significantly between regions. Similarly, the costs of raw materials, direct labor, maintenance, and overhead have been included. It is assumed that the gasification plant's thermal energy generation is sufficient to meet its energy requirements. The cost of transportation outside of the plant's immediate neighborhood is not considered into the economic analysis. For process operations, specified capacity of plant from 1-10 tons per h have been considered along with a shutdown period for maintenance activities. Linear depreciation of plants has been considered with 10 years of operational life of plant while the

inflation rate is not considered this economic analysis. Furthermore, some operational assumptions have been considered which include the consistency of plant operations, and availability of the raw material. According to Eq. 3.66-3.70, the IRR has been calculated [207]. IRR is defined as an interest rate which equates the present worth of cash flow to zero [207]. The IRR of the base and optimized process has been calculated at different efficiencies levels of the plant given in Chapter 4-7.

For the calculation of IRR, the following assumptions have been considered:

- Plant operational efficiency is consistent with respect to the applied case.
- Installed plant setup operational life is 10 years with linear depreciation.
- No inflation rate has been considered.
- For some cases, subsidy of $10-20 per ton or 50% waste disposal cost which is $50 in high-income and $17.5 per ton in low-income countries have been considered in chapter 7 [208].
- Cost of land, legal or regulatory duties, consultation, and administrative costs are not included in the initial investment.
- There is no shortage of raw material, and it is available as per requirement.
- Electricity generation in the plant is sufficient to meet the operational needs.

$$0 = \sum_{t=0}^{n} \frac{C_t}{(1 + IRR)^t} - C_o \tag{3.66}$$

where IRR is the internal rate of return, C_t is the net cash inflow during time period t, i is the discount rate, C_o is the initial investment, and t is the time period (yr.)

$$C_o = C_p + C_b + C_e \tag{3.67}$$

where C_o the initial investment, C_p cost of plant equipment, C_b cost of building/civil work, and C_e cost of electrical installations.

$$OPR = C_r + C_l + C_o + C_m + C_T + C_d \quad (3.68)$$

where OPR is the operational cost, C_r cost of raw material, C_l cost of labor, C_o overhead cost, C_m cost of engineering maintenance, C_T transportation cost, and C_d cost of plant depreciation.

$$C_t = P_c . Q_t \quad (3.69)$$

Where C_t is the net cash inflow during time period *t*, P_c is per unit cost of product, and Q_t product quantity produced.

$$PBP = \frac{C_o}{R_{wrt}} \quad (3.70)$$

where *PBP* payback period, R_{wrt} is the profit from revenue with respect to specific time.

3.3.8 Environment performance

Environment feasibility of the valorization process is being carried out using life cycle assessment (LCA) approach by applying ISO 14040 framework of defining goal and scope, inventory analysis, impact assessment, and interpretation [209]. LCA is a framework which is used for analyzing the environmental impact of the process or product throughout its life. For LCA calculations, SimaPro software's Ecoinvent libraries and the IMPACT 2002+ methodology was used. It is not a full cradle to grave LCA, but rather a gate-to-gate LCA, beginning with biomass waste collection from the farm and ending with the valorization process at the treatment plant. The environmental impact of building and plant installation is not considered in this research. The environmental impact of valorizing biomass waste per kilogram unit basis has been compared to land disposal or with other produced products as per respective chapter. For life cycle inventory (LCI) which has the vital role in the LCA, data is being obtained from respective chapter simulation model or different literatures [210] and Ecoinvent database using SimaPro software [211].

Life Cycle Impact Assessment (LCIA) has been carried out using the IMPACT 2002+ method with 15 midpoints impact categories including non-carcinogens, carcinogens, ionizing radiation, respiratory inorganics, respiratory organics, ozone layer depletion, aquatic

ecotoxicity, terrestrial acid, terrestrial ecotoxicity, land occupation, aquatic eutrophication, aquatic acidification, mineral extraction, global warming, non-renewable energy, and four end point (damage) categories including human health, climate change, ecosystem quality, and resources [212]. It is not a thorough LCA because the goal is to compare the environmental impact of biomass land disposal and valorization processes; hence, the default settings of the categories, weighting factor, and method structure have been used in SimaPro calculations. Final LCA results have been better examined in terms of midpoint, endpoint, and single score. While a single point average impact reflects a single component that can be biased according to unique location or other circumstances, certain corrective elements are required to convert these regional values, which are typically difficult to collect [212,213]. Therefore, to address this issue three approaches including endpoint, midpoint and single score have been used for comparative results.

3.3.9 Safety analysis

There are different quantitative and qualitative approaches that have been adopted by the researchers for process safety risk analysis. Most of the methods are index-based which have adopted qualitative approach for the risk assessment like Inherent Safety Index (ISI), potential safety, health, and environmental (SHE), Prototype Inherent Safety Index (PIIS), Process Safety Index Analysis (PSIA), Inherent Chemical Process Properties Data (ICPD) [214]. In this study, both subjective and objective based safety techniques have been applied for risk assessment. Numeric Descriptive Inherent Safety Index (NuDISI) quantitative process safety-based risk assessment of biomass raw material has been evaluated for different final products considering process parameters related to the temperature, pressure, heat of reactions, and process inventory. While subjective technique safety index analysis (PSIA) and inherent safety index (ISI) techniques [215,216] have also applied in some cases. Eq. 3.71-3.73 has

been used for NuDISI safety assessment without being involving any subjective term like ratings, classifications etc. [214]

$$y = \frac{1}{1 + Ae^{-Bx}} \tag{3.71}$$

where y= variable represent parameter values, x= parameter value, B= maximum score limit,

A = parameter score

$$B = \frac{4m}{C} \tag{3.72}$$

where B= maximum score limit, m = mean safety value of parameter collected from literature/simulation models, C =100

$$A = e^{Bk} \tag{3.72}$$

A = parameter score, B= maximum score limit, k = slope cumulative curve of parameter

$$\text{PSTS} = (S_T)_{max} + (S_P)_{max} + (S_{HR})_{max} + (S_I)_{max} \tag{3.73}$$

where Process Safety Total Score (PSTS), the scores for temperature (S_T), pressure (S_P), heat of reaction (S_{HR}), and process inventory (S_{PI})

Thermal processes data like pressure, process temperature, heat of reactions, reactivity, and material flow rate have been collected from the literature including Aspen Plus simulation model results [57] and experimental analysis. Slopes and scores of the parameters have been calculated based on the collected data. Then, using calculations of the individual variable, total process safety score (PSTS) has been calculated which is summarized in the respective chapter.

3.3.10 Strategic decision making

In this study, the decision-making model application was to identify the sustainable valorization process. Section 3.3.10.1 methodology has been developed for valorization

process selection while section 3.3.10.2 provides the mechanism for sustainability index calculations.

3.3.10.1 Sustainable valorization process selection

Sustainable valorization process selection has been developed based on the following frameworks:

a. Research framework

The main aim of this investigation is to identify a sustainable waste valorization process, based on criteria including economic, technological, environmental, and socio-governance aspects. The conceptual model depicting the research framework is given in Fig. 3.I. To achieve this objective, the research is structured into five distinct phases, concisely outlined below:

Phase 1: Identification of criteria and potential MSW valorization process.

A systematic literature review has been undertaken to identify the pivotal factors highlighted by scholars for the discernment of waste valorization processes. Therefore, four methodologies—namely, pyrolysis, gasification, HTG, and anaerobic digestion (AND)—have been selected as viable alternatives based on expert recommendations and prior research. The sixteen criteria, as given in Table 8.1 (chapter 8), have been substantiated through various research endeavors.

Phase 2 Calculating the main and sub-criteria weight through AHP.

On the basis of selected indicators for the waste valorization process, a survey instrument has been designed for data acquisition. The survey targets individuals recognized as field experts in this domain. The primary focus of data collection encompasses the following aspects:

- The criteria for the waste valorization process, shortlisted in the initial step, undergo evaluation by the researchers utilizing the AHP.

Primarily, weights are computed through the AHP method. This involves the development of four overarching main categories, namely economic, environmental, technological, and socio-governance considerations.

Phase 3 Ranking of MSW valorization processes through advanced IVFFS-CODAS method.

Expert perspectives on sustainable MSW valorization methods, specifically pyrolysis, gasification, HTG, and AND have been gathered with respect to the established criteria. Initially, the determination of criteria and sub-criteria weights was conducted using the AHP. These weights were subsequently employed for the ranking of the MSW valorization processes. The ultimate ranking of the processes was accomplished using IVFFS logic Dombi advanced CODAS method as given in section 3.3.10.1.d. Furthermore, the Shannon Entropy and CRITIC methods were also applied to ascertain weights for sensitivity analysis based on available quantitative data. Furthermore, quantitative data is gathered from over 30 diverse studies related to gasification, pyrolysis, HTG, and AND. The quantitative data will be predominantly classified within the aforementioned four criteria.

Phase 4 Performing a comprehensive sensitivity analysis.

Current model undergoes sensitivity analysis through varied weight assignments (utilizing AHP, Entropy, CRITIC, and Equal weighting methods) and the incorporation of different Dombi operator values ranging from 0.1 to 1. The adjustment of Dombi operator values within this specified range is carried out to assess its impact on the ultimate ranking. Furthermore, the rank reversal method is employed, involving the omission of certain criteria, to evaluate its influence on the final output. The final results of the sensitivity analysis are presented in section 8.5, where a variety of weights, encompassing both qualitative and quantitative methodologies, have been employed to rank the waste valorization processes.

Phase 5: Offering policy implications based on analysis findings.

Finally, policy implications for the short term, intermediate term, and long term have been outlined in accordance with the obtained results.

b. Fermatean fuzzy sets (FFS)

FFS is an extension of the Pythagorean Membership Grade (PMG), which, in turn, is an advanced iteration of the Intuitionistic Membership Grade (IMG) within fuzzy set theory introduced by Senapati and Yager [217]. In 2017, q-rung orthopair fuzzy sets have been introduced in which q^{th} power was supported by 1 but when q^{th} power is 3 then this type of fuzzy sets is considered as an FFS [218]. A visual depiction highlighting the distinctions among these three entities—IMS, PMG, and Fermatean Membership Grade (FMG)—can be found in Fig. 3.J. The constraint to holds for the sum of membership and non-membership functions to be less than or equal to 1 in all instances, but there are some situations in which IMS ($\alpha+\beta\leq1$) and PMG ($\alpha^2+\beta^2\leq1$) fail to adhere to this constraint. Consequently, a novel concept, FFS ($\alpha^3+\beta^3\leq1$) has been introduced to address this limitation. This new advancement can cover more space of acceptable orthopair as compared to previous models (i.e., IFS and PFS).

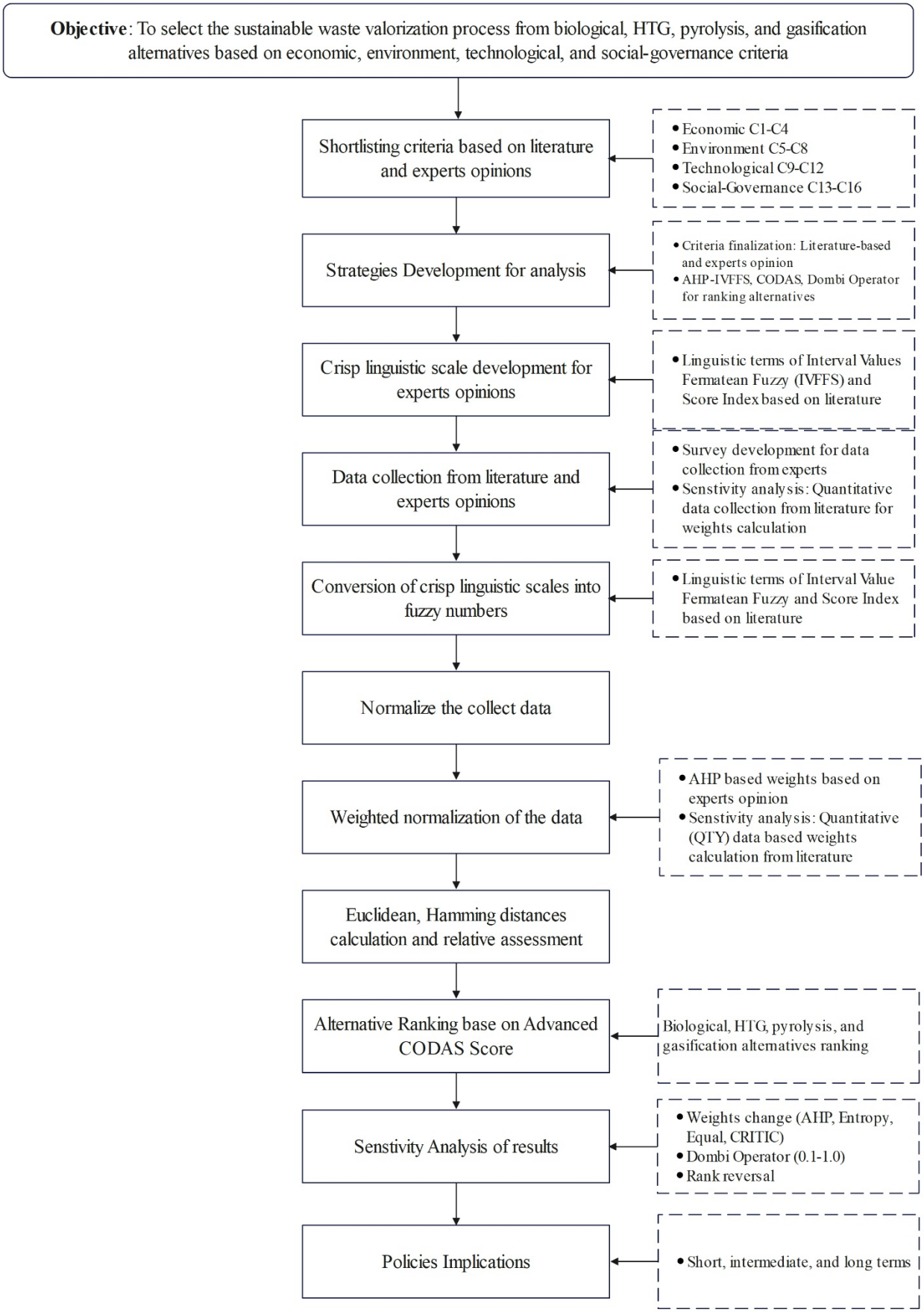

Fig. 3.I. Research framework for decision making model

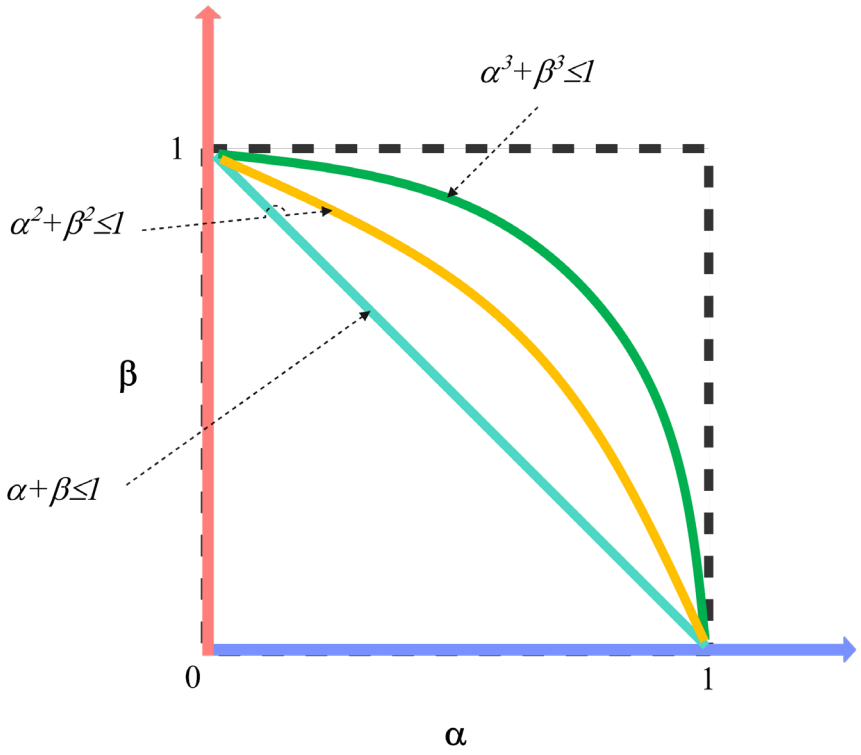

Fig. 3.J. Spaces among IMG, PMG, and FFS

Definition 1. Fermatean fuzzy set number (F) with a finite number universal set number ***X*** is expressed and given in Eq. 3.74 [217].

$$F = \left\{ \left(\left(x, \underset{f}{\alpha} \sim (x), \underset{f}{\beta} \sim (x) \right) \mid x \in X \right) \right\} \tag{3.74}$$

where the function $\underset{f}{\alpha} : X \rightarrow [0, 1]$ and $\underset{f}{\beta} : X \rightarrow [0, 1]$ are membership (MD) and non-membership (ND) degrees, respectively.

$$0 \leq \alpha_f^3 + \beta_f^3 \leq 1 \tag{3.75}$$

where the general rule of FFS

$$\underset{f}{\pi}(x) = \sqrt[3]{1 - \alpha_f(x)^3 - \beta_f(x)^3} \tag{3.76}$$

where degree of indeterminacy is represented as $\underset{f}{\pi}(x)$

Definition 2. Fermatean fuzzy set with a close sub-interval of *I* [0,1] in the universal set ***X*** can be defined as follow in Eq. 3.77 and 3.78 [219]:

$$F=\left\{\begin{array}{c}\left(x,\alpha_f\sim(x),\beta_f\sim(x)\right)\\ \left(\alpha_f^-\sim(x),\alpha_f^+\sim(x)\right)\in I[0,1],\\ \left(\beta_f^-\sim(x),\beta_f^-\sim(x)\right)\in I[0,1],x\in X\end{array}\right\} \tag{3.77}$$

where the function $\underset{f}{\alpha}: X\rightarrow I\ [0,\ 1]$ and $\underset{f}{\beta}: X\rightarrow I\ [0,\ 1]$ are the membership degree (MD) and non-membership degree (ND) of the component $I\in X$, satisfying $0\le\left(\alpha_f^+(x)\right)^3+\left(\beta_f^+(x)\right)^3\le 1$

where the indeterminacy degree is following: (3.78)

$$\vartheta_f^{\sim}(x)=[\vartheta_f^{-\sim}(x),\vartheta_f^{+\sim}(x)]=\left[\sqrt[3]{1-\left(\alpha_f^-(x)\right)^3+\left(\beta_f^-(x)\right)^3},\sqrt[3]{1-\left(\alpha_f^+(x)\right)^3+\left(\beta_f^+(x)\right)^3}\right]$$

This can be simplified as a $f=\left(\left[\alpha^-,\alpha^+\right],\left[\beta^-,\beta^+\right]\right)$ which fulfills the constraint given in Eq. 3.75.

Definition 3. Dombi t-norm (DTN) and Dombi-t-conorm (DTCN) operators have been introduced to balance between generality and specificity in fuzzy logic which can be explained in Eq. 3.79 as a function of two real numbers α and β [220,221]

where the indeterminacy degree is following:

$$DTN(\alpha,\beta)=\frac{1}{1+\left[\left(\frac{1-\alpha}{\alpha}\right)^{\lambda}+\left(\frac{1-\beta}{\beta}\right)^{\lambda}\right]^{1/\lambda}},DTCN(\alpha,\beta)=1-\frac{1}{1+\left[\left(\frac{1-\alpha}{\alpha}\right)^{\lambda}+\left(\frac{1-\beta}{\beta}\right)^{\lambda}\right]^{1/\lambda}} \tag{3.79}$$

where $\lambda>0$, and $(\alpha, \beta)\in[0,1]\times[0,1]$, for current study $\lambda=[0,1]$

Definition 4. Let the $\xi=\left(\left[\alpha^{-},\alpha^{+}\right],\left[\beta^{-},\beta^{+}\right]\right)$ are the FFS. Hence, the score and accuracy of the FFS ξ can be calculated through Eq. 3.80-3.81 [222].

$$\rho(\xi)=\frac{1}{2}\left(\frac{1}{2}\left(\left(\alpha^{-}\right)^{3}+\left(\alpha^{+}\right)^{3}-\left(\beta^{-}\right)^{3}-\left(\beta^{+}\right)^{3}\right)+1\right),\rho(\xi)\in[0,1] \tag{3.80}$$

$$\kappa(\xi)=\frac{1}{2}\left(\frac{1}{2}\left(\left(\alpha^{-}\right)^{3}+\left(\alpha^{+}\right)^{3}-\left(\beta^{-}\right)^{3}-\left(\beta^{+}\right)^{3}\right)+1\right),\kappa(\xi)\in[0,1] \tag{3.81}$$

Definition 5. The integration of DTN and DTCN operators in FFS can be stated as follows in Eq. 3.83. If the $\xi_1=\left(\left[\alpha_1{}^{-},\alpha_1{}^{+}\right],\left[\beta_1{}^{-},\beta_1{}^{+}\right]\right)$ and $\xi_2=\left(\left[\alpha_2{}^{-},\alpha_2{}^{+}\right],\left[\beta_2{}^{-},\beta_2{}^{+}\right]\right)$ are the FFS of $\xi=\left(\left[\alpha^{-},\alpha^{+}\right],\left[\beta^{-},\beta^{+}\right]\right)$ then the operation of DTN and DTCN for the real number $\gamma>0$ can be defined in Eq. 3.82-3.85 [223].

$$\rho(\xi)\oplus\kappa(\xi)=\left\langle\begin{array}{c}\sqrt[3]{1-\frac{1}{1+\left[\left(\frac{(\alpha_1^{-})^3}{1-(\alpha_1^{-})^3}\right)^{\lambda}+\left(\frac{(\alpha_2^{-})^3}{1-(\alpha_2^{-})^3}\right)^{\lambda}\right]^{1/\lambda}}},\sqrt[3]{1-\frac{1}{1+\left[\left(\frac{(\alpha_1^{+})^3}{1-(\alpha_1^{+})^3}\right)^{\lambda}+\left(\frac{(\alpha_2^{+})^3}{1-(\alpha_2^{+})^3}\right)^{\lambda}\right]^{1/\lambda}}},\\ \frac{1}{\sqrt[3]{1+\left[\left(\frac{1-(\beta_1^{-})^3}{(\beta_1^{-})^3}\right)^{\lambda}+\left(\frac{1-(\beta_2^{-})^3}{(\beta_2^{-})^3}\right)^{\lambda}\right]^{1/\lambda}}},\frac{1}{\sqrt[3]{1+\left[\left(\frac{1-(\beta_1^{+})^3}{(\beta_1^{+})^3}\right)^{\lambda}+\left(\frac{1-(\beta_2^{+})^3}{(\beta_2^{+})^3}\right)^{\lambda}\right]^{1/\lambda}}}\end{array}\right\rangle \tag{3.82}$$

$$\rho(\xi)\otimes\kappa(\xi)=\left\langle\begin{array}{c}\frac{1}{\sqrt[3]{1+\left[\left(\frac{1-(\alpha_1^{-})^3}{(\alpha_1^{-})^3}\right)^{\lambda}+\left(\frac{1-(\alpha_2^{-})^3}{(\alpha_2^{-})^3}\right)^{\lambda}\right]^{1/\lambda}}},\frac{1}{\sqrt[3]{1+\left[\left(\frac{1-(\alpha_1^{+})^3}{(\alpha_1^{+})^3}\right)^{\lambda}+\left(\frac{1-(\alpha_2^{+})^3}{(\alpha_2^{+})^3}\right)^{\lambda}\right]^{1/\lambda}}},\\ \sqrt[3]{1-\frac{1}{1+\left[\left(\frac{(\beta_1^{-})^3}{1-(\beta_1^{-})^3}\right)^{\lambda}+\left(\frac{(\beta_2^{-})^3}{1-(\beta_2^{-})^3}\right)^{\lambda}\right]^{1/\lambda}}},\sqrt[3]{1-\frac{1}{1+\left[\left(\frac{(\beta_1^{+})^3}{1-(\beta_1^{+})^3}\right)^{\lambda}+\left(\frac{(\beta_2^{+})^3}{1-(\beta_2^{+})^3}\right)^{\lambda}\right]^{1/\lambda}}}\end{array}\right\rangle \tag{3.83}$$

$$\gamma\xi = \left\langle \begin{array}{l} \sqrt[3]{1-\dfrac{1}{1+\left[\gamma\left(\dfrac{(\alpha_{\cdot}^{-})^3}{1-(\alpha_{\cdot}^{-})^3}\right)^{\lambda}\right]^{1/\lambda}}}, \sqrt[3]{1-\dfrac{1}{1+\left[\gamma\left(\dfrac{(\alpha_{\cdot}^{+})^3}{1-(\alpha_{\cdot}^{+})^3}\right)^{\lambda}\right]^{1/\lambda}}}, \\ \dfrac{1}{\sqrt[3]{1+\left[\gamma\left(\dfrac{1-(\beta_{\cdot}^{-})^3}{(\beta_{\cdot}^{-})^3}\right)^{\lambda}\right]^{1/\lambda}}}, \dfrac{1}{\sqrt[3]{1+\left[\gamma\left(\dfrac{1-(\beta_{2}^{+})^3}{(\beta_{2}^{+})^3}\right)^{\lambda}\right]^{1/\lambda}}} \end{array} \right\rangle \tag{3.84}$$

$$\xi^{\gamma} = \left\langle \begin{array}{l} \dfrac{1}{\sqrt[3]{1+\left[\gamma\left(\dfrac{1-(\alpha_{\cdot}^{-})^3}{(\alpha_{\cdot}^{-})^3}\right)^{\lambda}\right]^{1/\lambda}}}, \dfrac{1}{\sqrt[3]{1+\left[\gamma\left(\dfrac{1-(\alpha_{\cdot}^{+})^3}{(\alpha_{\cdot}^{+})^3}\right)^{\lambda}\right]^{1/\lambda}}}, \\ \sqrt[3]{1-\dfrac{1}{1+\left[\gamma\left(\dfrac{(\beta_{\cdot}^{-})^3}{1-(\beta_{\cdot}^{-})^3}\right)^{\lambda}\right]^{1/\lambda}}}, \sqrt[3]{1-\dfrac{1}{1+\left[\gamma\left(\dfrac{(\beta_{\cdot}^{+})^3}{1-(\beta_{\cdot}^{+})^3}\right)^{\lambda}\right]^{1/\lambda}}} \end{array} \right\rangle \tag{3.85}$$

Definition 6. The integration of DTN and DTCN operators average in the FFS has been done. For this purpose, an assumption has been taken. Let $\varphi_j = \left(\left[\vartheta_j^{-}, \vartheta_j^{+}\right], \left[\sigma_j^{-}, \sigma_j^{+}\right]\right)$ (j=1,2, 3…, k) is a collection IVFFS. FFSDW (Fermatean Fuzzy Dombi weightage) aggregated value is defined in Eq. 3.86 while the FFSDWG geometric operator is defined in Eq. 3.87 [223].

$$FFSDW(\varphi_1, \varphi_2, \varphi_3 \ldots, \varphi_j) = \left\langle \begin{array}{l} \left[\sqrt[3]{1-\dfrac{1}{1+\left\{\sum_{a=1}^{j}\tau_a\left(\dfrac{(\vartheta_a^{-})^3}{1-(\vartheta_a^{-})^3}\right)^{\lambda}\right\}^{1/\lambda}}}\right], \left[\sqrt[3]{1-\dfrac{1}{1+\left\{\sum_{a=1}^{j}\tau_a\left(\dfrac{(\vartheta_a^{+})^3}{1-(\vartheta_a^{+})^3}\right)^{\lambda}\right\}^{1/\lambda}}}\right], \\ \left[\dfrac{1}{\sqrt[3]{1+\left\{\sum_{a=1}^{j}\tau_a\left(\dfrac{(\sigma_a^{-})^3}{1-(\sigma_a^{-})^3}\right)^{\lambda}\right\}^{1/\lambda}}}\right], \left[\dfrac{1}{\sqrt[3]{1+\left\{\sum_{a=1}^{j}\tau_a\left(\dfrac{(\sigma_a^{+})^3}{1-(\sigma_a^{+})^3}\right)^{\lambda}\right\}^{1/\lambda}}}\right] \end{array} \right\rangle \tag{3.86}$$

where φ_j is the FFS, τ_a is the weight vector *(a= 1, 2, ..., n)* of φ_j *(j= 1, 2, 3.... k)* with $\tau > 0$ and $\sum_{j=1}^{n} \tau_j = 1$

$$FFSDWG(\varphi_1, \varphi_2, \varphi_3 ...., \varphi_j) = \left\langle \left[\frac{1}{\sqrt[3]{1 + \left\{ \sum_{a=1}^{j} \tau_a \left(\frac{(\vartheta_a^-)^3}{1-(\vartheta_a^-)^3} \right)^{\lambda} \right\}^{1/\lambda}}}, \frac{1}{\sqrt[3]{1 + \left\{ \sum_{a=1}^{j} \tau_a \left(\frac{(\vartheta_a^+)^3}{1-(\vartheta_a^+)^3} \right)^{\lambda} \right\}^{1/\lambda}}} \right], \left[\sqrt[3]{1 - \frac{1}{1 + \left\{ \sum_{a=1}^{j} \tau_a \left(\frac{(\sigma_a^-)^3}{1-(\sigma_a^-)^3} \right)^{\lambda} \right\}^{1/\lambda}}}, \sqrt[3]{1 - \frac{1}{1 + \left\{ \sum_{a=1}^{j} \tau_a \left(\frac{(\sigma_a^+)^3}{1-(\sigma_a^+)^3} \right)^{\lambda} \right\}^{1/\lambda}}} \right] \right\rangle \quad (3.87)$$

where φ_j is the FFS, τ_a is the weight vector *(a= 1, 2, ..., n)* of φ_j *(j= 1, 2, 3.... k)* with $\tau > 0$ and $\sum_{j=1}^{n} \tau_j = 1$

c. Weights calculation

In this study, the determination of weights was conducted through a qualitative approach using AHP. Subsequently, for the purpose of validation analysis, quantitative values of the criteria, as reported in the literature, were employed. These quantitative weights were derived from existing literature and explained below, detailing the procedures for weight calculation.

AHP weights

The methodology employed for the determination of criteria weights involves the application of the AHP. The utilization of linguistic numbers facilitates the transformation of subjective terms into objective weight calculations. The rationale behind selecting this integration lies in its efficacy in addressing subjective uncertainties inherent in expert decision-making, its enhanced sensitivity, and its alignment with real-world scenarios [224]. The sequential process for calculating AHP weights is as follows [225]:

Step 1: Commencing with the establishment of an objective to choose the most suitable option from the available alternatives based on the specified criteria.

Step 2: A pairwise comparison matrix has been formulated to facilitate the relative assessment of various criteria, as outlined in Eq. 3.88. The matrix elements represent the extent to which the i^{th} criterion is preferred over the j^{th} criterion. These comparative judgments are expressed in linguistic terms provided in Appendix A1, serving as the basis for transforming subjective ratings into an objective format for subsequent analysis.

$$A = \begin{array}{c} \\ C_1 \\ C_2 \\ C_3 \\ . \\ . \\ . \\ C_n \end{array} \begin{bmatrix} \\ x_{11} & x_{12} & x_{13} & .....x_{1n} \\ x_{21} & x_{22} & x_{23} & .....x_{2n} \\ x_{31} & x_{32} & x_{33} & .....x_{2n} \\ . & . & . & . \\ . & . & . & . \\ . & . & . & . \\ x_{n1} & x_{n2} & x_{n3} & .....x_{nn} \end{bmatrix} \tag{3.88}$$

where x_{ij} is the degree of preference of i^{th} criterion over j^{th} criterion.

Step 3: The data acquired from the pairwise comparison underwent normalization within the [0, 1] range by employing Eq. 3.89. The normalization process entails dividing the sum of column-wise values by the individual value in the corresponding column. It is being noted that the cumulative sum of values in each column after normalization equates to 1.

$$m_{ij} = \frac{x_{ij}}{\sum_{i=1}^{n} x_{ij}} \tag{3.89}$$

where x_{ij} is the degree of preference of i^{th} criterion over j^{th} criterion which is being divided by the sum of all degrees of preferences.

$$M = \begin{array}{c} C_1 \\ C_2 \\ C_3 \\ . \\ . \\ . \\ C_n \end{array} \begin{bmatrix} m_{11} & m_{12} & m_{13} & .....m_{1n} \\ m_{21} & m_{22} & m_{23} & .....m_{2n} \\ m_{31} & m_{32} & m_{33} & .....m_{2n} \\ . & . & . & . \\ . & . & . & . \\ . & . & . & . \\ m_{n1} & m_{n2} & m_{n3} & .....m_{nn} \end{bmatrix} \tag{3.90}$$

where m_{ij} is the normalized response of respective criteria in range of [0,1].

Step 4: Compute the Consistency Index (CI) within the framework of the AHP to assess the inconsistency inherent in expert opinions. The calculation of the inconsistency index for the pairwise matrix is accomplished using Eq. 3.91. The hunt of minimizing the *CI*, approaching the value of '0', is deemed as improved consistency in expert opinions. According to this study, if the *CI* falls below 0.10, the AHP results are considered acceptable; otherwise, a reassessment is warranted to attain a consistent outcome [226].

$$CI = \frac{\lambda_{\max} - N}{N - 1} \tag{3.91}$$

where λ_{max} is the principal eigenvalue of the expert opinion matrix, and *N* is the order of the matrix

Shannon Entropy weights

The weight determination for quantitative data obtained from the existing literature was conducted using the Shannon Entropy method. The application of the Entropy method involves utilizing relative information to predict quantitative values, subsequently calculating the

weights [227]. Shannon and Weaver utilized the entropy method to assess the uncertainty of components by employing the information probability function given in Eq. 3.92 [228]. The greater value of the entropy refers to the smaller weight. Another non-probabilistic entropy value was introduced by De Luca and Termini given in Eq. 3.93 [229] which have been utilized in this research to calculate the weights based on the available criterion for sensitivity analysis given in section 8.5.

$$E(px) = -k\sum_{k=1}^{q} p(x)\ln p(x) \tag{3.92}$$

where $E(px)$ is the entropy level, and k is the constant

$$E(\tilde{A}x) = -k\sum_{k=1}^{q} \mu_{\tilde{A}}(x_k)\ln \mu_{\tilde{A}}(x_k) \tag{3.93}$$

where $E(Ax)$ is the non-probabilistic entropy level, and k is the normalized value which is equal to $1/lnq$

d. Advanced CODAS method based on IVFFS

This study introduces a novel methodology involving the integration of IVFFS in CODAS method. The application of this approach aims to rank sustainable valorization processes for MSW, and the details of this integration are outlined in chapter 8. The process brief is structured based on the following sequential steps [230]:

Step 1: Shortlist the group of experts and determine the alternative along with the criterion based on which experts will relatively prioritize the alternatives in term of linguistics term based on the FFS (Eq. 3.94).

$$\varphi_{ij} = \left(\left[\vartheta_{ij}^{-}, \vartheta_{ij}^{+}\right], \left[\sigma_{ij}^{-}, \sigma_{ij}^{+}\right]\right) \tag{3.94}$$

where φ_{ij} is the performance value of i^{th} alternative with reference to the j^{th} criterion for each expert

The significance of weight in determining the ultimate ranking cannot be overstated. This calculation is derived from Section 3.3.10.1 for the AHP and Shannon Entropy.

Step 2: Calculate the expected membership ($MV(\vartheta_j)$) and non-membership ($MV(\sigma_j)$) values of the IVFFS based on the Eq. 3.95 and 3.96.

$$MV(\vartheta_j) = (1-\zeta)\vartheta^L + \zeta\vartheta^u \tag{3.95}$$

where $MV(\vartheta_j)$ is the membership value, ζ is the optimism degree of experts

$$MV(\sigma_j) = (1-\zeta)\sigma^L + \zeta\sigma^u \tag{3.96}$$

where $MV(\sigma_j)$ is the non-membership value

Step 3: Calculate the aggregated value of IVFFS decision matrix.

Step 4: Normalize the aggregated IVFFS decision matrix considering the cost and benefit types of criteria by applying the logic given in Eq. 3.97.

$$\tilde{N} = [\tilde{n}]_{n\otimes m} = \begin{Bmatrix} \left\{\left[\sigma^L, \sigma^u\right], \left[\vartheta^L, \vartheta^u\right], C_j \text{ is cost type}\right\} \\ \left\{\left[\vartheta^L, \vartheta^u\right], \left[\sigma^L, \sigma^u\right] C_j \text{ is benefit type}\right\} \end{Bmatrix} \tag{3.97}$$

where $[\tilde{n}]_{n\otimes m}$ is the normalized IVFFS matrix

Step 5: From the normalized IVFFS matrix, calculate the normalized weighted decision matrix based on Eq. 3.98.

$$\tilde{s}_{ij} = [\tilde{n}]_{ij} \otimes W_j \tag{3.98}$$

where W_j are the weights which are obtained based on AHP and Shannon Entropy with CRITIC for sensitivity analysis based on main criteria weights

Step 6: Calculate the negative ideal solution based on weighted normalized decision matrix as per Eq. 3.99.

$$\tilde{n}_{sj} = \left[\begin{matrix}\min\limits_{i} \vartheta_{ij}^{L}, & \min\limits_{i} \vartheta_{ij}^{u}\end{matrix}\right]\left[\begin{matrix}\max\limits_{i} \sigma_{ij}^{L}, & \max\limits_{i} \sigma_{ij}^{u}\end{matrix}\right], i = 1,2,3...,j \tag{3.99}$$

Step 7: Estimate the weighted Euclidean distances (*Ei*) and weighted Hamming distances (*Hi*) based on the negative ideal solution using Eq. 3.100 and 3.101.

$$E_i = \sum_{j=1}^{m} \sqrt{\left(\frac{1}{4}\left|\vartheta_{sij}^{L} - \vartheta_{nsj}^{L}\right|^2 + \frac{1}{4}\left|\vartheta_{sij}^{U} - \vartheta_{nsj}^{U}\right|^2 + \frac{1}{4}\left|\sigma_{sij}^{L} - \sigma_{nsj}^{L}\right|^2 + \frac{1}{4}\left|\sigma_{sij}^{L} - \sigma_{nsj}^{L}\right|^2\right)} \tag{3.100}$$

$$H_i = \frac{1}{4}\sum\left(\left|\vartheta_{sij}^{L} - \vartheta_{nsj}^{L}\right| + \left|\vartheta_{sij}^{U} - \vartheta_{nsj}^{U}\right| + \left|\sigma_{sij}^{L} - \sigma_{nsj}^{L}\right| + \left|\sigma_{sij}^{L} - \sigma_{nsj}^{L}\right|\right) \tag{3.101}$$

Step 8: Determine the relative assessment matrix (R_m) based on the *Ei* and *Hi* using Eq. 3.102-3.104.

$$R_i = [q_{it}]_{n \times n} \tag{3.102}$$

$$q_{it} = (E_i - E_t) + \psi(E_i - E_t) \times (H_i - H_t) \tag{3.103}$$

$$\psi(x) = \begin{cases} 1 \left|x\right| \geq \rho \\ 0 \left|x\right| < \rho \end{cases} \tag{3.104}$$

where $\psi \in \{1,2,3,...,n\}$ the threshold value of the ρ is taken between 0.01 and 0.05

Step 9: Calculate the final assessment (A_s) score q_{it} of each alternative based on the Eq. 3.105. The alternative with the highest positive value is regarded as the most favorable among all available alternatives.

$$A_s = \sum_{t=1}^{n} q_{it} \tag{3.105}$$

3.3.10.2 Process sustainability index calculation

The process's sustainability index was calculated using four indicators including energy, economics, safety, and biomass waste-based electric power generation (renewable resources). For each scenario, the sustainability index was calculated using Eq. 3.106. By application of Eqs. 3.107-3.111, all metrics (energy, economic, power, and safety norms) have been adjusted to ratios, allowing for a fair comparison of different solutions. As energy efficiency is measured in percentages (%), Eq. 3.107 can be used to convert it to a ratio. The IRR was calculated by multiplying different scenarios process efficiencies to get a percentage (%). Therefore, the IRR was averaged to account for various efficiency features (Eq. 3.108).

The power potential is computed in kW using the procedures described in section 3.8. Hence, it was converted to a ratio by comparing the highest power potential of the scope scenarios to the respective one (Eq. 3.109). Finally, in Eq. 3.110, the safety score was calculated by dividing the corresponding scenario by the greatest possible score and life cycle assessment with Eq. 3.111. Chapter 8 contains the EES calculations.

$$EES = W_1E_1 + W_2E_2 + W_3E_3 + W_4E_4 \ldots + W_nE_n \tag{3.106}$$

where ($0 \leq \text{EES} \leq 1$) W_1 is the weight of energy variable, E_1 is the energy based on Eq. 3.107, W_2 is the weight of economic variable, E_2 is the economic calculation on Eq. 3.108, W_3 is the weight of power potential, E_3 is the power potential based

on Eq. 3.109, W_4 is the weight of safety variable, and E_4 is the safety factor based on Eq. 3.110

$$E_1 = \frac{\eta_e}{100} \tag{3.107}$$

where $\boldsymbol{\eta_e}$ is the energy efficiency of respective scenarios

$$E_2 = \frac{\sum_{i=1}^{n} IRR_i}{n \times 100} \tag{3.108}$$

where $\boldsymbol{IRR_i}$ is the internal rate of return of respective scenarios, and $\boldsymbol{n}$ is the total *IRR* cases included

$$E_3 = \frac{P_i}{P_m} \tag{3.109}$$

where $\boldsymbol{P_i}$ is the calculated power potential of respective scenario, and $\boldsymbol{P_m}$ is the maximum power potential obtained in the scope scenarios

$$E_4 = 1 - \frac{SS_i}{SS_t} \tag{3.110}$$

where $\boldsymbol{SS_i}$ is the obtained safety score of respective scenarios, and $\boldsymbol{SS_t}$ is the maximum possible safety score

$$E_5 = \frac{1}{(\frac{\sum E_{m_i} + \sum E_{e_i}}{i_t}) \times 100 \times \eta_n} \tag{3.111}$$

where $\sum E_{m_i}$ is sum of mid-point indicators score, $\sum E_{e_i}$ is the sum of endpoint (damage impact), i_t is the total number of indicators included, and η_n is the base or the optimized process to the product ratio.

To calculate the weight of these four criteria, the BWM developed by Rezaei (2015) [231] has been used to determine the weights of the criteria. The procedure of this method has been shown in Fig. 3.K.

According to the steps presented in Fig. 3.K as well as the best worst method, the weights can be determined.

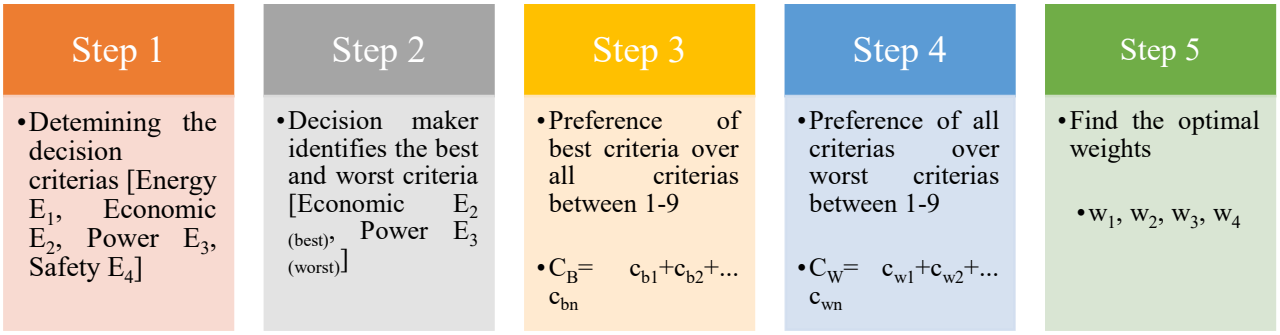

Fig. 3.K Best-worst method criteria for decision making

4 Chapter: HTG-based biomass waste valorization process

HTG is appropriate for high moisture or slurry feedstock type. Aspen software-based simulation model has been developed for HTG analysis. Proximate and ultimate analysis of the biomass type has been used as an input feed material. Simulation parameters like temperature, pressure, biomass concentration and stoichiometry reactions have been taken from the literature. The simulation model has been validated with the experimental study at four different points of temperature.

4.1 HTG process simulation development

The input parameters for the Aspen simulation model, such as biomass proximal, ultimate analysis, temperature, biomass concentration setting was taken from the literature of experimental work. Table 4.1 has the data of proximate and ultimate analysis of PL [232].

Table 4.1 Proximate and ultimate analysis of poultry litter for HTG

Water content		**Proximate analysis** [a]			**Ultimate analysis** [a]				
81.33	Mad	FC	VM	A	C	H	N	S	O[b]
Litter	2.10	9.12	61.94	26.84	33.14	4.41	2.65	0.57	32.39

a. On a dry basis
b. By difference (O%= 100% − Ash% − C% − H% − N% − S%)
FC = fix carbon, VM = volatile matter, A= Ash, C = Carbon, H = Hydrogen, N = Nitrogen, S = Sulphur, O= Oxygen

The HTG simulation model given in Fig. 4.A was developed using the Aspen Plus software. The feed rate of the materials has been set at 0.6:9.4 ratio with 6% biomass and 94% water which is based on the experimental study of poultry biomass [232]. Non-conventional biomass stream properties are obtained from the ultimate and proximate analysis as listed in Table 4.1. Simulation models have been executed at different parameters for validation. Further detailed attributes of the simulation model are given in Table 4.2 [232,233] and its stoichiometric reactions based on fraction conversions are given in Table 4.3.

Table 4.2 HTG simulation model attributes

Simulation Model Properties	
• Method	Peng Robinson
• Unit Set	METCBAR
• Stream Class	MIXCINC
• Phase system	Vapor-liquid
• Enthalpy	HCOALGEN
• Density	DCOALIGT
Operating Parameters	
• Feed Rate	1000 kg/h
• Biomass to Water Ratio	0.6:9.4 (6% and 94%)
• Feed Temperature	30 ºC
• HTG Reactor Temperature	500-620 ºC
• HTG Reactor Pressure	25 MPa
• Reformer Temperature	500-620 ºC

The molecular weights and weightage conversion of the input biomass proximate and ultimate analysis based on experimental study findings were used to calculate the stoichiometric fraction conversion of chemical processes [232]. This fractional conversion which is listed in Table 4.3 has been utilized to compute the yield of the HTG reactor for the RSTOIC reactor. The sum of fraction conversion of BM should be 1.

Reformer reactors have also been added to increase the quality of syngas by raising the fraction of hydrogen gas, bringing the results of this simulation model closer to the experimental investigation. Reaction kinetics were employed in the reformer reactor, which were taken from the literature. The details of these kinetics are given in Table 4.4 [232,234].

Table 4.3 Chemical reactions summary of biomass in HTG

Stoichiometric reaction equation					
Reactants	**R-Coefficient**	**Products**	**P-Coefficient**	**Fraction Conversion of BM**	**Reaction Number**
BM	-1	CH_4	0.062333414	0.1191260	1R
BM	-1	H_2	0.496061273	0.0252391	2R
BM	-1	CO	0.035701025	0.0000100	3R
BM	-1	CO_2	0.022722212	0.5299204	4R
BM	-1	H_2O	0.055508435	0.1330645	5R
BM	-1	BIOCHAR	1	0.1926400	6R

Table 4.4 Chemical reactions kinetics of HTG

Stoichiometric reaction equation				
Reaction	**Rate Constant** (K)	**n**	**Activation Energy** (cal/mol)	**No.**
$1.25C + O_2 \rightarrow 0.5\ CO + 0.75CO_2$	3.7×10^{10}	1	35826.9	R1
$C + O_2 \rightarrow CO_2$	1.78×10^{10}	0	42992.2	R2
$CH_4 + 0.5O_2 \rightarrow CO + 2H_2$	1.58×10^{12}	0	48246.9	R3
$C + H_2O \rightarrow H_2 + CO$	8×10^{-3}	0	11918.4	R4
$CH_4 + H_2O \rightarrow CO + 3H_2$	3×10^{11}	0	29855.7	R5
$C + 2H_2 \rightarrow CH_4$	1×10^{7}	1	19.21	R6

In the simulation model, Peng Robinson Equation of States (PR) method was applied due to its better results when the output is in the form of low molecular weight gases such as CO, CO_2, H_2, and CH_4 [124]. The model has been developed based on Gibbs free energy minimization given in these studies. Following the consolidated Eq. 4.1 and 4.2 for the total Gibbs Energy have been obtained from studies [235,236].

$$Total\ Gibbs\ Energy\ of\ the\ reaction\ (G_T) = \sum_{i=1}^{N} n_i \triangle G_{f,i}^{o} + \sum_{i=1}^{N} n_i\, RT\, ln \frac{n_i}{n_{tot}}. \quad (4.1)$$

where n_i represents the total concentration of mole, $\triangle G_{f,i}^{o}$ is the standardized form of Gibbs free energy formations, and R and T represent general gas constant and temperature, respectively.

By application of Lagranges multipliers method, Gibbs free energy can be minimized as given in Eq. 4.2. In Aspen Plus software, process simulation model has followed these equations for chemical process modeling [235,236].

Using Lagranges multipliers, Gibbs energy can be minimized as given in below equation:

$$\frac{\delta L}{\delta n_i} = \triangle G_{f,i}^{o} + n_i RT\, ln \frac{n_i}{n_{tot}} + \sum_{j=1}^{k} a_{ij} \varepsilon_j \quad (4.2)$$

where ε_j is the Lagrange multiplier, L is the Lagrange function, and a_{ij} represents the *j*-th element in the *i*-th mole of the compound

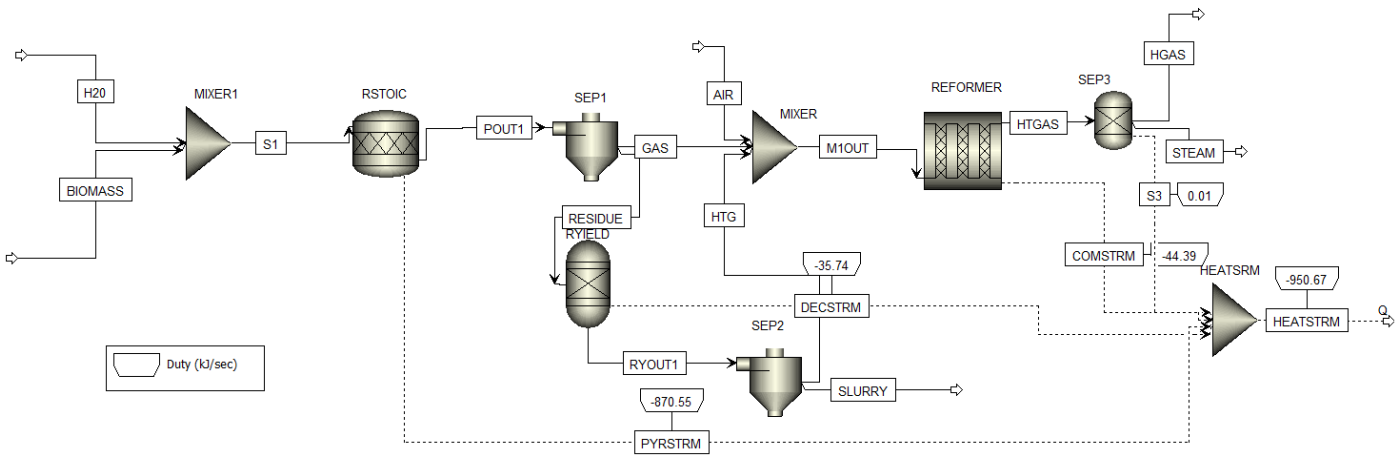

Fig. 4.A Aspen Plus HTG process simulation model

The HTG simulation model shown in Fig. 4.A begins with a 0.6:9.4 input feed of biomass and water into a mixture block that mixes the input material at a typical temperature of 25-30

ºC [11]. To make it more realistic, the output of this mixer was reacted into the primary reactors, which were subdivided into RSTOIC, RYield and reformer. At 500-620 ºC and 25 MPa pressure, the RSTOIC reactor performs the stoichiometry reactivity as shown in Table 4.3. SEP1, separates the generated gas and other residue for recovery in the RYield reactor. As a result, the output from both reactors was fed into the reforming reactor to improve the efficiency of the syngas product reforming by raising the hydrogen gas portion, as shown in the reactions presented in Table 4.4. Finally, SEP3 separates the high-quality syngas and steam produced during the HTG process from the biomass. This steam can be used for multiple purposes such as running turbines for power generation.

4.1.1 HTG process validation

The results in the experimental study [232] has been used to validate the simulation model. The percentage mole fractions of hydrogen, carbon monoxide, carbon dioxide, and

Fig. 4.B HTG process validation with experimental model

methane gases in syngas have been compared, as presented in Fig. 4.B. In addition, RMSE has been calculated. Root means square error percentage of each simulation at respective temperature has been taken using Eq. 3.27 as methodology defined in section 3.3.1. Fig. 4.B shows a point-by-point comparison of experimental and simulation data at four distinct temperatures (500, 540, 580, and 620 ºC). RMSE of the gases at each temperature has been given in the upper right corner of the respective graph in Fig. 4.B. At 500 ºC, it is 2.36%, similarly 0.74 %, 2.28% and 2.70% at 540 ºC, 580 ºC and 620 ºC.

4.2 HTG process optimization and prediction

Multi-objective optimization has been done by application of NLP (nonlinear programing) based problem model which is given in Eq. 4.3.

$$\begin{aligned} &min \quad f(x) \\ &s.t. \quad h_t(x) = 0 \\ &g_m(x) \leq 0 \end{aligned} \tag{4.3}$$

where $f: \boldsymbol{R}^n \rightarrow \boldsymbol{R},\ h: \boldsymbol{R}^n \rightarrow \boldsymbol{R}^t \ and\ g: \boldsymbol{R}^n \rightarrow \boldsymbol{R}^m$ are smooth functions. For solving easier, the nonlinear program (Eq. 4.3) could be replaced by a sequence of barrier subproblems of the form

$$\begin{aligned} &min \quad Z(x,s) = f(x) - \mu \sum_{i=1}^{m} ln\, s_i \\ &s.t. \quad h_t(x) = 0 \\ &g_m(x) + s = 0 \end{aligned} \tag{4.4}$$

where $\mu > 0$ is the barrier parameter and the slack variable s is assumed to be positive. By decreasing values of μ, the sequence of solutions to Eq. 4.4 should normally converge to a stationary point of the original nonlinear program Eq. 4.3.

According to MATLAB function "fmincon" used in this study, the process can be described as follows. The Lagrangian function associated with Eq. 4.5 is defined by [237]

$$L(x, s, \lambda_h, \lambda_g) = Z(x, s) + \lambda_h^T h(x) + \lambda_g^T (g(x) + s) \tag{4.5}$$

where $\lambda_h \; and \; \lambda_g$ are the Lagrange multipliers

The Karush-Kuhn-Tucker (KKT) conditions have been solved to:

$$\frac{\partial Z}{\partial x} = 0 \tag{4.6}$$

$$\lambda_i g_i(x) = 0$$

$$\lambda_i \geq 0$$

$$\lambda_i h_i(x) = 0$$

$$\lambda_i \geq 0$$

The Hessian H of $L(x, s, \lambda_h, \lambda_g)$ is

$$H = \nabla^2 f(x) + \sum_i \lambda_i \nabla^2 g_i(x) + \sum_j \lambda_j \nabla^2 h_j(x) \tag{4.7}$$

The Hessian (H) transforms into a matrix form, which can be solved by any Quasi-Newton methods. If the computation fails, conjugate gradient step is used to solve KKT conditions. It has been determined to minimize a quadratic approximation to the problem $Z(x, s)$ keeping the solution in the trust region. After determining the search direction, the appropriate step size needs to be found. Interior Point Method (IPM) uses a decrease in merit function approach until the final stop tolerance is achieved, where the resulted function is the combination of the objective function with the absolute value of the constraint violation times ν, as presented in Eq. 4.8 [238], if it is a better step or not.

$$Z(x,s) + \nu\|h(x), g(x) + s\| \quad (4.8)$$

where parameter ν may increase with the iterations for feasibility of solution

The maximum number of input variables *K*, as a hyperparameter, defines model complexity. The accuracy of the HDMR surrogate model varies with *K*, which has been explored in order to determine the best parameter *K* in the models for future use. A larger *K* value in the model can cause overfitting. Hence, to avoid overfitting, *K* values for HHV, LHV, NH, H_2, CO_2, and CO remain low. To avoid model overfitting, 10-fold cross-validation approaches were used in this phase. As illustrated in Fig. 4.C.a, increasing *K* greatly enhanced training performance (R^2). According to this, the training of models could get better R^2 when *K* is being increased from 1 to 8 but increasing *K* value also increases the risk of overfitting. Therefore, lower *K* value is better for the prediction model development. Specifically, R^2 for H_2, LHV, HHV, and NH models are greater than 0.95 when *K*=4 which means model can perform better prediction for these output variables. According to Fig. 4.C, the more complicated model (higher *K*) has better fitness (R^2) during the training phase. Hence, the training set was used to assess the model's output performance in terms of MAE, MSE, and percentage mean relative error (%MRE). The increasing *K* values of the test set in MAE (Fig. 4.C.b), MRE (Fig. 4.C.c), and MSE (Fig. 4.C.d) have been examined. Fig. 4.C.b shows that for *K*=5, the H_2, HHV, LHV, and NH models exhibited greater accuracies with MAE lower than 0.05. In Fig. 4.C.c, the MRE of these parameters is less than 3% at *K*=5. Mean square error (MSE) of H_2, LHV, HHV and NH is less than 0.01 at *K=2* which represents the better model performance in term of MSE prediction for these parameters. Therefore, based on Fig. 4.C data, *K=3* has been set for optimal prediction of H_2, HHV, LHV and NH with the lesser risk of overfitting.

To achieve the best prediction results, the dataset was split into test and training sets with 0.25 and 0.75 ratios based on different simulation runs. Fig. 4.C depicts the training performance of these models. The R^2 of these models ranged from 0.90-0.99, indicating that they were all well trained for better prediction. The outcomes of these models are given in Table 4.5. According to these findings, the LHV, HHV, and NH models perform best in the test set, with MAE, MRE, and MSE values ranging from 0.025-0.047, 1.9%-3.5%, and 0.001-0.004, respectively, followed by the H_2 model, which has MAE (0.054), MRE (3.5%), and MSE (0.001-0.004). While the CO and CO_2 model findings are not as good as those obtained by other models, their MAE, MRE, and MSE are around 0.06, 5%, and 0.009, respectively. The highest MRE, about 5% for CO_2 could be due to process parameter variation as shown in Table 4.5, particularly BMR, which has a more significant effect on CO and CO_2 yield than the others. Based on the data, the HDMR model was developed and the indicators MAE, MRE, and MSE were determined from it. The HHV, NHV, and NH models perform better in both training and testing. All models demonstrated remarkable generalization skills. Cross validations of the prediction model were performed using actual data, as shown in Fig. 4.D. The R^2 for the prediction of H_2 is 0.96, and the prediction values verses actual datapoints are quite close to each other in Fig. 4.D.a. Similarly, R^2 for NH, HHV, and LHV are 0.96, 0.99, and 0.99, respectively. The predicted values and actual datapoints for NH, HHV, and LHV are also near to each other, as shown in Fig. 4.D.b, 4.D.c, and 4.D.d, respectively. Therefore, the R^2, MSE, MRE, and MAE values are indicators of the model's predictability. Hence, the predicted values of all models match the simulated values well, demonstrating that the predictive model of these variables is robust.

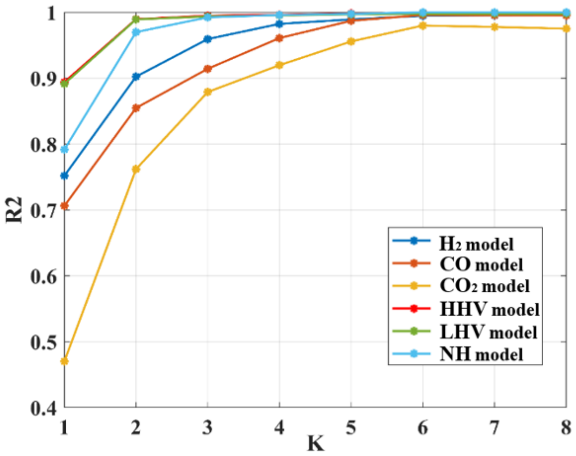

a. R^2 vs. K testing performance

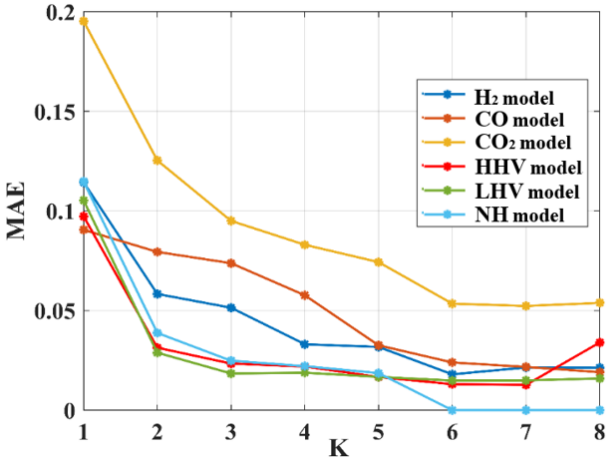

b. MAE vs. K testing performance

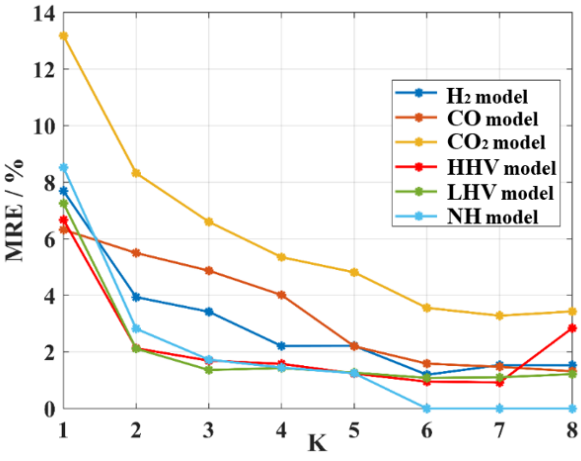

c. MRE vs. K testing performance

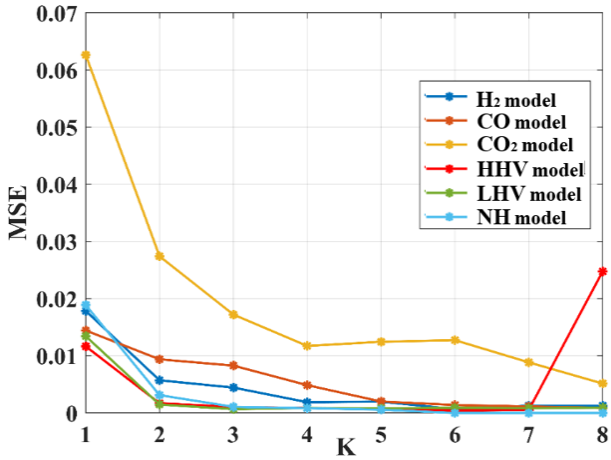

d. MSE vs. K testing performance

Fig. 4.C HDMR model testing performance with respect to K

Table 4.5 HDMR Models test performance summary

Model	MAE	MRE (%)	MSE
H_2 model	0.0540	3.49	0.0048
CO model	0.0522	3.51	0.0043
CO_2 model	0.0774	5.15	0.0093
HHV model	0.0275	2.00	0.0012
LHV model	0.0254	1.90	0.0011
NH model	0.0471	3.46	0.0043

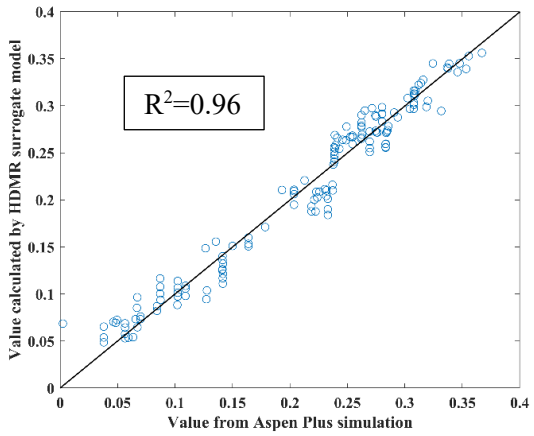

a. HDMR model prediction vs. Actual for H_2

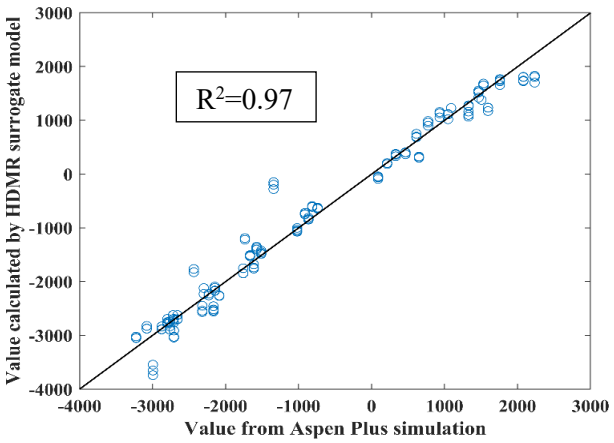

b. HDMR model prediction vs. Actual for NH

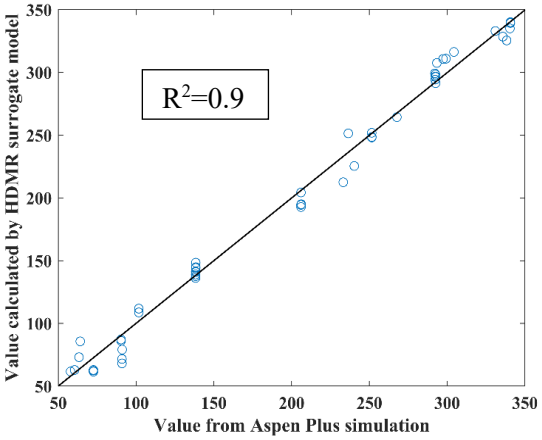

c. HDMR model prediction vs. Actual HHV

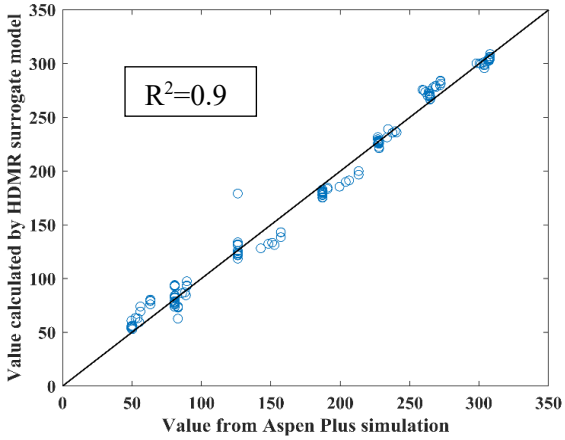

d. HDMR model prediction vs. Actual LHV

Fig. 4.D HDMR model prediction values vs. Actual values

4.2.1 HTG computational models' comparative analysis

For HTG prediction model development, data has been collected considering section 3.2.1.1, then five different models of AI (CNN, ANN, GBR, XGB and RFR) have been applied to predict the four different types of gases (H_2, CH_4, CO_2, and CO) in the syngas. These models have been tested based on R^2, MSE, MAE, and MAPE at three different training testing ratios. CNN model, R^2 values vary from 0.49 to 0.65 for different types of datasets and element. While MSE and MAE of CNN model varies from 0.01-0.03 and 0.07-0.14, respectively. MAPE of CNN model is also high (>20%) with exception of CO_2. For ANN, R^2 values vary from 0.10 to 0.55 for different simulation runs which are quite low for any model. MSE, MAE and MAPE of ANN vary from 0.02-0.04, 0.11-0.15, and 0.9-2.5% with exception of CO where it is >20%. GBR has the better results in terms of R^2, MSE, MAE, and MAPE (Table 4.6). For GBR, R^2 varies 0.75-0.95 which is maximum 0.95 in case of H_2 and minimum in case of CH_4. Similarly, for XGB and RGR, coefficient of determinant varies from 0.81-0.93 and 0.78-90 respectively. The poor performance of CNN and ANN models could be linked to data type and limits, as it is totally quantitative data with high fluctuation, and some researchers suggested CNN and ANN are better suited for subjective datatypes [239]. The number of epochs in NN has also increased to 1000 but it become almost stable after 300. Furthermore, potential cause for the ANN poor prediction results due to gradient descent learning which are susceptible to local minima existence [240]. Results show, regressor models GBR, XGB, and RFR perform better as compared to neural network CNN and ANN models for predicting the output of syngas elements. Especially, XGB model results perform equally better in predicting syngas elements where coefficient of determinant approaches to 0.93, 0.90, 0.85, 0.87 and MAPE 0.4%, 0.7%, 0.4%, 6.9% for H_2, CH_4, CO_2, and CO respectively (Table 4.6). Followed by RFR, as a second-best model among this research study models whose R^2 approaches to 0.90, 0.85, 0.90, and 0.83 for H_2, CH_4, CO_2, and CO respectively. Possible reason could be the quantitative datatype

for which regressor models are more suitable as in previous research, some researchers have applied the regression models which have an optimal result for model prediction [241,242]. But for XGB case, this is the advanced version of the GBR due to which its results are far better than other regressor models. Therefore, based on these results XGB model can be used to predict the syngas output in hydrothermal gasification process.

Table 4.6 CNN, ANN, GBR, XGB, and RFR experimental results comparison for HTG

Model Type	R^2 (90-10)	R^2 (80-20)	R^2 (70-30)	MAPE (90-10)	MSE (90-10)	MSE (80-20)	MSE (70-30)	MAE (90-10)	MAE (80-20)	MAE (70-30)	Element
CNN	0.60-0.65	0.49-0.55	0.59-0.65	>20%	0.01	0.01	0.01	0.09	0.09	0.08	**H_2**
ANN	0.50-0.55	0.34-0.40	0.42-0.46	2.1%	0.02	0.02	0.02	0.11	0.11	0.10	**H_2**
GBR	0.91-0.95	0.79-0.82	0.80-0.85	2.5%	0.004	0.01	0.007	0.05	0.06	0.05	**H_2**
XGB	0.89-0.93	0.82-0.86	0.78-0.82	0.4%	0.005	0.008	0.009	0.05	0.06	0.06	**H_2**
RFR	0.84-0.90	0.75-0.80	0.78-0.82	0.4%	0.007	0.009	0.01	0.06	0.06	0.06	**H_2**
CNN	0.53-0.60	0.45-0.50	0.34-0.40	>20%	0.02	0.02	0.03	0.10	0.11	0.11	**CH_4**
ANN	0.22-0.25	0.10-0.20	0.12-0.20	1.5%	0.03	0.03	0.03	0.12	0.14	0.13	**CH_4**
GBR	0.75-0.80	0.60-0.70	0.57-0.65	1.6%	0.009	0.01	0.01	0.07	0.08	0.08	**CH_4**
XGB	0.85-0.90	0.54-0.65	0.50-0.60	0.7%	0.005	0.02	0.02	0.06	0.11	0.11	**CH_4**
RFR	0.80-0.85	0.75-0.80	0.72-0.80	0.7%	0.01	0.01	0.01	0.06	0.07	0.07	**CH_4**
CNN	0.58-0.63	0.38-0.40	0.31-0.35	0.9%	0.02	0.03	0.03	0.12	0.12	0.14	**CO_2**
ANN	0.23-0.30	0.17-0.25	0.15-0.20	0.9%	0.04	0.04	0.04	0.15	0.15	0.15	**CO_2**
GBR	0.72-0.76	0.79-0.85	0.79-0.85	0.3%	0.01	0.01	0.01	0.08	0.06	0.06	**CO_2**
XGB	0.81-0.85	0.75-0.85	0.69-0.75	0.4%	0.01	0.01	0.01	0.07	0.08	0.09	**CO_2**
RFR	0.86-0.90	0.83-0.87	0.82-0.85	0.3%	0.01	0.008	0.01	0.06	0.06	0.06	**CO_2**
CNN	0.49-0.55	0.56-0.65	0.49-0.55	>20%	0.01	0.02	0.02	0.07	0.09	0.10	**CO**
ANN	0.19-0.25	0.19-0.25	0.17-0.20	>20%	0.03	0.03	0.03	0.12	0.12	0.11	**CO**
GBR	0.76-0.80	0.76-0.82	0.78-0.82	>20%	0.01	0.01	0.01	0.06	0.06	0.05	**CO**
XGB	0.84-0.87	0.68-0.75	0.69-0.74	6.9%	0.007	0.01	0.01	0.05	0.07	0.06	**CO**
RFR	0.78-0.83	0.76-0.82	0.73-0.78	7.1%	0.008	0.01	0.01	0.05	0.05	0.06	**CO**

4.3 HTG process sustainability evaluation

Process sustainability evaluation has been done by energy, economic, and environment life cycle assessment of the process as per procedure defined in section 3.3.8. While process yield performance has been done based on the effect of process parameters such as temperature,

pressure, and resident time on H_2, NH, HHV, and LHV. Process sustainability analysis is given in 4.3 sub-sections.

4.3.1 HTG energy analysis

Energy feasibility analysis of the HTG process has been carried out based on the results of Aspen plus simulation considering section 3.3.2. Energy analysis has been performed based on using one ton of the feed flow (6% BM, 94% water) into the system as the function unit. The reactor has been fed with 3984.9 kilowatt (kW) of energy equivalent biomass, which is processed through the mixer before entering the main reactor. The biomass conversion reaction has taken place in the main reactor. Resultantly, there are certain energy losses in terms of material waste, heat loss, and electricity usage, as shown in Fig. 4.E with outward arrows. Material and heat losses are the two most common types of losses in the main reactor that are not used in the following process. Material loss in the form of sludge residue, which is reprocessed to recover energy, and wastage, which can be used in agriculture. Net biomass efficiency is calculated by subtracting the energy outflows from the intake energy. The overall

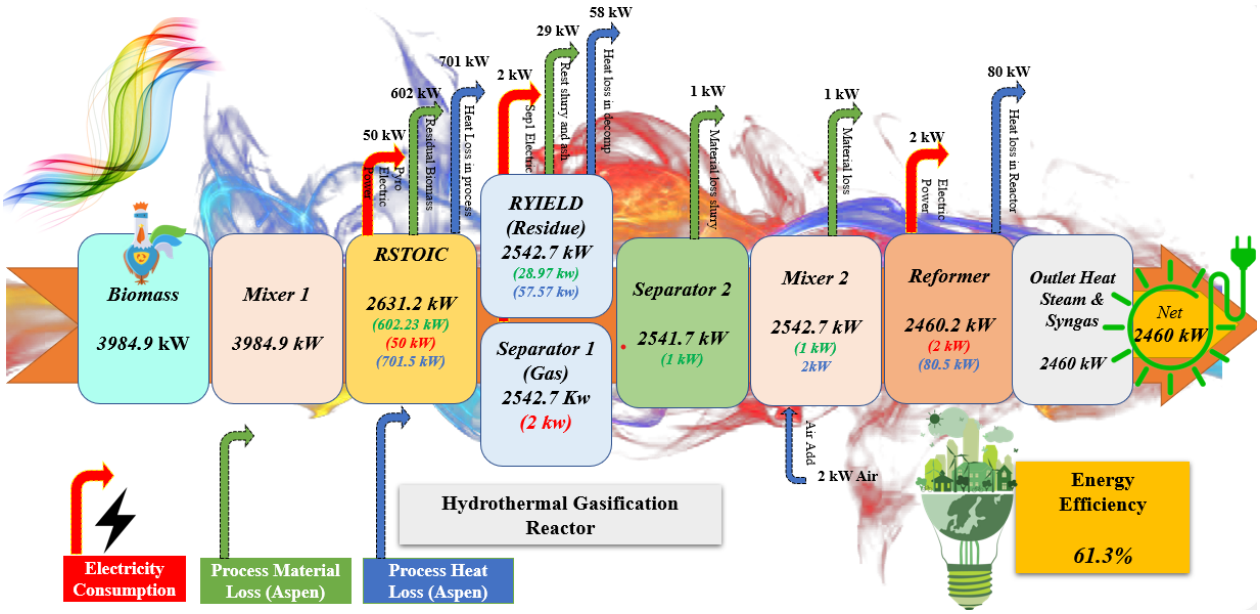

Fig. 4.E HTG process energy analysis

net energy has reduced from 3984 kW to 2460 kW, rest is the loss. Therefore, the overall net energy efficiency of this process is about 61%.

4.3.2 HTG economic analysis

The methodology outlined in section 3.3.7 is used to conduct economic analysis of HTG process. EA is being carried out with a small-scale plant that can be installed on 10,000 square feet of land and produce 5-10 megawatts of electricity. In EA, the cost of the net heat steam produced by biomass has been compared to the cost of other commonly used fuels such as coal, natural gas, and distillate oil. The estimated cost of the plant taken from vendor has been graphically presented in Fig. 4.F [20]. According to EA, equipment and machinery have the major cost around 71% and 14% for shed structure cost, rest are storage, electric, transportation and miscellaneous costs. The cost of land and other regulatory duties are not included in this cost as it varies significantly for different regions.

The cost of steam generation was determined based on both direct and indirect costs into account. Electricity costs, labor requirements, maintenance costs, and overhead costs were taken from the vendor's estimation [20]. The direct cost of materials is obtained from India and Pakistan's local markets. The plant usable life claim by the vendor has been subdivided to obtain simple depreciation cost of the plant, and this cost has been included in this computation,

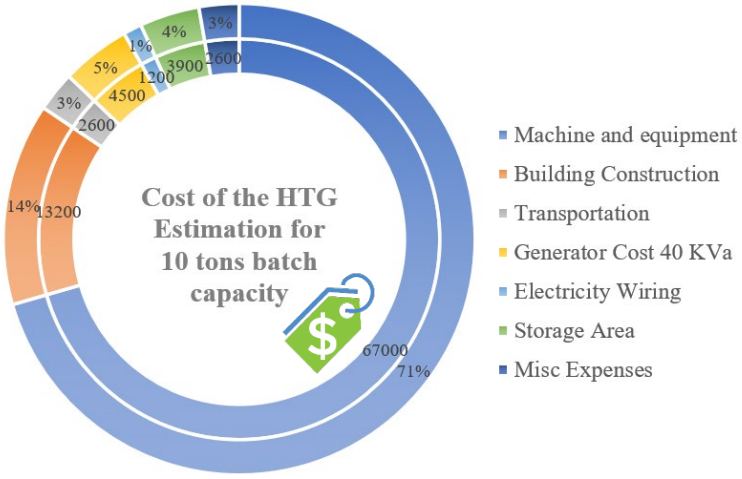

Fig. 4.F HTG capital cost analysis

Table 4.7 HTG Plant operational cost analysis

Utilities	Per day $	Per Month $	% Cost
Electricity Cost	93	2790	13.0%
Operating and Maintenance			
Manpower Cost (Plant Manager 1, Admin 1, Maintenance 1, Operator 6, Watchman 1)	150	4500	21.0%
Maintenance	90	2700	12.6%
Overhead Cost	50	1500	7.0%
Poultry litter price (10 × 2 tons)	200	6000	28.0%
Handling transportation cost	100	3000	14.0%
Depreciation Cost			
Plant depreciation/day (10 yrs.)	32	960	4.5%
Cost based on 20 tons biomass per day treatment	**715**	**21450**	

which is equal to 715 $ for 20 tons of poultry waste conversion. Raw material, transportation and manpower have the major monthly operational costs of this HTG plant which is around 63% as per Table 4.7.

Steam generation cost calculation methodology proposed by the United States Department of Energy has been used to calculate the cost of steam. Heat steam cost is determined by the factors, including the per unit price of fuel (natural gas, coal, distilled oil), fuel energy content, and percentage combustion efficiency, which is being calculated using boilers with feedwater economizers or air preheaters and considering, 3% oxygen in the flue gas. This is summarized in Eq. 4.9 and 4.10 [243] while the prices of natural gas, coal and distilled fuel have been taken from the international market [244]. These values have been used to calculate the steam cost per 1000 pounds.

$$\textbf{Steam Cost per lbs } (S_c) = \left(\frac{P_c \times 1006}{E_c \eta}\right) \tag{4.9}$$

$$\textbf{Steam Cost per 1000 lbs} = S_c \times 1000 \tag{4.10}$$

where, P_c fuel price per MMBTU, E_c fuel energy content BTU/sales unit, η fuel combustion efficiency

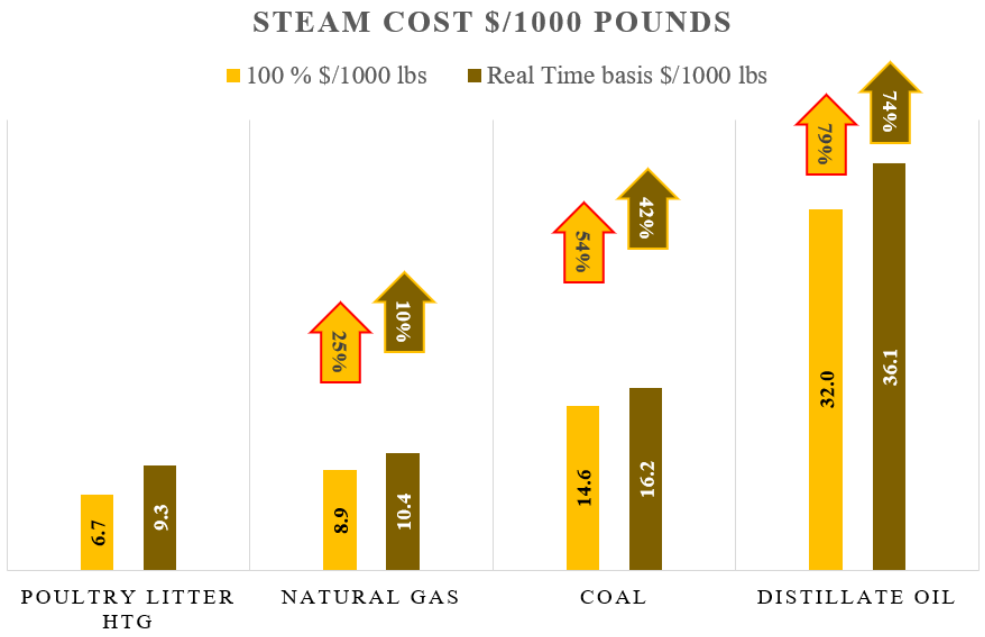

Fig. 4.G. Steam cost from HTG process

The cost of steam for coal, natural gas, and distillate oil has been calculated at both 100% and real-time basis efficiency which is assumed 60% of the calculated output. In Fig. 4.G, the cost of steam is shown as $/1000 lbs. In both 100% and real-time basis efficiency, poultry litter-based HTG has the lowest cost when comparing with other energy sources such as natural gas, coal, and distillate fuel. PL HTG process has 25%, 54%, and 79% lower cost of steam as compared with natural gas, coal, and distilled oil at 100% efficiency, respectively. While PL based HTG process has the 10%, 42%, and 74% lower cost of steam generation as compared with natural gas, coal, and distilled oil at real time basis efficiency, respectively [22]. The natural gas process is quite economical as compared with coal and distilled oil, but it is still

10% more costly as compared with PL HTG process, as illustrated in Fig. 4.G. Therefore, PL HTG process is more economical as compared with natural gas, coal, and distilled oil.

4.3.3 HTG environment life cycle assessment (LCA)

Environmental impacts of the poultry waste by comparing direct land disposal and HTG process treatment as per method defined in section 3.3.8. In Figs. 4.H.a, 4.H.b, and 4.H.c, LCA results are shown in the form of a midpoint, normalized endpoint, and single score comparison between direct land disposal and syngas high energy steam (HTG). The midpoint impact category represents the short-term environmental impact, but the endpoint impact category is primarily concerned with the long-term environmental impact on human health, ecosystem quality, climate change, and resources, all of which are derived from the midpoints [245]. The lower the percentage (%) and point (µPt) values in Figs. 4.H, represents the better the environmental performance. Therefore, the midpoints impact in Fig. 4.H.a shows that land disposal has a higher environmental impact in terms of respiratory organics, respiratory inorganics, terrestrial acidification, aquatic ecotoxicity, and aquatic acidification as compared to HTG (syngas generation), whereas land disposal results are better in terms of carcinogens, ionizing radiation, ozone layer depletion, and aquatic ecotoxicity. But these are short-term consequences caused mostly by a few specific characteristics.

End point category results reveal that land disposal has a negative long-term environmental impact, which can have an influence on human health, ecosystem quality, and climatic change. HTG has a 66% better performance in terms of human health than direct land disposal. Similarly, HTG has a better environmental performance than land disposal in terms of ecosystem quality and climate change. Although, some impact points in the HTG midpoints impact category, such as mineral extraction, non-renewable energy, aquatic ecotoxicity, and so on, have higher results than land disposal, the result of the single score Fig. 4.H.c HTG with 250 µPt and land disposal with 360 µPt shows that direct land disposal of biomass waste is

more environmentally damaging. Based on this environmental analysis, it can be concluded that the HTG process for syngas high energy steam generation is more environmentally friendly than direct land disposal. The LCA results of this investigation supported the LCA research of Raaj R. Bora et al. 2020 [210].

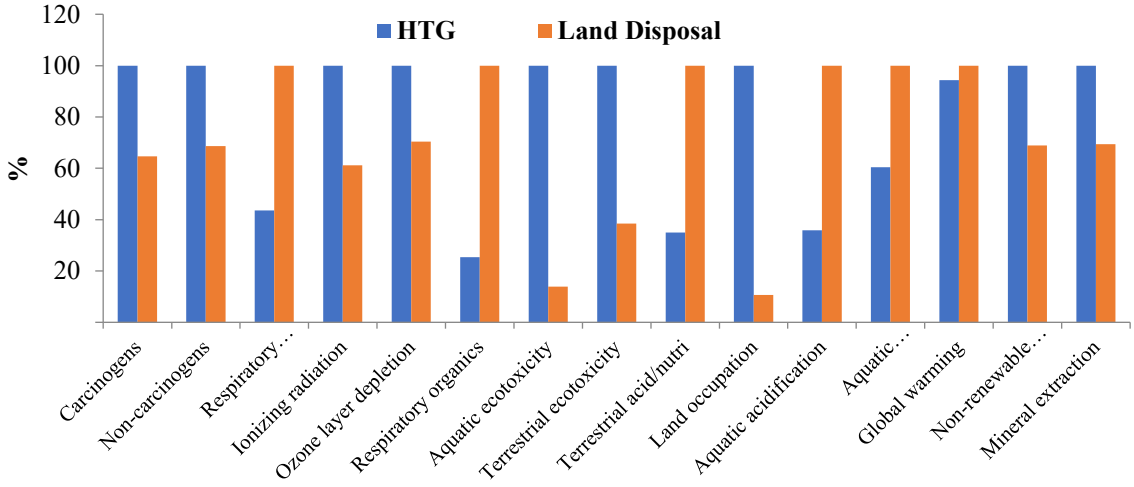

(a) Midpoint based environmental impact (%)

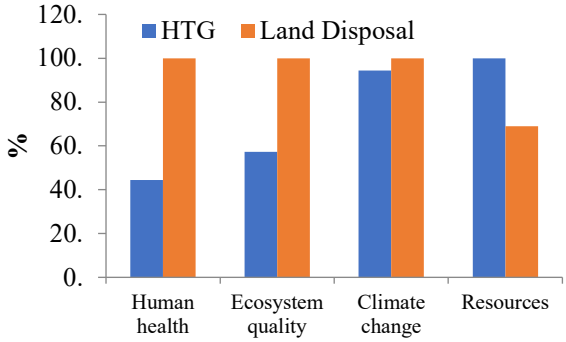

(b) Endpoint based impact (%)

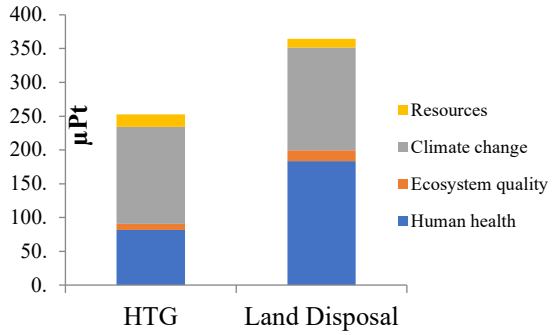

(c) Single Score/Method: IMPACT 2002+

Fig. 4.H LCA Comparative Results

4.4 Conclusion: HTG

In this chapter, the HTG simulation model has been used to analyze the production of syngas, particularly hydrogen, methane, carbon dioxide gas, and heat steam. The effect of three independent parameters including temperature, pressure, biomass concentration in feed has been analyzed using this model. Following the key findings of this case study:

- HTG process has better quality of syngas with highest mole fractions of hydrogen and methane at 540 ^{o}C temperature, 20-25 MPa pressure, and 20% biomass concentration in the feed.
- LCA results show that HTG method is environmentally friendly as compared to direct land disposal especially in term of human health, ecosystem quality and climate change.
- HTG is also an energy and cost-effective conversion method with a net energy efficiency of about 61%, and at least 10% cheaper steam production using natural gas, coal, or distillated oil.
- The economic analysis is restricted to the production of heat steam, which may then be used to generate electricity via a steam turbine generator. Similarly, this process is economical and energy-efficient, but the life cycle assessment of this process is not conducted in this research which will be done in future study. AI-based prediction models performance conclude, XGB model is better with coefficient of determinant from 0.85-0.95 and lower MSE, MAE, and MAPE for H_2, CH_4, CO_2, and CO [246].
- Correlation analysis results show that mole fractions of hydrogen, methane, and carbon monoxide can be increased by using biomass having more hydrogen and oxygen in ultimate analysis.
- Increasing temperature and biomass resident time in the gasification process can also increase the mole fractions of H_2 and CH_4 in final syngas.

Therefore, XGB algorithm model can be used to predict the HTG output in actual environment without being development of complex simulation models and experimental setups because it outperformed rest of the algorithms in the research scope to predict the amount of H_2, CH_4, CO_2, and CO in the syngas. Similarly, HDMR model training performances (R^2) are 0.96, 0.97, 0.99, and 0.99 for H_2, NH, HHV, and LHV, respectively which indicates the less error in predicting output. Although the HTG-based process is

sustainable for high moisture or slurry biomass, severe process parameters such as high pressure make the process less reliable and difficult for stakeholders. Furthermore, it is only applicable to slurry or high moisture biomass. Therefore, other valorization processes can be used to solve the issues outlined in the next section.

5 Chapter: Gasification based poly-generation process

Primary biomass waste gasification process has been integrated with the secondary or tertiary processes in this chapter to increase the overall sustainability. Different secondary and tertiary processes integrations have been evaluated in this section. This is the advanced integration of previous chapter 4 to valorize the biomass waste in a sustainable manner.

5.1 Gasification based poly-generation process simulation development

The gasification process simulation model has been developed for biomass waste valorization which has been further extended to secondary and tertiary processes are defined in below section 5.1.1.

5.1.1 Process G1: Tri-generation process for gasification to SOFC, and CHP

Integration of another secondary process with primary process has been developed to make process more sustainable. For this, a schematic diagram of the methods used in this investigation has been given in Fig. 5.A. In the current tri-generation process, the Aspen Plus simulation software was used to create a hybrid process simulation model that includes primary gasification process along with secondary solid oxide fuel cell (SOFC). Experimental study was used to validate the primary simulation model. To obtain data for AI-based prediction, a validated version of the simulation was utilized to run the multi-level factorial design. A total of 1372 simulations run data were collected from the validate model using a multi-level factorial approach. This simulation data was utilized as an input for the creation of an AI model for prediction and optimization as described in section 3.2. Ultimately, the Aspen Plus simulation model was used to obtain the energy flow values needed to perform exergy analysis.

Gasification is the primary process 1, with auxiliary processes such as cyclones for solid particle removal, gas separators with filtration, and scrubbers to separate gases for hydrogen production as given in Fig. 5.A. In process 2, hydrogen is fed into a SOFC for direct conversion

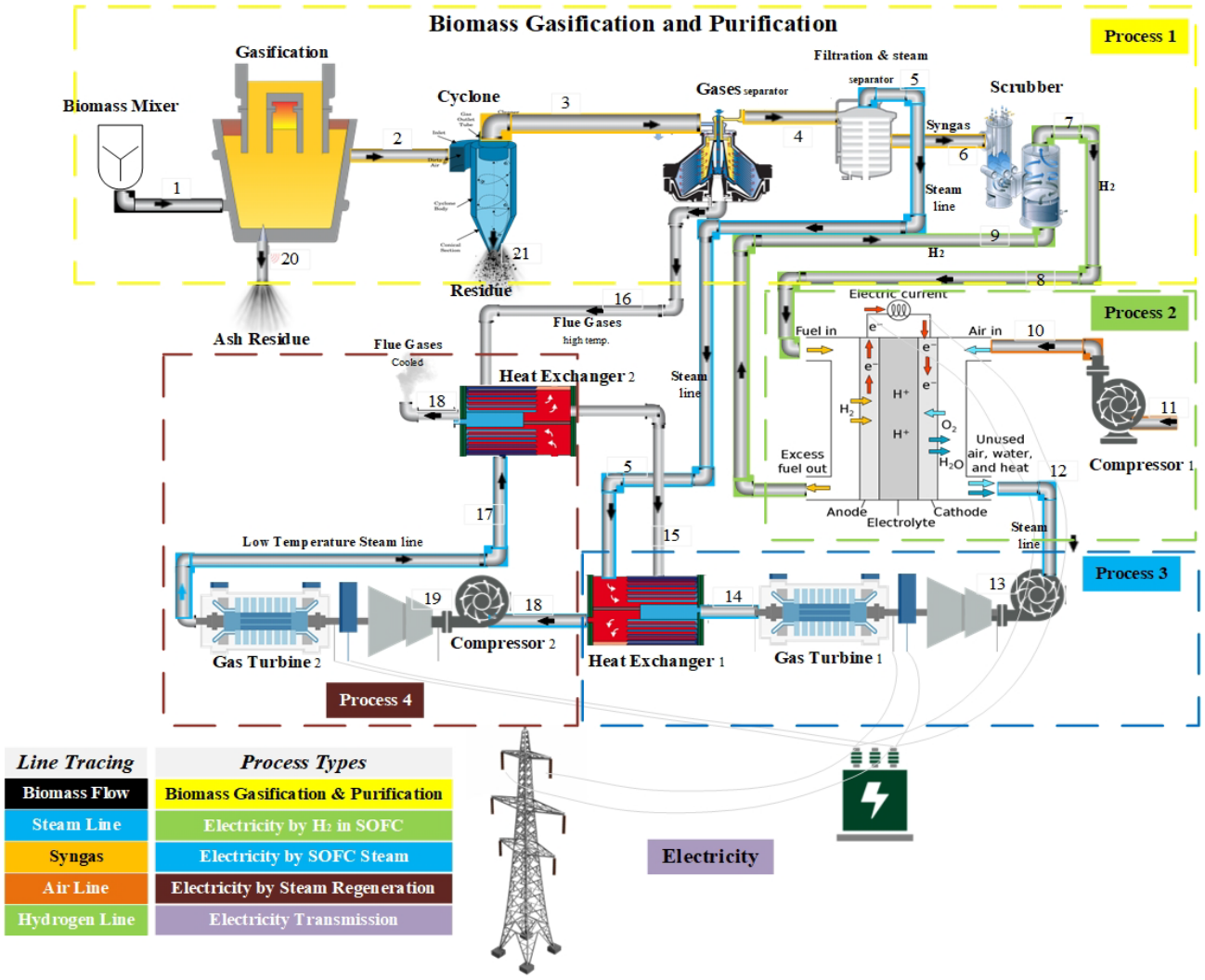

Fig. 5.A Gasification, SOFC, and CHP based tri-generation process

to power via an oxidation reaction, while some excess hydrogen gas is extracted from the SOFC's output side which is added back into the hydrogen stream. In SOFC, hydrogen reacts with oxygen to release electrons as a result of the redox reaction between H_2 and O_2, as well as the formation of high temperature (800 ^oC) steam that is passed into the thermos-compressor to boost its kinetic energy. In process 3, this high-temperature steam is used in a steam turbine to generate electricity. While steam from previous operations is combined with exiting steam for heating and power generation by a heat exchanger and thermos-compressor before being used in the second steam turbine for power generation. Hence, the valorization of biomass waste tri-energy generation has been done through primary gasification, SOFC, and a combined heating process.

Aspen Plus is a simulation model for biomass gasification and solid oxide fuel cells. In this simulation, certain assumptions have been made, such as the amount of fuel (hydrogen) and electron emission due to the oxidation process at SOFC, which is the key behind the working concept. Hence, these two factors were considered while determining power (current and voltage). Other materials, such as electrolytes, have not been considered. Striugas et al. 2014 [247] established a primary gasification technique for biomass. Proximal and ultimate analysis (Table 5.1) of biomass was used as a non-conventional material in the simulation method. The Aspen Plus gasification simulation model was developed using the Gibbs free energy minimization approach [236,248,249] which has been summarized in Table 5.2. The Peng Robinson equation of state model was chosen for the gasification process because PR is a good model if the ultimate product output is light gases such as H_2, CO, CO_2, H_2S, and N_2 [124]. The remaining parameters, such as stoichiometric data, feed rate, temperature, pressure, and BMR, were obtained from the literature [247,250,251]. Therefore, a gasification and SOFC model based on the data supplied in Tables 5.2 has been built, as shown in Appendix A4 model. This simulation procedure began with biomass input in RStoic reactor with determined reaction stoichiometry and specified temperature and pressure. The non-conventional biomass stream reacted in the RStoic reactor, and SEP1 separated the biomass into a gas mixture and a residue solid, which was then processed. Gases from the RStoic reactor are transferred to the RPlug, where they are mixed with air in the necessary ratio to carry out combustion and reduction activities [70]. Eventually, syngas reforming was performed to make this simulation process more realistic and to obtain higher quality syngas with a larger percentage of H_2. The final gas is a mixture of H_2, steam, carbon oxides, and a trace of higher hydrocarbons. Hydrogen gas is separated and transferred into the SOFC's anode, while air from the cathode side reacts to generate water and power through electron release in the oxidation reaction [92].

Table 5.1 Proximate and ultimate analysis of poultry litter for process G1

	Proximate analysis [a]				Ultimate analysis [a]				
Poultry Litter	Moisture	VM	FC	A	C	H	S	N	O[b]
	7.6	63.6	15.3	13.5	43.98	5.16	0.75	4.63	31.98

a. Dry basis
b. Based on difference (O%= 100% − H% − C% − N% − S% − Ash%)
FC = fix carbon, VM = volatile matter, A= Ash, C = Carbon, N = Nitrogen, H = Hydrogen, S = Sulphur, O= Oxygen

Table 5.2 Attributes of the Gasification-SOFC based simulation model (Process G1)

Simulation Model Properties	
• Method	Peng Robinson Equation of State (PR)
• Stream Class	MIXCINC
• Density	DCOALIGT
• Enthalpy	HCOALGEN
• Phase system	Vapor-liquid
Simulation Model Operating Parameters	
• Feed Rate	1000 kg/h
• Reactors Pressure (bar)	1-4
• Biomass to Air Ratio	0.25-4.00
• Reactors Temperature	400-1000 ºC
• SOFC Pressure (bar)	1-4
• SOFC Temperature	400-1000 ºC

5.1.1.1 SOFC output calculations

The tubular SOFC system is an advanced technology with commercialization potential. For output calculations, a similar 120 kW tubular SOFC model manufactured by Siemens Power Generation Inc. was employed in this study. The same model has been employed by different researchers in different studies [98,252]. While ion transfer is not achievable using this simulation model, the current simulation model used the same methods to reproduce the SOFC simulation in Aspen Plus. Therefore, the following full reaction (5.3) has occurred at anode [92]:

Water gas (reformer): $CO + H_2O \rightarrow CO_2 + H_2$ (5.1)

Complete Reaction (SOFC): $H_2 + 0.5O_2 \rightarrow H_2O$ (5.2)

Molar flow of hydrogen to oxygen: $nH_{2,\,cons} = 0.5nO_{2,\,cons}$ (5.3)

The important factor here is the modification of incoming air (O_2) for better efficiency and proper SOFC use. The molar flow of H_2 on the anode side and O_2 on the cathode side should be regulated according to a 2:1 ratio. If air is utilized on the cathode side, the air molar flow must be adjusted proportionately. H_2, cons are calculated using the fuel utilization factor (U_f), and then nO_2, cons are modified using Eq (5.3).

Voltage calculation has been done by calculating the ideal voltage V_{id} at standard potential and pressure of the SOFC. Ideal voltage V_{id}, and actual voltage V_{act} has been calculated by omitting the wastages from the Nernst voltage (V_{Nr}) by incorporating the Activation, Ohmic, and Concentration losses at cathode and anode of the SOFC as given in Eq. 5.4-5.13 while current and current density is being calculated using Eq. 5.14-5.17 [253,254]. Ideal voltage is dependent on the Gibbs free energy formation $-\triangle g_f$ and the Faraday's constant (F) which is equal to 96485 Coulomb/mol. Finally, Eq. 5.13 represent the V_{id}, where factor 2 in respective equation represents the number of electrons moles release in the anode half of the SOFC. For each water molecule formation as per Eq. 5.3, two electrons have been released for each reaction. Therefore, for one mole of water formation according to Eq. 5.2, releases two moles of the electrons. V_{Nr} is the equilibrium or reversible potential which is closer to the actual cell voltage as compared to V_{id}. V_{Nr} is being calculated using Nernst equation which is Eq. 5.12. This equation shows, how V_{id} is dependent on the gas concentration and pressure etc. where R̈ is the general gas constant 8.314 J/mol. K, and T is the average temperature (K) of outlet and inlet stream of SOFC. P_o is the reference pressure (1 bar) while P_i is the partial pressure of each species which is being computed based on inlet and outlet

streams at the anode and cathode. The rest of the parameters have been defined in respective Eq. 5.14-5.17. SOFC parameters values have been taken from research studies which have been used for Siemens Power Generation Inc. SOFC model [92,98,252]. SOFC actual voltage, ideal voltage, current, current density etc. calculations have been done using Eq. 5.4 to 5.17. Equation-wise calculations have been given in Appendix A5.

Voltage Activation Losses (A=Anode, C=Cathode)

Voltage activation loss in terms of resistance at SOFC anode is being determined by Eq. 5.4. [92,98,252]

$$\frac{1}{\ddot{\mathrm{R}}_{A,A}} = \frac{2FK_{AN}}{\ddot{\mathrm{R}}_g T_{op}} \left(\frac{P_{H_2}}{P^o}\right) m_{exp} \left(\frac{-E_{AN}}{\ddot{\mathrm{R}}_g T_{op}}\right) \tag{5.4}$$

where $\ddot{\mathrm{R}}_{A,A}$ is the specific resistance of anode, F= Faraday's constant, K_{AN} are the pre-exponential factor of anode, $\mathrm{P_o}$ is the reference pressure (1 bar), $\mathrm{P_i}$ is the partial pressure of each species, E_{AN} is the activation energy of anode, $\ddot{\mathrm{R}}_g$is the general gas constant, T_{op} is the operating temperature, and m is slope.

Voltage activation resistance due to cathode activation at SOFC is determined by Eq. 5.5. [92,98,252]

$$\frac{1}{\ddot{\mathrm{R}}_{A,C}} = \frac{4FK_{CA}}{\ddot{\mathrm{R}}_g T_{op}} \left(\frac{P_{O_2}}{P^o}\right) m_{exp} \left(\frac{-E_{CA}}{\ddot{\mathrm{R}}_g T_{op}}\right) \tag{5.5}$$

where $\ddot{\mathrm{R}}_{A,C}$ is the specific resistance of cathode, K_{CA} are the pre-exponential factor of cathode, $E_{CA}$is the activation energy of cathode.

Voltage Ohmic Losses (A=Anode, C=Cathode)

Voltage Ohmic losses due to anode activation at SOFC is determined by the Eq. 5.6. [92,98,252]

$$V_{O,A} = \frac{j\rho_{AN}(A\pi D_{mA})^2}{8t_A} \tag{5.6}$$

where $V_{O,A}$ is the ohmic loss of anode, j is current density, ρ_{AN} is the anode resistance, A ohmic loss, D_{mA} is cell average diameter (m), t_A anode thickness (m).

Voltage Ohmic losses due to cathode activation at SOFC are determined by the Eq. 5.7. [92,98,252]

$$V_{O,C} = \frac{j\rho_{CA}(\pi D_{mA})^2 A[A + 2(1 - A - B)}{8t_C} \tag{5.7}$$

where $V_{O,C}$ is the ohmic loss of cathode, j is current density, ρ_{CA} is the cathode resistance, A and B ohmic loss, D_{mA} is cell average diameter (m), t_C cathode thickness (m).

Voltage interconnection Ohmic losses has been determined by Eq. 5.8 [92,98,252] which is being used to calculate the actual voltage.

$$V_{O,Int} = \frac{j\rho_{Int}t_{Int}(\pi D_{mA})}{W_{Int}} \tag{5.8}$$

where $V_{O,Int}$ is the ohmic loss of interconnection, j is current density, ρ_{Int} is the interconnection resistance, D_{mA} is cell average diameter (m), t_{Int} interconnection thickness (m), $W_{Int}$is the width of *Int.*

Voltage Ohmic loss of electrolyte is determined by Eq. 5.9 [19, 32, 44]

$$V_{O,E} = j\rho_E t_E \tag{5.9}$$

where $V_{O,E}$ is the ohmic loss of electrolyte, j is current density, ρ_E is the electrolyte resistance, t_E electrolyte thickness (m).

Voltage Concentration Losses (A=Anode, C=Cathode)

Voltage concentration losses at anode is determined by Eq. 5.10 [19, 32, 44]

$$V_{C,A} = \frac{\mathrm{R\!\!\!^{\circ}}_g T_{op}}{2F} ln\left[\frac{1-(\mathrm{R\!\!\!^{\circ}}_g T_{op}/2F)(t_A/D_{A,eff}\, y^0_{H_2} P_{SOFC})J}{1+(\mathrm{R\!\!\!^{\circ}}_g T_{op}/2F)(t_A/D_{A,eff}\, y^0_{H_2O} P_{SOFC})J}\right] \tag{5.10}$$

where $\mathrm{R\!\!\!^{\circ}}_g$is the general gas constant, F= Faraday's constant, P_{SOFC} is the pressure in SOFC, T_{op} is the operating temperature, $D_{A,eff}$ is the diffusion co-efficient of anode, $t_A$is anode thickness, $y^0_{H_2}$ is average H_2 molar fractions, $y^0_{H_2O}$ is average H_2O molar fractions.

Voltage concentration losses at cathode is determined by Eq. 5.11 [92,98,252]

$$V_{C,C} = \frac{\ddot{\mathrm{R}}_g T_{op}}{4F} ln \left[\frac{(^{P_{SOFC}}/_{\delta_{0_2}}) - [(^{P_{SOFC}}/_{\delta_{0_2}}) - y^0_{H_2} P_{SOFC}] exp[(\ddot{\mathrm{R}}_g T_{op}/4F)(\delta_{0_2} t_C / D_{C,eff} P_{SOFC}}{y^0_{O_2} P_{SOFC}} \right] \quad (5.11)$$

where $\ddot{\mathrm{R}}_g$ is the general gas constant, F= Faraday's constant, P_{SOFC} is the pressure in SOFC, T_{op} is the operating temperature, $D_{C,eff}$ is the diffusion co-efficient of cathode, t_C is cathode thickness, $y^0_{H_2}$ is average H_2 molar fractions, δ_{0_2} is oxygen density.

Nernst voltage is determined by Eq. 5.12 [19, 32, 44] by including the ideal voltage

$$\text{Nernst voltage } V_{Nr} = V_{id} + \frac{\ddot{\mathrm{R}}T}{2F} ln \frac{P_{H_2O} P^{0.5}_{O_2}}{P_{H_2O}} \quad (5.12)$$

where $\ddot{\mathrm{R}}$ is the general gas constant, F= Faraday's constant, V_{id} is ideal voltage, P_{H_2O} is the pressure of H_2O, P_{O_2} is the partial pressure of oxygen.

Ideal voltage of SOFC is determined by Eq. 5.13 which is primarily based on the Gibbs free energy formation of the used fuel in SOFC [92,98,252]

$$\text{Ideal voltage } V_{id} = \frac{-\triangle g_f}{2F} \quad (5.13)$$

where $-\triangle g_f$ Gibbs free energy formation, F= Faraday's constant.

Current generated by the SOFC is mainly dependent on the concentration of the fuel (H_2 gas) which is calculated by Eq. 5.14. [92,98,252]

$$\text{Current generated by SOFC } (I) = 2F(H_{2,cons} \times \frac{1000}{3600}) \quad (5.14)$$

where I is the current, F= Faraday's constant, and $H_{2,cons}$ is hydrogen concentration.

SOFC current density of the SOFC is dependent on the current produced per unit active areas of SOFC which can be determined by Eq. 5.15 [92,98,252]

$$\text{Current Density by SOFC } (J) = \frac{I}{A} \quad (5.15)$$

where current generated by SOFC (I) and A is the SOFC active area.

Actual voltage generated by the SOFC is determined by the ohmic, activation, and concentration losses subtraction from the Nernst voltage using Eq. 5.16. [92,98,252]

$$V_{act} = V_{Nr} - (V_o + V_a + V_c) \tag{5.16}$$

V_{act} actual voltage of the SOFC, V_o ohmic voltage lose, V_o activation voltage losses, and V_c concentrate voltage losses.

The direct current power of the SOFC is the product of actual voltage and current generated by SOFC which is determined by Eq. 5.17. [92,98,252]

$$DCP = V_{act} \times I \tag{5.17}$$

DCP represents Direct Current Power, V_{act} is actual voltage of the SOFC, $and\ I$ is current generated by SOFC.

5.1.1.2 Process G1 validation: Gasification to SOFC, and CHP

The root means square error with experimental study [247] was calculated to validate the basic gasification simulation model as procedure defined in section 3.3.1. Figure 5.B shows a bar graph comparing mole fractions and RMSE. For H_2, CO_2, CO, CH_4, and N_2, the RMSE of the gasification simulation result is 1.56%. Whereas the SOFC's current density (J) and actual voltage (V_{act}) are compared with previous research [98,255], which is also shown in bar graphs in Fig. 5.B. The present gasification and SOFC simulation findings differ slightly from

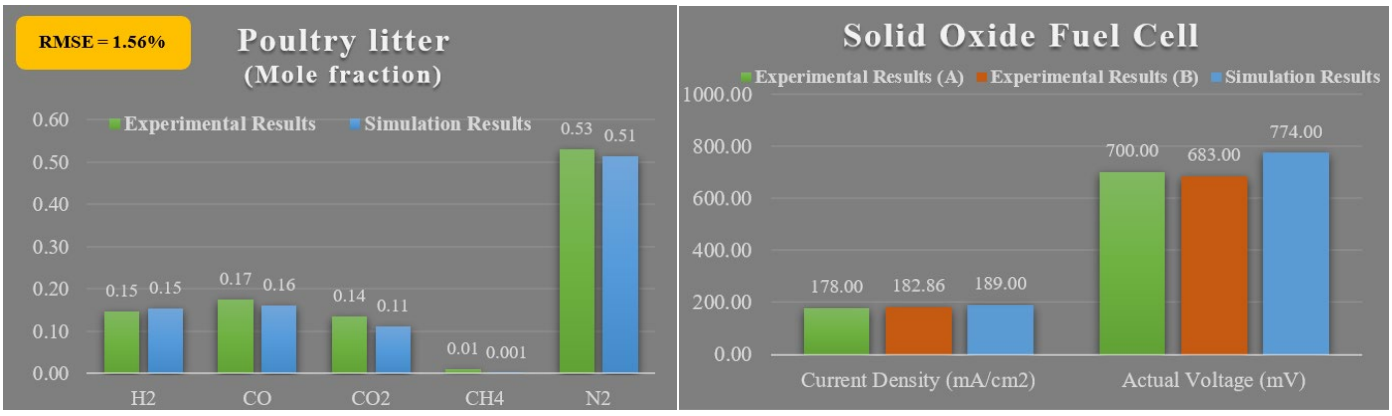

Fig. 5.B Validation of process G1 model

the reference studies; possible causes for this difference include feedstock kinds and new process usage for the gasification and SOFC.

5.1.2 Process G2: Tri- generation through gasification, DME, and CHP

A schematic representation of the tri-generation process for PL valorization through gasification to DME and CHP is illustrated in Fig. 5.C based on the work of Iaquaniello *et al.* (2017) and Salman *et al*. (2018) [93,94]. Primary process was the gasification of PL, starting with the pre-drying of biomass. In the pre-drying process, it was assumed that the moisture content (MC) was completely removed from the biomass via evaporation. This high-energy MC was utilised in the steam reforming of syngas. The dried PL was transferred into the main gasifier, where the gasification of the PL was performed in the presence of a gasifying agent (air) with an equivalence ratio of ~0.25–0.30 (Ramzan et al., 2011; Striugas et al., 2014) at high temperature (600–800 °C). In the gasifiers, PL was converted to syngas and a small amount of ash [257]. The ash particles were separated upon application of a cyclone and the refined syngas passed through the filters, which removed other unwanted elements. Finally, the refined syngas was mixed with steam for the reforming process, which improves the quality of syngas by converting CH_4 into H_2 and CO. The temperature of the reformed syngas (800 °C) was reduced to 220 °C using a heat exchanger (HXC1) prior to further reaction in the continuous stirrer reactor (RSCTR1), which transfers heat into high-temperature steam to run the turbine for power generation. Syngas was converted into methanol along with fractions of residual syngas. The temperature of the reactant mixture in the continuous stirrer (RSCTR1) was further reduced using a heat exchanger (HXC2) for the separation of the liquid and gas phases. Methanol was recovered in the liquid phase and dehydrated to obtain DME in RSCTR2 in secondary process. Both DME and methanol were separated, and the remaining gas phase was sent back to the cyclone, where it was further recovered to obtain a high yield of DME and methanol. The thermal energy recovered by reducing the syngas temperature from 800 to 220

°C and RSCTR2 was used to generate electricity through a steam turbine generator in tertiary process. A detailed description of this process is given in below.

The PL valorization process for gasification and DME production was simulated using Aspen Plus. This was a reaction kinetics and equilibrium-based simulation process, which can be divided into three different processes. The first process was the gasification of PL biomass to produce syngas, which can be further reformed to produce methanol in the second process. Finally, methanol was dehydrated to obtain DME, which is refined using continuous stirrer reactors to obtain high-purity DME in the third process. The following assumptions have been considered in this process:

- It is a steady state process.
- It is an isothermal system assuming the temperature remains constant in the reactor throughout the process [256]
- No sulphur and nitrogen compounds are produced in syngas.

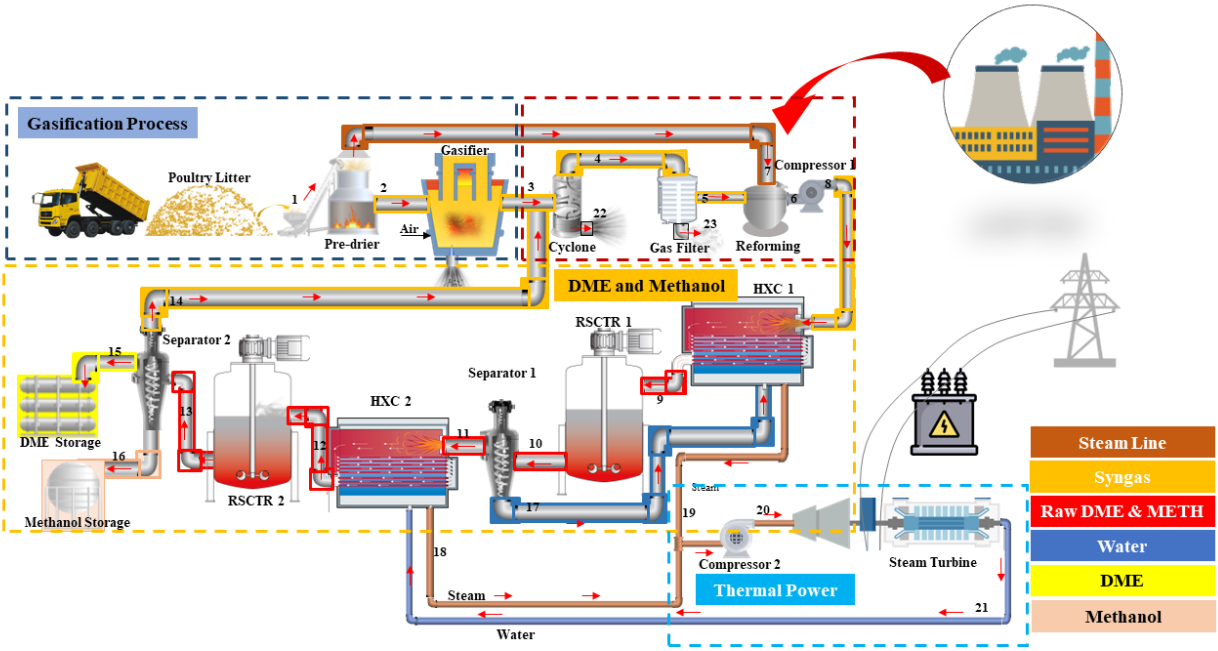

Fig. 5.C Gasification to DME production-based tri-generation process

- Nitrogen is considered inert.
- Tar and higher hydrocarbon chain compounds are not considered (Emun et al., 2010).

The Peng-Robinson (PR) equation of state method was applied to calculate the physical properties of the conventional compounds because of its suitability for low molecular weight gaseous compounds [124]. The density and enthalpy of the ash and biomass were determined using DCOALIGT and HCOALGEN [256]. Biomass is a non-conventional compound and therefore, proximate, and ultimate analyses were used as the biomass inputs. This proximate and ultimate analysis is given in Table 5.3 based on the work of Striugas *et al.* (2014) [247]. The primary process was developed using PL proximate and ultimate analyses, while mixed wood, soft wood, and sewage sludge-sawdust were used for the validation of our simulation model, as shown in Fig. 5.D. The DME yield was also validated by comparing it with experimental studies, as illustrated in Fig. 5.E. In addition, the description of the Aspen Plus blocks is given in Table 5.4 and the Aspen-based simulation model is given in Appendix A6.

Table 5.3 Proximate and ultimate analysis of different types of biomasses (Process G2)

Parameters	Poultry litter (PL)	Mix wood (MW)	Soft wood (SW)	Sewage sludge-sawdust (SS)
Proximate analysis (wt.%)				
Moisture	7.6	10.6	5.2	4.4
Volatile	63.6	75.8	79.2	59.5
Fix carbon	15.3	12.8	15.2	14.3
Ash	13.5	0.8	0.4	21.8
Ultimate analysis (wt.%)				
Carbon	43.98	48.77	49.2	41.08
Hydrogen	5.16	5.85	6.2	5.51
Oxygen	31.98	44.52	44.06	26.90
Nitrogen	4.63	0.05	0.08	3.77
Sulphur	0.75	0.01	0.06	0.94

Detailed descriptions of the Aspen Plus block IDs used for our simulation model of the PL gasification, methanol production, and DME production process are given in Table 5.4. This simulation model has been developed based on the literature and Aspen Plus software guidelines. Rstoic, Rplug, Ryield, and RCSTR reactors were used in the model development process, as described in similar studies reported in the literature [256,259]. The reactions occurring in the gasifier were split into the pyrolysis zone (PYROLYS), combustion zone (COMBUST), gasification zone (REDUCT), and inert char zone (DECOMP), as recommended in a study [256]. A schematic representation of a similar integrated downdraft gasifier has been proposed in an experimental study, which was used in our process validation process. A description of each reactor is given in Table 5.4. Furthermore, different chemical reactions were performed in these reactors and the details of the reaction kinetics given in Table 5.5 [256,259,260]. Finally, DME, methanol, steam, and syngas were separated at different stages, as shown in Appendix A6. In this simulation, the net heat stream was also calculated by introducing the HEATSRM (mixer block). All heat streams (endothermic and exothermic) from the reactors were joined at the HEATSRM mixer block (Appendix A6), which ultimately calculated the net heat stream. The positive value of this HEATSRM block indicates that the overall heat energy was being released (exothermic) from the process. This heat energy can be used for power generation using a turbine and generator set-up. The whole process has been validated using the application of different experimental studies, as described in section 5.1.2.1.

Table 5.4 Description of the Aspen Plus blocks for process G2 (Appendix A6)

Aspen ID	Model ID	Description
Rstoic	DRIER	Drying PL biomass at 100 °C for the gasification process.
Sep	H2OSP1	Separation of the moisture (H_2O) from PL biomass.
Rstoic	PYROLYS	Dis-integration of the PL into gases and biochar (1 bar, 600–800 °C).

Ssplit	SEP2	Separation of the solid particles (biochar) and gases received from PYROLYS.
Ryield	DECOMP	Conversion of biochar into gases at 1 bar and 600–800 °C.
Mixer	MIXER	Mixing the gases from SEP2 and SEP3 along with gasifying agent (air) (0.25–0.3 ER).
Rplug	COMBUST	Gasification in the presence of the gasifying agent (1 bar, 600–800 °C).
Rplug	REDUCT	Reduction of the gases to improve the H_2 content in syngas (1 bar, 600–800 °C).
Mixer	MIXER2	Mixing the syngas with steam generated from the drying process.
Rplug	CONV	Steam reforming of syngas to convert CH_4 into CO and H_2 (1 bar, 600–800 °C).
Compr	COMP	Compression of syngas to increase the pressure.
RCSTR	RSTR1	CO_2 conversion into CO for methanol preparation at 600–800 °C in the continuous stirrer reactor.
Heater	COOL1	Reduce the temperature to 50 °C for liquid gas separation.
Flash1	FLASH1	Separation of the liquid and other gases for further reaction to produce DME and methanol.
Heater	HEAT2	Increase the temperature of the gases to 220 °C for reaction at RSTR2.
RCSTR	RSTR2	Conversion of H_2 and CO to methanol and DME at 220 °C.
Heater	COOL2	Decrease the temperature to 50 °C for liquid and gases separation.
Flash2	FLASH2	Separation of the liquid (methanol) and gases (DME, trace syngas).
Sep	SEP5	Column separator for DME and separation of the remaining gases.
Sep	SEP4	Methanol separation from H_2O.
Mixer	HEATSTRM	Calculation of the net heat stream from all the blocks in the simulation model.

Table 5.5 Reaction kinetics of process G2

Reaction	Rate constant (K)	n	Activation energy (cal/mol)	Reaction number	Block ID
$1.25C + O_2 \rightarrow 0.5\ CO + 0.75CO_2$	3.7×10^{10}	1	35826.9	R1	COMBUST
$CO + 0.5O_2 \rightarrow CO_2$	1.78×10^{10}	0	42992.2	R2	
$CH_4 + 0.5O_2 \rightarrow CO + 2H_2$	1.58×10^{12}	0	48246.9	R3	
$H_2 + 0.5O_2 \rightarrow H_2O$	1.08×10^{7}	0	2779.54	R4	
$C + O_2 \rightarrow CO_2$	1.78×10^{10}	0	42992.2	R5	
$C + H_2O \rightarrow H_2 + CO$	8×10^{-3}	0	11918.4	R6	REDUCT
$CH_4 + H_2O \rightarrow CO + 3H_2$	3×10^{11}	0	29855.7	R7	
$C + H_2O \rightarrow CO + H_2$	0.008	0	11918.4	R8	
$1.25C + O_2 \rightarrow 0.5CO + 0.75CO_2$	3.7×10^{10}	1	35826.8	R9	CONV
$CO + 0.5O_2 \rightarrow CO_2$	1.78×10^{10}	0	42992.3	R10	
$CH_4 + 0.5O_2 \rightarrow CO + 2H_2$	1.58×10^{12}	0	48246.9	R11	
$H_2 + 0.5O_2 \rightarrow H_2O$	1.08×10^{7}	0	2579.54	R12	
Equilibrium basis	**A**	**B**	**C**	**D**	
$H_2 + CO_2 \rightarrow CO + H_2O$	13.148	–5639.5	–1.077	0.000544	RSTR1
$2H_2 + CO \rightarrow CH_3OH$	12.343	9143.6	–7.492	0.004076	RSTR2
$2\ CH_3OH \rightarrow DME + H_2O$	–2.27	2609.5	0.00823	-8.2×10^{-6}	

5.1.2.1 Process G2 validation: Gasification, DME, and CHP

The simulation model for the PL gasification process was developed based on the descriptive details presented in Section 5.1.2. This model was validated by comparing it with an experimental study prior to further analysis. The process validation was performed in two different ways, including validation of the gasification process using the application of four different types of biomasses and DME yield. The results of the gasification process and related

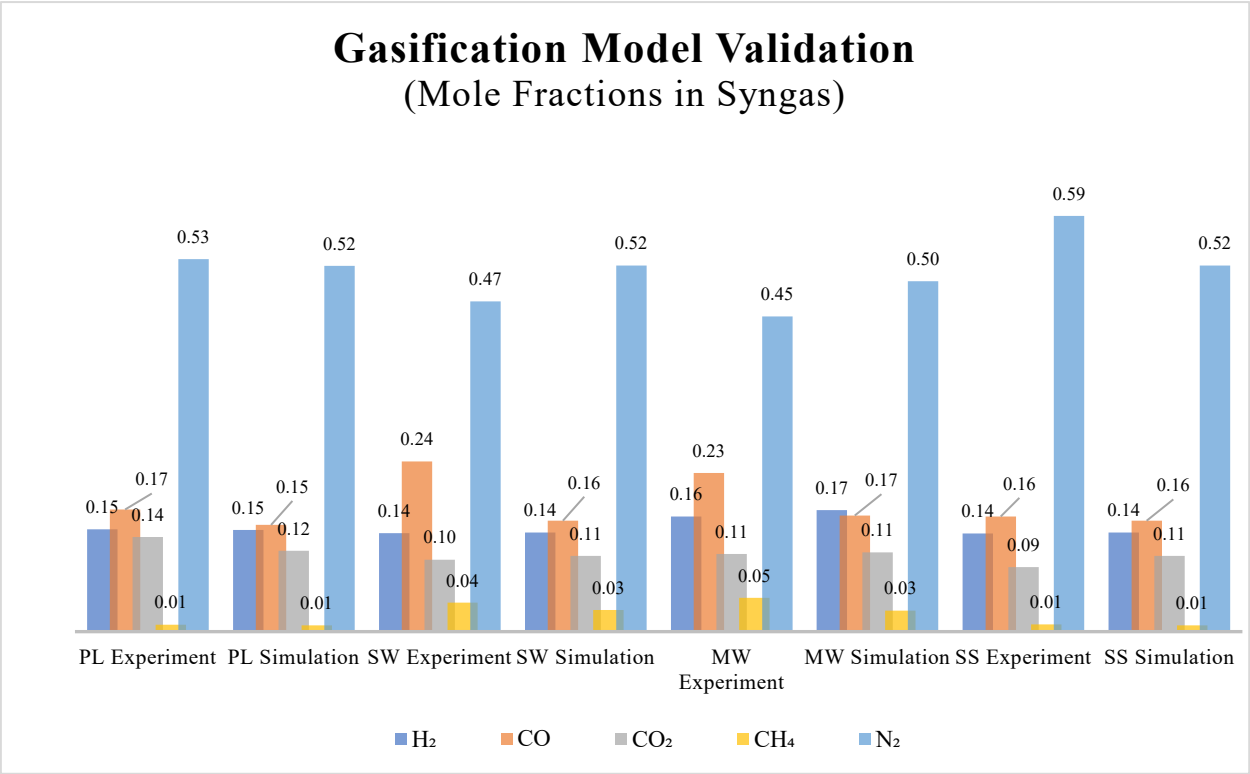

Fig. 5.D. Model validation using syngas composition for process G2

experimental studies are shown in Fig. 5.D [247]. The molar fractions of syngas, including H_2, CH_4, CO, CO_2, and N_2, were compared. This model was validated using the experimental results obtained for four different types of biomasses, including PL, SW, MW, and SS.

The results of the model validation process (see Fig. 5.D) show that there was no significant difference between the simulation results and those determined in the experimental

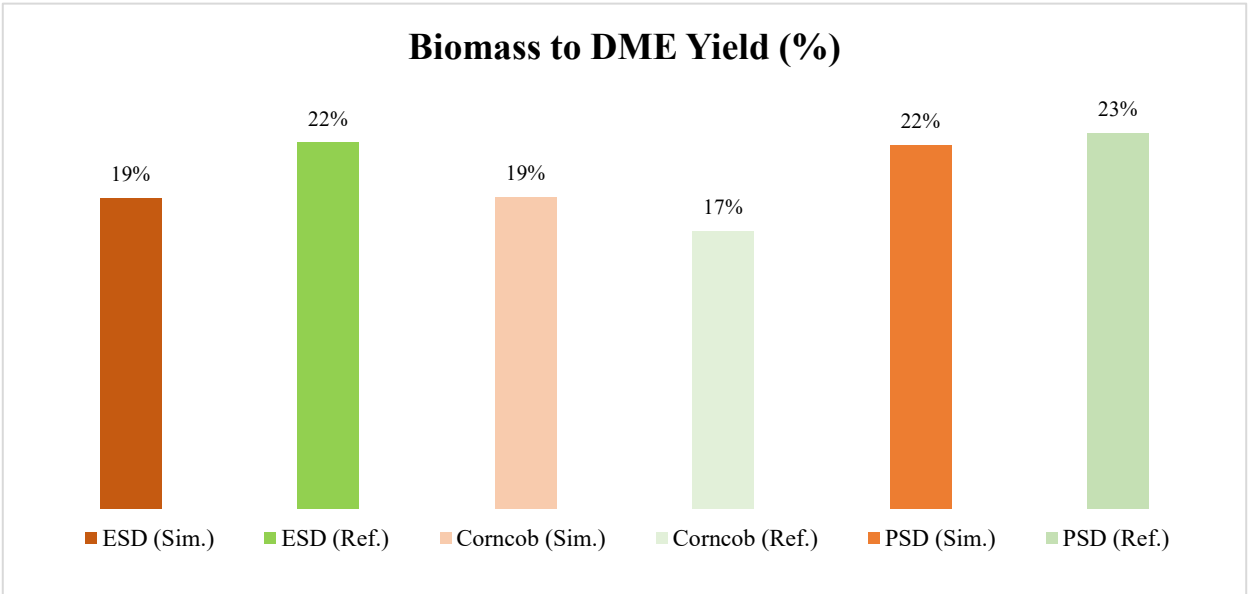

Fig. 5.E. Model validation using the DME yield (%) for process G2

studies for the four types of biomasses (PL, SW, MW, and SS) studied. In particular, the molar fraction of H_2 was within ±0.02 (2%) for PL, SW, MW, and SS. The molar fractions of CH_4, CO, CO_2, and N_2 were within ±2%. To validate the model of the secondary process (DME production), the biomass to DME yield (%) was utilised. Different types of biomasses, including corncob, pine saw dust (PSD), and eucalyptus saw dust (ESD), based on three different experimental studies were included to estimate the output of DME, as shown in Fig. 5.E [178,261,262]. The absolute error obtained for the biomass to DME yield (%) was within 1–3% (Fig. 5.E). Therefore, the primary gasification and secondary syngas to DME process have a reliable result using seven different types of biomasses because the absolute errors were <3%, which shows the robustness of the developed process. This validated model was further utilised in the optimization and sustainability evaluation based on the methodology described in chapter 3.

5.1.3 Process G3: Co-gasification for blue, and green hydrogen production

The initial phase of the study involved the gasification of both biomass and plastic waste, with steam serving as the gasifying agent. Steam was selected as a gasifying agent due to the synergistic effect of steam in production of H_2 [263,264]. Subsequently, the thermal energy generated during the gasification process was recovered by converting it into steam, which, in turn, was utilized for the generation of electric power. This generated electric power was employed to meet the operational requirements of the system, and any surplus energy was directed towards the production of green hydrogen through electrolysis process by application of alkaline electrolysis cell (AEC). In the final step, the gases comprising H_2, CH_4, and CO_2 were separated from the syngas. To facilitate these processes, a simulation model for co-gasification was developed using Aspen Plus. Fig. 5.F illustrates the process flow diagram of the simulation model, while the actual simulation figure can be found in Appendix A2 and A3.

The current simulation process is divided into four distinct stages. It begins with feedstock pre-treatment, encompassing feedstock mixing and drying. Subsequently, the pre-treated feedstock is transferred to the gasifier, where gasification occurs in the presence of steam acting as a gasifying agent. The second section focuses on the purification and recovery of heat energy from the produced syngas. In this phase, the syngas is passed through a cyclone to separate tar particles, and steam reforming of this refined syngas is done to increase the hydrogen fraction while converting CO into CO_2. The water-gas shift reaction is also carried out to facilitate the conversion of CO into CO_2, which will be recovered in later stages. Subsequently, the high-temperature reformed syngas is directed through a heat exchanger, where water is pumped to recover heat from the syngas. This results in the transfer of heat from the syngas to the water, leading to the production of high-temperature steam, which is then utilized for electricity generation through a steam turbine. In the third stage, any excess electricity generated in this process is used to produce green hydrogen through water electrolysis using AEC. Finally, in the fourth stage, CO_2, CH_4, and H_2 are recovered through a series of column separators based on liquefaction conditions.

The process details are outlined in below, along with the following assumptions:

- It’s a steady state simulation.
- No heat or pressure losses occurred during the simulation process, maintaining a closed system [149,265].

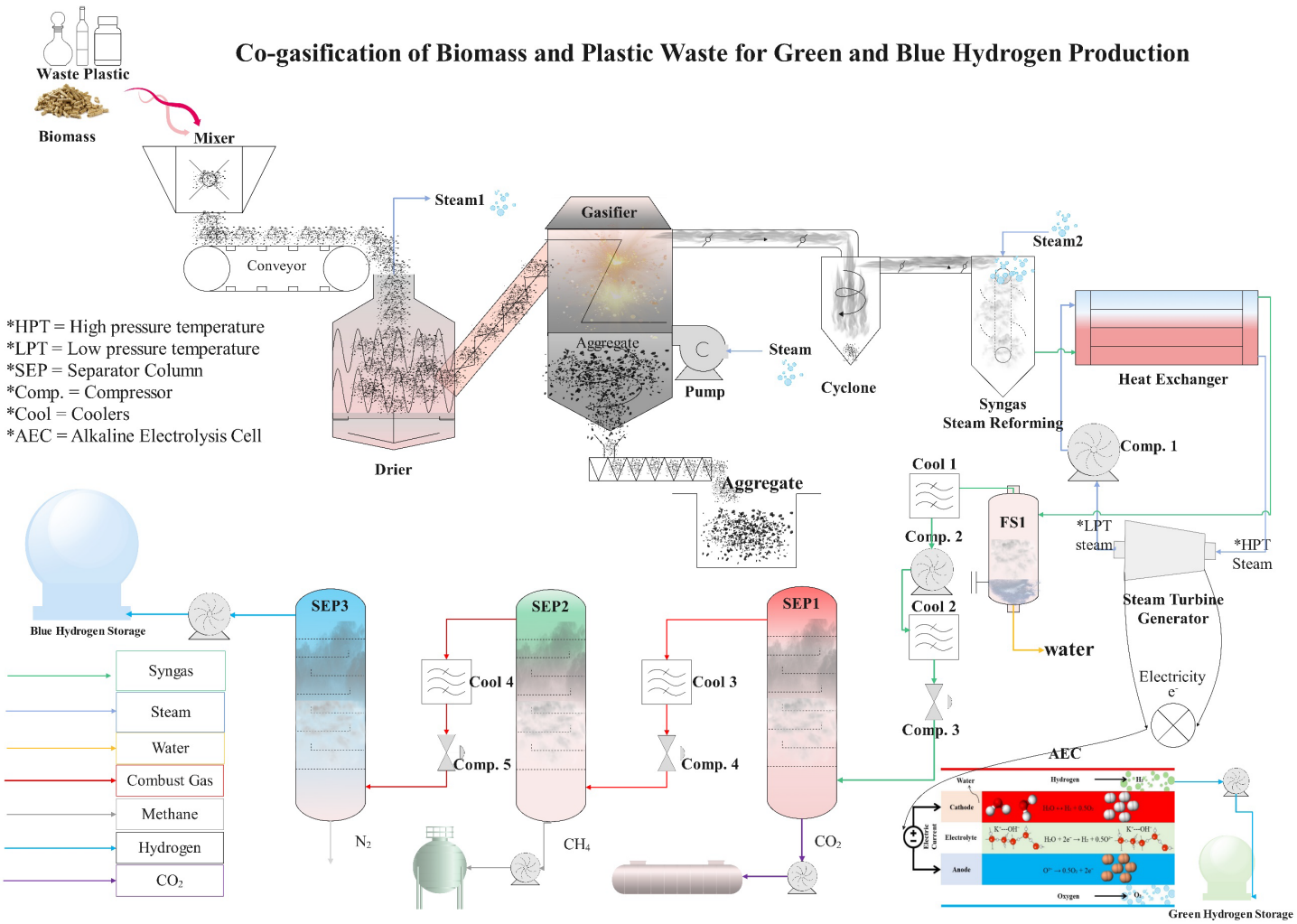

Fig. 5.F. Co-gasification and AEC based green hydrogen production process

- Ash is considered inert.
- Tar, composed of carbon, has been eliminated and plays no role downstream. Nitrogen is considered an inert.
- Feedstock decomposition produces syngas with H_2, CO, CO_2, and CH_4 as a main component [150,266].

The simulation of co-gasification involving lignocellulose biomass and plastic waste was developed using Aspen Plus. However, the software lacks the inclusion of non-conventional (NC) compounds like biomass. To address this limitation, these compounds were defined using the proximate and ultimate analyses of the feedstock. The enthalpy and density of the NC compounds were determined using HCOALGEN and DCOALIGT setups as specified in the

material properties. The model was developed based on the principles of Gibbs free energy minimization and reaction kinetics [149]. For handling the complex gas-liquid equilibrium and small molecular weight compounds, the Peng-Robinson equation of state with the Boston Mathias function was applied [124,150]. This equation of state has been employed in similar research by various researchers. A detailed illustration of the process simulation can be found in Fig. 5.G. The simulation model utilized proximate and ultimate analyses for the feedstock, which consists of wood and high-density polyethylene (HDPE). The details are provided in Table 5.6, sourced from an experimental study [267,268].

Table 5.6 Proximate and ultimate analysis of feedstock for process G3

Proximate analysis		
	Biomass Waste	Plastic Waste
Moisture	8%	0%
Volatile matter	17.7%	0.3%
Fixed carbon	73.7%	99.7%
Ash	0.6%	0%
Ultimate analysis		
	Biomass Waste	Plastic Waste
Carbon	50.6%	85.71%
Hydrogen	6.5%	14.29%
Nitrogen	0.2%	0%
Oxygen	42%	0%

Fig. 5.G serves as a technical representation of the simulation model, which was developed based on experimental and simulation studies [266,268,269]. These experimental and simulation-based studies have been used to develop the process and validate the model's integrity [266,268]. The feedstock consists of a 1:1 mixture of wood and HDPE, with a feed rate of 20,000 kg/h, introduced into the process at 30 °C and 1 bar pressure. The characterization of the non-conventional (NC) feed was determined through proximate and ultimate analyses, as given in Table 5.6. The initial step involves the pre-treatment of this

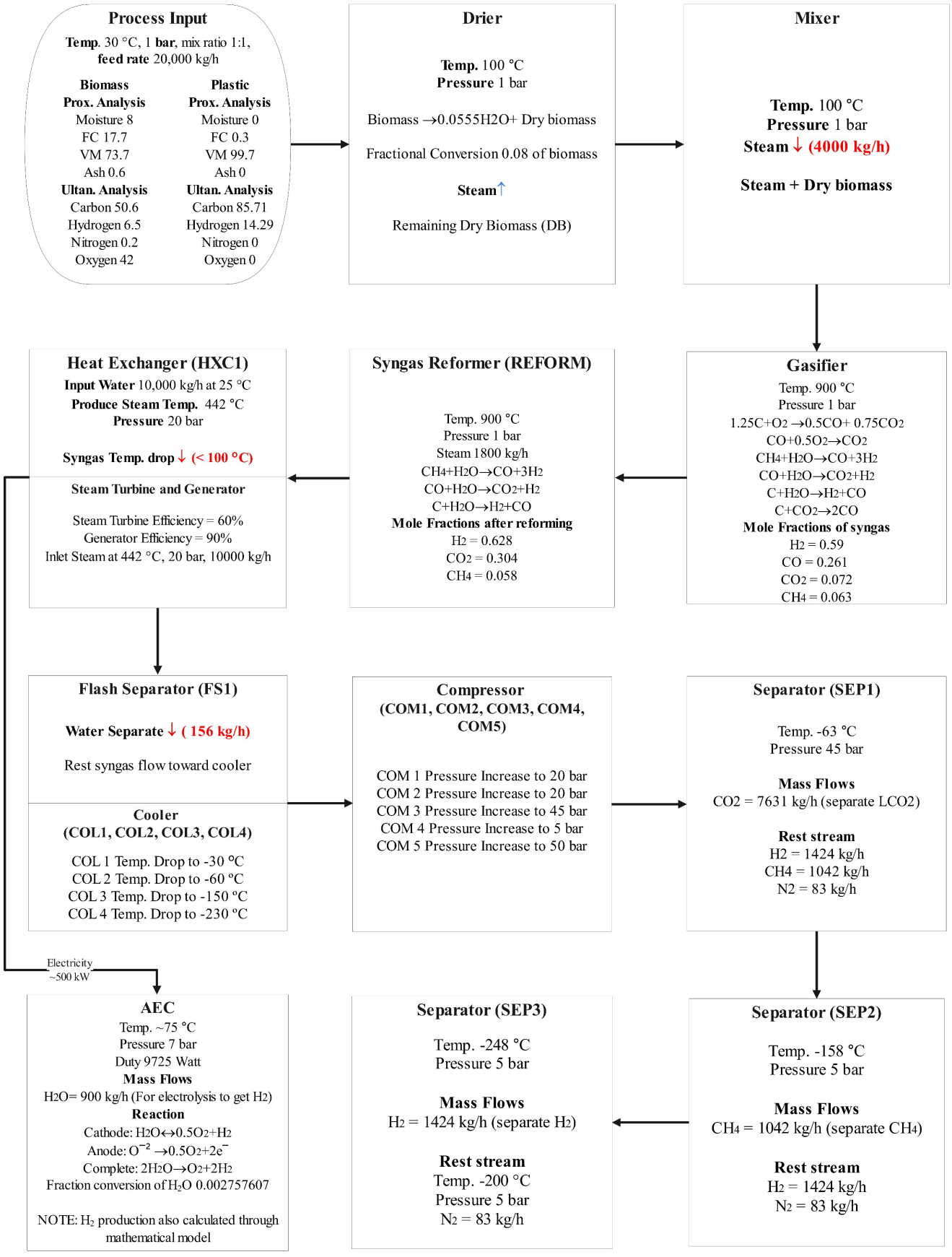

Fig. 5.G. Process flow of simulation model

feedstock through drying at 100°C, as indicated by the stoichiometric reaction provided in

Table 5.7 [266,270,271]. Subsequently, the dried materials are mixed to form a homogeneous mixture which undergoes a gasification process in the presence of steam as the gasifying agent, with a feed rate of 4,000 kg/h, operating at 900°C and 1 bar pressure. During the gasification process, a significant amount of CH_4 and CO is generated, which is further reformed through steam methane and water gas reforming reactions outlined in Table 5.7. The resulting reformed syngas is produced at a high temperature of around 900°C. To facilitate the separation of the desired gases from the syngas, it is necessary to reduce the temperature. To achieve this, thermal energy is recovered from the reformed syngas using a heat exchanger, with water serving as the heat transfer medium at a rate of 10,000 kg/h and 20 bars. This process effectively lowers the syngas temperature to below 100°C which ultimately assists in the separation of required gases from syngas.

The next phase involves the separation of the primary gases from syngas starting from moisture or liquid removal through a flash separator before proceeding with the further liquefaction of H_2, CH_4, and CO_2. Simultaneously, the steam generated through heat recovery from syngas is utilized for electric power generation through a steam turbine. Any excess electricity, beyond process requirements is employed to produce green hydrogen through an AEC. For CO_2 recovery from syngas, temperature is gradually reduced through a series of coolers and compressors. Separator columns are utilized to recover various gas components. Starting with the recovery of CO_2 in separator 1 (SEP1) at -63°C and 45 bars using cooler and compressor 1-2, the remaining gas undergoes further temperature reduction through cooler and compressor 3. The temperature and pressure of the gas have been reduced to -158°C and 5 bars, respectively. Resultantly, CH_4 is being recovered in separator 2 (SEP2), while the remaining gas, primarily composed of H_2, is recovered in separator 3 (SEP3) with the help of cooler and compressor 4. These reclaimed gases can be stored in cryogenic liquid tanks through the application of a compressor. For AEC, there is no standardized module available in the Aspen

Plus library. Therefore, literature-based data has been used to develop an AEC model stack through application of RSTOIC which has been given in Appendix A3. The potential of electric power to H_2 production potential calculated through electrochemical analysis given in section 5.1.3.1.

5.1.3.1 Alkaline electrolysis cell (AEC) calculations

The AEC serves as an important for the generation of H_2 and O_2 through electrolysis of water. This process occurs in the presence of a concentrated alkaline electrolyte solution, commonly potassium hydroxide (KOH) or sodium hydroxide (NaOH). The AEC primarily consists of two electrodes: a cathode and an anode, both immersed in the alkaline electrolyte solution. When electricity is supplied to AEC, a redox reaction occurs at the anode, leading to the oxidation of H_2O and the release of O_2 and electrons. While reduction occurs at cathode, resulting in the production of H_2. If the electricity used to power the AEC is sourced from renewable resources, the resultant hydrogen is considered as green hydrogen [271,272].

In this study, the electricity utilized in the AEC derives from the thermal energy recovery process. Resultantly, the H_2 produced is considered as "green hydrogen". Aspen Plus simulation of the AEC has been developed given in section 5.1.3. Furthermore, the hydrogen production potential from the AEC was calculated using the electrochemical model as given in Eq. 5.18-5.25 taken from literature. [271,273]. The fundamental concept underlying the electrochemical model involves the chemical decomposition of water molecules through the application of electricity. To achieve this, AEC requires electrical energy input, which corresponds to the Gibbs energy ($\underline{\Delta} G$) of 237 kJ/mol for water [271]. Eq. 5.18-5.21 specifically represents the calculation of electric energy in terms of the voltage required to disintegrate a water molecule into H_2 and O_2.

$$V_{rev} = \frac{\triangleq G}{zF} \tag{5.18}$$

where V_{rev} is reversible cell voltage, $\triangleq G$ is Gibbs energy of water, F is Faraday constant (96,485 C/mol), z is the no. of electron per reaction which is 2.

$$V_{tn} = \frac{\triangleq H}{zF} \tag{5.19}$$

where V_{tn} is Thermoneutral cell voltage, $\triangleq H$ is Enthalpy change of water, F is Faraday constant (96,485 C/mol), z is the no. of electron per reaction which is 2.

$$V = V_{rev} + \frac{r}{A} I + s \log\left(\frac{t}{A} I + 1\right) \tag{5.20}$$

where V is voltage, r is the ohmic resistance parameter, A is the area of electrodes (m^2), I is current while s is the coefficient for overvoltage on electrodes

$$V = V_{rev} + \left(\frac{r_1 + r_2 T}{A} I\right) + s \log\left(\frac{t_1 + {}^{t_2}/_{T} + {}^{t_3}/_{T^2}}{A} I + 1\right) \tag{5.21}$$

where V is voltage, $r_1$is the ohmic resistance parameter, $r_2 T$ is the ohmic resistance parameter with respect to temperature, A is the area of electrodes (m^2), I is current, s is the coefficient for overvoltage on electrodes, t_1 is the coefficient of overvoltage on electrodes

$$\eta_F = \frac{({}^{I}/_{A})^2}{f_1 + ({}^{I}/_{A})^2} f_2 \tag{5.22}$$

where η_F is Faraday efficiency while f_1 and f_2 are Faraday efficiency constants

$$n_{H_2} = \eta_F \frac{n_c I}{zF} \tag{5.23}$$

where n_{H_2} is H_2 production rate, η_F is Faraday efficiency, n_c is the number. of cells in series per stack

$$n_{H_2O} = n_{H_2} = 2n_{O_2} \tag{5.24}$$

where n_{H_2O} is the amount of water, n_{H_2} is the amount of hydrogen while n_{O_2} is the amount of oxygen

$$\eta_e = \frac{V_{tn}}{V} \tag{5.25}$$

where η_e is the energy efficiency while V_{tn} is Thermoneutral cell voltage (Eq. 5.19)

Table 5.7 Stoichiometric reaction in simulation model for process G3

No.	Reaction	Type	Process
(i)	$C+H_2O \leftrightarrow CO+H_2$ (+131 kJ/mol)	Water-gas reaction	Drying
(ii)	$C+2H_2 \leftrightarrow CH_4$ (-74.8 kJ/mol)	Hydrogasification	Gasification
(iii)	$C+0.5O_2 \rightarrow 2CO$ (-111 kJ/mol)	Carbon partial oxidation	Gasification
(iv)	$C+O_2 \rightarrow CO_2$ (-394 kJ/mol)	Carbon oxidation	Gasification
(v)	$CO+0.5O_2 \rightarrow CO_2$ (-283 kJ/mol)	Carbon monoxide oxidation	Oxidation
(vi)	$CH_4+2O_2 \leftrightarrow CO_2+2H_2O$(-803 kJ/mol)	Methane combustion	Oxidation
(vii)	$CO+H_2O \leftrightarrow CO_2+H_2$(-41.2 kJ/mol)	Water-gas shift	Oxidation
(viii)	$C+CO_2 \leftrightarrow 2CO$ (+172 kJ/mol)	Boundard reaction	Oxidation
(ix)	$CH_4+H_2O \rightarrow CO+3H_2$ (+206 kJ/mol)	Steam methane reforming	Reforming
(x)	$CO+H_2O \rightarrow CO_2+H_2$	Water gas (reformer)	Reforming
(xi)	$2OH^- \rightarrow 0.5O_2+H_2O+2e^-$	Anode	AEC
(xii)	$2H_2O+ 2e^- \rightarrow 2OH^-+H_2$	Cathode	AEC
(xiii)	$H_2O \rightarrow H_2+0.5O_2$	Complete reaction	AEC

5.1.3.2 Process G3 validation: Co-gasification, blue, and green hydrogen

Process validation has been done with the experimental and simulation study of similar work. Validation results show (Fig. 5.H) the robustness of the current simulation model for co-gasification of biomass and plastic waste [266,268]. This validation process employed the calculation of the RMSE between the mole fractions of gases in the current model and those from experimental studies based on section 3.3.1 [274]. The RMSE analysis revealed a mere 1.51% deviation, indicating strong alignment between our model and experimental findings. Furthermore, a detailed comparison was made between the mole fractions of H_2, CO, CO_2, and CH_4 in the experimental work and simulation model as shown in Fig. 5.H. The findings revealed that there is minimal variation between the mole fractions of the current simulation model and those from the experimental studies. For instance, as shown in Fig. 5.H, the mole fraction of H_2 in the experimental study was 0.57, while it was 0.59 in the current simulation, which is close to each other. Similarly, the mole fractions for CO, CO_2, and CH_4 in the experimental study were 0.28, 0.08, and 0.06, respectively which are closely aligned with the current simulation values of 0.26, 0.07, and 0.06 for CO, CO_2, and CH_4, respectively. Overall,

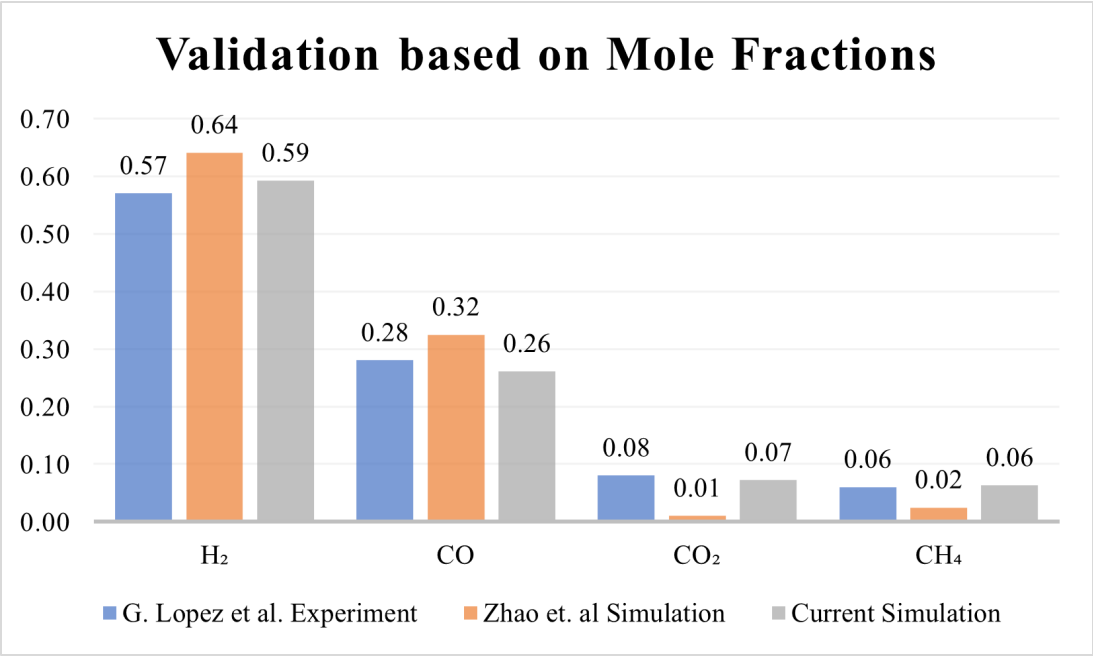

Fig. 5.H. Process G3 simulation model validation

our current simulation model's results exhibit a closer match with the experimental study, surpassing the performance of another simulation study [266]. Therefore, this model has been utilized for further secondary process of gases liquification and sustainability analysis.

5.2 Gasification based poly-generation process prediction, and optimization

Gasification based poly-generation process prediction and optimization has been done to improve the process sustainability considering methodology defined in chapter 3.

5.2.1 Process G1: Gasification to SOFC, and CHP parametric effect on output

Process parameters primary and secondary processes temperature, biomass to gasifying agent ratio, and pressure etc. effect on the process yield has been analyzed in sections 5.2.1.1 to 5.2.1.5.

5.2.1.1 Effect of gasification temperature and BMR

The temperature of the gasification process and the BMR are two essential elements that determine or can affect the hydrogen yield and the Gibbs Energy in the modeling process. The graphical representations of these behaviors are shown in Fig. 5.I.a and 5.I.b. Increased BMR supports higher Gibbs Energy up to 500 ºC, but the trend reverses after that. In Fig. 5.I.a, lower BMR has higher GE, which could be due to temperature superiority over BMR on GE. In Fig. 5.I.b, a similar pattern can be seen in the hydrogen mole fractions. Raising BMR decreases hydrogen moles and vice versa; this trend has become steady beyond 600 ºC. There is no increase in hydrogen moles after 600 ºC. Therefore, based on simulation data trend in Fig. 5.I, BMR inversely relates with GE and H_2 moles while there is no significant effect of temperature after 600 ºC.

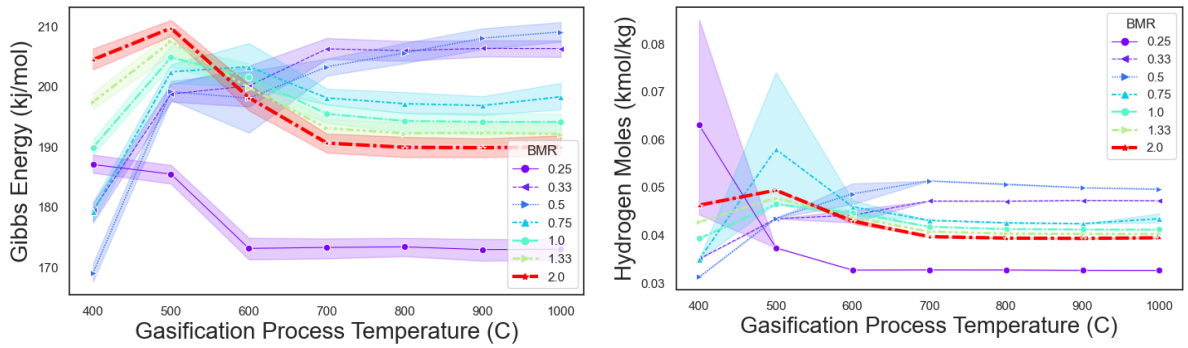

(a) (b)

Fig. 5.I Effect of gasification temperature and BMR on Gibbs energy and hydrogen moles

5.2.1.2 Effect of gasification pressure and temperature

Pressure is another key aspect that affects or might alter the GE and H_2 moles is pressure. Fig. 5.J illustrates the pressure and gasification process temperature correlation on GE and H_2 moles. Pressure has an inverse relationship with GE; increasing pressure decreases GE regardless of temperature. However, at 500 ºC and 1 bar pressure, GE had the highest value, which has since been reduced. A similar tendency may be seen for H_2 moles, which have a maximum value at 500 ºC regardless of pressure. Therefore, 500-600 ºC and 1 bar are the best conditions for the GE and H_2 moles.

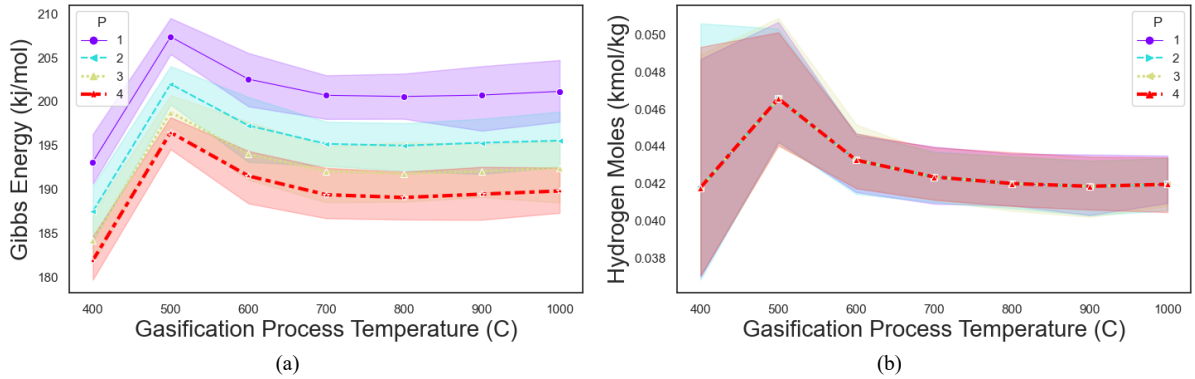

(a) (b)

Fig. 5.J Effect of gasification temperature and pressure on Gibbs energy and H_2 moles

5.2.1.3 Effect of SOFC temperature and BMR on current and current density

Current density is dependent on current (I); both are directly related. Hence, increasing current increases current density in SOFC. The influence of BMR and SOFC temperature is

depicted in Fig. 5.K. For all temperatures except 850-950 ºC, where BMR value 0.25 suppressed all other BMR, but BMR value 0.5 produced the best results for current and current density. Therefore, if the SOFC is operated between 850 and 950 ºC, 0.25 BMR produces the best output. For the remaining SOFC operational temperatures, 0.5 BMR produces the highest current and current density outputs.

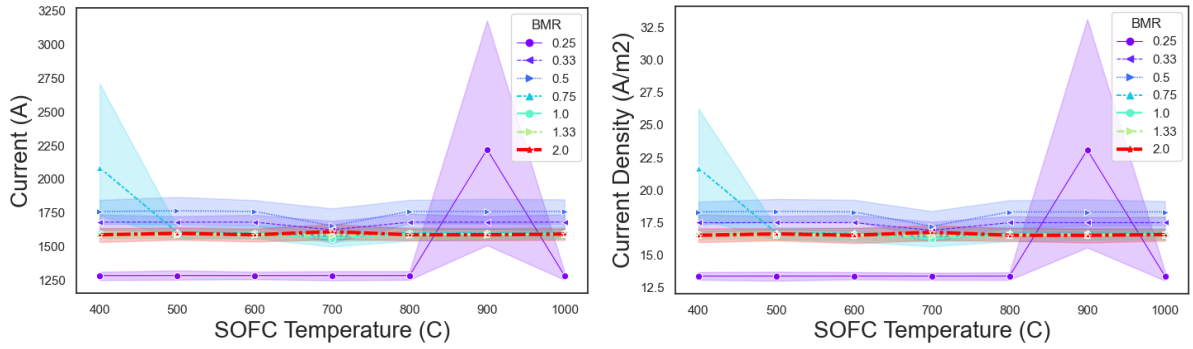

(a) (b)

Fig. 5.K Effect of temperature and BMR on SOFC current and current density

5.2.1.4 Effect of SOFC parameters on actual voltage and current density

The influence of pressure on SOFC real voltage and current density was shown in Fig. 5.L. According to Fig. 5.L.a, increasing SOFC pressure reduces real voltage whereas temperature has no influence on pressure. Similarly, Fig. 5.L.b shows that pressure has no effect on current density. However, the maximal value of current density is between 850 and 950 ºC. Therefore, (Fig. 5.L) it can be assumed that 1 bar pressure and temperatures ranging from 850 to 950 ºC have the best actual voltage and current density.

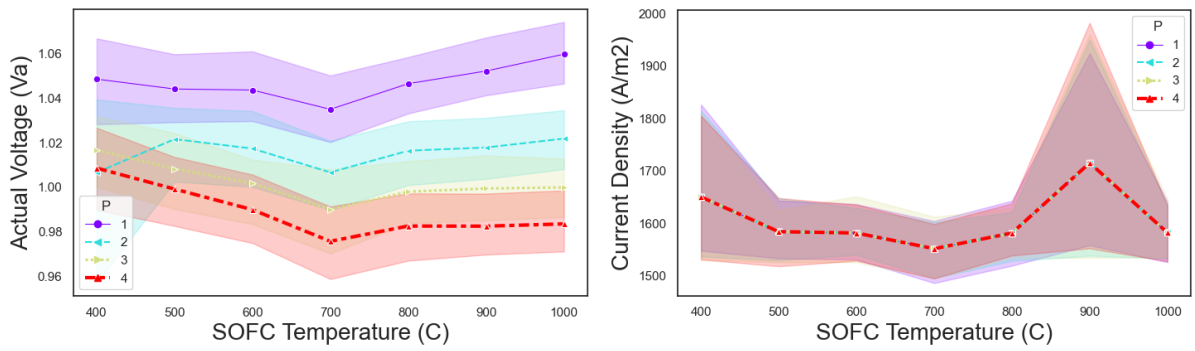

(a) (b)

Fig. 5.L Effect of temperature and pressure on SOFC actual voltage and current density

5.2.1.5 Effect of process parameters on Net-heat

Net heat is the total amount of energy (kJ/mol) that remains after eliminating the process energy use. This is estimated using the Aspen Plus simulation model. To obtain the net heat stream, all heat fluxes from various reactors and processes were combined in the HEATSTRM block. The NH simulation data was used to create Fig. 5.M. Figures 5.M.a and 5.M.b show the effect of gasification process temperature on BMR and pressure. With decreased BMR, NH has been raised, but it has essentially no influence on temperature. The maximal NH is between 0.25 and 0.33 BMR, while pressure has little impact on the NH. Therefore, to make a process more energy efficient, BMR should be 0.25-0.33.

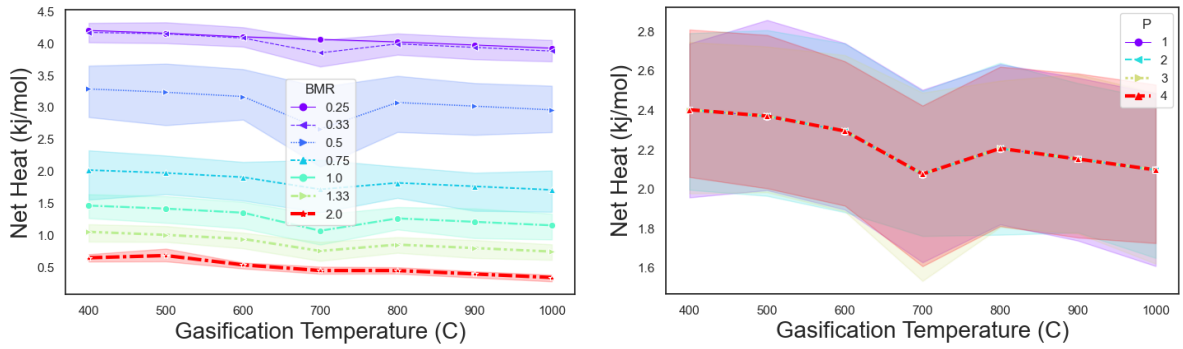

(a) (b)

Fig. 5.M Effect of temperature and pressure on Net Heat

5.2.2 Process G1: Gasification to SOFC, and CHP prediction model

To undertake the data analysis based on the Fig. 5.A model, the extreme gradient boosting AI method was loaded from the Python programming library. This model was run using the simulation dataset.

5.2.2.1 Process G1: Data collection for model development

For data collection, an experiment design has been devised. The output at different parameters was obtained using a factorial design with multi-levels, which is difficult to acquire in such a systematic manner using the Aspen Plus sensitivity analysis method. A total of 1372 simulations were run using a factorial approach, altering the elements that affect or can affect

syngas and SOFC production based on Fig. 5.N correlation analysis. Table 5.8 has the criteria that were determined after doing a literature review. For factorial design, four factors were selected including gasification process temperature, biomass to air ratio (BMR), SOFC pressure, and temperature. Temperature gasification and SOFC both have seven levels, while BMR and pressure have seven and four levels, respectively. Hence, a total of 1372 (7747) simulation runs were performed.

To conduct process parametric analysis, Pearson correlation has been drawn based on 1372 simulation runs results. A matrix format correlation has been drawn between input and output variables of the model. Fig. 5.N has the matrix diagram of this correlation results. Correlation value closer to the '1', represents strongly direct correlation among the respective parameters while value closer to the '-1', represents the strongly inverse correlation [51]. Whereas correlation value closer to '0' shows that there is insignificant correlation among the

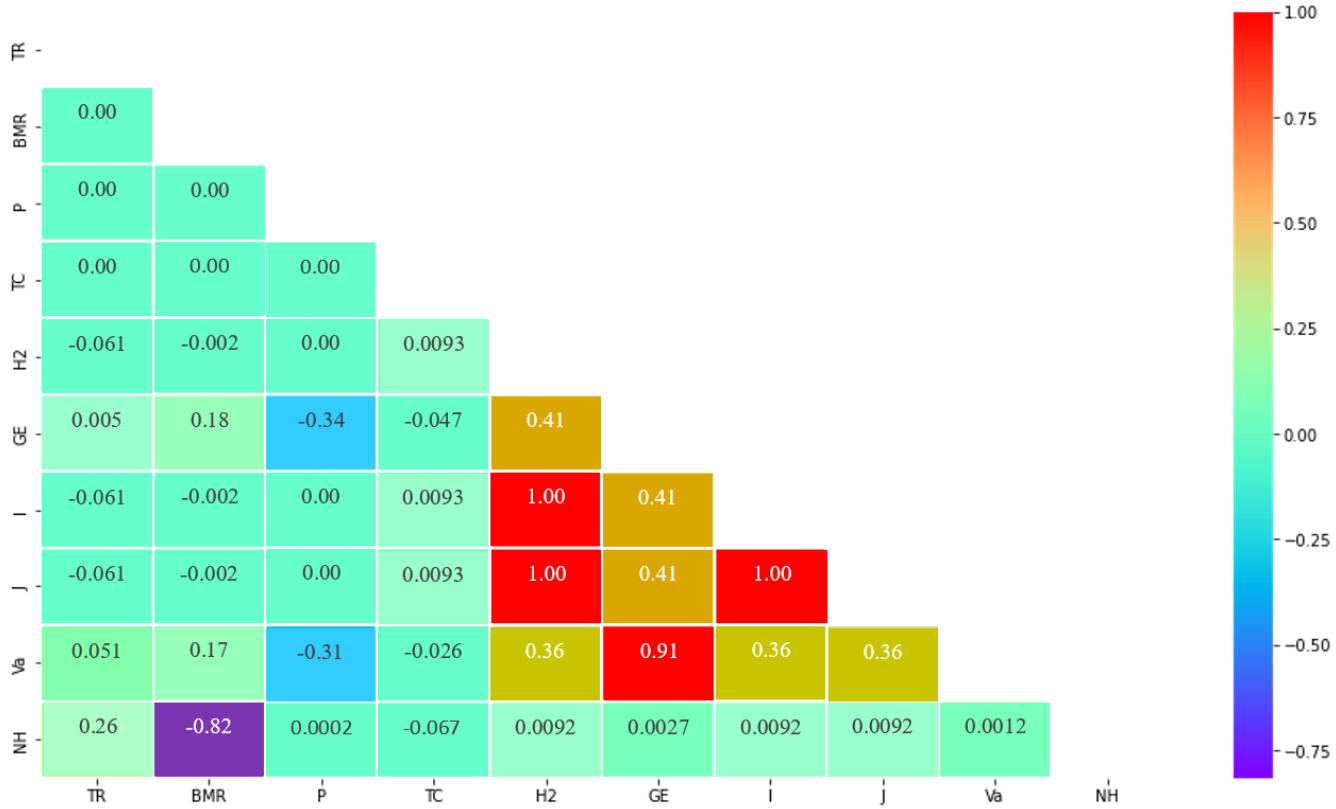

Fig. 5.N Pearson Correlation with process G1 parameters

respective parameters. Therefore, reactor temperature (TR) has a correlation with only net heat (NH) while it has insignificant correlation with other parameters. BMR has strong inverse correlation with NH which shows increasing BMR, decreases NH while it has a little

Table 5.8 Multilevel factorial design for process G1

GT (°C)	BMR (ratio)	P (bar)	SOFC (°C)	Total (1372)
400	0.25	1	400	7×7×4×1 = 196
500	0.33	2	500	7×7×4×1 = 196
600	0.50	3	600	7×7×4×1 = 196
700	0.75	4	700	7×7×4×1 = 196
800	1.00		800	7×7×4×1 = 196
900	1.33		900	7×7×4×1 = 196
1000	2.0		1000	7×7×4×1 = 196

correlation with actual voltage and Gibbs Energy. Pressure (P) has no significant correlation with dependent variable with the exception of actual voltage and Gibbs Energy, where it inversely correlates. H_2 has a strong direct correlation with current, current density, actual voltage, and Gibbs Energy. GE is responsible for better Va. Hence, correlation results show that higher pressure in SOFC contributes to better performance, but it has no effect on primary gasification process. Similarly, higher BMR generates more GE but at the cost of lower net heat.

5.2.2.2 XGB Model Performance Analysis

The performance of the XGB model was assessed using the R^2, MSE, and MAE. For the evaluation, section 3.2 was used. Instead of evaluating or calculating with a calculator, built-in programming code has been utilized. The performance of the XGB model was evaluated using three different types of training and testing datasets. Combinations of 90:10, 80:20, and 70:30 training and testing data sets were used to achieve the best results for the model in terms of R^2, MSE, and MAE. Table 5.9 shows the detailed results of these various parameters. The XGB algorithm was used to estimate the H_2, Current (I), and Current Density (J) for training and testing data sets of 90:10, 80:20, and 70:30. According to Table 5.9, XGB predicts better for 90:10 training-testing datasets due to higher R^2 (0.97-0.99), lower MSE, and MAE values when compared to 80:20 and 70:30 training-testing datasets. MAE shows the model's correctness because it has a greater R^2 (near to 1) and a lower MSE. Therefore, XGB has the better R^2, MSE, and MAE in the prediction of H_2, I, and J at 90:10.

Table 5.9 XGB model results at different parameters

Model Type	**R^2** (90-10)	**R^2** (80-20)	**R^2** (70-30)	**MSE** (90-10)	**MSE** (80-20)	**MSE** (70-30)	**MAE** (90-10)	**MAE** (80-20)	**MAE** (70-30)	**Element**
XGB	0.97-0.99	0.95-0.96	0.94-0.97	<0.01	0.04	0.05	<0.01	0.10	0.11	**H_2**
XGB	0.97-0.99	0.95-0.96	0.94-0.97	14.99	20.16	25.31	1.56	2.51	2.93	**Current (I)**
XGB	0.97-0.99	0.95-0.96	0.94-0.97	0.04	<0.01	<0.01	0.16	<0.01	<0.01	**Current Density**

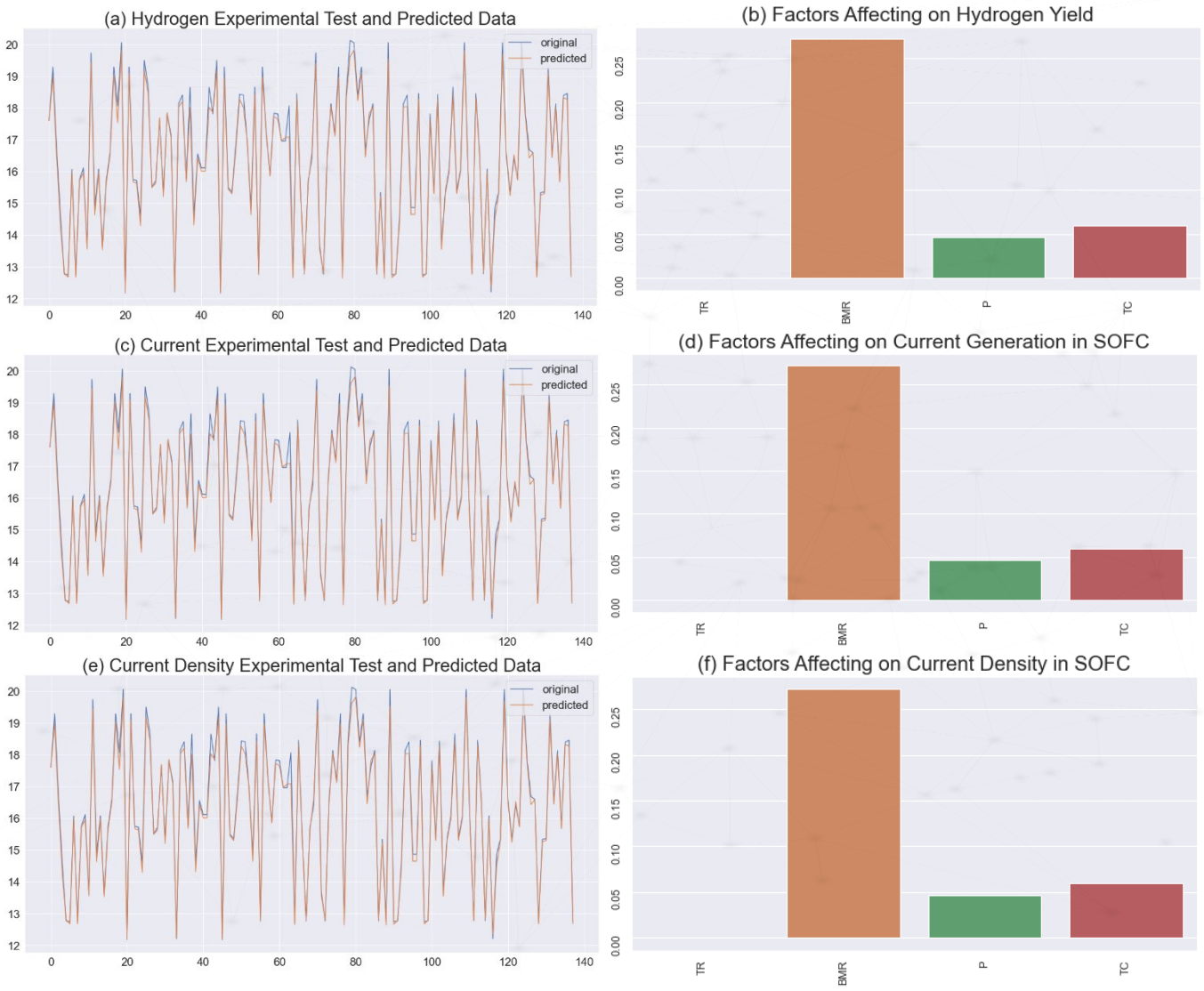

Fig. 5.O XGB model results analysis (90:10)

The graphical analysis of the XGB model findings is shown in Fig. 5.O. In Fig. 5.O.a hydrogen projection based on TR, P, BMR, and TC. The hydrogen experimental test and predicted data graph demonstrated that, with a few exceptions, the model is almost able to predict the data, with BMR being the most significant factor among all input values that affect the hydrogen moles, while P, TR, and TC have no significant effect on the H_2 results. Similar Fig. 5.O.b, 5.O.d, and 5.O.f, BMR remains a significant factor when compared to TR, P, and TC, all of which can influence the output results of current (I) and current density (J). Hence, BMR is the most important element in predicting datasets.

5.2.3 Process G2: Gasification, DME, and CHP; PSO based optimization

Process optimization was performed by applying PSO with MATLAB and Aspen Plus integration using the Component Object Model in the ActiveX Automation Server for which the methodology has been defined in Section 3.2.2.2 [275]. A total of 300 iterations of the PSO were performed to obtain the optimum DME output. After 150 iterations, the output of DME becomes almost stable, as shown in Fig. 5.P. The process parameters are summarised in Table 5.10. In the gasification process, the optimum operating conditions were determined to be 800 °C, 1 bar, and an air in-flow of 20000 kg/h with a feed rate of 10000 kg/h of PL. The base process produces 1908 kg/h of DME with a net heat of 46422 kJ/s. However, the results of the PSO model show that the optimum operating conditions (667 °C, 2 bar, and air in-flow of 17832 kg/h in the gasifier and 400 °C in RSTR1 to 100 °C in RSTR2 for DME) can help to

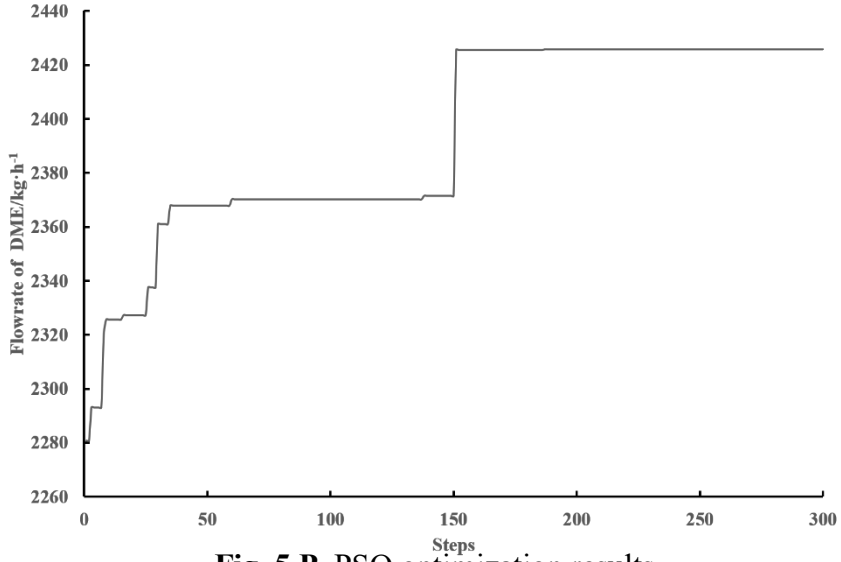

Fig. 5.P. PSO optimization results.

produce more DME as the output. Under these optimum operating conditions, 2426 kg/h of DME was produced along with a net heat of 44146 kJ/s, as summarised in Table 5.10. The simulation error of the current model was negligible because it is an integration of PSO in Aspen Plus, which runs the simulation models at a faster rate to obtain the optimum value without any human interference. Therefore, the maximum amount of DME can be produced

by setting the parameters (see Table 5.10) in the process without significantly compromising the net heat stream, which is an indicator of an energy-efficient process.

Table 5.10 Estimated optimum process parameters using PSO

Parameter	Range	Normal operation*	Optimum solution
Gasification temperature	400–800 ℃	800 ℃	667 ℃
Gasification pressure	1–4 bar	1 bar	2.0 bar
RSTR1 temperature	400–800 ℃	800 ℃	400 ℃
RSTR2 temperature	100–300 ℃	220 ℃	100 ℃
Air flow rate	2500–40000 kg/h	20000 kg/h	17832 kg/h
Flow rate of DME	-	1908 kg/h	2426 kg/h
PL biomass	10000 kg/h	-	-
Net heat stream	-	46422 kJ/s	44146 kJ/s

*[256,259,260]

5.2.4 Process G3: Co-gasification, blue, and green hydrogen

Green hydrogen production relies on renewable energy sources, including a range of options such as biochemical, photoelectric, thermal-biological, photo-thermal, thermal, electrical, etc. In this process, green hydrogen was produced through the utilization of an alkaline electrolysis cell for which some reference values have been taken from different studies [271,272]. This process involved the use of excess electricity derived from renewable energy sources (waste) to electrolyze water, yielding H_2 and O_2, as described in section 5.1.3.

Electrochemical analysis was employed to assess the potential H_2 output based on the electricity input, and the final results are summarized in Table 5.11. According to these calculations, the current process exhibits the potential to generate approximately 213.5 kg/day of H_2 using the surplus electricity produced from renewable resources (as described in section 5.1.3). The energy efficiency of this electrolysis cell is estimated at around 73%. This production of green hydrogen significantly contributes to the overall economic viability of the process.

Table 5.11 Green hydrogen production potential

Variables	Value	Variables	Values
V (res)	1.230 V	f_2	0.96
Current density	4000.0 A/m^2	Cell number	12.0
Process temperature	70.0 C	Active electrode area	0.10 m^2
r_1	4.4515×10^{-5}ohm m^2	H_2O conversion	4.604 kmol/h
r_2	7.0×10^{-9}ohm m^2/C	Molar mass of H_2O	18.015 kg/mol
S	0.33824 V	Fraction conversion of H_2O	0.141779706
t_1	-0.01539 m^2/A	P(Stack)	5×10^5 W
t_2	2.00181 m^{2}C/A		1.2789 mol/s
t_3	15.2418 m^{2}C/A	H_2 Production	4.60 kmol/h~9.3 kg/h
V (Cell)	2.026 V		213.5 kg/day
Thermoneutral cell volt V_{tn}	1.482 V	Energy Efficiency	73%
f_1	250	Faraday Efficiency	92%

5.3 Gasification based poly-generation process sustainability evaluation

Gasification based poly-generation process sustainability evaluation in terms of energy, exergy, economic, environmental, and safety analysis have been performed in this section.

5.3.1 Gasification energy analysis

Energy analysis of the process simulation modeling has been performed to calculate the overall process energy efficiency.

5.3.1.1 Process G2: Gasification, DME, and CHP Energy analysis

The Sankey diagram was developed based on the process-related energy input values from Aspen Plus. Heat, material, steam/water loss, and electricity utilisation have been considered in the Sankey diagram for our energy efficiency calculations. The efficiency of the steam turbine was set to 35% for power generation [276]. Therefore, the Sankey diagram for the base process is shown in Fig. 5.Q considering these aspects and the methodology defined in section 3.3.2. According to the results presented in the Sankey diagram, the net energy efficiency of the existing gasification process was 45%, which could be increased to 57% using the tri-generation process of thermal energy utilisation for power generation along with DME

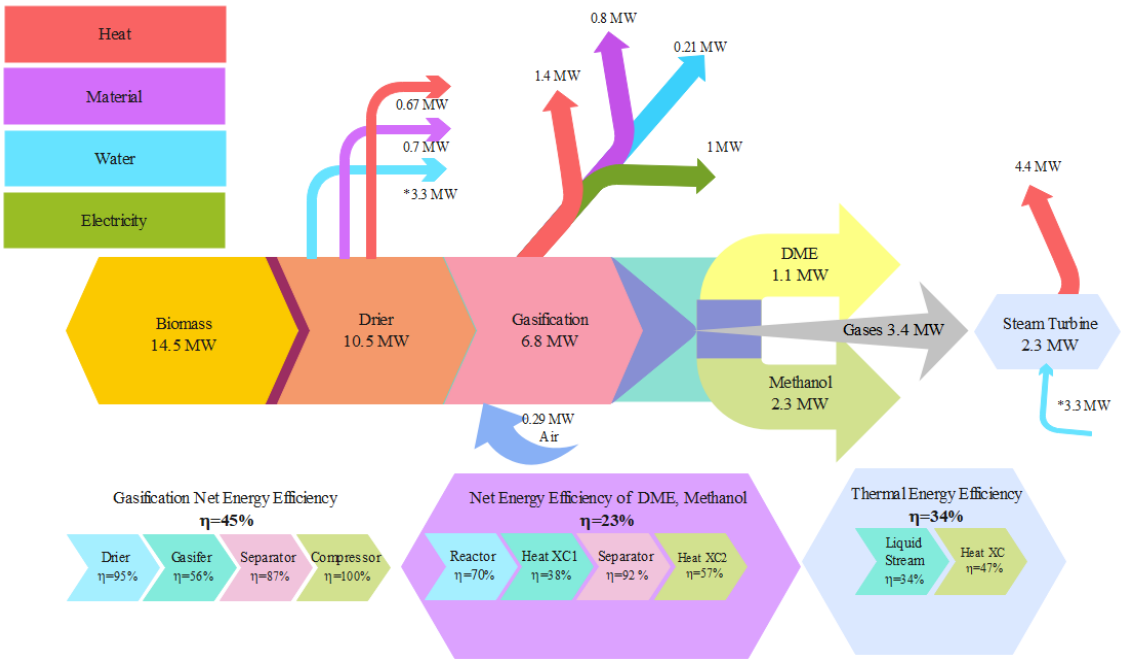

Fig. 5.Q. Energy analysis of the base model of process G2

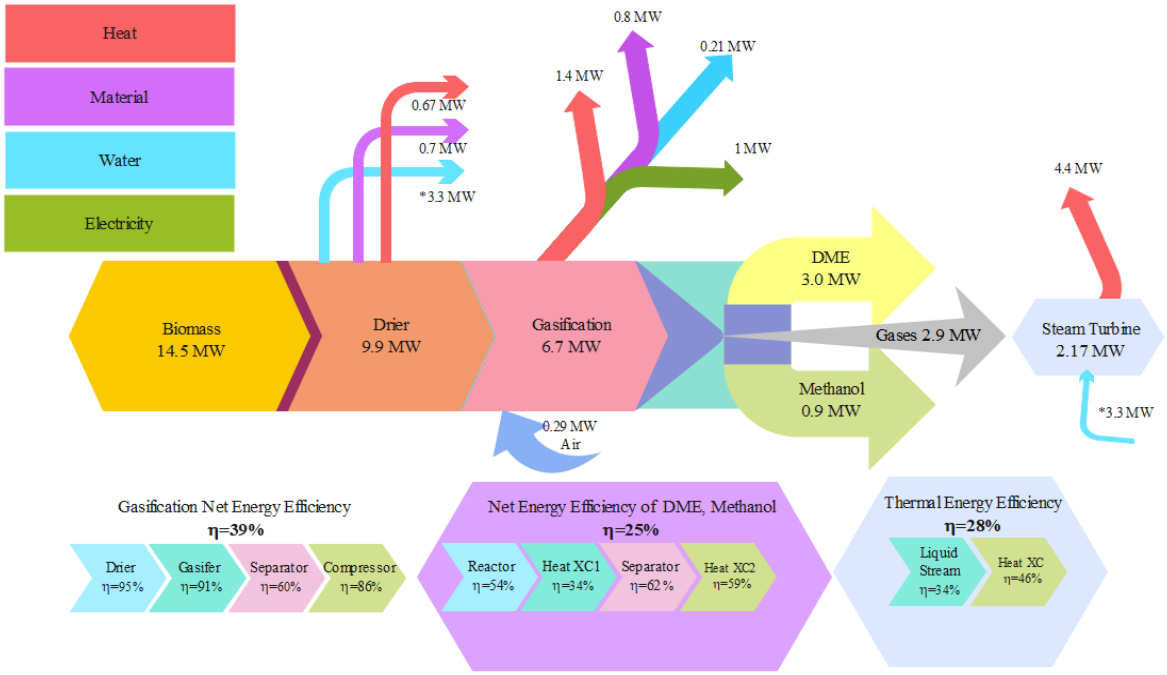

Fig. 5.R. Energy analysis of the optimized model of process G2

and methanol production. In addition, the final products (DME and methanol) of the current tri-generation process also have commercial value and can be sold as commercial fuels.

Energy analysis of the optimized process for DME production from PL was conducted by adjusting the process parameters given in Table 5.10. These optimized parameters were set in the Aspen simulation model to perform energy analysis under the optimum operating conditions. According to the results presented in Fig. 5.R, the energy efficiency of the gasification process was reduced to 39%, while the energy efficiency of the DME and methanol production process increased to 25%. Finally, the thermal efficiency (heat recovered) of the process was also reduced to 28%. Therefore, the energy efficiency of the optimized process was 4% lower when compared to the existing base process due to less thermal energy, but the DME output was improved from 23 to 25% due to the increased DME production, which was the objective of PSO.

5.3.2 Gasification exergy analysis

Simulation process exergy analysis has been performed to identify the lowest exergy efficient component; hence, it can be targeted to improve the overall process exergy efficiency.

5.3.2.1 Process G1: Gasification to SOFC, and CHP Exergy analysis

Sankey diagram has been created for exergy efficiency based on section 3.3.3. The calculations were performed in kilowatts of energy generated per ton of biomass. Several assumptions have been made regarding the power consumption of the reactors. The gasification process reactor has a capacity of 10 tons and a power consumption of 50 kW. Similarly, the efficiency of SOFCs and turbines has been estimated to be 70% and 65%, respectively [277,278]. Exhaust steam with low kinetic energy (KE) has been reused by increasing KE using a heat exchanger and compressor. The Aspen Plus simulation model was used to calculate material and heat losses (enthalpy). Exergy efficiencies of gasification, SOFC, and tri-generation through turbines have been estimated and given in Fig. 5.S. The gasification process has an overall net exergy efficiency of 63%, which has been enhanced to 69.8% by the use of SOFCs. However, if tri-generation through turbines is used, this method has overall 34.6%

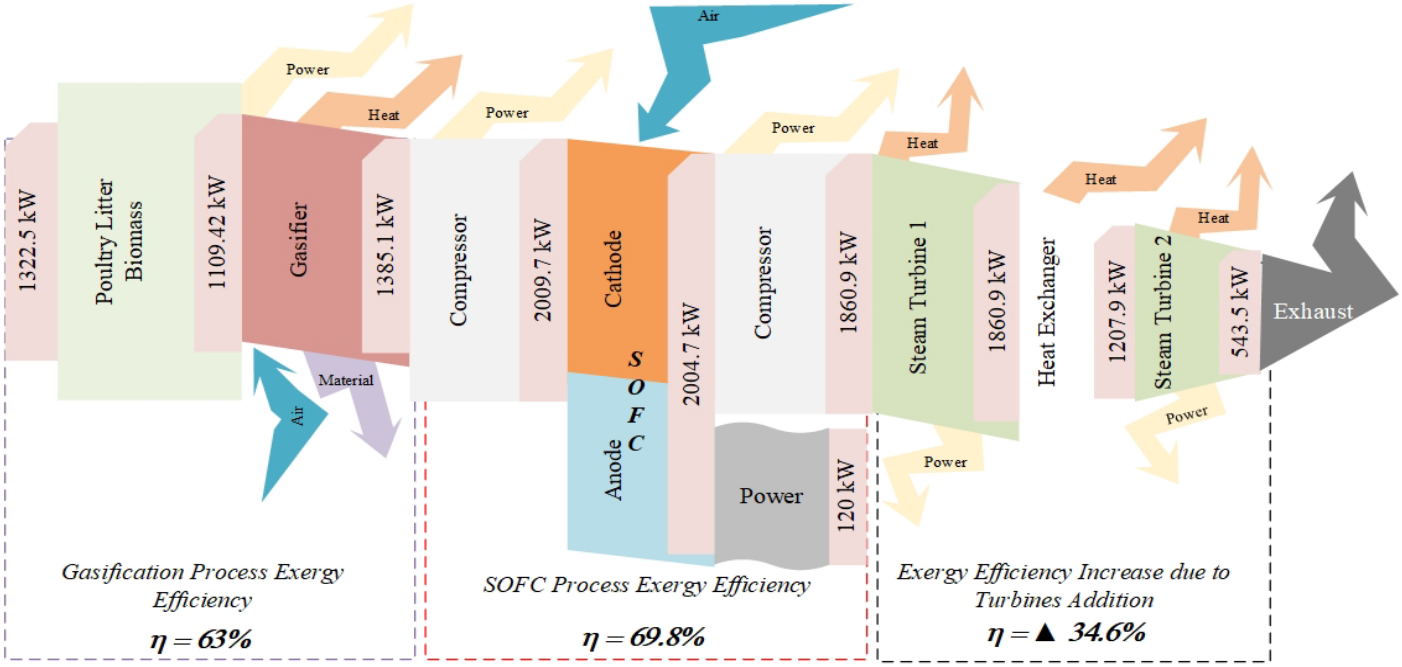

Fig. 5.S Exergy efficiency analysis of process G1

efficiency. Therefore, the suggested tri-generation process is more exergy efficient than the gasification process.

5.3.2.2 Process G3: Co-gasification, blue, and green hydrogen exergy analysis

Exergy analysis of the process was performed to identify the components with the greatest exergy destruction which highlighted the potential areas of improvement in terms of exergy. The exergy analysis was done based on the methodology outlined in section 3.3.3, and the final results are presented in Table 5.12. These results encompass both calculated values and data sourced from the Aspen Plus simulation model. The exergy analysis reveals that the gasifier, heat exchanger, and steam turbine emerge as the components with the lowest exergy efficiencies of 62.2%, 64.2%, and 61.0%, respectively. Therefore, these particular components need to be focused to enhance the overall exergy efficiency of the process. This strategic improvement effort can ultimately contribute to improving the overall sustainability of the entire process.

Table 5.12 Exergy analysis of process G3

	Input Exergy (Ex_{in}) kW	**Output Exergy** (Ex_{out}) kW	**Exergy destruction** (E_D) kW	**Efficiency (η)**
Drier	23345	19065	4280	81.7%
Gasifier	26407	16427	9979.5	62.2%
Compressor 1	44340	44333	7.0	100.0%
HeatXC	25808	16563	9245	64.2%
Steam Turbine	35088	21404	13684	61.0%
AEC	7100	5183	1917	73.0%
Flash Sep	25808	25228	580	97.8%
Cooler 1	26025	25228	797	96.9%
Compressor 2	26025	26020	5.0	100.0%

Compressor 3	26536	26020	516	98.1%
Separator 1	26536	26097	439	98.3%
Cooler 3	2478	1911	567	77.1%
Separator 2	2622	2478	144	94.5%
Cooler 4	1540	1018	522	66.1%
Separator 3	1687	1540	147	91.3%

5.3.3 Process G3: Exergoeconomic analysis

Economic co-relation and cost-effectiveness associated with exergy production and destruction within the process have been assessed through exergoeconomics analysis. The conclusive outcomes of this exergoeconomics analysis, including destruction costs and investment costs are given in Process G3 economic analysis in section 5.3.5 which has been calculated based on Appendix A7. The results of the exergoeconomics destruction cost analysis reveal that the highest destruction cost is due to the AEC, around $6,647.0 per hour, followed by the gasifier at approximately $6,561.3 per hour, and the heat exchanger $6,541.9 per hour in Table 5.13. Especially, the cost of destruction for the AEC is high, primarily due to the substantial investment costs associated with it around 28.6% of the total investment cost (as given in section 5.3.5, Table 5.16). Among these costs, $4,852.3 per hour apply to endogenous destruction, while the remaining is exogenous destruction. Therefore, the primary factor driving the high destruction cost in the AEC is its significant self-associated factors. While the cost of destruction for the gasifier, heat exchanger, and steam turbine is higher due to the considerable advanced exergy destruction within these components. However, it is significant that the exogenous destruction costs for the gasifier, heat exchanger, and steam turbine surpass that of the AEC, around $2,479.6, $2,343.4, and $2,538.8 per hour, respectively (Table 5.13). Therefore, the investment costs in these alternative components have a substantial impact on reducing the destruction costs associated with them.

Table 5.13 Exergoeconomics cost destruction analysis for process G3

	$C_{F,k}$ ($/h)	$C_{D,k}^{En}$ ($/h)	$C_{D,k}^{Ex}$ ($/h)	$C_{D,k}^{av}$ ($/h)	$C_{D,k}^{uv}$ ($/h)	$C_{D,k}^{av,En}$ ($/h)	$C_{D,k}^{av,Ex}$ ($/h)	$C_{D,k}^{un,En}$ ($/h)	$C_{D,k}^{un,Ex}$ ($/h)
Drier	6513.2	5319.1	1194.1	5861.9	651.3	5315.7	546.2	3.4	647.9
Gasifier	6561.3	4081.7	2479.6	6233.2	328.1	-2375.3	8608.5	6457.0	-6128.9
Compressor 1	6508.4	6507.4	1.0	5857.6	650.8	0.0	5857.6	6507.4	-5856.6
Heat XC	6541.9	4198.4	2343.4	6476.4	65.4	-2492.2	8968.7	6690.7	-6625.2
Steam Turbine	6509.9	3971.1	2538.8	5858.9	651.0	-844.2	6703.1	4815.3	-4164.3
AEC	6647.0	4852.3	1794.7	3921.7	2725.3	-1152.9	5074.6	6005.2	-3279.9
Flash Separate	6507.0	6360.8	146.2	5856.3	650.7	-3.3	5859.5	6364.0	-5713.3
Cooler 1	6509.9	6310.5	199.4	3905.9	2603.9	-6.0	3911.9	6316.5	-3712.6
Compressor 2	6512.7	6511.5	1.3	5861.4	651.3	0.0	5861.4	6511.5	-5860.2
Compressor 3	6512.7	6386.1	126.6	6121.9	390.8	-2.4	6124.4	6388.5	-5997.7
Separator 1	6535.0	6426.9	108.1	5881.5	653.5	-1.8	5883.3	6428.7	-5775.2
Cooler 3	6509.9	5020.3	1489.5	6184.4	325.5	-307.5	6491.9	5327.8	-5002.3
Separator 2	6535.0	6176.1	358.9	6273.6	261.4	-19.2	6292.8	6195.3	-5933.9
Cooler 4	6509.9	4303.3	2206.6	6184.4	325.5	-648.2	6832.6	4951.5	-4626.0
Separator 3	6535.0	5965.6	569.4	6273.6	261.4	-47.6	6321.2	6013.1	-5751.7

In terms of exergoeconomics investment costs, the AEC ranks as the highest, with a value of $193.60 per hour, followed by the gasifier at $107.89 per hour in Table 5.14 based on Appendix A7. AEC and gasifier both exhibit higher endogenous investment costs, with the AEC at $141.33 per hour and the gasifier at $67.11 per hour, compared to the other components. Furthermore, the exogenous investment costs for the AEC and gasifier are also higher $52.27 and $40.77 per hour, respectively. These results show the substantial influence that investments in other components can reduce the exergoeconomics advanced investment costs of the AEC and gasifier. Therefore, allocating investments to the other components within the valorization plant can play a pivotal role in reducing the overall exergoeconomics investment costs for these

specific components, ultimately contributing to the enhanced sustainability of the entire process.

Table 5.14 Exergoeconomic advanced investment analysis for process G3

	I ($/h)	I_k^{En} ($/h)	I_k^{Ex} ($/h)	I_k^{av} ($/h)	I_k^{uv} ($/h)	$I_k^{av,En}$ ($/h)	$I_k^{av,Ex}$ ($/h)	$I_k^{uv,En}$ ($/h)	$I_k^{uv,Ex}$ ($/h)
Drier	59.89	48.91	10.98	53.90	5.99	48.88	5.02	0.03	5.96
Gasifier	107.89	67.11	40.77	102.49	5.39	-39.06	141.55	106.17	-100.78
Compressor 1	55.03	55.02	0.01	49.53	5.50	0.00	49.53	55.02	-49.52
Heat XC	88.46	56.77	31.69	87.57	0.88	-33.70	121.27	90.47	-89.58
Steam Turbine	56.46	34.44	22.02	50.81	5.65	-7.32	58.13	41.76	-36.12
AEC	193.60	141.33	52.27	114.22	79.38	-33.58	147.80	174.91	-95.53
Flash Separate	53.60	52.40	1.20	48.24	5.36	-0.03	48.27	52.42	-47.06
Cooler 1	56.46	54.73	1.73	33.87	22.58	-0.05	33.93	54.78	-32.20
Compressor 2	59.31	59.30	0.01	53.38	5.93	0.00	53.38	59.30	-53.37
Compressor 3	59.31	58.16	1.15	55.76	3.56	-0.02	55.78	58.18	-54.62
Separator 1	81.60	80.25	1.35	73.44	8.16	-0.02	73.46	80.27	-72.11
Cooler 3	56.46	43.54	12.92	53.63	2.82	-2.67	56.30	46.21	-43.38
Separator 2	81.60	77.12	4.48	78.34	3.26	-0.24	78.58	77.36	-74.09
Cooler 4	56.46	37.32	19.14	53.63	2.82	-5.62	59.26	42.94	-40.12
Separator 3	81.60	74.49	7.11	78.34	3.26	-0.59	78.93	75.08	-71.82

5.3.4 Electricity production from thermal energy

Gasification process thermal energy has been transferred into steam turbine generators to estimate the potential electricity generation. The following section has the details of it.

5.3.4.1 Process G3: Electric power potential analysis

The syngas generated within the current process contains a substantial amount of thermal energy. This energy has been recuperated through a heat exchanger employing water as the medium for energy transfer. Consequently, this process yields high-temperature and high-pressure steam. To assess the potential for steam-to-electricity conversion, the methodology in

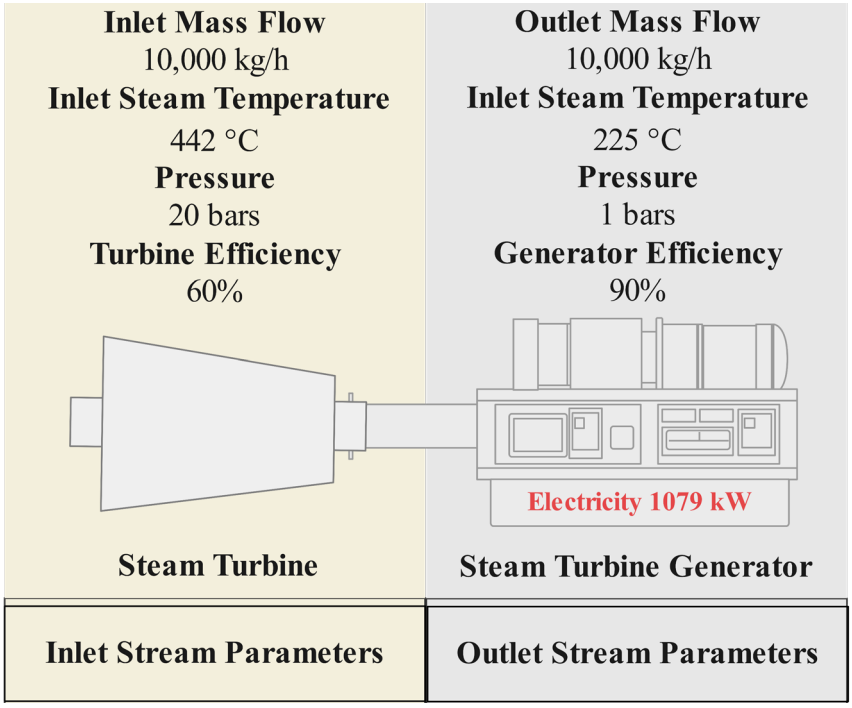

Fig. 5.T. Steam to electricity potential for process G3

section 3.3.6 has been applied. The analytical findings, as given in Fig. 5.T, indicate that the current process has an electricity generation potential of approximately 1079 kW through the recovery of heat from syngas. This is accomplished by employing a turbine with an efficiency of 60% and an attached generator with an efficiency of 90%. Most of the recovered thermal energy has been wasted in the steam turbine. The electricity production capacity of the plant is approximately 579 kWh (as indicated in Table 5.16), leaving an excess power of 500 kW that can be harnessed for the production of green hydrogen using an electrolysis cell.

5.3.5 Gasification process economic analysis

5.3.5.1 Process G2: Gasification, DME, and CHP economic analysis

Economic analysis (EA) of the PL to DME process was performed based on the methodology presented in Section 3.3.7. The EA results are summarised in Table 5.15 with the breakdown given in Appendix A8. A cost-benefit analysis was performed for a pilot plant with a 1 t/h biomass valorization capacity with the assumption that the maximum plant working time was 23 h/day with a 1-hour breakdown time. According to the results presented in Table

5.15, only 2861 USD/d revenue can be generated from the conversion of PL to DME without process optimization, and the cost of DME was ~0.54 $/kg. However, 3,683 USD/d revenue can be generated from the conversion of PL to DME after process optimization, and the cost of DME was ~0.43 $/kg, which is <1.66 $/kg from the direct system synthesis [22], and is also market competitive (0.65 $/kg) [23]. In addition, the breakdown of the plant capital cost was performed, as shown in Fig. 5.U. It was apparent that the gasifier and electric power generation set-up cover almost half of the total capital cost. Similarly, the cost of raw materials and manpower accounts for 50% of the total operating costs, as shown in Fig. 5.V. Sensitivity analysis of the economic performance of PL in the DME production process was carried out by applying the IRR as an economic indicator according to the method presented in Section 3.3.7.

According to the results of our sensitivity analysis (see Fig. 5.W), the maximum IRR was 15.1% at 100% plant efficiency for the base DME production process, whereas it was 26.8% for the optimized process. However, it is difficult to achieve 100% plant process efficiency and therefore, different efficiency points were selected for our IRR calculations. At 90% plant process efficiency (Fig. 5.W), the IRR was ~5% for the base process and 22.6% for the optimized process. When the efficiency is <90%, DME production in the base process was not feasible until it is subsidized, while the optimized process remains feasible up to an 80% process efficiency with an IRR of 3.3%, which is quite low. Therefore, another scenario was incorporated for economic analysis, which included a subsidy of $50 per ton basis. The results for $50 per ton subsidy on biomass waste valorization were quite encouraging. According to these results (Fig. 5.W), the IRR of the subsidized base process was 30.2% at 100% process efficiency, which varies from 27.7 to 5.3% when the process efficiency varies from 90 to 50%. The IRR of the subsidized optimized process was 35.4% at 100% process efficiency, which varies from 33.2 to 17.5% when the process efficiency varies from 90 to 50%. Therefore, the

optimized process using PSO was more economically stringent than the base process, while the energy efficiency was slightly compromised.

Table 5.15 Cost-benefit analysis of 23 t/d plant capacity for process G2.

Cost category		**Cost ($)**	
Capital cost		424400	
Operational cost/day		2385	
Estimated revenue	**DME (tons)**	**Market value**	**Cost $/t**
DME (base process) ratio 0.1908	4.3884	2861	652
DME (optimum) ratio 0.2426	5.5798	3638	

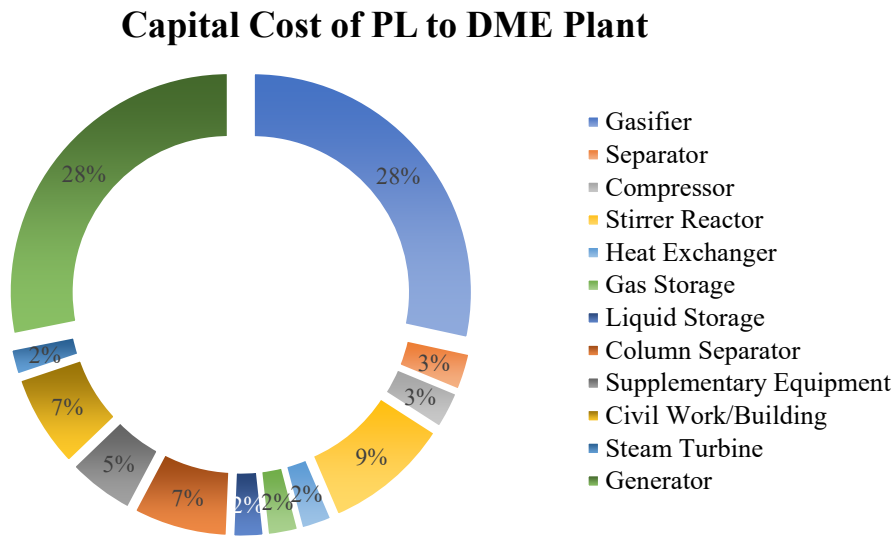

Fig. 5.U. The capital cost of DME plant (process G2)

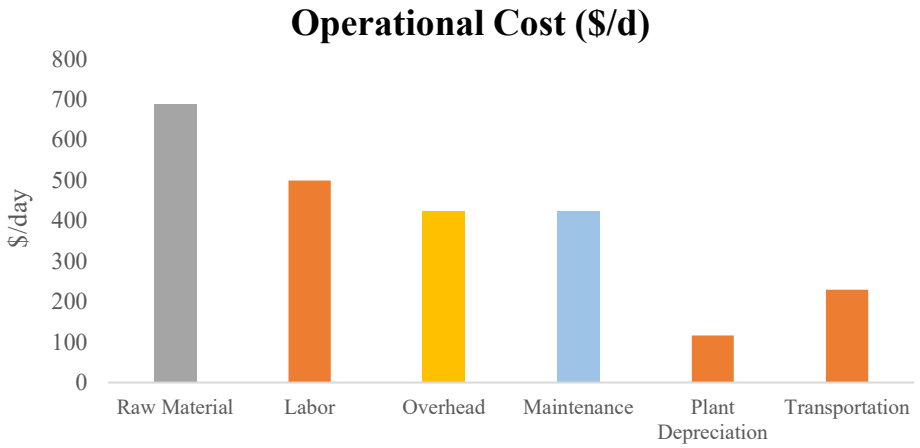

Fig. 5.V. Operational cost ($) of the PL to DME process (process G2)

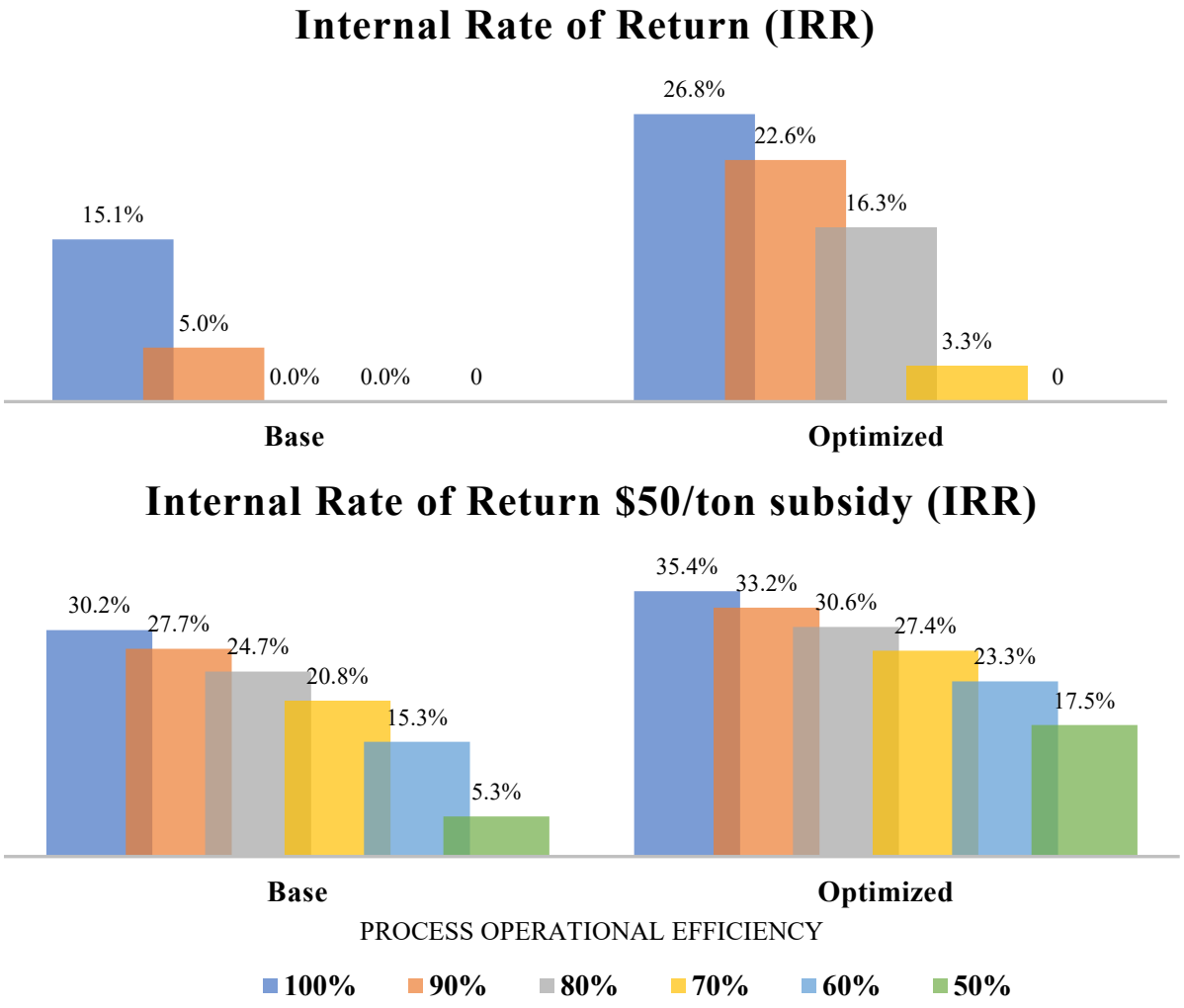

Fig. 5.W. Process payback period and IRR (process G2)

5.3.5.2 Process G3: Co-gasification, blue, and green hydrogen economic analysis

The economic analysis of the process was conducted following the methodology outlined in section 3.3.7. The economic analysis utilized data sourced from literature and equipment suppliers, summarized in Table 5.16. Specifically, the capital cost estimation is focused on a primary plant with a capacity of 20 t/h, and secondary equipment such as 1.5-megawatt steam turbine, a generator, and an electrolysis cell with a 500-kWh capacity. Certain assumptions were considered during the economic analysis, as described in section 3.3.7. Furthermore, the revenue cost of the product (Table 5.18) is estimated based on the average or lowest product

prices due to price fluctuation in different regions as given in Table 5.18. According to estimates, the capital cost assessment for the 20 t/h plant was around 1.726 million USD. Particularly, the electrolysis cell, column separator, and gasifier collectively accounted for more than half of the total investment. The daily operational costs of the plant are summarized in Table 5.17. Within these operational costs, the primary cost drivers are the raw materials. Developing strategies aimed at minimizing these costs, especially during site selection and transportation phases, can significantly contribute to reducing raw material expenses. Transportation costs often represent a major portion of raw material expenses. Therefore, implementing effective supply chain strategic planning can mitigate the costs incurred in acquiring raw materials, ultimately leading to reduced operational cost.

Considering the capital and operational costs (as summarized in Tables 5.16 and 5.17), the IRR was calculated and given in Fig. 5.X. The IRR results indicate that the current process is economically viable, achieving an IRR of 37% at a process efficiency of 90%. It should be noted that this efficiency threshold may be considered high for processes of a similar nature [279]. Therefore, the current process which involves sustainable waste valorization may be eligible for subsidies in the form of carbon credits. To explore this possibility, an alternative economic scenario was analyzed, assuming a subsidy of 10 $/t for waste valorization. In this scenario, as shown in Fig. 5.X, the subsidized process becomes economically feasible at a plant efficiency level of 60%, achieving an IRR of 8%. Therefore, the subsidized process presents a more economically attractive option for developing this process.

Table 5.16 Capital cost of waste valorization plant for process G3

Item	Qty	Price/unit	Cost (%)	Equipment ($000)	Power (kW)	Ref.
Drier	1	32,000	1.9%	32	37	[280]
Gasifier	1	200000	11.6%	200	40	[281]
Steam Pump	2	15000	1.7%	30	44	[282]
Feedstock mixer	2	22500	2.6%	45	180	[283]
Heat Exchanger	1	132000	7.7%	132	0	[284]
Flash Separator	1	10000	0.6%	10	10	[285]
Column Separator	3	108000	18.9%	324	0	[286]
Air Valve	3	6000	1.0%	18	0	[287]
Compressor	3	10000	1.7%	30	18.5	[288]
Water Pump	1	15000	0.9%	15	100	[289]
Cooler	2	20000	2.3%	40	130	[290]
Steam Turbine	1	20000	1.2%	20	0	[291]
Generator (1.5 MW)	1.5	120000	10.5%	180	0	[292]
Cryogenic liquid tank	5	20000	5.8%	100	0	[293]
AEC Electrolysis cell	500	1000	28.6%	500	(500)	[294]
Shed Area (m^2)	1000	50	2.9%	50	20	[295]
Grand total				1726	1079.5	

Table 5.17 Operational cost per day basis for process G3

Items	QTY	Cost ($/day)	Cost (%)	Ref.
Biomass ($/day)	240	12000	14.3%	[296]
Plastic Waste ($/day)	240	60000	71.5%	[297]
Labor ($/day)	-	4500	5.4%	[298]
Overhead ($/day)	1	2000	2.4%	[298]
Maintenance/Engineering ($/day)	1	4500	5.4%	[298]
Utility (kW)	579.5		Self-sufficient (Table 5.16)	
Water ($/day)	160	400	0.5%	[299]
Plant linear depreciation ($/day)		491	0.6%	Table 5.16
Total (Cost/day)		***83,891***		

Table 5.18 Process revenue per day basis for process G3

Items	QTY	Market Value ($)	Price ($)	Ref.
Hydrogen (Blue)	32.20 ton	64400	~2000/ton	[300]
Hydrogen (Green)	213.4 kg	1280	~6/kg	[300]
LPG (Methane)	23.92 ton	4784	~200/ton	[301]
CO_2 (Liquid)	175 ton	35000	~200/ton	[302]
Total (Revenue/day)		***105464***		

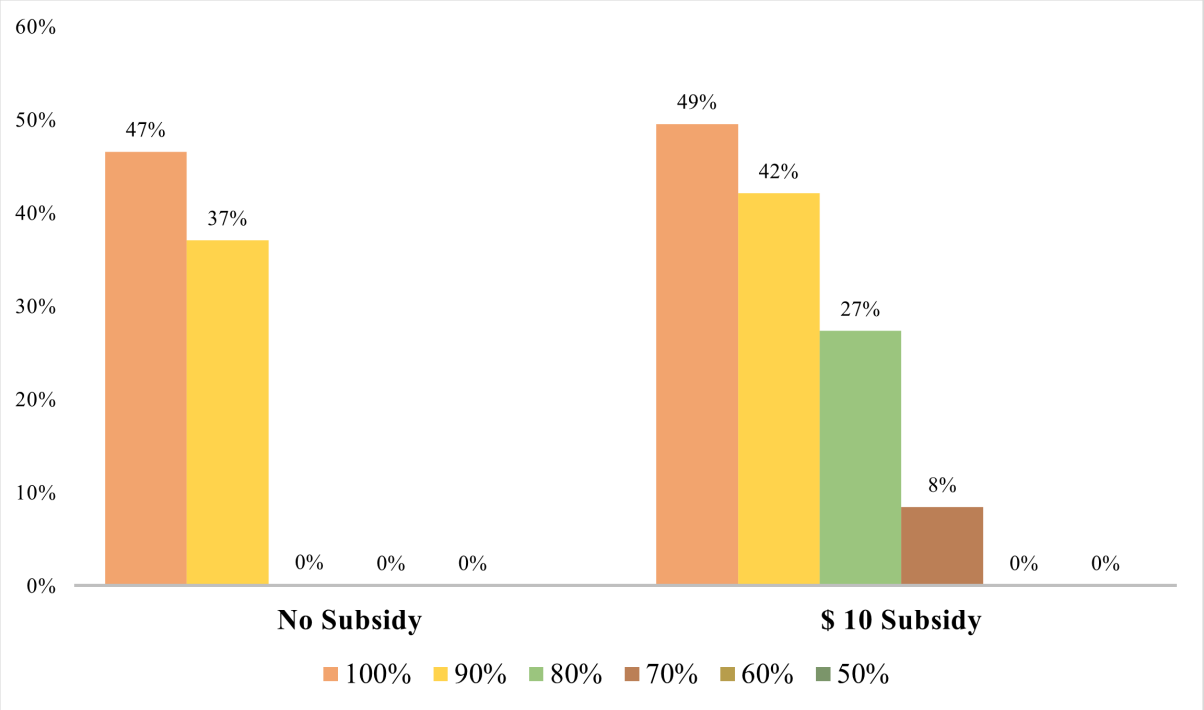

Fig. 5.X. Internal rate of return (IRR) for process G3 at different efficiencies

5.3.6 Gasification process environment life cycle assessment

5.3.6.1 Process G2: Gasification, DME, and CHP Environment LCA

The LCA results including LCA midpoint, endpoint, and single scores for PL to gasification, and PL to DME processes are given in Fig. 5.Y to 5.AA, respectively. A higher process score negatively impacts the environment. According to the midpoint results shown in Fig. 5.Y, the PL gasification process has better performance in carcinogens, non-carcinogens, ozone layer depletion, respiratory organics, and aquatic eutrophication when compared with the other three processes. The PL to DME process has lower performance than the gasification process in terms of carcinogens, non-carcinogens, non-carcinogens, ozone layer depletion,

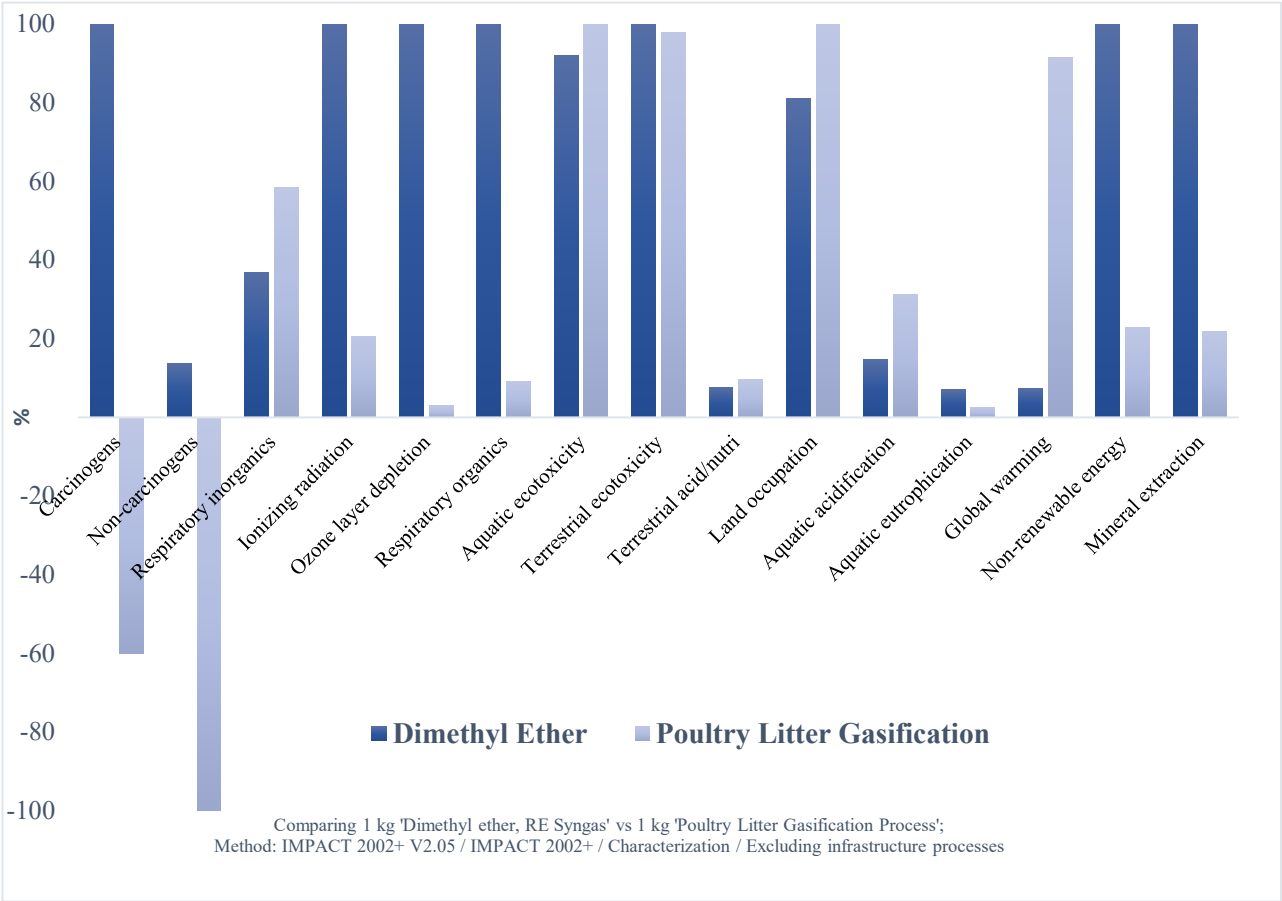

Fig. 5.Y. Midpoint LCA of PL gasification vs. PL gasification to DME (Process G2)

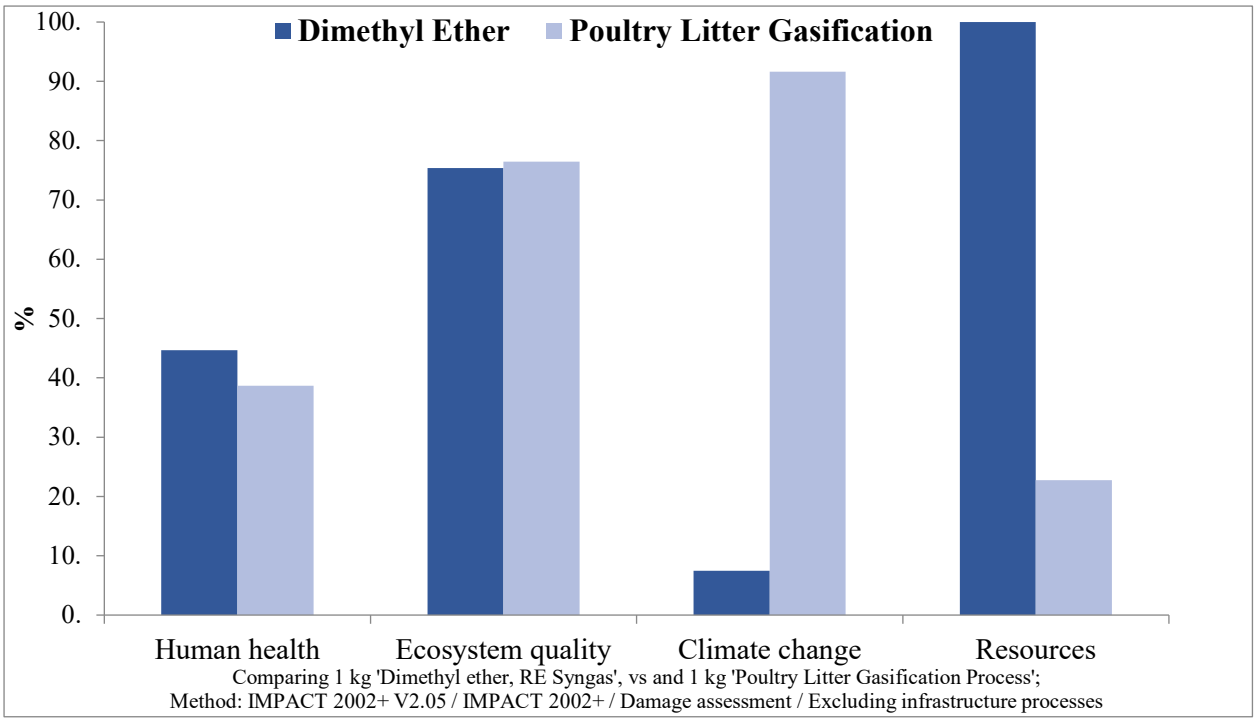

Fig. 5.Z. Endpoint LCA PL gasification vs. PL gasification to DME (Process G2)

respiratory inorganics, and non- renewable energy. However, the endpoint impact analysis showed a different result, as presented in Fig. 5.Z. The results determined by the endpoint (damage category) approach show that the PL to gasification process has a higher score for

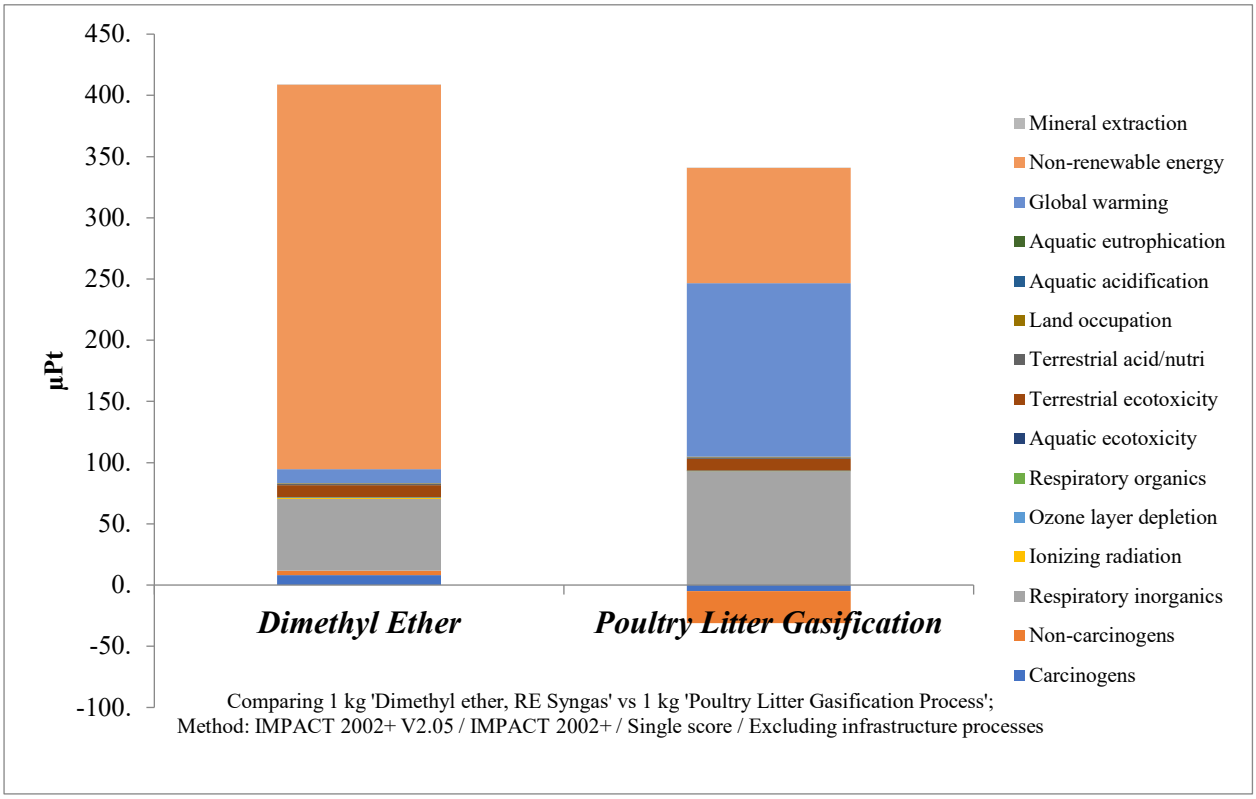

Fig. 5.AA. LCA single score PL gasification vs. PL gasification to DME (Process G2)

climate change. PL to DME production has a higher resource score. Therefore, based on both the midpoint and endpoint results, the PL-to-gasification process appears to be more environmentally friendly than the DME production process.

While the comparison of the PL gasification to DME production process with the PL to gasification process, the results obtained using the LCA single score approach have been determined to obtain the breakdown of the 15 LCA indicators in terms of μPt instead of a percentage. According to the single point score presented in Fig. 5. AA, the negative impacts of gasification on the environment are mainly caused by ozone layer depletion and respiratory inorganics. The PL to DME manufacturing process from syngas has higher single scores because of the non-renewable energy utilisation for PL processing. Therefore, if renewable energy is generated from the PL gasification-based tri-generation process used in the PL to DME process, then this process could be more eco-friendly than the PL gasification process.

5.3.7 Gasification process safety analysis

The total process safety total scores (PSTS) for each thermal technology (HTG, gasification, and pyrolysis) have been calculated based on section 3.3.9, and the individual score with respect to each parameter has also been determined, as presented in Fig. 5.BB. The HTG has a total process safety score of 210.2, followed by pyrolysis (226.4) and gasification (228.5). The PSTS of conventional gasification is the highest followed by pyrolysis process, while HTG has the lowest score. Lower scores represent safer processes; hence, HTG is the safest among these three technologies. When temperature scores are compared between HTG, conventional gasification, and pyrolysis, HTG has the lowest individual temperature score since its operating temperature lies in 374-400 ^{o}C, which is lower than those of the other two thermal processes. Therefore, lower operating temperature usually means that the process is safer while pressure score of HTG is higher compared with others because the pressure required by HTG is 20-25 MPa. Hence, higher pressure means that more hazards will exist in the process, resultantly, process safety score of pressure is higher. Heat of reaction for gasification and

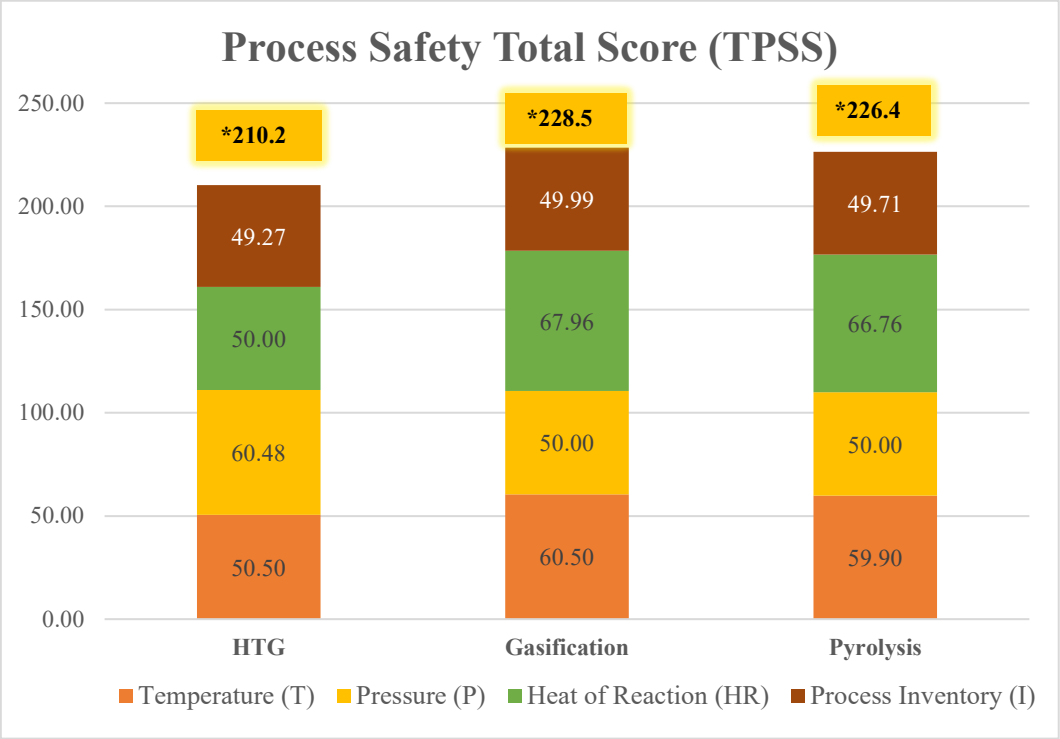

Fig. 5.BB. Process safety total score for HTG, Gasification, and Pyrolysis

pyrolysis are higher than that of the HTG as both processes are more exothermic compared with HTG, thus gasification and pyrolysis have higher PSTS than HTG which represents that these processes have higher level of hazards than HTG. Finally, process inventory in terms of yield which has almost equivalent score, consequently all these processes have same level of hazards in term of process inventory. Therefore, HTG process has outperformed gasification and pyrolysis in temperature and heat of reaction scores despite having higher PSTS due to pressure. For all these processes, the process inventory score is nearly equal. Based on these findings, it can be concluded that HTG process is safer than gasification and pyrolysis in this case.

5.4 Conclusion: Gasification G1, G2, and G3 Process

In process G1: Gasification to SOFC, and CHP economic analysis an Aspen Plus simulation-based tri-generation approach has been devised for biomass waste valorization. Following the key findings of process G1:

- XGB model predictions of H_2, I, J, theR^2 value is greater than 0.97, indicating that the XGB model has good prediction accuracy.
- Optimization research reveals that the gasification process at 600 ºC, 1 bar pressure, 0.25-0.33 BMR, and 850-950 ºC SOFC temperature produces the best results when compared to other parameters.
- Pressure has no effect on the gasification process; however, it has the inverse result on SOFC real voltage and Gibbs Energy.
- BMR is the most significant factor influencing H_2, I, and J among all input parameters, followed by SOFC temperature and pressure.
- Exergy efficiency analysis results demonstrate that this tri-generation method is energy efficient, with a 34.6% higher exergy efficiency than gasification process [303].

Therefore, these findings are based on a simulation model with supporting evidence from the literature. Similarly, economic analysis of this trigeneration is not performed in this chapter because our primary research focus is on prediction and optimization, as well as exergy analysis. Based on exergy research, it appears that this tri-generation method could be more cost effective than gasification in terms of converting biomass waste to energy, but at the cost of a greater plant capital expenditure.

Process G2: Gasification, DME, and CHP is mainly focused on tri-generation process design, optimization, energy, environment, and economic analysis for converting PL to DME. Following the key findings of process G2:

- PSO-based optimization results have a better DME yield from 190.8 kg/t to 242.6 kg/t of biomass.
- The energy efficiency of the tri-generation process is 57%, which is comparatively higher (45%) than that of the gasification process. It was 53% for the optimized tri-generation process and 39% for the gasification process.
- The PL to DME process is economically feasible and the IRR of the optimized process varies from 26.8 to 3.3% when the process efficiency drops from 100 to 70%, whereas the base process is not feasible when the process efficiency is <90%.
- Subsidized optimized process, the IRR varies from 30.2 to 17.5% when the process efficiency decreases from 100 to 50%. However, the IRR of the base process varied from 30.2 to 5.3% when the process efficiency varied from 100 to 50%.
- The cost of DME produced by this process ranges from 0.43 to 0.54 $/kg, which is market competitive, and the optimized process is more sustainable than the base process due to its higher SI score of 0.290.

Process G3: An innovative process for the integrated production of blue and green hydrogen have been developed through the co-gasification of biomass and plastic waste. Sustainability analysis has been conducted which include the economic considerations, energy potential, exergy, advanced exergy, and exergoeconomics aspects [304]. Following the key findings of process G1:

- The process demonstrates economic feasibility when operational efficiency is more than 90%, yielding an IRR of 37%. For the subsidized process, economic viability is maintained within a process efficiency of 100-70%, and IRR of ranging from 49% to 8%.
- The process has a potential to generate 1079 kW of electricity from syngas thermal energy, with 500 kW of surplus electricity available for use in the electrolysis cell, resulting in the production of around 213.5 kg/day of H_2.
- Gasifier, heat exchanger, and steam turbine exhibit higher exergy destruction levels compared to other components, with values around 62.2%, 64.2%, and 61.0%, respectively.
- Advanced exergy analysis indicates that the steam turbine and gasifier experience the most substantial exergy destruction around 13,684 kW and 9,979.54 kW, respectively. The AEC incurs the highest destruction cost $6,647.0 per hour, followed by the gasifier at $6,561.3 per hour, and the heat exchanger at $6,541.9 per hour.

The gasification process for valorizing biomass waste is widely used, and its technology is more mature than that of other sustainable thermal processes. Although the gasification process is sustainable, it can be made more environmentally friendly by incorporating secondary or tertiary processes, as proposed in section 5.1. The high moisture content of biomass waste makes the gasification process less sustainable, but this can be overcome by

incorporating pre-processing methods such as torrefaction. However, the gasification process is preferred over HTG, and the decision-making model (Section 8) in this study also supports gasification. Though, additional processes, such as plasma gasification and pyrolysis integration, have been investigated in chapter 6 and 7.

6 Chapter: Plasma gasification-based tri-generation process

In this chapter plasma gasification-based valorization process of biomass waste has been developed and its sustainability evaluation has been done. PG is more versatile to valorization of feedstock types with lower emissions due to better disintegration of feedstock organic pollutant at higher temperature.

6.1 Plasma gasification simulation process development

The schematic diagram of the PG based tri-generation process is developed and given in Fig. 6.A based on the work of Wang *et. al* 2011 [261]. The dry biomass is transferred into plasma gasifier where plasma torch at high temperature converts PL biomass into syngas and aggregate (biochar). The temperature of plasma gasifier torch is up to 3000 ^{o}C due to which biomass has been converted into syngas with a negligible amount of the tar particles production, which is a non-conventional (NC) component consist of C, H, N, S and O (Table 6.1) at this high temperature. In this process, leftover aggregate particles in syngas have been considered as a tar which have been separated from the syngas through cyclone before being used at the next process where reaction has been taken place to convert syngas into methanol. This methanol further dehydrated to form a DME at gaseous phase. A mixture of DME and syngas has been produced which has a high temperature of around 1000 ^{o}C. For the synthesis of DME from syngas, the temperature of the gas has been reduced to less than 100 ^{o}C by transferring the gas heat into water through heat exchanger. This syngas (mainly include H_2) and DME mixture has been transferred to the flash separator where DME has been separated while the syngas has been transferred to the DME reactor for further recovery. Heat recovery from the syngas converts the water into high temperature and pressure (~212 ^{o}C, ~20 bar) steam which has been transferred into the steam turbine for power generation. This electric power can be further utilized in the plant operations. While the low temperature and pressure steam has been

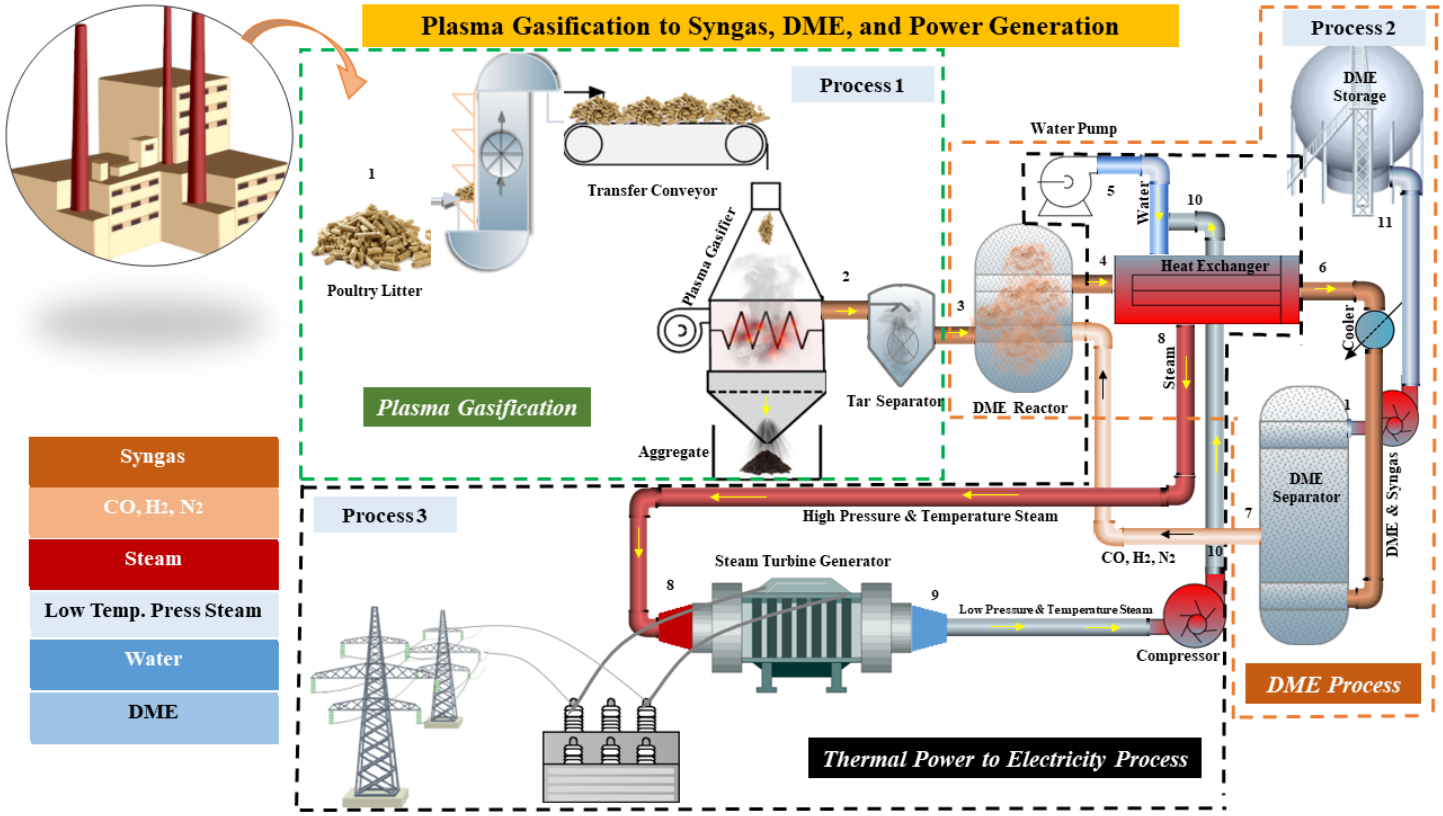

Fig. 6.A. Plasma gasification schematic diagram

further transferred to the heat exchanger to get thermal energy from the syngas, hence, it is a cyclic process. DME which has been produced in this process will be stored into the bowser at high pressure generated through compressor.

The PG tri-generation process simulation model for PL valorization has been developed by using Aspen Plus. The process flow of the developed model has been given in Appendix A11 and the description and the key parameters of the used blocks have been given in Table 6.2 based on existing literature [305–308]. PL biomass has been used as a feedstock in this developed model. The proximate and ultimate analysis of PL feedstock given in Table 6.1 has been used as an input in the simulation model [247,309]. Furthermore, different simulation blocks have been utilized which have been described in Table 6.2. In this simulation model, the following assumptions have been considered [307]:

- It is a steady state simulation;
- Isothermal process with no heat loss;

- C, H, O, S and N elements have been taken as an NC biomass input;
- All C, H, O, and N elements (reactants) conversion have been taken place;
- Inorganic material like S is inert; and
- Due to high temperature, negligible tar and ash have been produced which has no effect on the reactions.

Table 6.1 Proximate and ultimate analysis for plasma gasification model

Proximate analysis wt. %			**Ultimate analysis wt. %**		
	Biomass	**Biochar**		**Biomass**	**Biochar**
Moisture	7.6		Carbon	43.98	46.4
Fixed Carbon	15.3	46.7	Hydrogen	5.16	0.7
Volatile Matter	63.6	7.9	Nitrogen	4.63	2.0
Ash	13.5	47.9	Sulphur	0.75	0.02
HHV (MJ/kg)	16.8		Oxygen	31.98*	2.8
*Based on difference					

PL biomass introduced at the rate of 10 t/h, the temperature of 30 ºC and the pressure of 1 bar is dried by using the RSTOIC block at the temperature of 100 ºC. The Peng Robinson equation of state with Boston-Mathias modification (PR-BM) has been used in the simulation process when the output is in the form of low molecular weight compounds [124,310]. The moisture separated from the biomass and dried biomass (PL) reacted further at 1000 ºC which breakdown the PL into C, H, O, N, and low molecular compounds. Finally, the PG has been established in the presence of air as a gasifying agent with equivalence ratio of 0.3-0.6 [247]. The produced syngas has been further reacted at the RCSTR-1 for steam reformation as given in Table 6.2. At this phase, the temperature of the syngas is around 1000 ºC which is extremely high for methanol to DME production, therefore, the temperature has been reduced by transferring the thermal energy into the water which produces a steam of around 212 ºC and 20

bars through heat exchanger. This steam can be further utilized in the steam turbine to generate electricity while the cooled syngas can further react at the temperature range of 200-220 ºC to form methanol and DME. The temperature of these mixed gases has been reduced further for DME separation through flash separator. A detailed description of the parameters has been given in Table 6.2 and the stoichiometric data were presented in Table 6.3 [306,307,311–313].

Table 6.2 Aspen Plus model specifications for base model of plasma gasification to DME

ID	Block	Parameters
DRIER	RSTOIC	Biomass drying at 100 ºC, 1 bar
H2OSP1	SEP	Steam and dry biomass separation
PYROLYS	RSTOIC	Temperature 1000 ºC, 1 bar
GSFA	HEAT1	Air as a gasifying agent 0.3-0.6 ER at 1000 ºC, 1 bar
MIXER	MIXER	Air mixture with gas
PLASMA	RPLUG	PG at 1000 ºC, 1 bar (reaction kinetics in Table 6.3)
RSTR1	RCSTR	Water gas at 1000 ºC, 1 bar
HXC1	HXC	Steam production10000 kg/h 20 bars from heat transfer
FLASH1	FLASH2	Gas and solid particles (tar) separator
HXC2	HXC	Heat transfer to gas for DME production at > 200 ºC, 1 bar
RSTR2	RCSTR	Methanol to DME at 220 ºC, 1 bar (reaction kinetics Table 6.3)
COOL	COOL	Cool down to less than 60 ºC DME separation from other gases
FLASH2	FLASH2	To separate DME and other gases

Table 6.3 Reaction kinetics of PL plasma gasification to DME production

Reaction	Rate Constant (K)	n	Activation Energy (cal/mol)
$1.25C + O_2 \rightarrow 0.5\ CO + 0.75CO_2$	3.7×10^{10}	1	35826.9
$CO + 0.5O_2 \rightarrow CO_2$	1.78×10^{10}	0	42992.2
$CH_4 + 0.5O_2 \rightarrow CO + 2H_2$	1.58×10^{12}	0	48246.9
$H_2 + 0.5O_2 \rightarrow H_2O$	1.08×10^{7}	0	2779.54
$C + H_2O \rightarrow H_2 + CO$	8.0×10^{-3}	0	11918.4
$CH_4 + H_2O \rightarrow CO + 3H_2$	3.0×10^{11}	0	29855.7
$C + CO_2 \rightarrow 2CO$	1.05×10^{23}	0	32244.2
$CH_4 + H_2O \rightarrow CO + 3H_2$	3.0×10^{11}	0	2985.7
$CO + H_2O \rightarrow CO_2 + H_2$	295000	0	900
$CH_4 + 0.5O_2 \rightarrow CO + 2H_2$	1.58×10^{12}	0	48246.9
	T (^oC)	*A (i)	*B (i)
$2H_2 + CO \rightarrow CH_3OH$	220	3.48×10^{-6}	54,689
$2\ CH_3OH \rightarrow CH_3OCH_3 + H_2O$	220	-2.27	2609.5

*Factors of reaction

6.1.1 Plasma gasification process validation

PG model validation has been performed by comparing the results determined in the experimental studies with those determined by the simulation model before having further analysis. There are two types of validations which have been done: syngas has been validated through different experimental studies with different types of biomasses while DME yield (%) validation has been done through two different types of biomasses. For validation purpose, the cross comparison of the produced syngas mole fractions in simulation model have been compared with that determined in the reference studies which are illustrated in Fig. 6B.a [305,307]. While biomass to DME yield (%) has been compared through experimental studies

(eucalyptus (ESD) and pine saw dust (PSD)) as given in Fig. 6B.b [178,262]. The root-mean-square error between simulation model and reference model output for syngas has been calculated by using section 3.3.1 [189]. According to the results presented in Fig. 6B.a, the RMSE of the results in the experimental study about softwood-sewage sludge (SW-SS, with ratio of 70-30%) PG and that determined by the simulation model in this study is less than 1% while it is also less than 4% in case of municipal waste. PG output of the developed model is quite good and very close to the results in the reference studies. Similarly, the RMSE with respect to biomass to DME yield (%) for eucalyptus saw dust (ESD) and pine saw dust (PSD) are also within 3-4%. Therefore, the simulation model validation results are quite good, and the results can be used for further analysis.

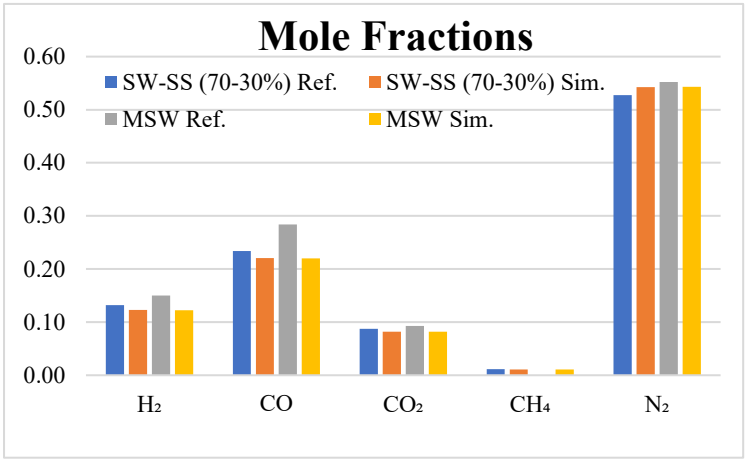

Fig. 6B.a. PG syngas validation

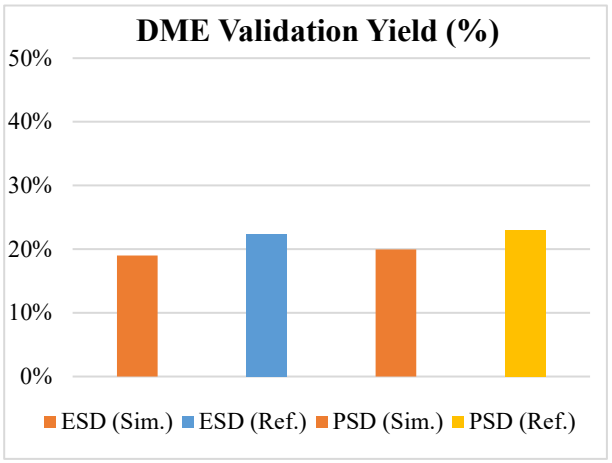

Fig. 6B.b. PG to DME validation

Fig. 6.B. PG simulation model validation

6.2 Plasma gasification process optimization

Process optimization has been carried out by importing Aspen Plus simulation file into MATLAB program. The results have been illustrated in Fig. 6.C while the pseudocode is given in Appendix A12 of the supplementary data. On the *x*-axis, there are a number of simulations runs to get the optimized value of DME (kg/h). The optimum result is found between 1800-1900 kg/h, to get the minimum value. It reaches a stable value with less than 50 objective function evaluations, which shows the high efficiency of the optimization method. Furthermore, each reset of surrogate model through the distribution of initial sampling points is random, i.e.,

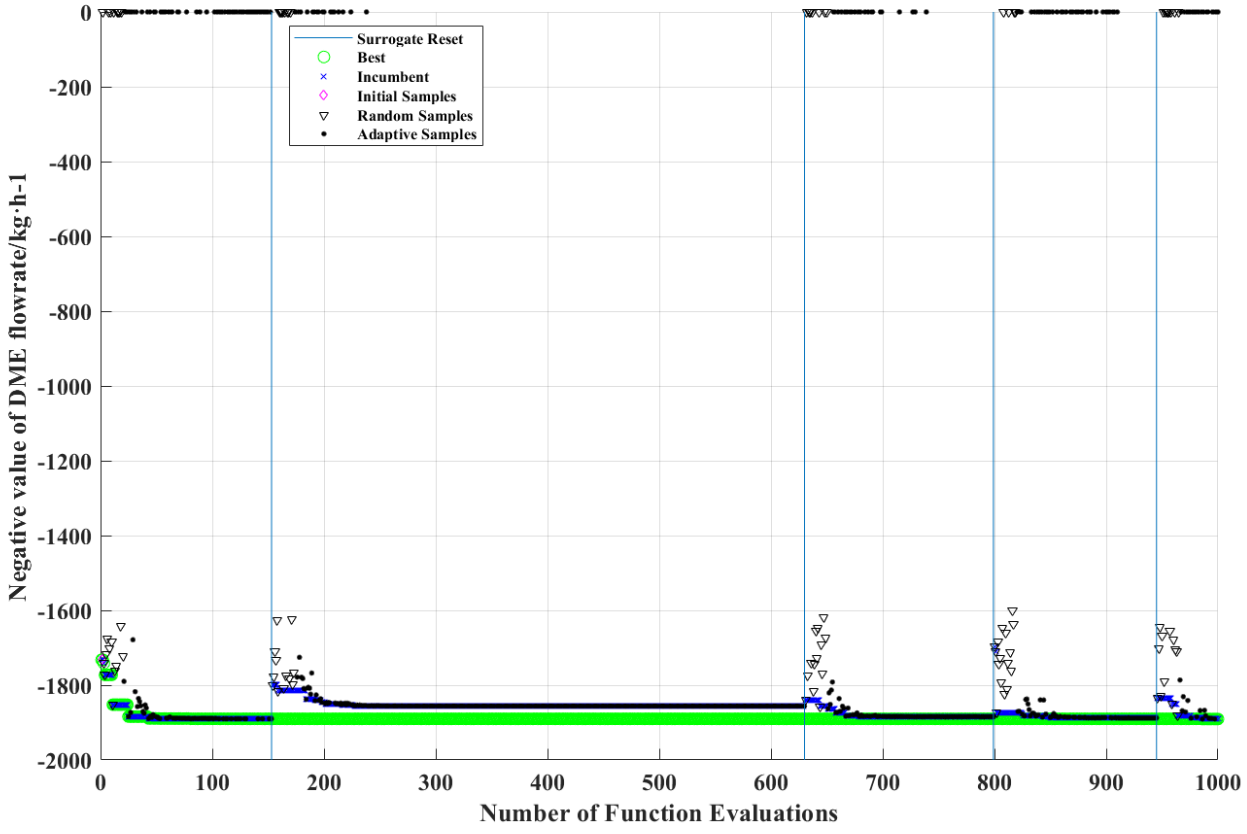

Fig. 6.C. Process of radial basis function-based surrogate optimization

the adaptive points converge quickly, indicating that the local minimum point can be easily found by radial basis function-based surrogate. Considering the computational cost, the maximum number of function evaluations was set up to 1000 and it could be found that the

minimum value of objective reaches around 1890 kg/h (i.e., it means that that the maximum flowrate of DME is 1890 kg/h) stably even when the surrogate is reset repeatedly.

The comparison of the optimum solution with the base solution is listed in Table 6.4. After optimization, the best temperature of PG (the temperature of PYROLYS reactor and the temperature of PLASMA reactor) is found to be 1147.6 ℃ while other variables reach the given bound. In the operational range, higher temperature of RSTR1 is helpful to produce more DME as per model result. Compared with the base solution, the DME flowrate of the optimum solution has been increased by ~6% from 1783 kg/h to 1890 kg/h, showing the positive effect of process optimization. Though the temperature of generated steam (heat generated) is higher in optimum solution while its gasification temperature (heat consumed) is also higher than that in the base solution due to which the energy efficiency is also affected in the optimization model as given in section 6.3.

Table 6.4 PG model optimization results

Variables	Range	Base solution	Optimum solution
Temperature of PG/℃	1000-3000	1000	1147.6
Temperature of RSTR1/℃	200-1000	1000	1000
Temperature of RSTR2/℃	150-350	150	150
Air flowrate kg/h	100-2000	100	170
DME flowrate kg/h	-	1783	1890
Temperature of generated steam/℃	-	195	198

6.3 Plasma gasification process sustainability analysis

Plasma gasification-based sustainability analysis has been done considering energy, exergy, economic, and environmental analysis.

6.3.1 Plasma gasification energy analysis

The comparative energy analysis of the DME tri-generation base and optimized model has been done. The energy efficiency of the base and the optimized process has been calculated based on some assumptions as given in section 3.3.2. According to the energy analysis results given in Fig. 6.D, the overall energy efficiency of the base process was around 48%, while it is around 44% for the optimized process. The energy efficiency after optimization is lower compared with that in the base case, and the possible reason could be that the increase of plasma gasifier temperature and more gasifying agent introduction in the process which assist in the production of more output (DME) but at the cost of some reduction in the energy efficiency. Therefore, the process efficiency after process optimization is less compared with that in the base case but there is around 6% additional DME produced which ultimately creates a significant impact on the economic output.

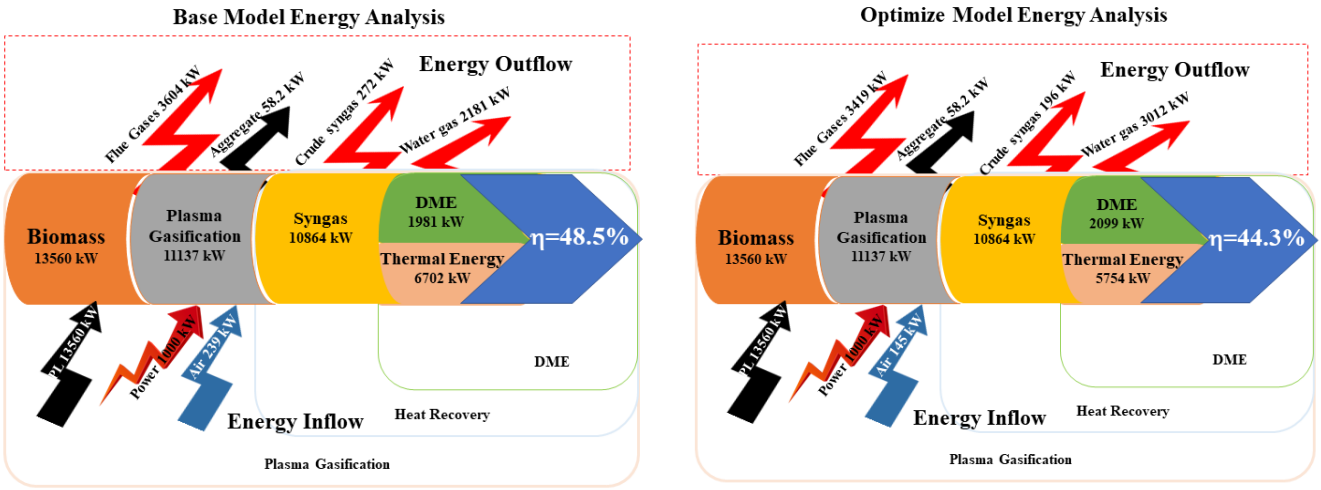

Fig. 6.D. PG energy analysis of the base process and optimized process

6.3.2 Plasma gasification exergy analysis

The exergy analysis of the PL-based biomass valorization in PG tri-generation process has been conducted based on the first and the second law of thermodynamics using section 3.3.3 methodology. All calculations have been done by using the unit kilowatt (kW). According to the exergy calculation results, the exergy efficiency of the base process is around 41% while the optimization process has a relatively higher exergy efficiency (42%) as given in Fig. 6.E. Therefore, there is no such a significant difference between the exergy analysis of the base and optimized process, but the overall exergy efficiency of the tri-generation process is higher compared with the single PG process.

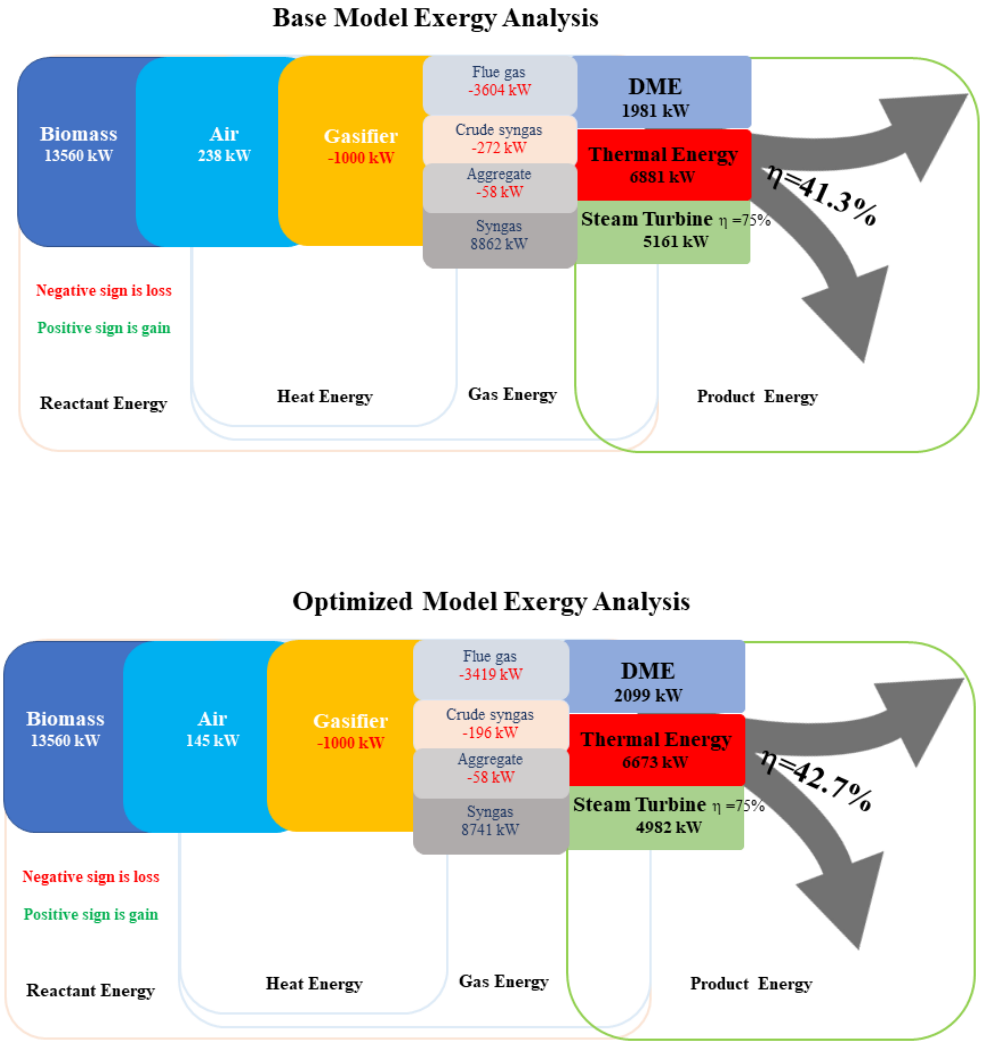

Fig. 6.E. PG exergy analysis of the base process and optimized process

6.3.3 Plasma gasification thermal energy to electric power potential

Thermal energy of the syngas has been transferred into water to convert it into high pressure steam which has been further utilized in the steam turbine to generate power by assuming that inlet mass flow is equal to the outlet mass flow. To calculate the potential of electrical power generation, the detailed processes have been summarized in section 3.3.6. The final calculation results have been summarized in Table 6.5. According to the results, the overall power output potential is 1271.8 kW by using the single stage steam turbine with the isentropic efficiency of 60% and the generator with efficiency of 93%. Therefore, the electrical energy generated in this process is enough to meet the plant energy demand which is around 1000 kW based on the vendor's estimation [314].

Table 6.5 Single stage steam turbine-based power calculation

Inlet Properties		**Outlet Properties**	
Steam Pressure	20 bar (290 psig)	Steam Pressure	4.9 (71 psig)
Steam Temperature	212 °C (413 °F)	Specific Entropy	0.545 btu/lbm/R
Specific Enthalpy	356.9 btu/lbm	Specific Enthalpy (Ideal)	353.4 btu/lbm (0.22 kWh)
Energy Flow	786.9 MMBtu/h	Specific Enthalpy	354.8 btu/lbm (0.23 kWh)
Efficiency		Temperature	158.2 °C (316.8 °F)
Isentropic efficiency [204]	60%	Energy Out	4.7 MMBtu/h
Generator efficiency [204]	90-93%	**Power Out**	**1271.8 kW**

6.3.4 Plasma gasification economic analysis

The economic analysis of PG to DME manufacturing process has been done based on the biomass waste valorization rate of 10 t/h (plant treatment capacity). For this purpose, the data has been taken from the related vendors and literatures by using methodology defined in

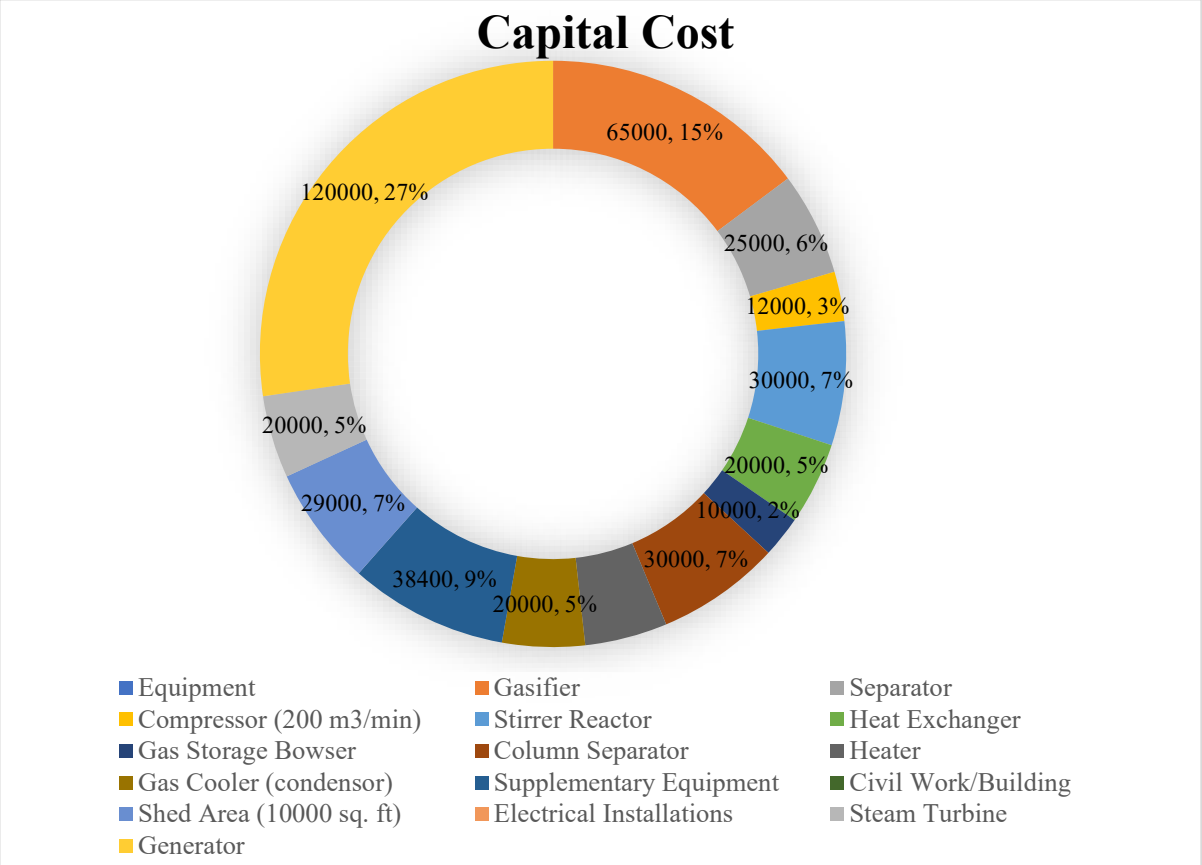

Fig. 6.F. Capital cost for 10 t/h capacity

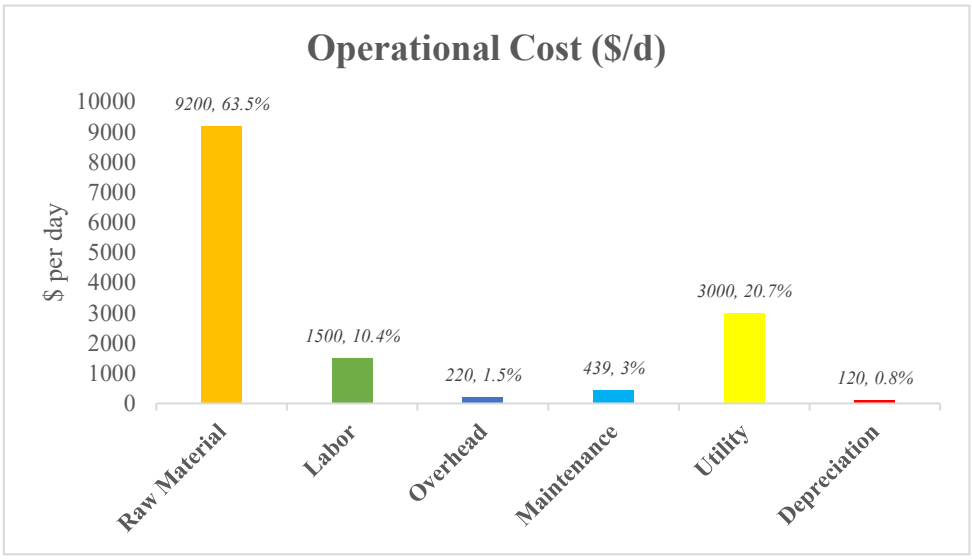

Fig. 6.G. Operational cost $/d

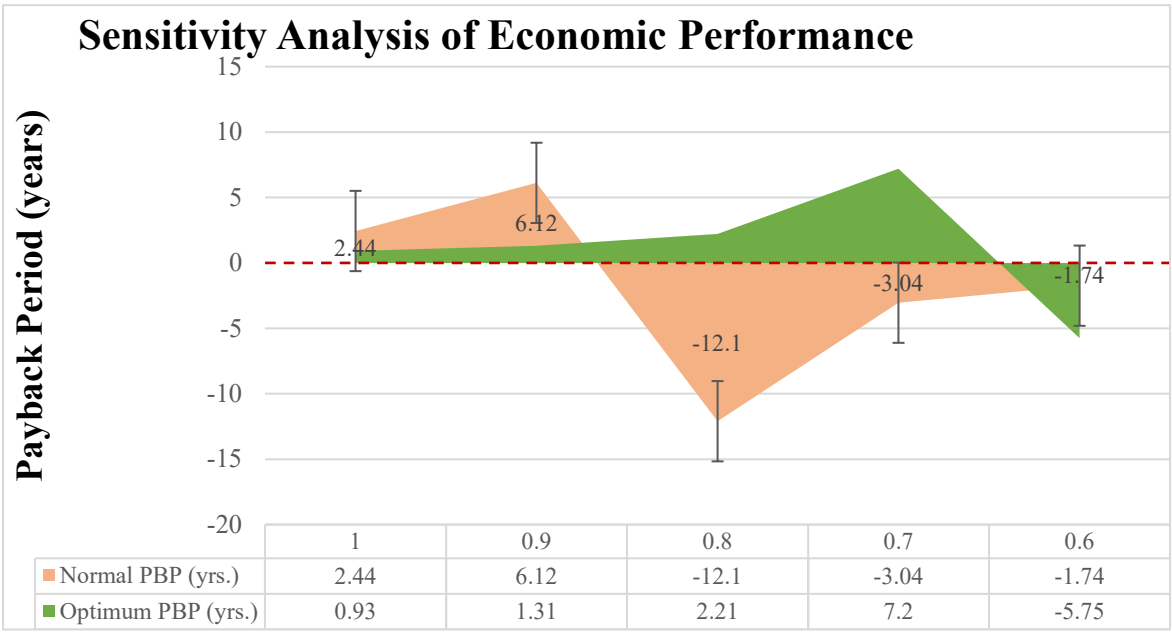

Fig. 6.H. Sensitivity analysis of economic performance

section 3.3.7. The detailed calculation of the data has been given in Appendix A13 of the supplementary material. The capital cost payback period of the installed process has been calculated based on the revenue and operational cost. According to the estimation presented in Fig. 6.F, the overall capital cost for the 10 t/h PG to DME processing process is around US $ 0.5 million without including any regulatory duties and taxes etc. as summarized in section 3.3.7. Gasifier and generator have the major equipment cost 15% and 27%, respectively. While raw material cost is the highest in operational cost which is account for 63% followed by utility and labor (manpower) as given in Fig. 6.G. The payback period has been calculated, considering that the process has been installed and operated at fully operational condition. Sensitivity analysis of the payback period has been conducted based on the process output efficiency. According to the results of sensitivity analysis as presented in Fig. 6.H, the payback period of the base process is 2.44 years at 100% efficiency while it is 6.12 yrs. at 90% efficiency. When the efficiency is lower than 90%, the base process is not feasible without any subsidies or external financial support. The scenario is different for the optimized process, according to the results of sensitivity analysis as shown in Fig. 6.H, the payback period for capital cost is between 1 to 7.2 yrs. with process efficiency (from 100% to 70%). However, the optimized

process is not feasible when the efficiency is lower than 70%. Therefore, the optimized process is more economical and faster in capital return which is feasible when the process efficiency is greater than 70% as compared with the base process which is not feasible when the process efficiency is lower than 90%.

6.3.5 Plasma gasification environmental life cycle assessment

Life cycle assessment of the proposed process has been done by using IMPACT 2002^{+} method in SimaPro software without considering the infrastructure of the process. As for life cycle inventory analysis, the data has been taken from the SimaPro and literatures [210,315]. The LCA inventory data have been given in the supplementary data. The environmental analysis of the developed processes has been done by comparative analysis of (i) PG of the PL verses PL composting process and (ii) DME manufacturing from coal verses syngas produced from plasma gasification of PL (PL-PG). The single score impact categories of 15 different LCA indicators have been given in Fig. 6.I. According to the results presented in Figs. 6.I and 6.J DME production through PG syngas of PL is more environmentally friendly compared with the DME production from coal. The score for DME-coal case is higher compared with the DME-PL. The most significant reason leading to the high score of DME-coal in Fig. 6.J is caused by the non-renewable energy utilization in DME production because coal is a non-renewable energy source. Furthermore, the overall score of PL-PG is lower compared with that of the PL composting process because there are high emissions of GHG (especially CH_4 and CO_2) in PL composting process due to which its global warming potential and respiratory inorganics scores are higher. While composting process has higher global warming, aquatic eutrophication, and acidification potential as compared with syngas and DME production, but relatively lower impact in term of carcinogens and non-carcinogens, as presented in Fig. 6.J.

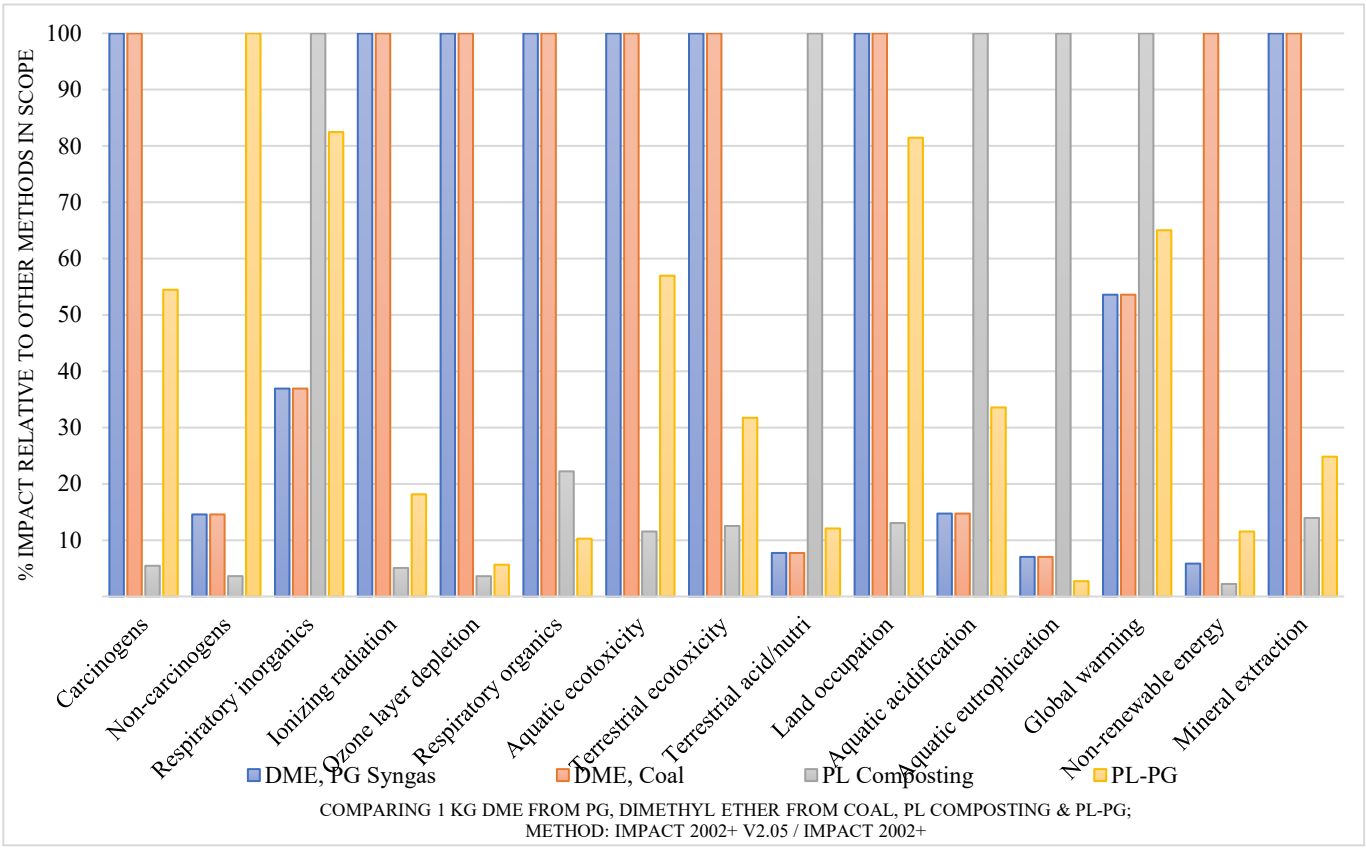

Fig. 6.J. PG life cycle assessment individual ranked

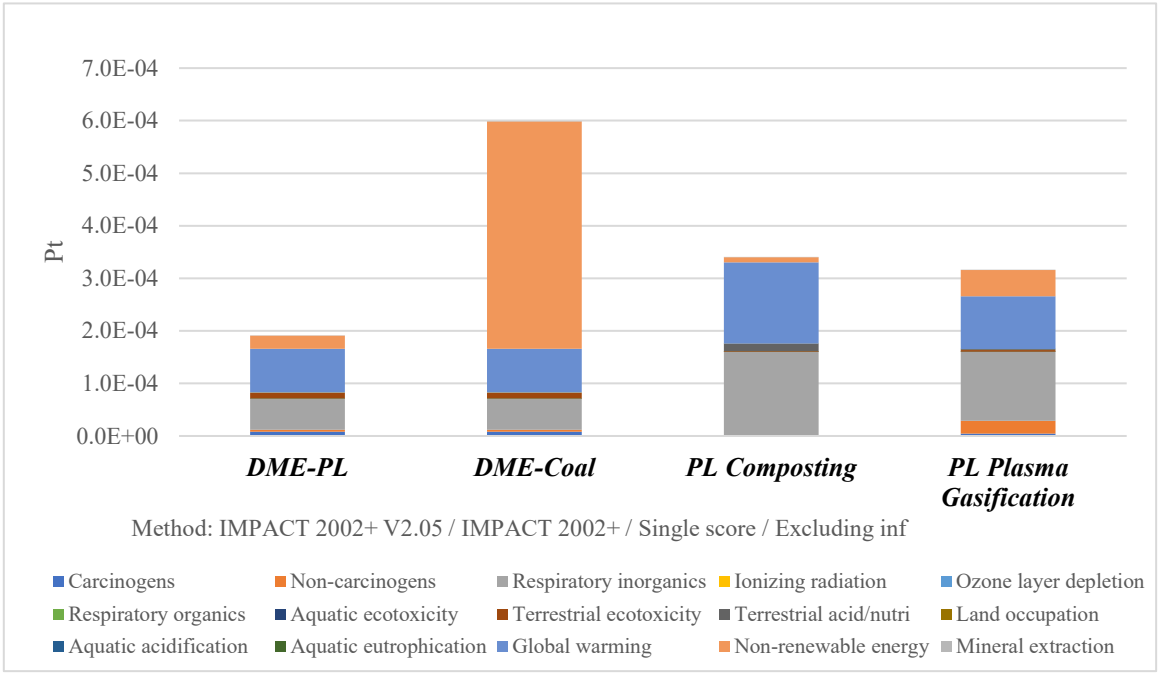

Fig. 6.I. PG Life cycle assessment single score impact analysis

Therefore, dimethyl ether from poultry litter (DME-PL) process is more eco-friendly comparing with DME manufacturing from coal (DME-Coal), while PG of PL process has overall better environmental performance comparing with PL composting process.

6.4 Conclusion: Plasma gasification

In this research, the PG based tri-generation process for PL valorization to produce DME and electrical power generation has been developed. The developed process is feasible based on 4E (energy, exergy, economic, and environmental) analysis of the process. The following are the key conclusions of this study:

- DME efficiency has been improved to 6% after process optimization.
- The energy efficiency in the base case is 48% which is better than that in the optimized process (44%).
- No significant difference of the exergy efficiency of the base from that of the optimized process.
- The thermal energy to electrical power generation capacity of the proposed process through steam is around 1271 kW.
- The optimized process has a shorter payback period as compared with the base process, and it is feasible when the process efficiency is equal to or greater than 70%while the base process is not economically feasible when the process efficiency is lower than 90%.
- The environmental performance of DME production from PL syngas is better than DME-coal while PL composting process has a worse environmental performance as compared with PL-PG valorization.

This study provides an overview of a new way to decision-makers, specifically the tri-generation for biomass waste valorization. The PG-based tri-generation technique has shown good performance in 4E analysis. Consequently, this technique has the potential to effectively valorize biomass waste. However, this process needs severe temperatures, which increases process safety risk and has an impact on the process's energy efficiency. Therefore, chapter 7 includes an assessment of the sustainability of the integrated pyrolysis and gasification process.

7 Chapter: Pyrolysis-gasification based integrated process

In this chapter, pyro-gasification based valorization process for biomass waste has been developed and its sustainability analysis has been done.

7.1 Pyrolysis process simulation development

Aspen plus was used to simulate the biomass waste valorization process. The integrated pyrolysis and gasification process is given (Fig. 7.A). The proximal and final analyses of PL biomass were employed as a reference in the current approach. Whereas the created model has been evaluated using three different types of biomasses at six different temperatures as indicated by the relevant experimental studies [316–318] in section 7.2. This validated model has been extended to include the secondary gasification and carbon dioxide liquefaction processes. The actual process, as shown in Appendix A14, can be separated into three stages: pyrolysis, gasification (including turbine steam generation), and carbon dioxide liquefaction. This approach was developed using the parameters defined in Fig. 7.B and which has been primarily obtained from different studies [316–319]. For economic analysis, the feed rate is

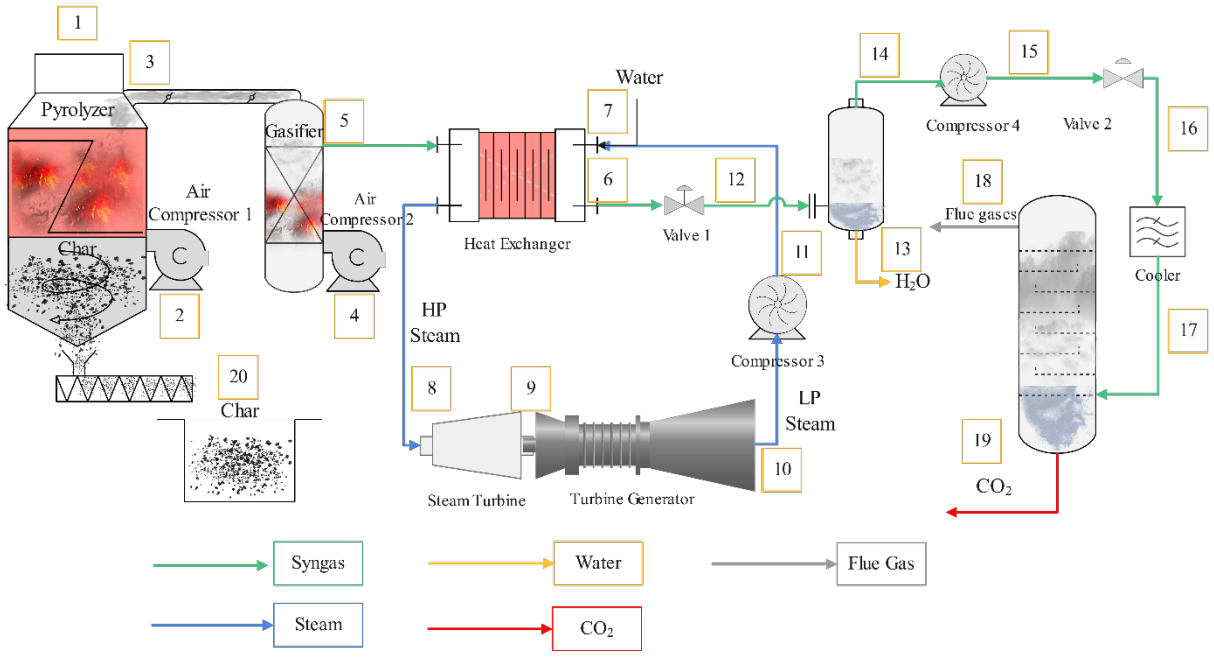

Fig. 7.A Pyro-gasification based process schematic diagram

estimated to be 10,000 kg/h based on the capacity of the selected plant. In terms of the basic process, biomass was pyrolyzed at 600 ºC and 1 atm, which yields approximately 4235 kg/h of biochar along with pyro-gas, which was then reacted with air for gasification, which increased the temperature due to combustion. This combustor heat has been transferred to water in a heat exchanger with a flow rate of 18,000 kg/h, resulting in high-pressure steam of approximately 25 atm and 540 ºC. During combustion syngas contains a significant amount of H_2O, N_2, and CO_2. By application of coolers and valve application, the temperature of the syngas has been decreased, and H_2O has been separated in the first phase at a rate of around 4903 kg/h. While the temperature of the syngas had dropped to -50 ºC, CO_2 was liquified (about 3246 kg/h) and separated from N_2. Biochar and CO_2 have immediate economic value, whereas this high temperature and pressure steam has the potential to generate approximately 2302 kW of electric

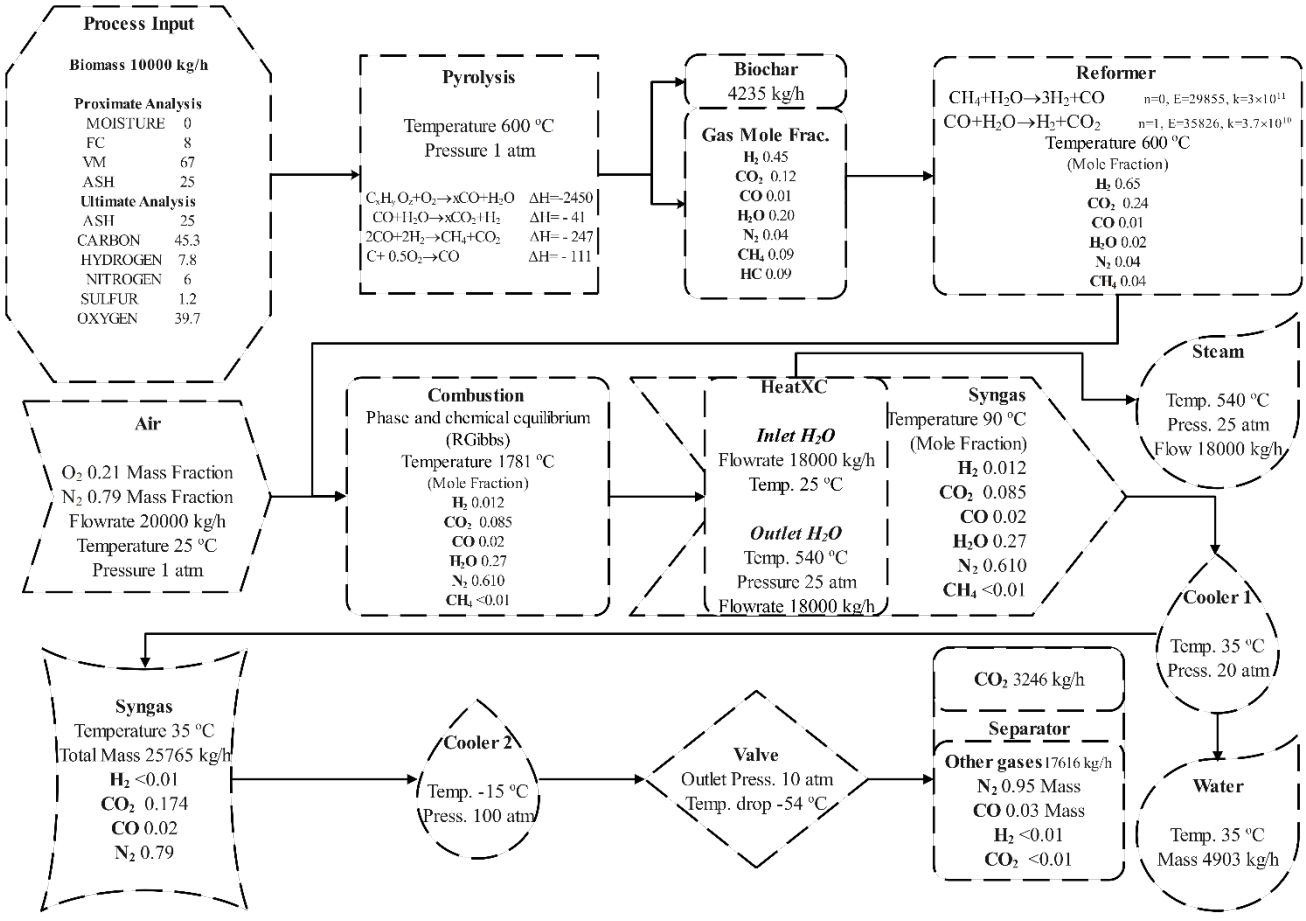

Fig. 7.B. Pyro-gasification base simulation process parameters

power, calculated based on section 3.3.6. In this basic model, the parameters were taken from the previously published literatures [316–319], and this process has been further optimized by using different optimization algorithms (see section 3.2.2 for the details). Therefore, this novel process has been optimized and different scenarios have been considered to provide a clear overview to the decision-makers/stakeholders.

7.2 Pyrolysis process validation

Pyrolysis model validation has been done by comparative analysis with the experimental studies [316–318]. For model validation, experiments focusing on the treatment of various forms of biomass such as rice straw (RS), sugar bagasse (SB), poultry litter (PL), and dry poultry litter (DLP) were used. These biomasses were compared to the simulation models' outputs at six different temperatures (ranging in 300-800 ºC). Fig. 7.C depicts the findings of the comparison analysis. The errors for the yield for all biomasses determined by the simulation model are between 0 and 9%, which is fairly good for such a complex process. Possible reasons

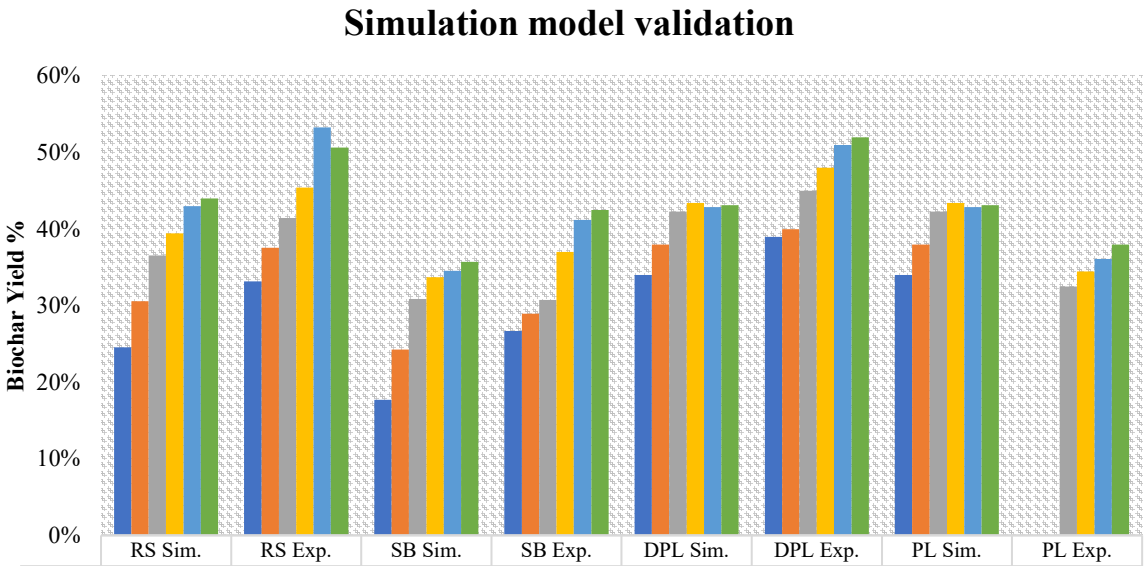

	RS Sim.	RS Exp.	SB Sim.	SB Exp.	DPL Sim.	DPL Exp.	PL Sim.	PL Exp.
800 C	25%	33%	18%	27%	34%	39%	34%	
700 C	31%	38%	24%	29%	38%	40%	38%	
600 C	37%	41%	31%	31%	42%	45%	42%	33%
500 C	39%	45%	34%	37%	43%	48%	43%	34%
400 C	43%	53%	35%	41%	43%	51%	43%	36%
300 C	44%	51%	36%	43%	43%	52%	43%	38%

Fig. 7.C. Pyro-gasification model validation

for these variances could be biomass composition and differences in the equipment utilized in this experimental research. Most of the time, the yield determined by the simulation model is lower than the yield determined by the actual research. Therefore, the limitations in the current simulation model appear to be more stringent toward the final goods, but these are acceptable and do not significantly vary from the actual conditions. Therefore, this validated model can be used for further study.

7.3 Pyro-gasification process sustainability evaluation

A multi-scenario sustainability analysis has been developed to assess the sustainability of the developed process by incorporating energy (section 3.3.2), economic (section 3.3.7), and safety (section 3.3.9) EES aspects simultaneously. The basic model and multi-scenarios pattern search based optimized model considering section 3.2.2 have been established for comparative analysis purpose. These determined process parameters can be further used for sustainability analysis by considering the EES indicators. There are three scenarios in this study, as defined in Table 7.1. The first scenario aims to focus on the "maximization of biochar production" considering the constraints as given in Table 7.1. The second scenario aims to focus on the "maximization of the electric power generation by application of process thermal energy and CO_2 liquefication as an economic indicator" with the defined constraints of scenario 2 as shown in Table 7.1. The third scenario aims to focus on the "optimum yield of biochar, liquified CO_2 and electric power simultaneously". All these scenarios have been evaluated based on the EES index which has been calculated according to section 3.3.10.2. The energy, economic, and safety criteria have been incorporated in the EES index by introducing the weighting factor for each criterion. The EES index has a score in the range of 0 to 1, and the closer to 1, the more sustainable the process will be. The methodology of energy, economic, and process safety methods are given in sections 3.3.2, 3.3.7, and 3.3.9, respectively. Therefore, a scenario which

has a better EES score due to higher energy efficiency, economic (IRR) return, and safety score is sustainable for biomass waste valorization.

Table 7.1 Pyro-gasification base process optimization scenarios

Scenario 1
Objective: Maximization of biochar production $max\ P_b$
Constraints: $s.t.\begin{cases} 400 \leq T_{pyro} \leq 800 \\ 400 \leq T_{ref} \leq 800 \\ 0.1 \leq R_{air} \leq 0.5 \\ NH > 0 \end{cases}$
Scenario 2
Objective: Maximization of electric power generation by application of process thermal energy and CO_2 liquefication an economic indicator $max\ (T_{steam}, F_{CO_2})$
Constraints: $s.t.\begin{cases} 400 \leq T_{pyro} \leq 800 \\ 400 \leq T_{ref} \leq 800 \\ 0.1 \leq R_{air} \leq 0.5 \\ NH > 0 \\ 300 \leq T_{steam} \leq 600 \end{cases}$
Scenario 3
Objective: To get an optimum yield of biochar, liquified CO_2, and electric power simultaneously $max\ (F_{bio}, T_{steam}, F_{CO2})$
Constraints: $s.t.\begin{cases} 400 \leq T_{pyro} \leq 800 \\ 400 \leq T_{ref} \leq 800 \\ 0.1 \leq R_{air} \leq 0.5 \\ NH > 0 \\ 300 \leq T_{steam} \leq 600 \end{cases}$
where P_b is flowrate of biochar, kg/h; T_{pyro} is the pyrolysis temperature, °C; T_{ref} is reformer temperature; R_{air} is the ratio of air to biomass; NH is net heat, kW; T_{steam} is the steam temperature, °C; F_{CO2} is the flowrate of liquid CO_2, kg/h.

7.3.1 Basic case

The basic process was established by employing the parameters defined in Fig. 7.B that were obtained through different studies [316–319]. This basic scenario was assessed in terms of energy efficiency, economic performance (IRR), process safety, and prospective power generation. The baseline scenario's sustainability index has been derived using the aforementioned criteria. The basic scenario has an overall process energy efficiency of approximately 59%, according to the energy efficiency results shown in Fig. 7.D. The heat exchanger and the pyrolysis process have both lost the most energy. The thermal energy of the process was turned into electrical power by the use of steam turbine generating, as described in section 3.3.6. According to the results shown in Appendix A15, the basic process has the ability to generate nearly 2302 kWh of electricity from the thermal energy produced. While the basic process's process safety index score is high (approximately 13 out of 16 (81%)) in Fig. 7.E, this represents the increased hazards inherent in this process. The basic process has been economically evaluated at various process efficiencies (100 to 50% or till IRR is negative), as shown in Fig. 7.F. Whereas the effects of various subsidy scenarios on IRR are also examined. The basic process is economical (IRR ranges from 37 to 2%) when the process efficiency is reduced from 100 to 80% without undermining any subsidies, but the IRR is too low (2%) when the process efficiency is reduced to 80%. If a subsidy of 17.5 $/t is provided, which is 50% of the cost of waste handling in low-income countries [208], the basic process is economically viable with an IRR of 13% when the process efficiency is up to 70%, and the process is economically viable with an IRR of 19% when the subsidy is 50 $/t, and the plant is up to 50%. Finally, the sustainability index (SI) was computed using the methodology described in section 3.3.10.2. (see Appendix A16). The fundamental process's BWM-based SI score is 0.503 out of 1.0, and it is 0.428 when all indications are given equal weightage, which is significantly lower (Appendix A16) when compared to other scenarios. Hence, process

optimization is required to make the basic process more sustainable in terms of economic, safety, and energy.

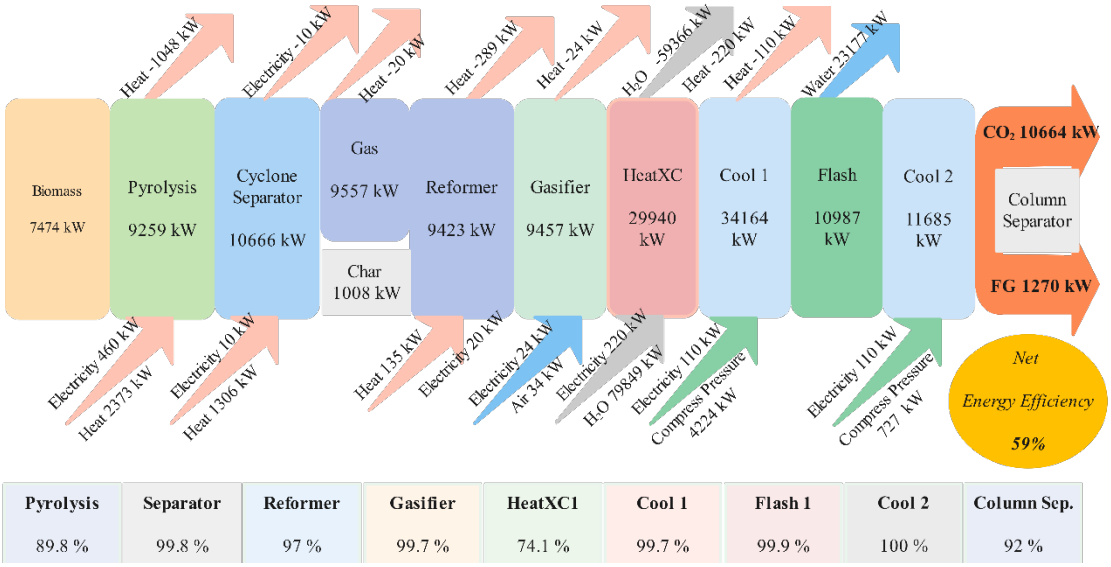

Pyrolysis	Separator	Reformer	Gasifier	HeatXC1	Cool 1	Flash 1	Cool 2	Column Sep.
89.8 %	99.8 %	97 %	99.7 %	74.1 %	99.7 %	99.9 %	100 %	92 %

Fig. 7.D Pyro-gasification Base process energy efficiency

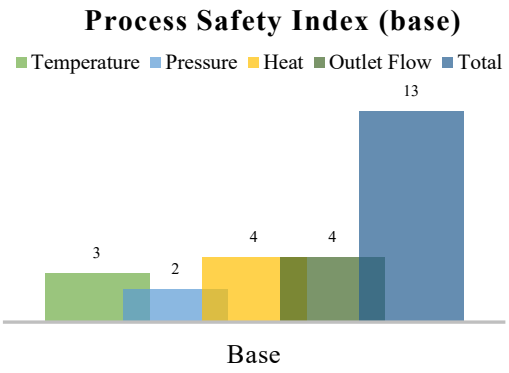

Fig. 7.E Pyro-gasification Base PSI

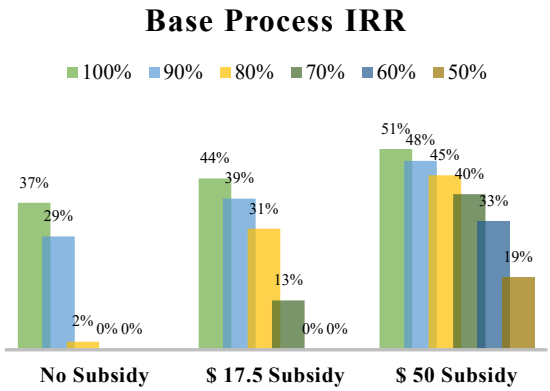

Fig. 7.F Pyro-gasification Base process EA

7.3.2 **Results of Scenario 1** (Maximization of biochar production)

Scenario 1 seeks to maximize biochar production by changing process parameters. The basic process has been optimized for this purpose by using the Pattern search algorithm described in section 3.2.2.4. The pyrolysis process temperature is 516 ^{o}C, the reformer temperature is 600 ^{o}C, and the air flow is 3500 kg/h, according to the optimization results. The

process can create the most biochar (approximately 423.2 kg/t of biomass) with 411.2 kg/t of CO_2 and 20,000 kg/h of high temperature (605 ^oC) and pressure (25 atm) steam under these operating parameters. This steam may be utilized to generate approximately 2788 kW of electricity (see Appendix A15). Scenario 1's overall process efficiency is 66% (see Fig. 7.G), which is pretty good and better than the basic process, and also the process safety index score (Fig. 7.H) is about the same (13 out of 16) as the basic process. Furthermore, the economic performance (as measured by IRR) of Scenario 1 is superior to that of the fundamental process (see Fig. 7.I). Even without any subsidies, the optimized process in Scenario 1 is economically viable with an IRR of 38 to 6% when the process efficiency is reduced from 100% to 80%. It is economically possible with an IRR ranging from 44 to 14% when the subsidy is 17.5 $/t and the process ranges from 100 to 70%. Similarly, when the subsidy becomes 50 $/t, the improved process in Scenario 1 becomes economically viable, with an IRR ranging from 51 to 19% when the process efficiency falls from 100 to 50%. According to the weights obtained by the BWM, the sustainability index score of the optimized process under scenario 1 is 0.563, which is likewise higher than that of the basic process (see Appendix A16). Hence, as compared to the basic process, the optimized process under Scenario 1 seems to be more sustainable in terms of economic, energy, and electric power generating potential.

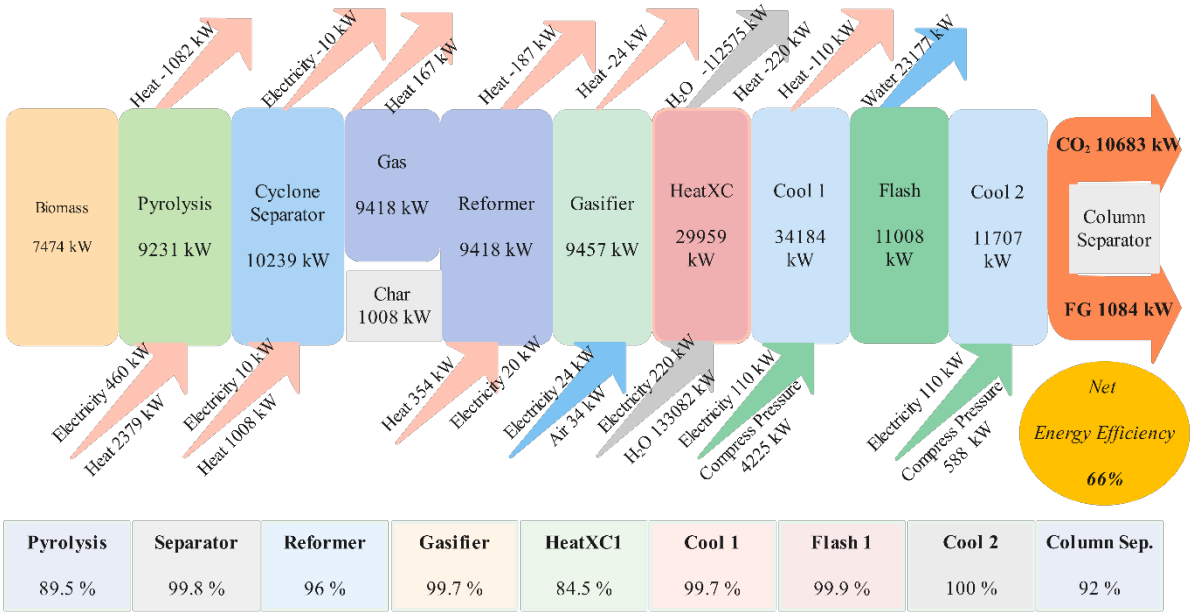

Fig. 7.G Pyro-gasification energy efficiency of the optimized process under scenario 1

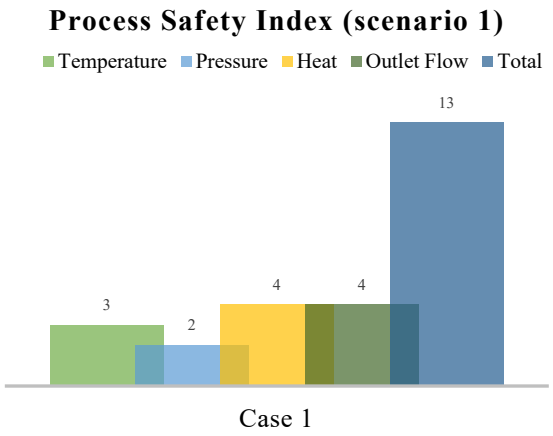

Fig. 7.H Pyro-gasification PSI for optimized process scenario 1

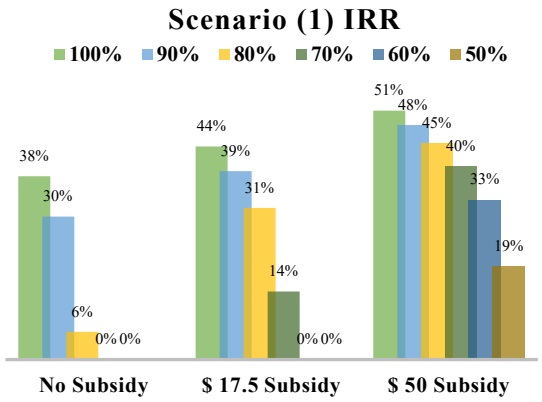

Fig. 7.I Pyro-gasification EA for optimized process scenario 1

7.3.3 **Results of Scenario 2** (Maximization of thermal power and CO_2 liquefaction)

The pattern search algorithm method was used for process optimization with the goal of maximization of thermal power generation and CO_2 production. The final optimization results are shown in Appendix A17, and the best one with the best CO_2 and thermal power production has been chosen. The pyrolysis temperature is 800 ºC, the reformer temperature is 512.5 ºC, and the air flowrate is 3125 kg/h, according to the optimization results. These ideal operating

parameters can generate the most CO_2 (6268.5 kg/h) and steam (30,000 kg/h at 579.5 ºC), which is more than the basic and optimized processes under scenario 1. Moreover, the energy efficiency of this process is only 47% (see Fig. 7.J), which is lower than the basic and improved processes under Scenario 1, but its thermal to electric energy potential is significantly larger (around 4044 Kw). In terms of economics, the IRR of the non-subsidized process (see Fig. 7.L) ranges from 44 to 28% when process efficiency changes from 100 to 80%, which is higher than the IRRs of the basic and optimal processes under Scenario 1. However, when the process efficiency is less than 80%, this optimized process (scenario 2) is not economically feasible without a subsidy. When the process efficiency changes from 100% to 70%, the IRR ranges dropped from 48% to 29%, with a subsidy of 17.5 $/t. But with the subsidy 50 $/t, it ranges dropped from 54 to 28%. The optimized process under scenario 2 has a slightly higher process safety index score (14 out of 16) than the basic process and the optimized process under scenario 1 (Fig. 7K). The final sustainability index score of the optimized process under scenario 2 by using BWM weights is 0.534 (see Appendix A16), which is greater than the basic process and the scenario 3 optimized process. In terms of economic, energy, power generation potential, and safety indicators, the optimized process of scenario 2 is a more sustainable process than the basic process and the optimal process of scenario 3.

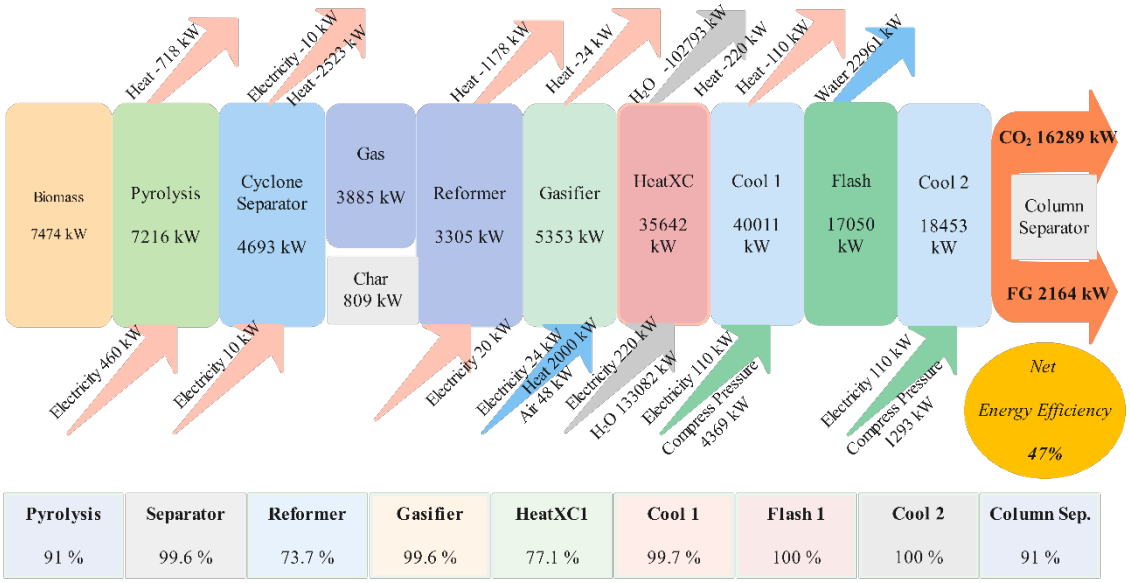

Fig. 7.J Energy efficiency of the optimized process under scenario 2

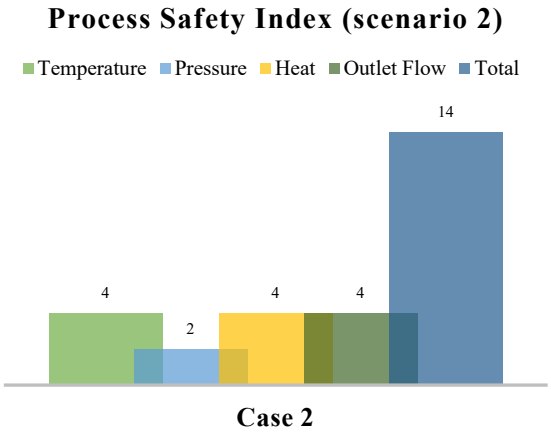

Fig. 7.K Pyro-gasification PSI for optimized process scenario 2

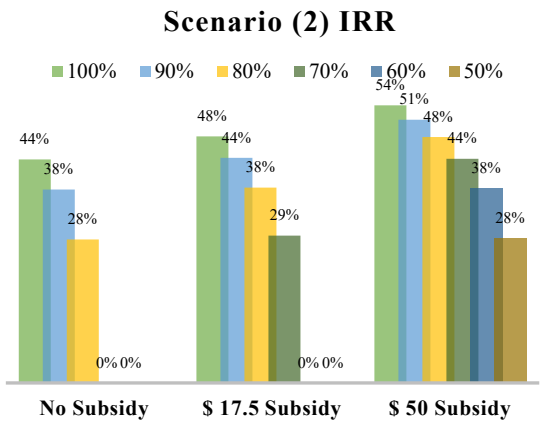

Fig. 7.L Pyro-gasification EA for optimized process scenario 2

7.3.4 **Results of Scenario 3** (Economic gain by optimization of biochar, CO_2, and electric power)

Scenario 3, economic advantage has been maximized by optimizing the production of biochar, CO_2, and electric power generation. To develop this, the pattern search technique described in section 3.2.4 was applied. The evaluation results are given in Appendix A18. The production of biochar and that of CO_2 have an inverse correlation, due to which the optimal results have been selected in which the yields of CO_2, biochar, and steam can reach a balance.

Increasing one reduces the yield of another. Resultantly, the optimum values of the parameters were chosen when the yields of both products could be balanced. The optimal operating conditions are 775 ºC pyrolysis temperature, 800 ºC reformer temperature, and 3562.5 kg/h airflow. In this case, the improved process in scenario 3 produces around 5946.9 kg/h of CO_2, 3471.2 kg/h of biochar, and 10 t/h steam from biomass at 582.6 ºC (see Appendix A18). Considering the process parameters, the energy efficiency of the optimized process in scenario 3 can also be computed. According to the energy efficiency statistics, the energy efficiency of the optimized process under scenario 3 is 46% (see Fig. 7.M), the lowest of all scenarios (including the basic process, the optimized process under scenario 1 and the optimized process under scenario 2). Similarly, the PSI score is 14 (see Fig. 7.N), which is comparable to the optimized process in scenario 2 but lower than the basic and optimized processes in scenario 1. A high PSI score highlights the process's increased safety-related risks. One likely reason is because scenario 3's goal is to maximize economic gain while taking safety performance into account. Therefore, the IRR has been calculated to assess economic sustainability performance. According to the IRR results (see Fig. 7.O), the optimized process under scenario 3 is an economically feasible process with an IRR ranging from 43 to 27% when process efficiency is up to 80% without considering any process subsidies. When the process efficiency is reduced from 100% to 70%, the optimized process under scenario 3 is economically sustainable with an IRR ranging from 48 to 28% (see Fig. 7.O). If the subsidy is 50 $/t, this process performs better with a maximum IRR of 54% at 100% process efficiency and is also economically viable with an IRR of 28% until process efficiency reaches 50%. Hence, the economic performance of the optimized process in scenario 3 outperforms all other scenarios. Ultimately, the optimized process's sustainability index under scenario 3 has been determined using energy, safety, economic, and power generation factors. According to the weights derived by the BWM technique, the sustainability index score of the optimized process under scenario 3 is 0.517 (see

Appendix A16), which is higher than that of the basic process. Therefore, it is lower than the improved process's sustainability index in scenarios 1 and 2. Hence, in terms of process sustainability, the optimized process under scenario 3 is inferior to the optimized processes under scenarios 1 and 2.

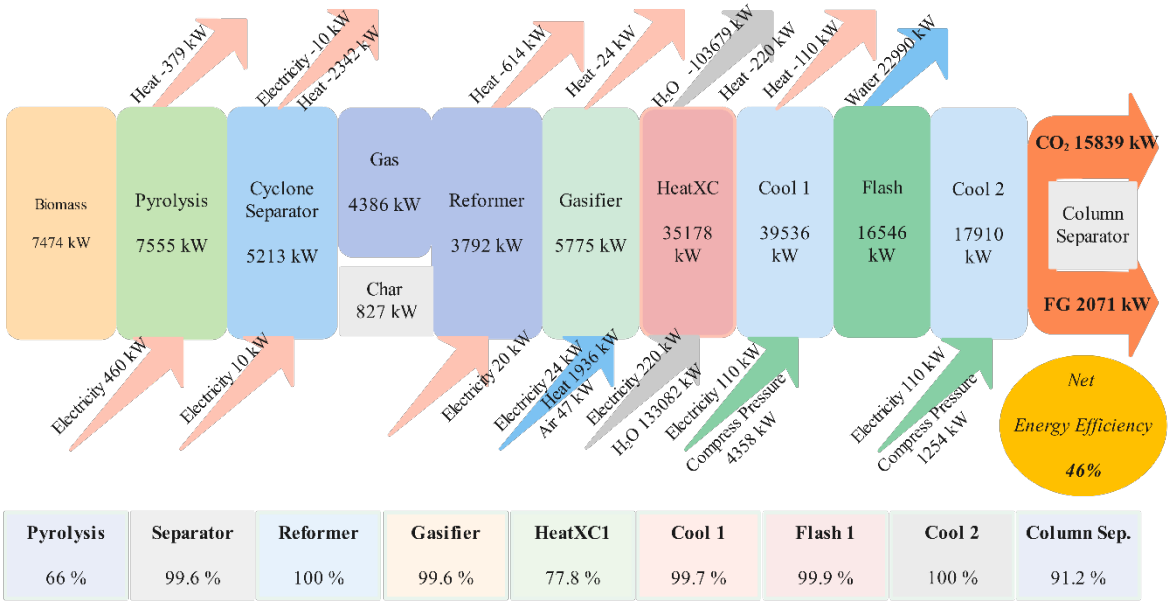

Fig. 7.M Energy efficiency of the optimized process under scenario 3

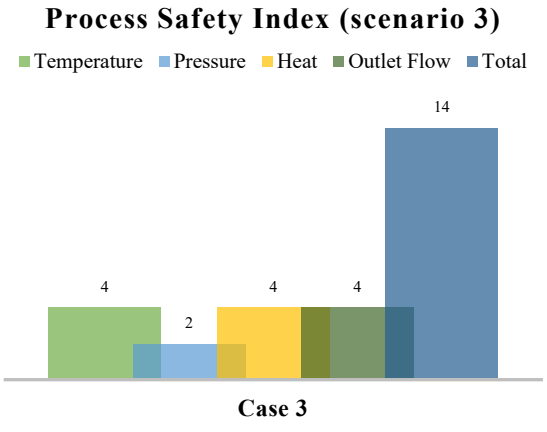

Fig. 7.N Pyro-gasification PSI for optimized process scenario 3

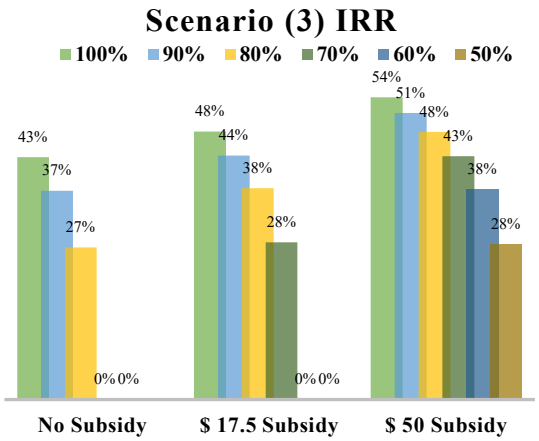

Fig. 7.O Pyro-gasification EA for optimized process scenario 3

7.3.5 Pyro-gasification process sensitivity analysis

The process inputs and outputs under different scenarios have been summarized in Table 7.2. The feed rate of biomass has been set the same for all the scenarios, which is 10 t/h. For basic cases, the simulation parameters have been set in Fig. 7.B taken from experimental studies. The sustainability index score of the basic process is 0.503 according to the weights determined by the BWM which is the lowest among all the scenarios in this study. The sustainability index of the optimized process under scenario 3 is ranked third position in terms of sustainability performance with a SI score of 0.517. The SI score of the optimized process under scenario 2 has been ranked in the second position with 0.534, and the optimized process under scenario 1 has the highest SI score of 0.563 with a major contribution by its performance regarding energy and economic aspect. Sensitivity analysis of the sustainability index score calculation has been done in Appendix A16 by assigning different weights to the indicators. Sensitivity analysis results show the basic process has the lowest sustainability index score in all cases. Among all scenarios, the optimized process under scenario 2 has the highest SI score-0.534 (see Appendix A16) due to its better performances in energy efficiency, economics, and power generation aspect. Therefore, the optimized processes are more sustainable as compared with the basic process, but the optimized process under scenario 2 is the most sustainable among all these processes when all sustainability indicators have equal preferences.

Table 7.2 Summary of pyro-gasification process inputs and outputs

Scenarios	Basic	Scenario 1	Scenario 2	Scenario 3
Biomass Flow Rate (kg/h)	10000	10000	10000	10000
Pyrolysis Temp. °C	600	516	800	775
Reformer Temp. °C	600	600	512	513
Steam Flow Rate (kg/h)	18000	20000	30000	30000

Steam Pressure (atm)	25	25	25	25
Steam Temp. °C	540	605	579	532
Air Flow (kg/h)	2000	3500	3125	3562
CO_2 (kg/h)	3246	4112	6268	6096
Biochar (kg/h)	4235	4332	3397	3471
Electric Power (kW)	2302	2788	4044	3796
Energy Efficiency (%)	59%	66%	47%	46%
IRR (%) No subsidy (η=100-80%)	37 to 2%	38 to 6%	44 to 28%	43 to 27%
Process Safety Risk (%)	81%	81%	88%	88%
Sustainability Index (BWM)	0.503	**0.563**	0.534	0.517
Sustainability Index (E_1 (0.25), E_2 (0.25), E_3 (0.25), E_4 (0.25))	0.428	0.477	**0.507**	0.488
Sustainability Index (E_1 (0.4), E_2 (0.2), E_3 (0.2), E_4 (0.2))	0.460	**0.514**	0.499	0.482
Sustainability Index (E_1 (0.2), E_2 (0.4), E_3 (0.2), E_4 (0.2))	0.380	0.420	**0.429**	0.414
Sustainability Index (E_1 (0.2), E_2 (0.2), E_3 (0.4), E_4 (0.2))	0.456	0.520	**0.605**	0.578
Sustainability Index (E_1 (0.2), E_2 (0.2), E_3 (0.2), E_4 (0.4))	0.415	0.455	**0.493**	0.477

7.4 Conclusion: Pyro-gasification

In this chapter, pyrolysis and gasification process integration basis sustainable process for biomass waste valorization has been established. Process optimization has been done and evaluated using energy, economic, and process safety indicators. Following the principal findings of this chapter:

- When compared to the basic process, the optimized process performs better in all scenarios.
- The basic process and the optimized process under scenarios 1-3 have an energy efficiency of 59%, 66%, 47%, and 46%, respectively with an electric power potential of 2304 kW, 2788 kW, 4044 kW, and 3796 kW in the respective case.
- In the non-subsidized situation, when the process efficiency varies from 100% to 80% in the economic evaluation, the IRR (%) varies between 37-2%, 38-6%, 44-28%, and 43-27% for the basic process and the optimized process under scenarios 1-3, respectively.
- Process safety risk (%) of the basic and scenario 1 optimized process is lower than that optimized scenarios 2-3.
- The optimized process under scenarios 1 has the highest SI score 0.563 based on the weights determined by the BWM, followed by the optimized process under scenarios 2 with a sustainability index score of 0.534, the optimized process under scenarios 3 with a sustainability index score of 0.517, and basic process with a sustainability score of 0.503.

Although the current integrated process of pyrolysis and gasification process is sustainable but still some other sustainability aspects need to be explored. All case studies included in this research work seem sustainable but overall sustainability analysis results will be varied with respect to regional constraint and stakeholder's interest. Therefore, to assess this variation and stakeholders' interest, a multi-criteria decision-making framework has been utilized in chapter 8 by application of both subjective and objective approach to identify the sustainable valorization process.

8 Chapter: Multi-criteria for sustainable valorization process selection

The current model has been implemented to assess its efficacy in addressing real-time issues. In this context, a sustainable waste valorization process, considering economic, environmental, technological, and socio-governance aspects, has been identified. Further elaboration on this is provided in Sections 3.3.10.1.

8.1 Problem statement

In this study, the selection of waste valorization processes is focused on developing countries, specifically targeting India, Pakistan, and Bangladesh. These countries collectively account for approximately one-fourth of the global population [320]. Consequently, substantial amounts of MSW are generated within these countries. According to various institutional estimates, India produces an average of approximately 165 million tons of MSW, Pakistan produces 30 million tons, and Bangladesh produces around 7.4 million tons [321–323]. But a considerable proportion of this waste is not managed in an environmentally sound manner. The generated waste harbors significant potential for sustainable energy production. For instance, an estimation suggests that poultry litter waste alone in India, Pakistan, and Bangladesh has the potential for daily electricity production of 8745, 8893, and 4803 MW, respectively [324]. Despite this potential, challenges arise due to a lack of technological advancement and financial constraints in these countries, hindering the implementation of sustainable valorization processes for waste management. Consequently, selecting a sustainable waste valorization technique based on economic, environmental, technological, and socio-governance considerations becomes paramount to address and harness the potential of this waste in an appropriate and sustainable manner.

8.2 Alternatives and selection criteria

The primary objective of this research is to find the most suitable and sustainable process for the valorization of MSW. The study focuses on the comparison of primary biological and thermal techniques, exploring four alternatives as depicted in Fig. 8.A while the application methodology is defined in section 3.3.10.1, 'Research framework'. Among the primary biological methods, AND is considered, involving the biological conversion of waste into biogas and slurry, both of which can serve as valuable sources of energy and fertilizer [325]. Within the thermal techniques, gasification, pyrolysis, and hydrothermal gasification have been shortlisted as alternatives. Gasification specifically entails the transformation of MSW into syngas within the constraints of a limited amount of gasifying agent. The final output of this procedure is syngas, which can be subsequently employed in secondary processes such as methanol, dimethyl ether, hydrogen, etc. [279]. The pyrolysis process transforms MSW into either bio-oil or char, contingent upon the operational parameters governing the process in the absence of a gasifying agent. The ultimate product of pyrolysis can undergo further refinement to yield a fuel of higher quality, thereby contributing to meeting energy requirements [326].

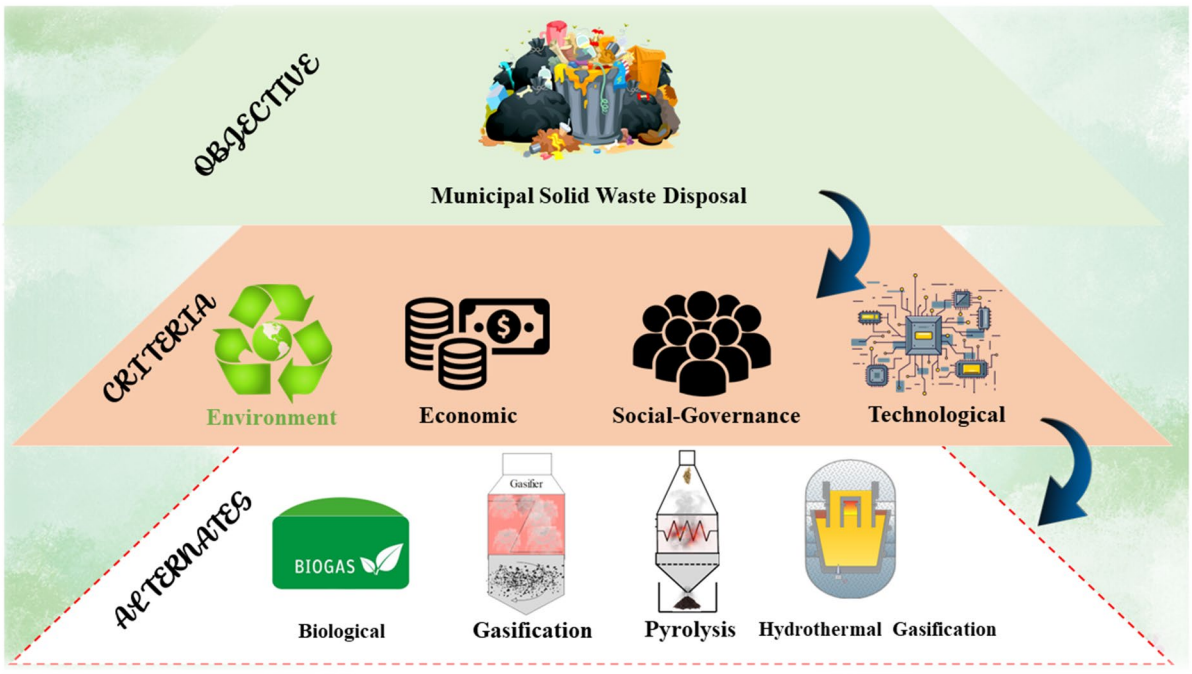

Fig. 8.A. Decision making model structure for biomass waste valorization processes

HTG represents a type of gasification process applicable to liquid biomass, under supercritical conditions of water—specifically, at pressures ranging from 20 to 30 MPa and temperatures between 350 and 450 ^{o}C. The principal output of this process is primarily hydrogen [327]. Therefore, these four biological and thermal processes have been shortlisted based on the economic, environment, and technological advantages as described in literature while environment, economic, technological, and social governance have been utilized as a criterion to select an optimum process from different alternatives.

There are primarily four major criteria—environmental, economic, social-governance, and technological—that have been thoroughly identified from the existing literature. These criteria have been shortlisted through a systematic way which included following steps:

Step 1: A primary discussion related to MSW valorization process has been conducted with three academic experts who have more than 10 years of relevant research experience in this field.

Step 2: A systematic literature review has been carried out to identify and shortlist criteria based on snowball approach of inclusion and exclusion criteria adopted in previous research [220,324]. Different keywords like “waste valorization”; “sustainable waste valorization processes”; “decision making models”; “pyrolysis process sustainability”; “gasification process”, “hydrothermal gasification”; “thermal valorization 3E analysis”; “anaerobic digestion”; “carbon neutral waste disposal”; “Fuzzy logics”; “CODAS” etc. have been searched in Scopus, Google Scholar, Elsevier database.

Step 3: Finally, these shortlisted criteria have been shared with three academic experts for their opinion and based on which ‘16’ criteria have been finalized.

Each primary criterion has been further divided into four sub-criteria. Consequently, a total of 16 sub-criteria have been employed in this research for evaluative purposes, with references cited in Table 8.1. The economic criteria, denoted as C1-C4, encompass various facets. 'C1' pertains to the 'Capital cost and operational cost of the process,' representing a cash outflow. 'C2' focuses on the 'Marketability of the final products,' serving as an indicator for a more favorable return on investment; a higher final product price or market demand correlates with improved returns. 'C3' involves the 'Rate of return on investment,' which integrates the IRR as an indicator for investment return. 'C4' addresses 'Maintenance and personnel cost,' serving as an indicator of the operational challenges associated with the process, with higher costs generally indicative of more technical or less mature processes. The environmental criteria, designated as C5-C8, include 'C5,' which examines 'GHG/Particulate matter emissions' originating from the relevant process. The eco-sustainability of a process is inversely proportional to its emissions; higher emissions correspond to lower eco-sustainability, and vice versa. 'C6' assesses 'Soil/Land/Aquatic pollution' resulting from the operational activities of the process, where elevated pollution levels indicate reduced eco-sustainability. 'C7' evaluates 'Land use,' with processes necessitating greater land considered less eco-friendly due to the assumed increased likelihood of land contamination and environmental damage. 'C8' focuses on 'Product emission throughout the product life cycle,' where a higher final product price is indicative of economic sustainability. However, it is essential that the environmental impact of the product is minimized for overall sustainability. These environmental criteria are derived from the existing literature.

Technological criteria, denoted as C9-C12, encompass several dimensions. 'C9' evaluates 'Process energy and exergy recovery,' serving as an indicator of the overall energy efficiency of the process. 'C10' analyses the 'Access and technology adaptability' of the pertinent process, with increased technological maturity enhancing the likelihood of process sustainability. 'C11'

assesses 'Waste treatment effectiveness and volume reduction,' where the greater reductions in waste volume correlate with improved process sustainability. 'C12' considers the 'Diversification of material handling,' recognizing that certain processes are sensitive to the type of material involved. For instance, processes like HTG and anaerobic digestion are limited in valorizing solid waste until it undergoes conversion into slurry or liquid. Hence, gasification and pyrolysis are suitable for solid or dry waste. Therefore, the availability of the requisite material that can be valorized by these processes is deemed a crucial factor.

Social-governance criteria, identified as C13-C16, are instrumental in the evaluation of available alternatives. 'C13' pertains to 'Process occupational safety hazards,' recognizing that processes with intense operational parameters may entail heightened occupational safety hazards. Consequently, 'C13' is incorporated into the evaluation criteria. 'C14' addresses 'Public acceptance and employment generation,' acknowledging that certain processes may necessitate more manpower and garner public acceptance due to their operational or environmental sustainability. Therefore, it is included in the analysis. 'C15' and 'C16' encompass 'Political support through existing policies' and 'Promoting social responsibility (Carbon credit),' respectively. Hence, processes receiving support through various policies and promoting social responsibility, particularly through mechanisms such as carbon credits, are considered superior in comparison to their counterparts.

Table 8.1 Selection criteria for biomass waste valorization processes

No.	Criteria	Category	Ref.
C1	Capital cost and operational cost of process	Economic	[328,329]
C2	Marketability of the final products	Economic	[328,329]
C3	Rate of return on investment	Economic	[328,330]
C4	Maintenance and personnel cost	Economic	[328]
C5	GHG/Particulate matter emissions	Environment	[329,331]
C6	Soil/Land/Aquatic pollution	Environment	[328,332]
C7	Land use	Environment	[333]
C8	Product emission throughout product life cycle	Environment	[327,334]
C9	Process energy and exergy recovery	Technological	[327,335]
C10	Access and technology adaptability	Technological	[330]
C11	Waste treatment effectiveness and volume reduction	Technological	[336]
C12	Diversification of material handling	Technological	[329]
C13	Process occupational safety hazards	Social-Governance	[337]
C14	Public acceptance and employment generation	Social-Governance	[328,330]
C15	Political support through existing policies	Social-Governance	[328,330]
C16	Promoting social responsibility (Carbon credit)	Social-Governance	This study

8.3 Data collection and analysis

Data collection and evaluation based on the problem statement defined in section 8.1 and alternatives and criteria selection based on section 8.2 has been divided into different steps.

Step 1: The study data was acquired through the development of a survey, the details of which are provided in Appendix A19. All available alternatives underwent a comprehensive evaluation based on the '16' criteria outlined in Table 8.1. The survey construction and evaluation were conducted with the guidance of experts as defined in section 8.2. The entire research framework is given in Fig. 8.A, starting from survey development to data collection

and final analysis. For this particular study, '7' experts were selected from '3' distinct developing countries, including Pakistan and Bangladesh. These experts comprised individuals with backgrounds in academia and industry, each possessing a minimum of '8' years of relevant experience with graduation. To facilitate data collection through the survey, an online survey link was shared with the experts. The survey sought their relative assessments of the processes based on the economic, environmental, technological, and social-governance criteria given in Table 8.1. This survey includes the criteria comparison based on IVFFS and also relative comparison among the criteria to prioritize them based on AHP. A sample of this survey is given in Appendix A19. Thorough measures were taken to ensure that all experts completed the surveys accurately and comprehensively. Final survey results are given in Appendix A20.

Step 2: For analysis purposes, all data of AHP weights calculation and IVFFS, in the form of expert opinions, underwent systematic analysis. For AHP weights, experts' opinions have been converted into crisp values, and further analysis has been done. The consistency index of the AHP has been identified as less than 0.10. After that expert opinions regarding IVFFS which were initially presented in linguistic form, an initial conversion was executed, transforming them into IVFFS -based crisp values as detailed given in Appendix A20.

Step 3: Aggregated decision matrix has been calculated through Eq. 3.80-3.87 given in section 3.3.10 while results are summarized in Table 8.3 which has been normalized through Eq. 3.91 and final normalized results are given in Table 8.4. The calculation of weights, as outlined in Section 3.12.1.3 and final weights calculation are presented in Table 8.2 and Appendix A21. These weights were utilized to compute the weighted normalized matrix in Table 8.5 based on the normalized aggregated Interval Fermatean fuzzy values (Table 8.4). Shannon Entropy (Eq. 3.92 and 9.93) and CRITIC weights are also included based on main criteria for sensitivity analysis. Primarily, AHP weights have been utilized for the analysis of results while entropy,

CRITIC, and equal weights have been only utilized for sensitivity analysis purpose which are given in section 8.5. The Dombi operator (0.1-1) has been utilized to calculate the aggregate score of the Interval Value Fermatean Fuzzy Numbers (IVFFS) based on the methodology defined in section 3.3.10.1 as given in Table 8.3.

Step 4: Subsequently, the negative ideal solution has been calculated based on the weighted normalized decision matrix in Table 8.5.

Table 8.2 Criteria's weights based on different methods

	AHP		AHP Local	AHP Global
Economic	0.4426	C1	0.2315	0.1025
		C2	0.1906	0.0844
		C3	0.3245	0.1436
Environment	0.2242	C4	0.2534	0.1121
		C5	0.3547	0.1570
		C6	0.2546	0.1127
		C7	0.1987	0.0879
		C8	0.1920	0.0850
Social	0.1264	C9	0.2879	0.1274
		C10	0.2976	0.1317
		C11	0.1434	0.0635
Technology	0.2068	C12	0.2711	0.1200
		C13	0.3357	0.1486
		C14	0.1876	0.0830
		C15	0.2597	0.1149
		C16	0.2170	0.0960

Table 8.3 Aggregate decision matrix of IVFFS

		Economic				Environment				Technology				Social Governance			
		C1	C2	C3	C4	C5	C6	C7	C8	C9	C10	C11	C12	C13	C14	C15	C16
Gasification	ϑ^-	0.704	0.683	0.607	0.631	0.552	0.519	0.567	0.573	0.626	0.593	0.679	0.672	0.612	0.619	0.581	0.623
	ϑ^+	0.767	0.747	0.674	0.686	0.607	0.575	0.643	0.647	0.697	0.656	0.741	0.725	0.674	0.685	0.639	0.672
	σ^-	0.389	0.510	0.563	0.544	0.624	0.650	0.595	0.556	0.495	0.595	0.435	0.538	0.553	0.490	0.584	0.574
	σ^+	0.495	0.579	0.618	0.586	0.685	0.695	0.656	0.630	0.587	0.659	0.499	0.564	0.617	0.556	0.648	0.629
Pyrolysis	ϑ^-	0.691	0.616	0.613	0.638	0.623	0.619	0.576	0.616	0.620	0.662	0.646	0.601	0.667	0.652	0.595	0.601
	ϑ^+	0.741	0.679	0.677	0.703	0.685	0.675	0.616	0.675	0.686	0.726	0.692	0.650	0.740	0.708	0.646	0.650
	σ^-	0.489	0.548	0.551	0.450	0.515	0.574	0.627	0.540	0.530	0.588	0.574	0.587	0.407	0.561	0.622	0.587
	σ^+	0.529	0.617	0.612	0.514	0.584	0.613	0.675	0.610	0.591	0.645	0.603	0.636	0.508	0.605	0.645	0.636
HTG	ϑ^-	0.712	0.644	0.680	0.681	0.573	0.570	0.594	0.585	0.630	0.490	0.664	0.671	0.693	0.620	0.588	0.610
	ϑ^+	0.749	0.708	0.731	0.745	0.649	0.594	0.644	0.628	0.692	0.566	0.709	0.733	0.753	0.669	0.636	0.668
	σ^-	0.496	0.481	0.536	0.435	0.555	0.660	0.597	0.613	0.486	0.649	0.583	0.493	0.470	0.566	0.606	0.582
	σ^+	0.547	0.548	0.577	0.499	0.628	0.705	0.639	0.660	0.553	0.715	0.614	0.551	0.537	0.612	0.654	0.641
AND	ϑ^-	0.574	0.663	0.595	0.640	0.637	0.604	0.626	0.666	0.579	0.682	0.626	0.549	0.644	0.682	0.656	0.685
	ϑ^+	0.646	0.701	0.664	0.704	0.704	0.683	0.691	0.729	0.640	0.745	0.666	0.602	0.682	0.741	0.719	0.732
	σ^-	0.559	0.561	0.540	0.512	0.511	0.515	0.515	0.518	0.587	0.448	0.601	0.628	0.610	0.474	0.477	0.535
	σ^+	0.646	0.594	0.622	0.581	0.570	0.587	0.584	0.576	0.645	0.545	0.645	0.685	0.647	0.541	0.545	0.561

Table 8.4 Normalized decision matrix of IVFFS

		Economic				Environment				Technology				Social Governance			
		C1	C2	C3	C4	C5	C6	C7	C8	C9	C10	C11	C12	C13	C14	C15	C16
Gasification	ϑ^-	0.389	0.683	0.607	0.544	0.624	0.650	0.595	0.556	0.626	0.593	0.679	0.672	0.553	0.619	0.581	0.623
	ϑ^+	0.495	0.747	0.674	0.586	0.685	0.695	0.656	0.630	0.697	0.656	0.741	0.725	0.617	0.685	0.639	0.672
	σ^-	0.704	0.510	0.563	0.631	0.552	0.519	0.567	0.573	0.495	0.595	0.435	0.538	0.612	0.490	0.584	0.574
	σ^+	0.767	0.579	0.618	0.686	0.607	0.575	0.643	0.647	0.587	0.659	0.499	0.564	0.674	0.556	0.648	0.629
Pyrolysis	ϑ^-	0.489	0.616	0.613	0.450	0.515	0.574	0.627	0.540	0.620	0.662	0.646	0.601	0.407	0.652	0.595	0.601
	ϑ^+	0.529	0.679	0.677	0.514	0.584	0.613	0.675	0.610	0.686	0.726	0.692	0.650	0.508	0.708	0.646	0.650
	σ^-	0.691	0.548	0.551	0.638	0.623	0.619	0.576	0.616	0.530	0.588	0.574	0.587	0.667	0.561	0.622	0.587
	σ^+	0.741	0.617	0.612	0.703	0.685	0.675	0.616	0.675	0.591	0.645	0.603	0.636	0.740	0.605	0.645	0.636
HTG	ϑ^-	0.496	0.644	0.680	0.435	0.555	0.660	0.597	0.613	0.630	0.490	0.664	0.671	0.470	0.620	0.588	0.610

	ϑ^+	0.547	0.708	0.731	0.499	0.628	0.705	0.639	0.660	0.692	0.566	0.709	0.733	0.537	0.669	0.636	0.668
	σ^-	0.712	0.481	0.536	0.681	0.573	0.570	0.594	0.585	0.486	0.649	0.583	0.493	0.693	0.566	0.606	0.582
	σ^+	0.749	0.548	0.577	0.745	0.649	0.594	0.644	0.628	0.553	0.715	0.614	0.551	0.753	0.612	0.654	0.641
AND	ϑ^-	0.559	0.663	0.595	0.512	0.511	0.515	0.515	0.518	0.579	0.682	0.626	0.549	0.610	0.682	0.656	0.685
	ϑ^+	0.646	0.701	0.664	0.581	0.570	0.587	0.584	0.576	0.640	0.745	0.666	0.602	0.647	0.741	0.719	0.732
	σ^-	0.574	0.561	0.540	0.640	0.637	0.604	0.626	0.666	0.587	0.448	0.601	0.628	0.644	0.474	0.477	0.535
	σ^+	0.646	0.594	0.622	0.704	0.704	0.683	0.691	0.729	0.645	0.545	0.645	0.685	0.682	0.541	0.545	0.561

Table 8.5 AHP weighted normalized decision matrix of IVFFS

		Economic				**Environment**				**Technology**				**Social Governance**			
		C1	**C2**	**C3**	**C4**	**C5**	**C6**	**C7**	**C8**	**C9**	**C10**	**C11**	**C12**	**C13**	**C14**	**C15**	**C16**
Gasification	ϑ^-	0.040	0.058	0.087	0.061	0.098	0.073	0.052	0.047	0.080	0.078	0.043	0.081	0.082	0.051	0.067	0.060
	ϑ^+	0.051	0.063	0.097	0.066	0.108	0.078	0.058	0.054	0.089	0.086	0.047	0.087	0.092	0.057	0.073	0.065
	σ^-	0.072	0.043	0.081	0.071	0.087	0.058	0.050	0.049	0.063	0.078	0.028	0.064	0.091	0.041	0.067	0.055
	σ^+	0.079	0.049	0.089	0.077	0.095	0.065	0.057	0.055	0.075	0.087	0.032	0.068	0.100	0.046	0.075	0.060
Pyrolysis	ϑ^-	0.050	0.052	0.088	0.050	0.081	0.065	0.055	0.046	0.079	0.087	0.041	0.072	0.060	0.054	0.068	0.058
	ϑ^+	0.054	0.057	0.097	0.058	0.092	0.069	0.059	0.052	0.087	0.096	0.044	0.078	0.076	0.059	0.074	0.062
	σ^-	0.071	0.046	0.079	0.072	0.098	0.070	0.051	0.052	0.068	0.077	0.036	0.070	0.099	0.047	0.072	0.056
	σ^+	0.076	0.052	0.088	0.079	0.108	0.076	0.054	0.057	0.075	0.085	0.038	0.076	0.110	0.050	0.074	0.061
HTG	ϑ^-	0.051	0.054	0.098	0.049	0.087	0.074	0.052	0.052	0.080	0.065	0.042	0.081	0.070	0.052	0.068	0.059
	ϑ^+	0.056	0.060	0.105	0.056	0.099	0.079	0.056	0.056	0.088	0.075	0.045	0.088	0.080	0.056	0.073	0.064
	σ^-	0.073	0.041	0.077	0.076	0.090	0.064	0.052	0.050	0.062	0.086	0.037	0.059	0.103	0.047	0.070	0.056
	σ^+	0.077	0.046	0.083	0.084	0.102	0.067	0.057	0.053	0.070	0.094	0.039	0.066	0.112	0.051	0.075	0.062
AND	ϑ^-	0.057	0.056	0.085	0.057	0.080	0.058	0.045	0.044	0.074	0.090	0.040	0.066	0.091	0.057	0.075	0.066
	ϑ^+	0.066	0.059	0.095	0.065	0.089	0.066	0.051	0.049	0.082	0.098	0.042	0.072	0.096	0.061	0.083	0.070
	σ^-	0.059	0.047	0.078	0.072	0.100	0.068	0.055	0.057	0.075	0.059	0.038	0.075	0.096	0.039	0.055	0.051
	σ^+	0.066	0.050	0.089	0.079	0.111	0.077	0.061	0.062	0.082	0.072	0.041	0.082	0.101	0.045	0.063	0.054

Step 5: Negative ideal solution has been identified (Table 8.6) based on weightage normalized decision matrix (Table 8.5) through application of Eq. 3.99. The advanced CODAS method, as described in Section 3.3.10.1.a, was applied for the computation of Euclidean and Hamming distances (Eq. 3.100 and 3.101) in Table 8.7 and 8.8, respectively. The relative assessment

matrix has been calculated based on Table 8.7 and 8.8 summarized in Table 8.9 based on Eq. 3.102-3.104. Finally, based on this matrix (Table 8.9), Relative Assessment Matrix *(R_m)* of the alternative ranks were determined, and using Eq. 3.105 final assessment score have been calculated given in Table 8.10. Further CODAS method validation performed, results of which are given in Section 8.5.

Table 8.6 Negative Ideal Solution

	C1	C2	C3	C4	C5	C6	C7	C8	C9	C10	C11	C12	C13	C14	C15	C16
ϑ^-	0.0399	0.0519	0.0855	0.0488	0.0803	0.0580	0.0453	0.0440	0.0738	0.0646	0.0397	0.0659	0.0604	0.0514	0.0668	0.0577
ϑ^+	0.0507	0.0573	0.0953	0.0560	0.0895	0.0661	0.0513	0.0490	0.0815	0.0745	0.0423	0.0722	0.0755	0.0556	0.0731	0.0624
σ^-	0.0729	0.0473	0.0808	0.0764	0.1000	0.0697	0.0551	0.0566	0.0748	0.0855	0.0381	0.0754	0.1029	0.0470	0.0715	0.0564
σ^+	0.0786	0.0521	0.0893	0.0835	0.1106	0.0769	0.0607	0.0619	0.0822	0.0941	0.0410	0.0821	0.1118	0.0508	0.0751	0.0616

Table 8.7 Euclidean distance calculation *Ei*

	C1	C2	C3	C4	C5	C6	C7	C8	C9	C10	C11	C12	C13	C14	C15	C16
ϑ^-	0.012	0.004	0.006	0.008	0.009	0.012	0.007	0.004	0.005	0.018	0.002	0.011	0.019	0.003	0.004	0.004
ϑ^+	0.008	0.003	0.005	0.007	0.010	0.009	0.006	0.004	0.006	0.017	0.003	0.011	0.013	0.003	0.005	0.004
σ^-	0.007	0.004	0.003	0.004	0.008	0.006	0.004	0.006	0.009	0.014	0.005	0.010	0.007	0.005	0.009	0.003
σ^+	0.006	0.003	0.003	0.005	0.009	0.008	0.004	0.006	0.008	0.013	0.005	0.011	0.008	0.004	0.006	0.004

Table 8.8 Hamming distance calculation *Hi*

	C1	C2	C3	C4	C5	C6	C7	C8	C9	C10	C11	C12	C13	C14	C15	C16
ϑ^-	0.039	0.012	0.016	0.023	0.025	0.038	0.024	0.013	0.018	0.061	0.007	0.036	0.061	0.008	0.011	0.011
ϑ^+	0.024	0.010	0.013	0.021	0.029	0.028	0.019	0.015	0.020	0.057	0.009	0.036	0.041	0.010	0.011	0.012
σ^-	0.017	0.012	0.009	0.015	0.025	0.018	0.012	0.019	0.032	0.042	0.013	0.032	0.023	0.014	0.023	0.007
σ^+	0.017	0.011	0.008	0.016	0.027	0.023	0.015	0.020	0.026	0.039	0.014	0.036	0.024	0.011	0.014	0.009

Table 8.9 Relative Assessment Matrix (R_m)

	Gasification	Pyrolysis	HTG	AND
Gasification	0.000	0.014	0.024	0.025
Pyrolysis	-0.014	0.000	0.010	0.012
HTG	-0.024	-0.010	0.000	0.002
AND	-0.025	-0.012	-0.002	0.000

Table 8.10 Assessment score calculation (AHP weights)

	A_s	Rank
Gasification	0.063	1
Pyrolysis	0.009	2
HTG	-0.033	3
AND	-0.039	4

8.4 Results and discussions on multi-criteria sustainability assessment

According to the Dombi operator based IVFFS-CODAS method, alternative ranks were computed. AHP results highlight the economic criteria as most important as compared to other. Similarly, for the entropy and CRITIC weights from the quantitative data from literature support this by attaining highest weights to the economic criteria. Among economic criteria, experts proposed 'C3' rate of return on investment with highest weight followed by 'C4' process maintenance and personnel cost. While 'C5' GHG/Particulate matter emissions in environment, 'C10' Access and technology adaptability in technology, and 'C13' Process occupational safety hazards in social governance have been ranked highest weights by the experts. Final ranked results of AHP-IVFFS proposed the gasification process as first ranked due to highest positive value, succeeded by pyrolysis and HTG, with the anaerobic digestion process attaining the lowest rank, as given in Table 8.10. Consequently, the gasification process is deemed the optimal choice among all alternatives, considering the economic, environmental, technological, and social-governance criteria.

Different studies have consistently demonstrated the better economic sustainability of thermal valorization processes compared to AND. Thermal processes typically offer a shorter payback period on investments than AND [324]. Furthermore, thermal processes tend to achieve greater reductions in GHG emissions compared to AND. According to estimates, thermal processes exhibit an average GHG reduction ranging from 63% to 66%, with gasification processes achieving approximately 66% reduction, whereas the reduction is

around 23% for AND [338,339]. The energy efficiency of thermal processes typically ranges from 45% to 60%, with gasification processes achieving approximately 50% to 60% efficiency across various studies [340]. The favorable economic, environmental, and energy performance of the gasification process may account for its highest assessment score (as indicated in Table 8.10), resulting in its top ranking. To enhance the robustness and validity of the findings, a sensitivity analysis of the data is presented in Section 8.5.

8.5 Validation through sensitivity analysis

The validation of the entire decision-making process was undertaken through a three-fold approach, incorporating both subjective and objective weightages, variations in the Dombi operator, and the rank reversal method. Fig. 8.B presents illustrative results in the form of a spider graph. According to Fig. 8Ba, with a Dombi operator value of 0.1, the gasification process consistently secured the 1st rank regardless of the application of AHP, equal, entropy, or CRITIC weightages (as detailed in Appendix A21). However, there was a change in the ranking of the pyrolysis process, transitioning from 2nd to 3rd and 4th positions in the case of entropy (QT Analysis) and equal weights, respectively. Conversely, altering the Dombi operator from 0.1 to 0.3 (Fig. 8Bb) yielded no significant impact on the rankings of the alternatives. While when criteria 9 and 16 were omitted, the gasification process consistently secured the 1st rank. Meanwhile, the rankings of AND and pyrolysis experienced a reversal, with AND occupying the 2nd rank and pyrolysis falling to the 3rd position. Tables 8.11 and 8.12 provide a comprehensive summary of the sensitivity analysis under various parameters. In all three-fold validation cases, involving variations in the Dombi operator or the omission of criteria at different weights, the gasification process consistently held the 1st rank, followed by pyrolysis and AND at the 2nd or 3rd positions, while HTG consistently ranked at the bottom. This trend of HTG may be attributed to the lack of process

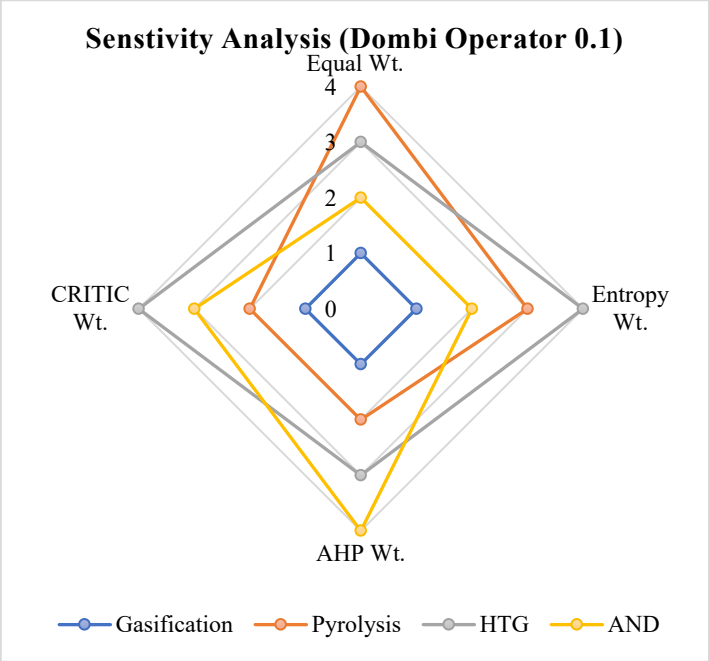

Fig. 8Ba. Sensitivity analysis with Dombi Operator 0.1

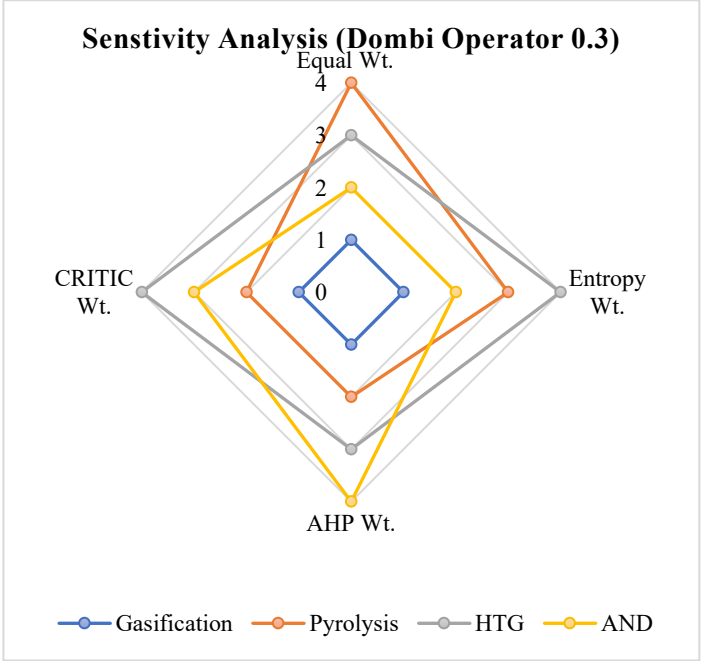

Fig. 8Bb. Sensitivity analysis with Dombi Operator 0.3

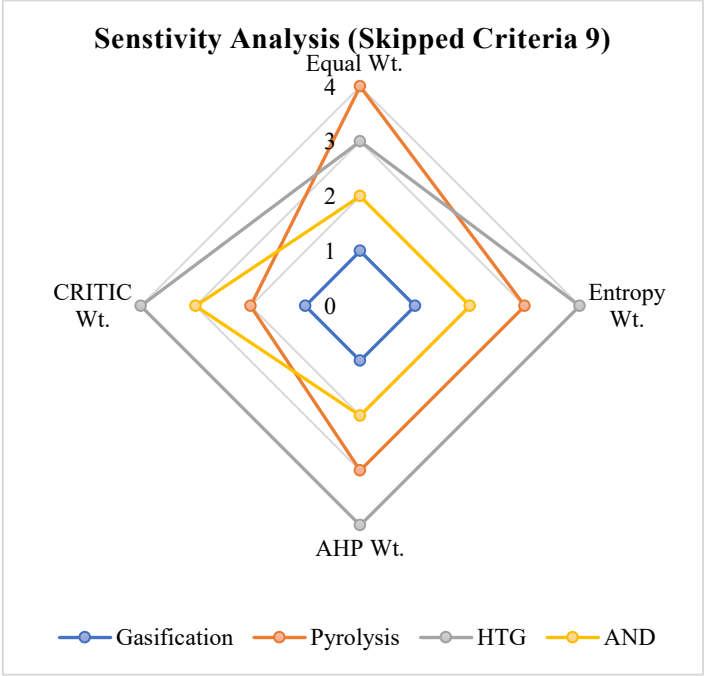

Fig. 8Bc. Sensitivity analysis skipped criteria '9'

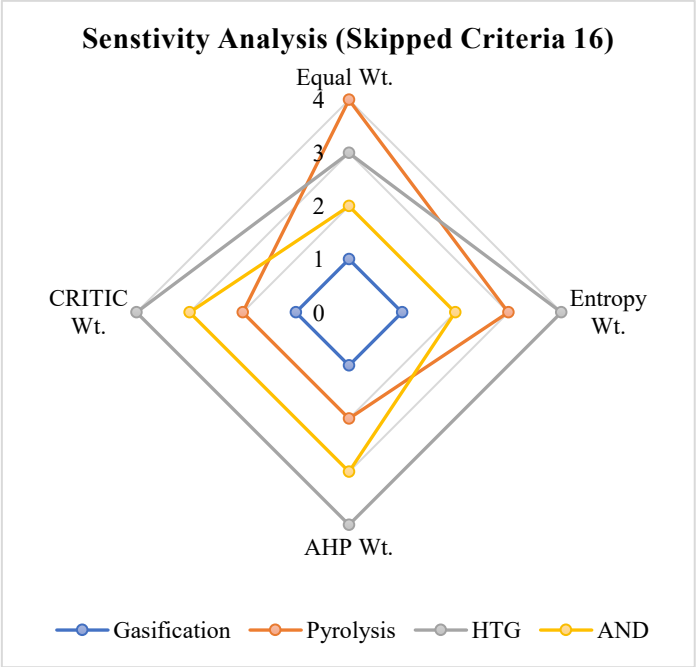

Fig. 8Bd. Sensitivity analysis skipped criteria '16'

Fig. 8.B. Sensitivity analysis of waste valorization process selection

maturity, extreme temperature and pressure requirements, and the necessity for liquid waste feed, which is not frequently available in the case of MSW. Therefore, based on this sensitivity analysis, it can be concluded that the gasification process is more sustainable compared to

pyrolysis, HTG, and AND, considering economic, environmental, technological, and social-governance aspects.

Table 8.11 Sensitivity analysis at different Dombi Operator and weights

	Dombi Operator	Equal Wt.	Entropy Wt.	AHP Wt.	CRITIC Wt.
Gasification	0.1	*1*	*1*	*1*	*1*
Pyrolysis		4	3	3	2
HTG		3	4	3	4
AND		2	2	4	3
Gasification	0.2	1	1	1	1
Pyrolysis		4	3	2	2
HTG		3	4	3	4
AND		2	2	4	3
Gasification	0.3	***1***	***1***	***1***	***1***
Pyrolysis		4	3	2	2
HTG		3	4	3	4
AND		2	2	4	3
Gasification	0.4	1	1	1	1
Pyrolysis		4	3	2	2
HTG		3	4	3	4
AND		2	2	4	3
Gasification	0.5	1	1	1	1
Pyrolysis		4	3	3	3
HTG		3	4	4	4
AND		2	2	2	2
Gasification	0.6	***1***	***1***	***1***	***1***
Pyrolysis		4	3	2	2
HTG		3	4	4	4
AND		2	2	3	3
Gasification	0.7	***1***	***1***	***1***	***1***
Pyrolysis		3	3	2	2
HTG		4	4	4	4
AND		2	2	3	3
Gasification	0.8	***1***	***1***	***1***	***1***
Pyrolysis		4	3	2	2
HTG		3	4	4	4
AND		2	2	3	3
Gasification	0.9	***1***	***1***	***1***	***1***
Pyrolysis		3	3	2	2
HTG		4	4	4	3
AND		2	2	3	4

Table 8.12 Sensitivity analysis of ranking results with skipped criteria and different weights

	Criteria skipped	Equal Wt.	Entropy Wt.	AHP Wt.	CRITIC Wt.
Gasification	16	***1***	***1***	***1***	***1***
Pyrolysis		4	3	2	2
HTG		3	4	4	4
AND		2	2	3	3
Gasification	13	***1***	***1***	***1***	***1***
Pyrolysis		4	3	2	2
HTG		3	4	4	4
AND		2	2	3	3
Gasification	9	***1***	***1***	***1***	***1***
Pyrolysis		4	3	3	2
HTG		3	4	4	4
AND		2	2	2	3
Gasification	8	***1***	***1***	***1***	***1***
Pyrolysis		4	3	3	2
HTG		3	4	4	4
AND		2	2	2	3

8.6 Conclusion: Multi-criteria for decision making

MSW constitutes a significant environmental concern; however, the prospect of converting this waste into a valuable resource emerges through effective valorization processes. For this first time, this study is conducting an in-depth analysis that integrates economic, environmental, technological, and social-governance considerations to assess gasification, pyrolysis, hydrothermal gasification, and anaerobic digestion. Following the key findings of decision making:

- The utilization of IVFFS-COADS with Dombi operator integration reveals "gasification" as the most sustainable process across economic, environmental, technological, and social-governance criteria, compared with HTG, which ranks as the least sustainable. Pyrolysis secures the 2nd rank, with AND following in 3rd place.
- A threefold sensitivity analysis, encompassing weightage, Dombi operator, and rank reversal methods, consistently corroborates the finding that gasification stands out as

the most sustainable process, while HTG consistently ranks as the least sustainable. Pyrolysis and AND interchange between 2nd and 3rd positions under different scenarios.

These findings underscore the pivotal role of government policies and public support in influencing the success of such waste valorization projects. Hence, governmental interventions, such as awareness campaigns and incentivization, can be pivotal in garnering public interest and ensuring the success of these projects, ultimately fostering a mutually beneficial outcome for all stakeholders involved.

Quantitative value weights calculations which are used in the sensitivity analysis are limited to the main criteria due to data limitations. All sixteen data criteria were not available, therefore, to perform sensitivity analysis equal number criteria weights have been calculated from the literature. Furthermore, to limit the scope of research only primary processes of MSW valorization have been compared in this study while secondary processes like gasification to methanol or dimethyl ether etc. are not the part of this research. In future, maybe an advanced MCDM model can be developed to integrate qualitative and quantitative data simultaneously to make an informed decision.

9 Policy and managerial implications

Governments can address biomass waste disposal issues along with sustainable energy production by using thermal valorization technologies. This is especially effective in remote areas where livestock and poultry farms produce a lot of biomass waste. However, specific policies and actions in the form of subsidies, tax breaks, or direct financial assistance are required to carry out the biomass waste valorization approach. There is also a need to adopt hybrid models by focusing on specific places for the proper usage of existing biomass waste potential to meet energy and agricultural needs. Furthermore, supply chain optimization along with geographical analysis can be utilized to determine the best locations for the installation of

these plants based on the availability of biomass feedstock and market demand to minimize the emissions.

Thermal valorization technologies offer better returns, more eco-friendly compared to direct land disposal of biomass waste. Among thermal processes; pyrolysis and gasification provide economic advantages over biological methods. However, they require significant capital investment and entail substantial operational costs. In South Asian countries, although legislation and plans exist for biogas plants, other conversion methods, such as pyrolysis and gasification, have been largely overlooked by governments. Therefore, to attract stakeholder interest, it is essential to commercialize final products like biochar, biofuel, and biogas, and to provide financial incentives for these technologies.

Another aspect of this study is the valorization of biomass through the integration of pyrolysis and gasification processes to enhance sustainability in terms of energy efficiency, economic viability, process safety, and power generation potential. Different scenarios for process optimization have been explored in chapter 4-7 to identify the most sustainable approach based on economic performance, electric power potential, energy efficiency, and safety. The sustainability index is evaluated by assigning different preference weights for SI score calculation using the BWM. Economic analysis indicates that the government should provide a subsidy per ton basis to make this process economically attractive to investors, as the process remains economically feasible at this subsidy level even if efficiency drops from 100% to 70%. Policymakers can prioritize indicators based on these scenarios, while investors can adjust process input parameters to enhance sustainability. Therefore, the analysis of economic performance, safety, electric power potential, and energy efficiency offers valuable insights for policymakers to develop policies that attract investors and promote the sustainable valorization of biomass waste.

A novel approach has been developed and applied to evaluate different waste valorization methodologies. The IVFFS method, integrated with CODAS, has been used to identify and rank these processes. This study offers insights for stakeholders on selecting sustainable waste valorization methods for biomass. Specifically, the study identifies the optimal alternative based on four criteria: economic, environmental, technological, and social governance. These

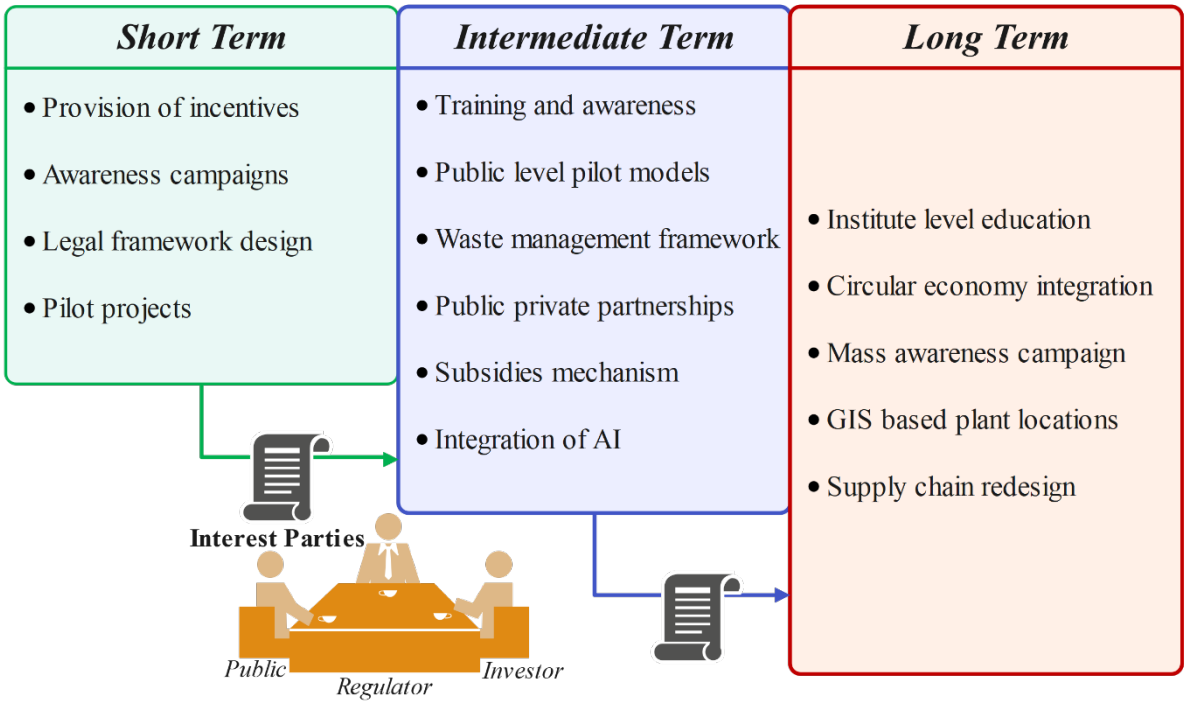

Fig. 9.A. Policy framework

criteria were identified from the literature and evaluated by experts. Based on the results, short-term, intermediate-term, and long-term action plans are proposed which are also depicted in Fig. 9.A:

Short-term actions: Current waste valorization processes necessitate substantial investments and technical assistance. However, solely relying on investor contributions may not be feasible. Consequently, there is a requirement to advocate for the establishment of technical support programs and investment opportunities that encompass not only individual investors but also financial institutions. By involving financial institutions, interested parties seeking to implement waste valorization processes can benefit both technically and financially, thereby

fostering a more conducive environment for the adoption and execution of these biomass waste valorization processes. Furthermore, environment-based incentives awareness and incentive programs need to be initiated. As 100% operational efficiency of the installed capacity does not seem feasible to achieve and therefore, operational efficiency-based scenarios can be analysed considering the economic aspects. Stakeholders can estimate the economic results of this process at different efficiencies to estimate realistic economic conditions.

Intermediate-term actions: Regulatory institutions hold a pivotal responsibility with public sector support to plan the establishment of pilot projects for waste valorization. This entails not only the execution of pilot initiatives but also the implementation of workforce training programs within these projects. The active involvement of academic and industrial experts becomes imperative to ensure the efficacy and success of these pilot endeavors. These pilot projects, besides serving as platforms for workforce development, carry the added benefit of incentivizing investors to deploy waste valorization plants strategically. Integration of AI can be done with these valorization processes to optimize the process sustainability. To make these technologies more affordable, regulators might introduce give-and-take schemes. The government will provide subsidies and financial benefit through carbon credits against these installations, which will cost at least $40-100 per 1000 kg CO_2 [210] and cost saving in the form of litter disposal.

Long-term actions: The significance of public awareness stands as a decisive factor that can either make or break initiatives of this nature. To ensure a sustained impact and foster a long-term perspective, comprehensive awareness and training programs should be initiated in the targeted areas. This needs not only the establishment of development and training modules within technical institutes but also the incorporation of waste technologies and related awareness into educational textbooks. Furthermore, periodic awareness campaigns should be conducted to actively promote these action plans and strategies, thereby fostering a continuous

and informed engagement with the community. Optimal plant location is a crucial factor in the implementation of biomass waste processes. Redesign of supply chain network along with application of geo-graphical information system (GIS). Furthermore, governmental support can be extended through subsidies to incentivize investors participating in these setups, further strengthening the viability and attractiveness of biomass waste processes. Similarly, long-term regulatory framework can also be a part of this policy framework.

The implementation of these short-term, intermediate, and long-term plans assumes a crucial role in expediting the biomass waste valorization process within developing countries. This multifaceted approach not only addresses immediate needs but also establishes a framework for sustained progress and advancement in waste management practices. The strategic incorporation of comprehensive planning across various temporal horizons serves to enhance the efficiency and effectiveness of biomass waste valorization endeavors, contributing significantly to the overarching goal of sustainable waste management in developing nations.

10 Research conclusions, limitations, and future directions

10.1 Major contribution

This study evaluated biomass thermal and biological conversion technologies and land disposal in South Asia, focusing on economic feasibility, SWOT-PEST analysis, and environmental impact. A complete summary of this study is given in Table 10.1. Findings indicate that utilizing 60% of poultry litter could provide significant electricity potential—8893 MW/d in Pakistan, 8745 MW/d in India, and 4803 MW/d in Bangladesh. Fast pyrolysis emerged as economically and technologically feasible, but it is hindered by insufficient policies, while anaerobic digestion benefits politically. The HTG simulation model showed that HTG is environmentally friendly and efficient, though less sustainable compared to gasification, which ranked highest in a comprehensive analysis integrating economic, environmental,

technological, and social-governance criteria. Gasification was found to be the most sustainable process, while HTG was the least, with pyrolysis and anaerobic digestion varying between second and third place depending on the scenario. Government policies and public support are crucial for the success of waste valorization projects.

The tri-generation processes for biomass waste valorization, including G1: Gasification to SOFC and CHP, G2: Gasification to DME and CHP, and G3: Co-gasification for hydrogen production, demonstrate significant advancements in energy efficiency and sustainability. The G1 process, optimized using AI model, shows a 34.6% improvement in exergy efficiency over traditional gasification, although it requires higher capital investment. The G2 process, optimized through PSO, achieves 57% energy efficiency and produces DME at competitive market rates, proving economically feasible with an IRR up to 26.8%. The G3 process for hydrogen production is economically viable at operational efficiencies above 90%, with potential to generate substantial electricity and hydrogen, despite high exergy destruction costs in key components. These findings (Table 10.1) underline the potential for sustainable biomass valorization through advanced tri-generation methods, highlighting the need for further economic analysis and optimization to enhance feasibility and attractiveness to investors.

PG-based tri-generation process has been developed for PL valorization to produce DME and electrical power using a comprehensive 4E (energy, exergy, economic, and environmental) analysis. The optimized process improved DME efficiency by 6%, achieved a thermal energy to electrical power capacity of 1271 kW, and demonstrated economic feasibility at efficiencies of 70% or higher. Environmentally, DME production from PL syngas is better than coal-based DME and PL composting. Furthermore, the integration of pyrolysis and gasification for biomass waste valorization showed better performance across all scenarios compared to the basic process, with energy efficiencies of 46%-66% and electric power potentials of 2304-4044 kWh. The process safety risks were lower for the optimized scenario 1, which had the highest

sustainability index score (0.563). These findings are summarized in Table 10.1 which provide valuable insights for policymakers and stakeholders on sustainable biomass valorization.

CNN, ANN, GBR, XGB, and RFR based AI-models have been developed to predict H_2, CH_4, CO_2, and CO levels in syngas produced by the gasification process. Using different dataset combinations, the study aimed to find the most reliable prediction model with higher R^2 and lower MSE, MAE, and MAPE. A 90:10 training-to-testing dataset ratio yielded the best results across all AI algorithms. The XGB model outperformed others, achieving coefficients of determination between 0.85 and 0.95 with low error metrics. AI results indicate that hydrogen, methane, and carbon monoxide mole fractions can be increased by using biomass with higher hydrogen and oxygen content and by increasing temperature and biomass residence time during gasification. Hence, the XGB algorithm is recommended for predicting gasification outputs, as it surpassed other models in accuracy without requiring complex simulations or experimental setups.

Table 10.1 Summary of the research work

Study	Phase	Novelty	Process	Output	Study Conclusion
[324]	1	SWOT, economic, electric potential and environment analysis of waste valorization techniques	AND, FP, SP, AD	SWOT, EA, LCA, and power (MW)	FP payback period is 299 days, while SP 5036, and AND in loss. AND is eco-friendly compared to FP and SP. Pakistan, India, and Bangladesh have a potential of 8893 MW/d, 8745 MW/d, and 4803 MW/d electricity
[327]	2	HTG PL economic, environment, energy analysis	HTG	Syngas, steam	10% cheaper steam production compared to coal or gas from PL HTG Energy efficiency of process is 61.3% HTG is eco-friendly with 250 µt as compared to land disposal 360 µt
[158]	2	H_2 Prediction through Neural Network, optimize H_2, HHV, LHV	Gasification	H_2, HHV, LHV	PSO, RSM, CNN models applied to predict output with process R^2>0.95 and MSE<0.01
[246]	2	Quality syngas prediction in HTG process; CNN, ANN, GBR, XGB, RFR.	HTG	H_2, CO_2, CO, CH4	CNN, ANN, GBR, XGB, and RFR models applied but XGB model has better predictability results. R^2 0.85-0.95, MAE 0.05-0.15, MAPE 0.4-7.1%. Hence, XGB is a better predictability algorithm for similar processes.
[303]	2	PL to gasification process by integration of SOFC, CHP, XGB prediction model for H_2, steam, electric power	Gasification, SOFC, CHP	H_2, steam, electric power	Process Exergy efficiency is 34.6% and XGB model (R^2>0.97) is suitable for process prediction.

[337]	2	HTG, gasification, pyrolysis safety analysis and strategies for risk reduction.	Gasification, Pyrolysis, HTG	NuDIST safety score, and Hierarchy of risk control	SI for HTG is 210.2 while it is 228.5, 226.4 for Gasification and pyrolysis. A hierarchy of risk control in these processes was also proposed.
[193]	3	Develop a novel multi-generation valorization process for syngas utilization in SOFC, CO_2 liquification, and CHP	Gasification, SOFC, CHP	Electric power, CO_2	Process payback period is 1888 days at 100-90% η; while 610 days at 5$ subsidy IRR of process is 7% for base and 20% subsidy at 100% η; Process steam to electric power potential is 1331 kW for 10 t/h
[170]	2	Prediction and optimization of yield (H_2), HHV, and LHV	HTG	Optimization of H_2, LHV, HHV	HDMR model optimization MAE 0.02-0.05, MSE 0.001-0.009, and MAPE 1.9-3.49%. Hence, this optimization model can be applied for waste valorization.
[41]	1	Gasification process review including technological, process parameters routes for output optimization	Gasification	Optimized parameters, technology, catalyst, LCA	**LCA** concludes that biomass waste gasification process can reduce 60 to 75 CO_2 as compared to land disposal. China, USA, Brazil, Pakistan, India, and Bangladesh have the potential to reduce CO_2 by 68.8, 71.3, 45.6, 10.1, 9.9, and 5.4 million t/yr by only application of poultry litter gasification as compared to land disposal.
[64]	1	Critical review of cause-and-effect analysis, economic, environment, safety analysis	HTG	HTG review analysis from literature	Syngas quality can be improved by managing process parameters such as 500-550 ℃, 25-28 MPa, 120-150 min resident time, and 10-20% of the solid biomass content. H_2 cost 1.94 to 7.0 $/kg with a payback period of 3.3-5.16 yrs.
[279]	2,3	PL gasification to DME process has been developed and 3E, 1S Sustainability analysis of this process has been performed by optimization of PSO.	Gasification, DME, CHP	DME, CHP, and CO_2	The IRR of PSO based optimized model is 16% at 80% η with energy efficiency of 57%. LCA predict DME 442 µt PL gas 309 µt. This tri-generation process exhibits 57% energy efficiency, which is 12% higher than that of PL gasification (45%)
[334]	2,3	Plasma gasification tri-generation for DME, CHP has been developed and its sustainability analysis in terms of techno-economic, environment, energy, exergy, and emergy have been done. This process has been optimized by radial base function.	PG, DME, CHP	DME, power	Process PBP is 2.21 yrs. for optimized process while it is not feasible without optimization below 90% η. Process energy efficiency is 44.3-48.5% and exergy efficiency are 41.3-42.7%. LCA (µt) DME PL is eco-friendly with 191 µt as compared to DME Coal 599 µt. Thermal energy to electric power potential is 1271 kWh per 10 t/h
[335]	2,3, 4	BM waste valorization by the co-generation of pyrolysis and gasification processes through techno-economic, energy, and safety analysis. Process sustainability enhanced by pattern search algorithm.	Pyro-gasification, CHP, CO_2	DME, power, CO_2	IRR (%) of the basic process varies from 37 to 2% when the process efficiency dropped from 100 to 80%, and it varies from 44 to 6% for the optimized process without any subsidy. The optimized process has a potential of 2,788-4,044 kW of electric power generation from the thermal energy of the process while it is only 2,302 kW for basic scenario.
[304]	2,3	To produce blue H_2, and green H_2 by comixing feedstock comprising biomass and plastic waste. Furthermore, an advanced exergy and exergoeconomics analysis have been performed.	Co-gasification, AEC, CHP	Blue H_2, green H_2, CH_4, CO_2 and power	Process IRR is 8% at 70% η $10 subsidy; while 47-37% at 100-90% η no subsidy. Exergy efficiency loss at the gasifier is around 40%, and 36% for HeatXC. Therma energy has a potential of 1079 kWh electricity per 20 t/h
[339]	4	Identification of economic, environment, technological, and social governance indicators for selection and CODAS for ranking of the sustainable valorization process by comparing quantitative and Qualitative criteria	HTG, gasification, pyrolysis, AND	Gasification is sustainable with A_S of 0.063.	The thermal valorization technique gasification identified as the sustainable process with assessment score (A_s) of 0.063, followed by pyrolysis and HTG with A_s of 0.009 and -0.033, respectively. The threefold validation, encompassing weights variation, rank reversal, and changing DO, consistently supported the finding that gasification stands out as the most sustainable process.

[341]	2,3	Gasification process for ethanol and acetaldehyde production has been developed which is techno-economic and energy sustainable. Prediction and optimization have been done through ANN.	Gasification, Ethanol, Acetaldehyde, CHP	Acetaldehyde, power, ethanol	Process sustainability analysis demonstrated an energy efficiency of 64% while economic viability up to 80% process efficiency with an IRR of 6% and a PBP of 2107 days with energy efficiency 64%. 700 kWh of electricity has been produced from 10 t/h ANN prediction performance is R^2 0.92-0.98, MAE 0.03-0.1, and MAPE 0.1-1.12%	

Quantitative and qualitative decision-making analyses related to biomass waste valorization process, supported by expert opinion and existing literature, identify the gasification process as the most reliable and sustainable option among pyrolysis, hydrothermal gasification, and anaerobic processes in the developing countries. Therefore, a gasification-based thermal process is recommended for biomass waste valorization due to its biomass waste type processing flexibility, scalability, energy efficiency, economic viability, and technical process maturity.

Table 10.2 Summarized causes and effect relation of gasification process

Parameters	H_2	CO	CO_2	CH_4	Tar	Char	CGE	CCE	LHV	HHV	ROR
Temperature ↑	↑	↑	↓	↓	↓	↓	↑	↑	↑	↑	↑
Pressure ↑	↓	↓	↑	↑	↑	↑	↑	↑	↑	↑	↓
Gasifying Agent ↑	↑	↑	↓	↓	↓	↓	↑	↑	↓	↓	↑
Resident Time ↑	↓	↓	↑	↑	↓	↓	↑	↑	↑	↑	↑
Particle Size ↑	↓	↓	↑	↑	↑	↑	↑	↑	↓	↓	↓
Target (H_2) Catalyst ↑	↑	↑	↓	↓	↓	↓	↑	↑	↑	↑	↑

Table 10.2 [41] represents the general relationship between process parameters and gasification output through a cause-and-effect analysis based on this research findings with some exceptions. In Table 10.2, arrows pointing in the same direction between parameters and

output attributes indicate a directly proportional relationship (green color), whereas arrows pointing in opposite directions denote an inverse correlation (red color). According to the findings in Table 10.1, an increasing process temperature correlates with increased yields of H_2 and CO, while reduction in the quantities of CO_2 and CH_4. Furthermore, it also increases in CGE, CCE, LHV, HHV, and the rate of reaction (ROR) are observed, accompanied by reduction in tar and char generation from BM. While pressure does not have significant impact on syngas yield, it reduces the rate of reaction, contributing to a higher percentage of tar and char in the syngas. The influence of various GAs on the gasification process exhibits variability, specifically with O_2 and steam demonstrating a more concrete effect in enhancing the syngas quality compared to air. Otherwise, all GAs follows similar patterns, but the quantity of GA correlates with increased yields of H_2 and CO, simultaneously lessening the quantities of CO_2, CH_4, tar, and char in the syngas. Furthermore, there is an improvement observed in CCE, CGE, and the rate of reaction.

10.2 Limitations and future directions

All case studies from chapter 4-7 are based on some assumptions which have been summarized in methodology chapter 3. Economic analysis is limited to small-scale plants with some assumptions mentioned in chapter 3 and LCA is limited to system boundaries from waste transportation to final production at waste valorization plant while civil infrastructure work LCA is not being incorporated. Similarly, the social aspects of the valorization process, including plant location selection and occupational safety assessment, are not part of this study while only process safety index have been covered. But that was a macro-level study of the primary processes rather than the tri-generation process [342]. Electric power potential calculations relied on claimed efficiencies of steam turbines and generators, subject to change with improved component efficiencies. Therefore, the social aspects of the valorization process,

plant location selection, and operational occupational safety assessment will be incorporated in our future work to make this process more sustainable and safer.

An analysis has been conducted on the sustainability of gasification, focusing on its energy, economic, and safety aspects. There are some other social aspects in terms of job generation, contributions toward society, and macro/micro level contribution of the work towards the environment are still missing in the work, which will be covered in future work. Furthermore, due to regional aspects and techno-economic variations, some assumptions have been considered in the calculation of all indicators given in the respective sections. In current work, different tri-generation processes related to SOFC, dimethyl ether, methanol, carbon dioxide, hydrogen etc. production has been developed. Similarly, these processes can be optimized by the application of PSO (section 3.2.2.2) and pattern search algorithms (section 3.2.2.4). Decision making modeling regarding poly-generation optimal techniques selection based on energy, exergy, economic, environment, and safety perspectives. PESTL criteria are also under consideration which will be presented in future work. Furthermore, valorization process plant location selection is also an important factor which is also not included in this current work. Therefore, these works will be included in the future work.

References

[1] The World Bank, Trends in Solid Waste Management, (2023). https://datatopics.worldbank.org/what-a-waste/trends_in_solid_waste_management.html (accessed October 10, 2023).

[2] S. Mor, K. Ravindra, Municipal solid waste landfills in lower-and middle-income countries: Environmental impacts, challenges and sustainable management practices, Process Safety and Environmental Protection 174 (2023) 510–530. https://doi.org/10.1016/j.psep.2023.04.014.

[3] M. Margallo, M.B.M. Taddei, A. Hernández-Pellón, R. Aldaco, Á. Irabien, Environmental sustainability assessment of the management of municipal solid waste incineration residues: A review of the current situation, Clean Technol Environ Policy 17 (2015) 1333–1353. https://doi.org/10.1007/S10098-015-0961-6/TABLES/13.

[4] R. Joshi, S. Ahmed, Status and challenges of municipal solid waste management in India: A review, Cogent Environ Sci 2 (2016). https://doi.org/10.1080/23311843.2016.1139434.

[5] D.Q. Zhang, S.K. Tan, R.M. Gersberg, Municipal solid waste management in China: Status, problems and challenges, J Environ Manage 91 (2010) 1623–1633. https://doi.org/10.1016/J.JENVMAN.2010.03.012.

[6] Biomass explained - U.S. Energy Information Administration (EIA), (n.d.). https://www.eia.gov/energyexplained/biomass/ (accessed March 17, 2023).

[7] Z. Hameed, M. Aslam, Z. Khan, K. Maqsood, A.E. Atabani, M. Ghauri, M.S. Khurram, M. Rehan, A.S. Nizami, Gasification of municipal solid waste blends with biomass for energy production and resources recovery: Current status, hybrid technologies and

innovative prospects, Renewable and Sustainable Energy Reviews 136 (2021) 110375. https://doi.org/10.1016/J.RSER.2020.110375.

[8] Y. Ayub, A. Mehmood, J. Ren, C.K.M. Lee, Sustainable recycling of poultry litter to value-added products in developing countries of South Asia, J Clean Prod 357 (2022) 132029. https://doi.org/10.1016/J.JCLEPRO.2022.132029.

[9] Biomass explained - U.S. Energy Information Administration (EIA), (n.d.). https://www.eia.gov/energyexplained/biomass/ (accessed March 17, 2023).

[10] F.A. Agblevor, S. Beis, S.S. Kim, R. Tarrant, N.O. Mante, Biocrude oils from the fast pyrolysis of poultry litter and hardwood, Waste Management 30 (2010) 298–307. https://doi.org/10.1016/J.WASMAN.2009.09.042.

[11] A. Atimtay, S. Yurdakul, Combustion and Co-Combustion characteristics of torrefied poultry litter with lignite, Renew Energy 148 (2020) 1292–1301. https://doi.org/10.1016/j.renene.2019.10.068.

[12] H.K. Jeswani, A. Whiting, A. Martin, A. Azapagic, Environmental and economic sustainability of poultry litter gasification for electricity and heat generation, Waste Management 95 (2019) 182–191. https://doi.org/10.1016/j.wasman.2019.05.053.

[13] Y. Ayub, S. Tao, J. Ren, C.K.M. Lee, C. He, A. Manzardo, Poultry litter valorization by application of hydrothermal gasification: Process simulation, Economic, Energic, and Environmental analysis, Int J Energy Res (2022). https://doi.org/10.1002/er.8610.

[14] R. Segurado, S. Pereira, D. Correia, M. Costa, Techno-economic analysis of a trigeneration system based on biomass gasification, Renewable and Sustainable Energy Reviews 103 (2019) 501–514. https://doi.org/10.1016/J.RSER.2019.01.008.

[15] A. Ebrahimi, M. Ziabasharhagh, Energy and exergy analyses of a novel integrated process configuration for tri-generation heat, power and liquefied natural gas based on biomass gasification, Energy Convers Manag 209 (2020) 112624. https://doi.org/10.1016/J.ENCONMAN.2020.112624.

[16] J. Zhou, M. Ashraf Ali, A. Alizadeh, P. Kumar Singh, S. Fahad Almojil, A. Ibrahim Almohana, A. Fahmi Alali, Proposal of a tri-generation system by co-combustion of groundnut shell biomass and synthesis gas exiting from a solid oxide fuel cell: Environmental assessment and multi-objective optimization, Fuel 343 (2023) 127803. https://doi.org/10.1016/J.FUEL.2023.127803.

[17] Y. Ayub, J. Zhou, J. Ren, Y. Wang, W. Shen, C. He, L. Dong, S. Toniolo, Plasma gasification based monetization of poultry litter: System optimization and comprehensive 5E (Energy, Exergy, Emergy, Economic, and Environmental) analysis, Energy Convers Manag 282 (2023). https://doi.org/10.1016/j.enconman.2023.116878.

[18] I. Syazaidah, M.S. Abu Bakar, M.S. Reza, A.K. Azad, Ex-situ catalytic pyrolysis of chicken litter for bio-oil production: Experiment and characterization, J Environ Manage 297 (2021). https://doi.org/10.1016/j.jenvman.2021.113407.

[19] C. Ji, L. Shi, S. Wang, X. Cong, T. Su, M. Yu, Investigation on performance of a spark-ignition engine fueled with dimethyl ether and gasoline mixtures under idle and stoichiometric conditions, Energy 126 (2017) 335–342. https://doi.org/10.1016/j.energy.2017.03.045.

[20] D. Baruah, D.C. Baruah, Modeling of biomass gasification: A review, Renewable and Sustainable Energy Reviews 39 (2014) 806–815. https://doi.org/10.1016/j.rser.2014.07.129.

[21] C. Zhang, K.W. Jun, R. Gao, G. Kwak, H.G. Park, Carbon dioxide utilization in a gas-to-methanol process combined with CO2/Steam-mixed reforming: Techno-economic analysis, Fuel 190 (2017) 303–311. https://doi.org/10.1016/j.fuel.2016.11.008.

[22] T. Nakyai, Y. Patcharavorachot, A. Arpornwichanop, D. Saebea, Comparative exergoeconomic analysis of indirect and direct bio-dimethyl ether syntheses based on air-steam biomass gasification with CO2 utilization, Energy 209 (2020). https://doi.org/10.1016/j.energy.2020.118332.

[23] ECHEMI, Methyl ether Price and Market Analysis - ECHEMI, (2022). https://www.echemi.com/productsInformation/pid_Seven1867-dimethylether.html (accessed November 30, 2022).

[24] M. Singh, S.A. Salaudeen, B.H. Gilroyed, A. Dutta, Simulation of biomass-plastic co-gasification in a fluidized bed reactor using Aspen plus, Fuel 319 (2022). https://doi.org/10.1016/j.fuel.2022.123708.

[25] M.-N. Kaydouh, N. El Hassan, Thermodynamic simulation of the co-gasification of biomass and plastic waste for hydrogen-rich syngas production, Results in Engineering 16 (2022) 100771. https://doi.org/10.1016/j.rineng.2022.100771.

[26] J. Li, R.G. Burra, Z. Wang, X. Liu, A.K. Gupta, Co-gasification of high-density polyethylene and pretreated pine wood, Appl Energy 285 (2021). https://doi.org/10.1016/j.apenergy.2021.116472.

[27] J. Li, M. Suvarna, L. Pan, Y. Zhao, X. Wang, A hybrid data-driven and mechanistic modelling approach for hydrothermal gasification, Appl Energy 304 (2021). https://doi.org/10.1016/j.apenergy.2021.117674.

[28] H. Shahbeik, A. Shafizadeh, M.H. Nadian, D. Jeddi, S. Mirjalili, Y. Yang, S.S. Lam, J. Pan, M. Tabatabaei, M. Aghbashlo, Using evolutionary machine learning to characterize and optimize co-pyrolysis of biomass feedstocks and polymeric wastes, J Clean Prod 387 (2023). https://doi.org/10.1016/j.jclepro.2023.135881.

[29] C.C.E. Christopher, A. Dutta, S. Farooq, I.A. Karimi, Process Synthesis and Optimization of Propylene/Propane Separation Using Vapor Recompression and Self-Heat Recuperation, Ind Eng Chem Res 56 (2017) 14557–14564. https://doi.org/10.1021/acs.iecr.7b03432.

[30] J. Kennedy, R. Eberhart, bls gov, Particle Swarm Optimization, 1995.

[31] A. Jain, S. Sarsaiya, M. Kumar Awasthi, R. Singh, R. Rajput, U.C. Mishra, J. Chen, J. Shi, Bioenergy and bio-products from bio-waste and its associated modern circular economy: Current research trends, challenges, and future outlooks, Fuel 307 (2022). https://doi.org/10.1016/J.FUEL.2021.121859.

[32] D.J. Garcia, F. You, The water-energy-food nexus and process systems engineering: A new focus, Comput Chem Eng 91 (2016) 49–67. https://doi.org/10.1016/J.COMPCHEMENG.2016.03.003.

[33] C. Font-Palma, Characterisation, kinetics and modelling of gasification of poultry manure and litter: An overview, (2011). https://doi.org/10.1016/j.enconman.2011.08.017.

[34] L.E. Hubbard, C.E. Givens, D.W. Griffin, L.R. Iwanowicz, M.T. Meyer, D.W. Kolpin, Poultry litter as potential source of pathogens and other contaminants in groundwater and surface water proximal to large-scale confined poultry feeding operations, Science of the Total Environment 735 (2020). https://doi.org/10.1016/J.SCITOTENV.2020.139459.

[35] M.K. Mohammadi-Aragh, C.E. Stokes, Assessing Class 1 Integron Presence in Poultry Litter Amended with Wood Biochar and Wood Vinegar, Curr Microbiol 78 (2021) 3733–3740. https://doi.org/10.1007/S00284-021-02640-4/TABLES/1.

[36] K.L. Hwang, S.M. Choi, M.K. Kim, J.B. Heo, K.D. Zoh, Emission of greenhouse gases from waste incineration in Korea, J Environ Manage 196 (2017) 710–718. https://doi.org/10.1016/J.JENVMAN.2017.03.071.

[37] N. Nakatsuka, Y. Kishita, T. Kurafuchi, F. Akamatsu, Integrating wastewater treatment and incineration plants for energy-efficient urban biomass utilization: A life cycle analysis, J Clean Prod 243 (2019). https://doi.org/10.1016/j.jclepro.2019.118448.

[38] Y. Niu, Y. Lv, Y. Lei, S. Liu, Y. Liang, D. Wang, en Hui, Biomass torrefaction: properties, applications, challenges, and economy, Renewable and Sustainable Energy Reviews 115 (2019). https://doi.org/10.1016/j.rser.2019.109395.

[39] F. Safari, I. Dincer, Development and analysis of a novel biomass-based integrated system for multigeneration with hydrogen production, Int J Hydrogen Energy 44 (2019) 3511–3526. https://doi.org/10.1016/J.IJHYDENE.2018.12.101.

[40] M. Prestipino, A. Piccolo, M.F. Polito, A. Galvagno, Combined Bio-Hydrogen, Heat, and Power Production Based on Residual Biomass Gasification: Energy, Exergy, and Renewability Assessment of an Alternative Process Configuration, Energies 2022, Vol. 15, Page 5524 15 (2022) 5524. https://doi.org/10.3390/EN15155524.

[41] Y. Ayub, J. Ren, T. Shi, Exploring gasification process and technology for biomass-waste utilization: A comprehensive review on the path to sustainable energy, Process Safety and Environmental Protection 188 (2024) 1489–1501. https://doi.org/10.1016/J.PSEP.2024.06.056.

[42] Renewable energy statistics - Statistics Explained, (n.d.). https://ec.europa.eu/eurostat/statistics-explained/index.php?title=Renewable_energy_statistics (accessed March 17, 2023).

[43] Share of energy consumption from renewable sources in Europe, (n.d.). https://www.eea.europa.eu/ims/share-of-energy-consumption-from (accessed March 17, 2023).

[44] International Renewable Energy Agency., European Commission., Renewable Energy Prospects for the European Union, International Renewable Energy Agency (IRENA), 2018.

[45] N.S. Bolan, A.A. Szogi, T. Chuasavathi, B. Seshadri, M.J. Rothrock, P. Panneerselvam, Uses and management of poultry litter, Https://Doi.Org/10.1017/S0043933910000656 66 (2019) 673–698. https://doi.org/10.1017/S0043933910000656.

[46] Economic Adviser's Wing_Finance Division Government of Pakistan_Islamabad, (n.d.). www.finance.gov.pk (accessed March 17, 2023).

[47] India - livestock and poultry inventory 2019 | Statista, (n.d.). https://www.statista.com/statistics/622684/livestock-poultry-inventory-india/ (accessed March 17, 2023).

[48] N. Enterprise Agency, Poultry sector study Bangladesh Commissioned by the Netherlands Enterprise Agency, (n.d.).

[49] WBA, GLOBAL BIOENERGY STATISTICS 2021, World Bioenergy Association (2021). https://www.worldbioenergy.org/uploads/211214%20WBA%20GBS%202021.pdf (accessed August 16, 2023).

[50] Y. Ayub, J. Ren, Revealing the synergistic effect of feedstock compositions and process parameters in co-pyrolysis: A review based on bibliometric analysis and experimental studies, J Clean Prod 459 (2024). https://doi.org/10.1016/j.jclepro.2024.142540.

[51] Z.E. Zadeh, A. Abdulkhani, O. Aboelazayem, B. Saha, Recent Insights into Lignocellulosic Biomass Pyrolysis: A Critical Review on Pretreatment, Characterization, and Products Upgrading, Processes 2020, Vol. 8, Page 799 8 (2020) 799. https://doi.org/10.3390/PR8070799.

[52] C. Di Blasi, Modeling chemical and physical processes of wood and biomass pyrolysis, Prog Energy Combust Sci 34 (2008) 47–90. https://doi.org/10.1016/j.pecs.2006.12.001.

[53] O.A. Fakayode, E.A.A. Aboagarib, C. Zhou, H. Ma, Co-pyrolysis of lignocellulosic and macroalgae biomasses for the production of biochar – A review, Bioresour Technol 297 (2020) 122408. https://doi.org/10.1016/J.BIORTECH.2019.122408.

[54] S.A. Dhar, T.U. Sakib, L.N. Hilary, Effects of pyrolysis temperature on production and physicochemical characterization of biochar derived from coconut fiber biomass through slow pyrolysis process, Biomass Convers Biorefin 12 (2022) 2631–2647. https://doi.org/10.1007/S13399-020-01116-Y/FIGURES/2.

[55] Z. Hameed, M. Aslam, Z. Khan, K. Maqsood, A.E. Atabani, M. Ghauri, M.S. Khurram, M. Rehan, A.S. Nizami, Gasification of municipal solid waste blends with biomass for energy production and resources recovery: Current status, hybrid technologies and innovative prospects, Renewable and Sustainable Energy Reviews 136 (2021) 110375. https://doi.org/10.1016/J.RSER.2020.110375.

[56] J.A. Okolie, E.I. Epelle, M.E. Tabat, U. Orivri, A.N. Amenaghawon, P.U. Okoye, B. Gunes, Waste biomass valorization for the production of biofuels and value-added

products: A comprehensive review of thermochemical, biological and integrated processes, (2021). https://doi.org/10.1016/j.psep.2021.12.049.

[57] Y. Ayub, S. Tao, J. Ren, C.K.M. Lee, C. He, A. Manzardo, Poultry litter valorization by application of hydrothermal gasification: Process simulation, Economic, Energic, and Environmental analysis, Int J Energy Res 46 (2022) 23095–23109. https://doi.org/10.1002/ER.8610.

[58] J.A. Okolie, S. Nanda, A.K. Dalai, J.A. Kozinski, A.K. Dalai, Optimization and modeling of process parameters during hydrothermal gasification of biomass model compounds to generate hydrogen-rich gas products, (2019). https://doi.org/10.1016/j.ijhydene.2019.05.132.

[59] K. Babaei, A. Bozorg, A. Tavasoli, Hydrogen-rich gas production through supercritical water gasification of chicken manure over activated carbon/ceria-based nickel catalysts, J Anal Appl Pyrolysis 159 (2021) 105318. https://doi.org/10.1016/j.jaap.2021.105318.

[60] C. Cao, L. Xu, Y. He, L. Guo, H. Jin, Z. Huo, High-Efficiency Gasification of Wheat Straw Black Liquor in Supercritical Water at High Temperatures for Hydrogen Production, Energy and Fuels 31 (2017) 3970–3978. https://doi.org/10.1021/ACS.ENERGYFUELS.6B03002.

[61] M. Salimi, F. Safari, A. Tavasoli, A. Shakeri, Hydrothermal gasification of different agricultural wastes in supercritical water media for hydrogen production: a comparative study, International Journal of Industrial Chemistry 7 (2016) 277–285. https://doi.org/10.1007/S40090-016-0091-Y/FIGURES/7.

[62] C. Yang, S. Wang, J. Yang, D. Xu, Y. Li, J. Li, Y. Zhang, Hydrothermal liquefaction and gasification of biomass and model compounds: a review, Green Chemistry 22 (2020) 8210–8232. https://doi.org/10.1039/D0GC02802A.

[63] Z.R. Xu, W. Zhu, M. Gong, H.W. Zhang, Direct gasification of dewatered sewage sludge in supercritical water. Part 1: Effects of alkali salts, Int J Hydrogen Energy 38 (2013) 3963–3972. https://doi.org/10.1016/J.IJHYDENE.2013.01.164.

[64] Y. Ayub, J. Zhou, J. Ren, Critical reviews of hydrothermal gasification for poultry litter valorization: Process yield, economic viability, environmental sustainability and safety, J Clean Prod 415 (2023). https://doi.org/10.1016/j.jclepro.2023.137876.

[65] D. Hantoko, H. Su, M. Yan, E. Kanchanatip, H. Susanto, G. Wang, S. Zhang, Z. Xu, Thermodynamic study on the integrated supercritical water gasification with reforming process for hydrogen production: Effects of operating parameters, (2018). https://doi.org/10.1016/j.ijhydene.2018.07.198.

[66] W. Cao, W. Wei, H. Jin, L. Yi, L. Wang, Optimize hydrogen production from chicken manure gasification in supercritical water by experimental and kinetics study, J Environ Chem Eng 10 (2022) 2213–3437. https://doi.org/10.1016/j.jece.2022.107591.

[67] D. Castello, L. Fiori, Supercritical water gasification of biomass: Thermodynamic constraints, (2011). https://doi.org/10.1016/j.biortech.2011.05.017.

[68] F.J. Gutiérrez Ortiz, P. Ollero, A. Serrera, S. Galera, Process integration and exergy analysis of the autothermal reforming of glycerol using supercritical water, (2012). https://doi.org/10.1016/j.energy.2012.03.069.

[69] L. Fiori, M. Valbusa, D. Castello, Supercritical water gasification of biomass for H 2 production: Process design, (n.d.). https://doi.org/10.1016/j.biortech.2012.06.116.

[70] M. Puig-Gamero, D.T. Pio, L.A.C. Tarelho, P. Sánchez, L. Sanchez-Silva, Simulation of biomass gasification in bubbling fluidized bed reactor using aspen plus®, Energy Convers Manag 235 (2021) 113981. https://doi.org/10.1016/j.enconman.2021.113981.

[71] M. Niu, J. Xie, S. Liang, L. Liu, L. Wang, Y. Peng, Simulation of a new biomass integrated gasification combined cycle (BIGCC) power generation system using Aspen Plus: Performance analysis and energetic assessment, (2021). https://doi.org/10.1016/j.ijhydene.2021.04.076.

[72] A. Perna, M. Minutillo, A. Lubrano Lavadera, E. Jannelli, Combining plasma gasification and solid oxide cell technologies in advanced power plants for waste to energy and electric energy storage applications, Waste Management 73 (2018) 424–438. https://doi.org/10.1016/j.wasman.2017.09.022.

[73] P. Jiang, A. Mahmud Parvez, Y. Meng, X. Dong, M. Xu, X. Luo, K. Shi, T. Wu, Novel two-stage fluidized bed-plasma gasification integrated with SOFC and chemical looping combustion for the high efficiency power generation from MSW: A thermodynamic investigation, Energy Convers Manag 236 (2021). https://doi.org/10.1016/j.enconman.2021.114066.

[74] M. Materazzi, P. Lettieri, R. Taylor, C. Chapman, Performance analysis of RDF gasification in a two stage fluidized bed-plasma process, Waste Management 47 (2016) 256–266. https://doi.org/10.1016/j.wasman.2015.06.016.

[75] S. Consonni, F. Viganò, Waste gasification vs. conventional Waste-To-Energy: A comparative evaluation of two commercial technologies, Waste Management 32 (2012) 653–666. https://doi.org/10.1016/j.wasman.2011.12.019.

[76] U. Arena, Process and technological aspects of municipal solid waste gasification. A review, Waste Management 32 (2012) 625–639. https://doi.org/10.1016/j.wasman.2011.09.025.

[77] M. Minutillo, A. Perna, D. di Bona, Modelling and performance analysis of an integrated plasma gasification combined cycle (IPGCC) power plant, Energy Convers Manag 50 (2009) 2837–2842. https://doi.org/10.1016/j.enconman.2009.07.002.

[78] K. Chaump, M. Preisser, S.R. Shanmugam, R. Prasad, S. Adhikari, B.T. Higgins, Leaching and anaerobic digestion of poultry litter for biogas production and nutrient transformation, (2018). https://doi.org/10.1016/j.wasman.2018.11.024.

[79] B.P. Kelleher, J.J. Leahy, A.M. Henihan, T.F. O'dwyer, D. Sutton, M.J. Leahy, Advances in poultry litter disposal technology-a review, (n.d.).

[80] C. Mao, Y. Feng, X. Wang, G. Ren, Review on research achievements of biogas from anaerobic digestion, (2015). https://doi.org/10.1016/j.rser.2015.02.032.

[81] N. Zhao, J. Lehmann, F. You, Poultry Waste Valorization via Pyrolysis Technologies: Economic and Environmental Life Cycle Optimization for Sustainable Bioenergy Systems, ACS Sustain Chem Eng 8 (2020) 4633–4646. https://doi.org/10.1021/ACSSUSCHEMENG.0C00704/SUPPL_FILE/SC0C00704_SI_001.PDF.

[82] J. Gelegenis, D. Georgakakis, I. Angelidaki, V. Mavris, Optimization of biogas production by co-digesting whey with diluted poultry manure, Renew Energy 32 (2007) 2147–2160. https://doi.org/10.1016/j.renene.2006.11.015.

[83] E. Agyarko-Mintah, A. Cowie, L. Van Zwieten, B.P. Singh, R. Smillie, S. Harden, F. Fornasier, Biochar lowers ammonia emission and improves nitrogen retention in poultry litter composting, (2016). https://doi.org/10.1016/j.wasman.2016.12.009.

[84] J. Ma, F. You, Superstructure optimization of thermal conversion based poultry litter valorization process, J Clean Prod 228 (2019) 1111–1121. https://doi.org/10.1016/J.JCLEPRO.2019.04.346.

[85] H.I. Abdel-Shafy, M.S.M. Mansour, Solid waste issue: Sources, composition, disposal, recycling, and valorization, (2018). https://doi.org/10.1016/j.ejpe.2018.07.003.

[86] M. Baniasadi, A. Tugnoli, R. Conti, C. Torri, D. Fabbri, V. Cozzani, Waste to energy valorization of poultry litter by slow pyrolysis, (2016). https://doi.org/10.1016/j.renene.2016.01.018.

[87] S. Sarker, J.J. Lamb, D.R. Hjelme, K.M. Lien, A review of the role of critical parameters in the design and operation of biogas production plants, Applied Sciences (Switzerland) 9 (2019). https://doi.org/10.3390/APP9091915.

[88] V. Dhyani, T. Bhaskar, A comprehensive review on the pyrolysis of lignocellulosic biomass, (2017). https://doi.org/10.1016/j.renene.2017.04.035.

[89] V. Dhyani, T. Bhaskar, A comprehensive review on the pyrolysis of lignocellulosic biomass, Renew Energy 129 (2018) 695–716. https://doi.org/10.1016/J.RENENE.2017.04.035.

[90] C. Beausang, K. Mcdonnell, F. Murphy, Anaerobic digestion of poultry litter-A consequential life cycle assessment, (2020). https://doi.org/10.1016/j.scitotenv.2020.139494.

[91] D.S. Pandey, G. Katsaros, C. Lindfors, J.J. Leahy, S.A. Tassou, Fast pyrolysis of poultry litter in a bubbling fluidised bed reactor: Energy and nutrient recovery, Sustainability (Switzerland) 11 (2019). https://doi.org/10.3390/SU11092533.

[92] S. Sezer, F. Kartal, U. Gur¨ozverengur¨ Gur¨ozveren, Artificial Intelligence Approach in Gasification Integrated Solid Oxide Fuel Cell Cycle, Fuel 311 (2022) 122591. https://doi.org/10.1016/j.fuel.2021.122591.

[93] G. Iaquaniello, G. Centi, A. Salladini, E. Palo, S. Perathoner, L. Spadaccini, Waste-to-methanol: Process and economics assessment, Bioresour Technol 243 (2017) 611–619. https://doi.org/10.1016/j.biortech.2017.06.172.

[94] C.A. Salman, M. Naqvi, E. Thorin, J. Yan, Gasification process integration with existing combined heat and power plants for polygeneration of dimethyl ether or methanol: A detailed profitability analysis, Appl Energy 226 (2018) 116–128. https://doi.org/10.1016/j.apenergy.2018.05.069.

[95] Y. Ayub, J. Zhou, T. Shi, S. Toniolo, J. Ren, Sustainability assessment of blue hydrogen production through biomass gasification: A comparative analysis of thermal, solar, and wind energy sources, Bioresour Technol 418 (2025) 131798. https://doi.org/10.1016/J.BIORTECH.2024.131798.

[96] N. Millar, E. McLaughlin, T. Börger, The Circular Economy: Swings and Roundabouts?, Ecological Economics 158 (2019) 11–19. https://doi.org/10.1016/J.ECOLECON.2018.12.012.

[97] Goal 7 | Department of Economic and Social Affairs, (n.d.). https://sdgs.un.org/goals/goal7 (accessed March 18, 2023).

[98] W. Zhang, E. Croiset, P.L. Douglas, M.W. Fowler, E. Entchev, Simulation of a tubular solid oxide fuel cell stack using AspenPlus TM unit operation models, Energy Convers Manag 46 (2005) 181–196. https://doi.org/10.1016/j.enconman.2004.03.002.

[99] T. Detchusananard, S. Sharma, F. Maréchal, A. Arpornwichanop, Multi-objective optimization of sorption enhanced steam biomass gasification with solid oxide fuel cell, (2018). https://doi.org/10.1016/j.enconman.2018.12.047.

[100] C. Li, J. Li, L. Pan, X. Zhu, S. Xie, G. Yu, Y. Wang, X. Pan, G. Zhu, I. Angelidaki, Treatment of digestate residues for energy recovery and biochar production: From lab to pilot-scale verification, (2020). https://doi.org/10.1016/j.jclepro.2020.121852.

[101] S. Zhang, S. Zhu, H. Zhang, X. Liu, Y. Xiong, High quality H 2-rich syngas production from pyrolysis-gasification of biomass and plastic wastes by NieFe@Nanofibers/Porous carbon catalyst, (2019). https://doi.org/10.1016/j.ijhydene.2019.08.105.

[102] M. Cortazar, L. Santamaria, G. Lopez, J. Alvarez, M. Amutio, J. Bilbao, M. Olazar, Fe/olivine as primary catalyst in the biomass steam gasification in a fountain confined spouted bed reactor, Journal of Industrial and Engineering Chemistry 99 (2021) 364–379. https://doi.org/10.1016/j.jiec.2021.04.046.

[103] M. SHK Tushar, A. Dutta, C. Xu, Catalytic supercritical gasification of biocrude from hydrothermal liquefaction of cattle manure, Appl Catal B 189 (2016) 119–132. https://doi.org/10.1016/j.apcatb.2016.02.032.

[104] T. Shi, J. Zhou, Y. Ayub, S. Toniolo, J. Ren, Novel process optimization based on machine learning: A study on biohydrogen production from waste resources, Biomass Bioenergy 185 (2024) 107222. https://doi.org/10.1016/J.BIOMBIOE.2024.107222.

[105] L. Li, J.R. V Flora, J.M. Caicedo, N.D. Berge, Investigating the role of feedstock properties and process conditions on products formed during the hydrothermal carbonization of organics using regression techniques, (2015). https://doi.org/10.1016/j.biortech.2015.03.054.

[106] J. Li, X. Zhu, Y. Li, Y.W. Tong, Y. Sik Ok, X. Wang, Multi-task prediction and optimization of hydrochar properties from high-moisture municipal solid waste: Application of machine learning on waste-to-resource, (2020). https://doi.org/10.1016/j.jclepro.2020.123928.

[107] X. Zhu, Y. Li, X. Wang, Machine learning prediction of biochar yield and carbon contents in biochar based on biomass characteristics and pyrolysis conditions, (2019). https://doi.org/10.1016/j.biortech.2019.121527.

[108] Y. Ayub, J. Ren, Co-Pyrolysis of biomass and plastic waste: Process prediction and optimization based on Artificial Intelligence and response optimizer surrogate model, Process Safety and Environmental Protection 186 (2024) 612–624. https://doi.org/10.1016/J.PSEP.2024.04.049.

[109] A. Yener Mutlu, O. Yucel, An artificial intelligence based approach to predicting syngas composition for downdraft biomass gasification, (2018). https://doi.org/10.1016/j.energy.2018.09.131.

[110] F. Elmaz, O. Yücel, A.Y. Mutlu, Predictive modeling of biomass gasification with machine learning-based regression methods, (2019). https://doi.org/10.1016/j.energy.2019.116541.

[111] J. Zhou, Y. Ayub, T. Shi, J. Ren, C. He, Sustainable co-valorization of medical waste and biomass waste: Innovative process design, optimization and assessment, Energy 288 (2024) 129803. https://doi.org/10.1016/J.ENERGY.2023.129803.

[112] T. Shi, J. Zhou, J. Ren, Y. Ayub, H. Yu, W. Shen, Q. Li, A. Yang, Co-valorisation of sewage sludge and poultry litter waste for hydrogen production: Gasification process design, sustainability-oriented optimization, and systematic assessment, Energy 272 (2023) 127131. https://doi.org/10.1016/J.ENERGY.2023.127131.

[113] P. Baggio, M. Baratieri, L. Fiori, M. Grigiante, D. Avi, P. Tosi, Experimental and modeling analysis of a batch gasification/pyrolysis reactor, Energy Convers Manag 50 (2009) 1426–1435. https://doi.org/10.1016/j.enconman.2009.03.004.

[114] T. Srinivas, A.V.S.S.K.S. Gupta, B. V. Reddy, Thermodynamic equilibrium model and exergy analysis of a Biomass gasifier, Journal of Energy Resources Technology, Transactions of the ASME 131 (2009) 0318011–0318017. https://doi.org/10.1115/1.3185354/465017.

[115] R. Knappstein, G. Kuenne, H. Nicolai, F. Di Mare, A. Sadiki, J. Janicka, Description of the char conversion process in coal combustion based on premixed FGM chemistry, (2018). https://doi.org/10.1016/j.fuel.2018.08.158.

[116] M. Vascellari, R. Arora, C. Hasse, Simulation of entrained flow gasification with advanced coal conversion submodels. Part 2: Char conversion, (n.d.). https://doi.org/10.1016/j.fuel.2013.11.004.

[117] Q. Dang, X. Zhang, Y. Zhou, X. Jia, Prediction and optimization of syngas production from a kinetic-based biomass gasification process model, (2020). https://doi.org/10.1016/j.fuproc.2020.106604.

[118] N. Hashimoto, R. Kurose, S.-M. Hwang, H. Tsuji, H. Shirai, A numerical simulation of pulverized coal combustion employing a tabulated-devolatilization-process model (TDP model), (2011). https://doi.org/10.1016/j.combustflame.2011.05.024.

[119] S. Ascher, W. Sloan, I. Watson, S. You, A comprehensive artificial neural network model for gasification process prediction, (2022). https://doi.org/10.1016/j.apenergy.2022.119289.

[120] D. Shankar Pandey, S. Das, I. Pan, J.J. Leahy, W. Kwapinski, Artificial neural network based modelling approach for municipal solid waste gasification in a fluidized bed reactor, (2016). https://doi.org/10.1016/j.wasman.2016.08.023.

[121] J. Milewski, K.S.´ Wirski, Modelling the SOFC behaviours by artificial neural network, Int J Hydrogen Energy 34 (2009) 5546–5553. https://doi.org/10.1016/j.ijhydene.2009.04.068.

[122] G. Mert Yagli, D. Yang, D. Srinivasan, Automatic hourly solar forecasting using machine learning models, (2019). https://doi.org/10.1016/j.rser.2019.02.006.

[123] M.W. Ahmad, M. Mourshed, Y. Rezgui, Tree-based ensemble methods for predicting PV power generation and their comparison with support vector regression, (2018). https://doi.org/10.1016/j.energy.2018.08.207.

[124] Kamal I.M. Al-Malah, ASPEN PLUS ® Chemical Engineering Applications, New Jersey , 2017.

[125] M. Wetter, J. Wright, COMPARISON OF A GENERALIZED PATTERN SEARCH AND A GENETIC ALGORITHM OPTIMIZATION METHOD, (n.d.).

[126] H. Duan, Z. Zhang, M. Rahman, X. Guo, X. Zhang, J. Cai, Insight into torrefaction of woody biomass: Kinetic modeling using pattern search method, (2020). https://doi.org/10.1016/j.energy.2020.117648.

[127] H. Rabitz, Ö.F. Aliş, General foundations of high-dimensional model representations, J Math Chem 25 (1999) 197–233. https://doi.org/10.1023/A:1019188517934/METRICS.

[128] M. Pan, J. Sikorski, J. Akroyd, S. Mosbach, R. Lau, M. Kraft, Design technologies for eco-industrial parks: From unit operations to processes, plants and industrial networks, (2016). https://doi.org/10.1016/j.apenergy.2016.05.019.

[129] P. Azadi, G. Brownbridge, S. Mosbach, O. Inderwildi, M. Kraft, Simulation and life cycle assessment of algae gasification process in dual fluidized bed gasifiers, Green Chemistry 17 (2015) 1793–1801. https://doi.org/10.1039/C4GC01698J.

[130] W. Han, Z. Sun, A. Scholtissek, C. Hasse, Machine Learning of ignition delay times under dual-fuel engine conditions, Fuel 288 (2021) 119650. https://doi.org/10.1016/j.fuel.2020.119650.

[131] L.T. Biegler, Y.-D. Lang, W. Lin, Multi-scale optimization for process systems engineering, Comput Chem Eng 60 (2014) 17–30. https://doi.org/10.1016/j.compchemeng.2013.07.009.

[132] R. Shahraki Shahdabadi, A. Maleki, S. Haghighat, M. Ghalandari, Using multi-criteria decision-making methods to select the best location for the construction of a biomass power plant in Iran, J Therm Anal Calorim 145 (2021) 2105–2122. https://doi.org/10.1007/s10973-020-10281-1.

[133] G.N. Yücenur, Ş. Çaylak, G. Gönül, M. Postalcıoğlu, An integrated solution with SWARA&COPRAS methods in renewable energy production: City selection for biogas facility, Renew Energy 145 (2020) 2587–2597. https://doi.org/10.1016/J.RENENE.2019.08.011.

[134] D. Curto, M. Martín, Renewable based biogas upgrading, (2019). https://doi.org/10.1016/j.jclepro.2019.03.176.

[135] H.-C. Lee, C.-T. Chang, Comparative analysis of MCDM methods for ranking renewable energy sources in Taiwan, (2018). https://doi.org/10.1016/j.rser.2018.05.007.

[136] G. Sakthivel, R. Sivakumar, N. Saravanan, B.W. Ikua, A decision support system to evaluate the optimum fuel blend in an IC engine to enhance the energy efficiency and energy management, (2017). https://doi.org/10.1016/j.energy.2017.08.051.

[137] S.J.W. Klein, S. Whalley, Comparing the sustainability of U.S. electricity options through multi-criteria decision analysis, (n.d.). https://doi.org/10.1016/j.enpol.2015.01.007.

[138] H.I. Cobuloglu, _ I Esra Büyüktahtakın, A stochastic multi-criteria decision analysis for sustainable biomass crop selection, (2015). https://doi.org/10.1016/j.eswa.2015.04.006.

[139] M. Amer, T.U. Daim, Selection of renewable energy technologies for a developing county: A case of Pakistan, (2011). https://doi.org/10.1016/j.esd.2011.09.001.

[140] S. Rahimi, A. Hafezalkotob, S.M. Monavari, A. Hafezalkotob, R. Rahimi, Sustainable landfill site selection for municipal solid waste based on a hybrid decision-making approach: Fuzzy group BWM-MULTIMOORA-GIS, J Clean Prod 248 (2020) 119186. https://doi.org/10.1016/J.JCLEPRO.2019.119186.

[141] A. Makan, D. Malamis, O. Assobhei, M. Loizidou, M. Mountadar, Multi-criteria decision aid approach for the selection of the best compromise management scheme for the treatment of municipal solid waste in Morocco, Int J Environ Waste Manag 12 (2013) 300–317. https://doi.org/10.1504/IJEWM.2013.056197.

[142] M.L. Tseng, Application of ANP and DEMATEL to evaluate the decision-making of municipal solid waste management in Metro Manila, Environ Monit Assess 156 (2009) 181–197. https://doi.org/10.1007/S10661-008-0477-1.

[143] S. and A.H. CHAUDHARY, A Fuzzy Analytical Hierarchy Process Approach for Landfill Site Selection: A Case Study in Allahabad City, India, International Journal of Earth Sciences and Engineering 10 (2015) 1110–1117.

[144] T.L. Saaty, Decision making with the analytic hierarchy process, Int. J. Services Sciences 1 (2008) 83–98.

[145] N. Munier, E. Hontoria, Management for Professionals Uses and Limitations of the AHP Method A Non-Mathematical and Rational Analysis, Springer, 2021. https://doi.org/https://doi.org/10.1007/978-3-030-60392-2.

[146] T. Senapati, R.R. Yager, Fermatean fuzzy weighted averaging/geometric operators and its application in multi-criteria decision-making methods, Eng Appl Artif Intell 85 (2019) 112–121. https://doi.org/10.1016/J.ENGAPPAI.2019.05.012.

[147] J. Dombi, Towards a general class of operators for fuzzy systems, IEEE Transactions on Fuzzy Systems 16 (2008) 477–484. https://doi.org/10.1109/TFUZZ.2007.905910.

[148] S.B. Aydemir, S. Yilmaz Gunduz, Fermatean fuzzy TOPSIS method with Dombi aggregation operators and its application in multi-criteria decision making, Journal of Intelligent & Fuzzy Systems 39 (2020) 851–869. https://doi.org/10.3233/JIFS-191763.

[149] A. Okati, M.R. Khani, B. Shokri, E. Monteiro, A. Rouboa, Parametric studies over a plasma co-gasification process of biomass and coal through a restricted model in Aspen plus, Fuel 331 (2022). https://doi.org/10.1016/j.fuel.2022.125952.

[150] L. Prasad, R. Pala, Q. Wang, G. Kolb, V. Hessel, Steam gasification of biomass with subsequent syngas adjustment using shift reaction for syngas production: An Aspen Plus model, (2016). https://doi.org/10.1016/j.renene.2016.08.069.

[151] Y. Ayub, J. Ren, Co-Pyrolysis of biomass and plastic waste: Process prediction and optimization based on Artificial Intelligence and response optimizer surrogate model, Process Safety and Environmental Protection 186 (2024) 612–624. https://doi.org/10.1016/J.PSEP.2024.04.049.

[152] X. Zhu, X. Wang, Y.S. Ok, The application of machine learning methods for prediction of metal sorption onto biochars, (2019). https://doi.org/10.1016/j.jhazmat.2019.06.004.

[153] K. Teilo, O.' Shea, K. O'shea, R. Nash, An Introduction to Convolutional Neural Networks Identification and Validation of Low-Cost, High-Throughput Microbial and Metabolite Biomarker Assays for Lung Cancer Status, Stage and Type View project An Introduction to Convolutional Neural Networks, Neural and Evolutionary Computing (2015) 1–11. https://click.endnote.com/viewer?doi=arxiv%3A1511.08458&token=WzM1ODg5OTIsImFyeGl2OjE1MTEuMDg0NTgiXQ.-Objq7Xlm2KXQvMJBuo2ORfZrfw (accessed March 24, 2023).

[154] L. Wang, C. Wu, L. Tang, W. Zhang, S. Lacasse, H. Liu, L. Gao, Efficient reliability analysis of earth dam slope stability using extreme gradient boosting method, Acta Geotech 15 (2020) 3135–3150. https://doi.org/10.1007/S11440-020-00962-4.

[155] Z. Li, F. Liu, W. Yang, S. Peng, J. Zhou, A Survey of Convolutional Neural Networks: Analysis, Applications, and Prospects, IEEE Trans Neural Netw Learn Syst 33 (2022) 6999–7019. https://doi.org/10.1109/TNNLS.2021.3084827.

[156] A. Kathirgamanathan, A. Patel, A.S. Khwaja, B. Venkatesh, A. Anpalagan, Performance comparison of single and ensemble CNN, LSTM and traditional ANN models for short-term electricity load forecasting, The Journal of Engineering 2022 (2022) 550–565. https://doi.org/10.1049/TJE2.12132.

[157] Y. Tian, X. Zhou, S. Lin, X. Ji, J. Bai, M. Xu, Syngas production from air-steam gasification of biomass with natural catalysts, (2018). https://doi.org/10.1016/j.scitotenv.2018.07.071.

[158] Y. Ayub, Y. Hu, J. Ren, W. Shen, C.K.M. Lee, Hydrogen prediction in poultry litter gasification process based on hybrid data-driven deep learning with multilevel factorial design and process simulation: A surrogate model, Eng Appl Artif Intell 126 (2023) 107018. https://doi.org/10.1016/j.engappai.2023.107018.

[159] K.G. Sheela, S.N. Deepa, Review on methods to fix number of hidden neurons in neural networks, Math Probl Eng 2013 (2013). https://doi.org/10.1155/2013/425740.

[160] 5 Convolutional Neural Networks | The Mathematical Engineering of Deep Learning, (n.d.). https://deeplearningmath.org/convolutional-neural-networks.html (accessed March 24, 2023).

[161] J.H. Friedman, Greedy function approximation: A gradient boosting machine, Ann Stat 29 (2001) 1189–1232. https://doi.org/10.1214/AOS/1013203451.

[162] O. González-Recio, J.A. Jiménez-Montero, R. Alenda, The gradient boosting algorithm and random boosting for genome-assisted evaluation in large data sets, J Dairy Sci 96 (2013) 614–624. https://doi.org/10.3168/JDS.2012-5630.

[163] M.W. Ahmad, M. Mourshed, Y. Rezgui, Tree-based ensemble methods for predicting PV power generation and their comparison with support vector regression, (2018). https://doi.org/10.1016/j.energy.2018.08.207.

[164] G. Mert Yagli, D. Yang, D. Srinivasan, Automatic hourly solar forecasting using machine learning models, (2019). https://doi.org/10.1016/j.rser.2019.02.006.

[165] R.P. Sheridan, W.M. Wang, A. Liaw, J. Ma, E.M. Gifford, Extreme Gradient Boosting as a Method for Quantitative Structure-Activity Relationships, J Chem Inf Model 56 (2016) 2353–2360. https://doi.org/10.1021/ACS.JCIM.6B00591.

[166] P. Kumari, D. Toshniwal, Extreme gradient boosting and deep neural network based ensemble learning approach to forecast hourly solar irradiance, J Clean Prod 279 (2021) 123285. https://doi.org/10.1016/J.JCLEPRO.2020.123285.

[167] H.P. Piepho, A coefficient of determination (R2) for generalized linear mixed models, Biometrical Journal 61 (2019) 860–872. https://doi.org/10.1002/BIMJ.201800270.

[168] H. Rabitz, F. Alıs¸b, A. Alıs¸b, General foundations of high-dimensional model representations, J Math Chem 25 (1999) 197–233.

[169] G. Li, H. Rabitz, Ratio control variate method for efficiently determining high-dimensional model representations, J Comput Chem 27 (2006) 1112–1118. https://doi.org/10.1002/JCC.20435.

[170] Y. Ayub, J. Zhou, J. Ren, T. Shi, W. Shen, C. He, High-Dimensional Model Representation-Based Surrogate Model for Optimization and Prediction of Biomass Gasification Process, Int J Energy Res 2023 (2023) 1–14. https://doi.org/10.1155/2023/7787947.

[171] M. Pan, J. Sikorski, J. Akroyd, S. Mosbach, R. Lau, M. Kraft, Design technologies for eco-industrial parks: From unit operations to processes, plants and industrial networks, Appl Energy 175 (2016) 305–323. https://doi.org/10.1016/J.APENERGY.2016.05.019.

[172] W. Wang, Y. Lu, Analysis of the Mean Absolute Error (MAE) and the Root Mean Square Error (RMSE) in Assessing Rounding Model, IOP Conf Ser Mater Sci Eng 324 (2018). https://doi.org/10.1088/1757-899X/324/1/012049.

[173] M. Pan, J. Sikorski, J. Akroyd, S. Mosbach, R. Lau, M. Kraft, Design technologies for eco-industrial parks: From unit operations to processes, plants and industrial networks, Appl Energy 175 (2016) 305–323. https://doi.org/10.1016/J.APENERGY.2016.05.019.

[174] H.J. Yang, K.S. Hwang, C.J. Lee, Stochastic Optimization of a Natural Gas Liquefaction Process Considering Seawater Temperature Variation Based on Particle Swarm Optimization, Ind Eng Chem Res 57 (2018) 2200–2207. https://doi.org/10.1021/ACS.IECR.7B04546.

[175] X. Wang, J. Li, Y. Zheng, J. Li, Smart systems engineering contributing to an intelligent carbon-neutral future: opportunities, challenges, and prospects, Front Chem Sci Eng 16 (2022) 1023–1029. https://doi.org/10.1007/s11705-022-2142-6.

[176] M. Clerc, Standard Particle Swarm Optimisation, HAL Open Science 1 (2012). https://hal.archives-ouvertes.fr/hal-00764996 (accessed December 3, 2022).

[177] N. Striugas, K. Zakarauskas, A. Džiugys, R. Navakas, R. Paulauskas, An evaluation of performance of automatically operated multi-fuel downdraft gasifier for energy production, Appl Therm Eng 73 (2014) 1151–1159. https://doi.org/10.1016/j.applthermaleng.2014.09.007.

[178] Tiejun Wang, Jie Chang, Yan Fu, Qi Zhang, Yuping Li, An integrated biomass-derived syngas/dimethyl ether process, Korean Journal of Chemical Engineering 24 (2007) 181–185. https://doi.org/https://doi.org/10.1007/s11814-007-5029-9.

[179] G. Baglietto, S. Maccarini, A. Traverso, P. Bruttini, Techno-Economic Comparison of Supercritical CO2, Steam, and ORC Cycles for WHR Applications, J Eng Gas Turbine Power (2022). https://doi.org/10.1115/1.4055727.

[180] J. Lampe, S. Menz, K. Akinci, K. Böhm, T. Seeger, T. Fend, Optimizing the operational strategy of a solar-driven reactor for thermochemical hydrogen production, Int J Hydrogen Energy 47 (2022) 14453–14468. https://doi.org/10.1016/j.ijhydene.2022.02.193.

[181] H.-M. Gutmann, A Radial Basis Function Method for Global Optimization, 2001.

[182] Inc. The MathWorks, Surrogate optimization for global minimization of time-consuming objective functions, (n.d.). https://ww2.mathworks.cn/help/gads/surrogateopt.html (accessed January 4, 2023).

[183] R. Hooke, T.A. Jeeves, "Direct Search" Solution of Numerical and Statistical Problems*, Association for Computing Machinery 8 (1960). https://doi.org/https://doi.org/10.1145/321062.321069.

[184] J. Na, Y. Lim, C. Han, A modified DIRECT algorithm for hidden constraints in an LNG process optimization, Energy 126 (2017) 488–500. https://doi.org/10.1016/j.energy.2017.03.047.

[185] J.S. Al-Sumait, A.K. AL-Othman, J.K. Sykulski, Application of pattern search method to power system valve-point economic load dispatch, International Journal of Electrical Power and Energy Systems 29 (2007) 720–730. https://doi.org/10.1016/j.ijepes.2007.06.016.

[186] C. Audet, V. Béchard, J. Chaouki, Spent potliner treatment process optimization using a MADS algorithm, Optimization and Engineering 9 (2008) 143–160. https://doi.org/10.1007/s11081-007-9030-2.

[187] How Pattern Search Polling Works - MATLAB & Simulink, (n.d.). https://www.mathworks.com/help/gads/how-pattern-search-polling-works.html (accessed March 24, 2023).

[188] A.T. Abbas, A.A. Al-Abduljabbar, M.M. el Rayes, F. Benyahia, I.H. Abdelgaliel, A. Elkaseer, Multi-Objective Optimization of Performance Indicators in Turning of AISI 1045 under Dry Cutting Conditions, Metals (Basel) 13 (2023). https://doi.org/10.3390/met13010096.

[189] T. Chai, R.R. Draxler, Root mean square error (RMSE) or mean absolute error (MAE)? -Arguments against avoiding RMSE in the literature, Geosci Model Dev 7 (2014) 1247–1250. https://doi.org/10.5194/gmd-7-1247-2014.

[190] R.A. Herendeen, Energy analysis and EMERGY analysis - A comparison, Ecol Modell 178 (2004) 227–237. https://doi.org/10.1016/j.ecolmodel.2003.12.017.

[191] D. Buentello-Montoya, X. Zhang, An Energy and Exergy Analysis of Biomass Gasification Integrated with a Char-Catalytic Tar Reforming System, Energy and Fuels 33 (2019) 8746–8757. https://doi.org/10.1021/acs.energyfuels.9b01808.

[192] L.F. Pellegrini, S. de Oliveira, Exergy analysis of sugarcane bagasse gasification, Energy 32 (2007) 314–327. https://doi.org/10.1016/j.energy.2006.07.028.

[193] Y. Ayub, J. Zhou, J. Ren, C. He, An innovative integration of torrefaction, gasification, and solid oxide fuel cell for carbon–neutral utilization of biomass waste: Process development, economic, exergy, advanced exergy, and exergoeconomics analysis, Energy Convers Manag 292 (2023). https://doi.org/10.1016/j.enconman.2023.117426.

[194] E. Açıkkalp, H. Caliskan, O. Altuntas, A. Hepbasli, Novel combined extended-advanced exergy analysis methodology as a new tool to assess thermodynamic systems, (2021). https://doi.org/10.1016/j.enconman.2021.114019.

[195] H. Caliskan, Energy, exergy, environmental, enviroeconomic, exergoenvironmental (EXEN) and exergoenviroeconomic (EXENEC) analyses of solar collectors, Renewable and Sustainable Energy Reviews 69 (2017) 488–492. https://doi.org/10.1016/J.RSER.2016.11.203.

[196] H. Caglayan, H. Caliskan, Advanced exergy analyses and optimization of a cogeneration system for ceramic industry by considering endogenous, exogenous, avoidable and unavoidable exergies under different environmental conditions, Renewable and Sustainable Energy Reviews 140 (2021) 110730. https://doi.org/10.1016/j.rser.2021.110730.

[197] G.O. Erol, E. Açıkkalp, A. Hepbasli, Performance assessment of an ice rink refrigeration system through advanced exergoeconomic analysis method, Energy Build 138 (2017) 118–126. https://doi.org/10.1016/J.ENBUILD.2016.12.025.

[198] E. Açikkalp, C.T. Yucer, A. Hepbasli, T.H. Karakoc, Advanced low exergy (ADLOWEX) modeling and analysis of a building from the primary energy transformation to the environment, Energy Build 81 (2014) 281–286. https://doi.org/10.1016/J.ENBUILD.2014.06.024.

[199] E. Açikkalp, H. Aras, A. Hepbasli, Advanced exergoeconomic analysis of a trigeneration system using a diesel-gas engine, Appl Therm Eng 67 (2014) 388–395. https://doi.org/10.1016/J.APPLTHERMALENG.2014.03.005.

[200] T. Morosuk, G. Tsatsaronis, Advanced exergetic evaluation of refrigeration machines using different working fluids, Energy 34 (2009) 2248–2258. https://doi.org/10.1016/J.ENERGY.2009.01.006.

[201] Steam Calculators: Steam Turbine Calculator, (n.d.). https://www4.eere.energy.gov/manufacturing/tech_deployment/amo_steam_tool/equip Turbine (accessed March 26, 2023).

[202] U.S. Department of Energy, Steam System Modeler Tool (SSMT), (2015). https://www4.eere.energy.gov/manufacturing/tech_deployment/amo_steam_tool/equip Turbine (accessed January 2, 2023).

[203] Luoyang Zhongtai Industries Co. Ltd, Suction Type 24t/H Steam Turbine Electric Generator 3000kw, (2022). https://citiczt.en.made-in-china.com/product/pFOtGEgdHnry/China-Suction-Type-24t-H-Steam-Turbine-Electric-Generator-3000kw.html (accessed December 28, 2022).

[204] NCON Turbo Tech Pvt. Ltd., Power Generation Calculator, (2020). http://www.nconturbines.com/calculate-power-from-steam.html (accessed January 2, 2023).

[205] C.A. Magni, The Internal Rate of Return Approach and the AIRR Paradigm: A Refutation and a Corroboration, Eng Econ 58 (2013) 73–111. https://doi.org/10.1080/0013791X.2012.745916.

[206] F. Lefley, The payback method of investment appraisal: A review and synthesis, Int J Prod Econ 44 (1996) 207–224. https://doi.org/10.1016/0925-5273(96)00022-9.

[207] J.C. Hartman, I.C. Schafrick, The relevant internal rate of return, Engineering Economist 49 (2004) 139–158. https://doi.org/10.1080/00137910490453419.

[208] The World Bank Group, Trends in Solid Waste Management, (2016). https://datatopics.worldbank.org/what-a-waste/trends_in_solid_waste_management.html (accessed February 1, 2023).

[209] ISO - ISO 14040:2006 - Environmental management — Life cycle assessment — Principles and framework, (n.d.). https://www.iso.org/standard/37456.html (accessed March 24, 2023).

[210] R.R. Bora, M. Lei, J.W. Tester, J. Lehmann, F. You, Life Cycle Assessment and Technoeconomic Analysis of Thermochemical Conversion Technologies Applied to Poultry Litter with Energy and Nutrient Recovery, ACS Sustain Chem Eng 8 (2020) 8436–8447. https://doi.org/10.1021/acssuschemeng.0c02860.

[211] G. Wernet, C. Bauer, B. Steubing, J. Reinhard, E. Moreno-Ruiz, B. Weidema, The ecoinvent database version 3 (part I): overview and methodology, International Journal of Life Cycle Assessment 21 (2016) 1218–1230. https://doi.org/10.1007/S11367-016-1087-8.

[212] S. Humbert, A. De Schryver, X. Bengoa, M. Margni, O. Jolliet, IMPACT 2002+: User Guide, (2014). https://doi.org/10.1007/BF02978505.

[213] A. Lautier, R.K. Rosenbaum, M. Margni, J. Bare, P.-O. Roy, L. Deschênes, Development of normalization factors for Canada and the United States and comparison with European factors, (2010). https://doi.org/10.1016/j.scitotenv.2010.09.016.

[214] S.I. Ahmad, H. Hashim, M.H. Hassim, Numerical Descriptive Inherent Safety Technique (NuDIST) for inherent safety assessment in petrochemical industry, Process Safety and Environmental Protection 92 (2014) 379–389. https://doi.org/10.1016/j.psep.2014.03.009.

[215] A.-M. Heikkilä, Inherent safety in process plant design An index-based approach 3 8 4, (1999). http://www.inf.vtt.fi/pdf/ (accessed March 25, 2023).

[216] D. Lawrence, Quantifying inherent safety of chemical process routes Quantifying inherent safety of chemical process routes PLEASE CITE THE PUBLISHED VERSION PUBLISHER © Duncan Lawrence LICENCE CC BY-NC-ND 4.0 REPOSITORY RECORD, 1996. https://hdl.handle.net/2134/7427.

[217] T. Senapati, R.R. Yager, Fermatean fuzzy sets, J Ambient Intell Humaniz Comput 11 (2020) 663–674. https://doi.org/10.1007/s12652-019-01377-0.

[218] T. Senapati, R.R. Yager, Fermatean fuzzy weighted averaging/geometric operators and its application in multi-criteria decision-making methods ☆, Eng Appl Artif Intell 85 (2019) 112–121. https://doi.org/10.1016/j.engappai.2019.05.012.

[219] J. S, Ordering of interval-valued Fermatean fuzzy sets and its applications, Expert Syst Appl 185 (2021) 115613. https://doi.org/10.1016/J.ESWA.2021.115613.

[220] M.A. Moktadir, J. Ren, Modeling challenges for Industry 4.0 implementation in new energy systems towards carbon neutrality: Implications for impact assessment policy and practice in emerging economies, Resour Conserv Recycl 199 (2023) 107246. https://doi.org/10.1016/J.RESCONREC.2023.107246.

[221] J. Dombi, A general class of fuzzy operators, the demorgan class of fuzzy operators and fuzziness measures induced by fuzzy operators, Fuzzy Sets Syst 8 (1982) 149–163. https://doi.org/10.1016/0165-0114(82)90005-7.

[222] P. Rani, A.R. Mishra, M. Deveci, J. Antucheviciene, New complex proportional assessment approach using Einstein aggregation operators and improved score function

for interval-valued Fermatean fuzzy sets, Comput Ind Eng 169 (2022) 108165. https://doi.org/10.1016/J.CIE.2022.108165.

[223] M.R. Seikh, U. Mandal, Interval-valued Fermatean fuzzy Dombi aggregation operators and SWARA based PROMETHEE II method to bio-medical waste management, Expert Syst Appl 226 (2023) 120082. https://doi.org/10.1016/J.ESWA.2023.120082.

[224] S. Lee, Determination of Priority Weights under Multiattribute Decision-Making Situations: AHP versus Fuzzy AHP, J Constr Eng Manag 141 (2014) 05014015. https://doi.org/10.1061/(ASCE)CO.1943-7862.0000897.

[225] F. Torfi, R.Z. Farahani, S. Rezapour, Fuzzy AHP to determine the relative weights of evaluation criteria and Fuzzy TOPSIS to rank the alternatives, Appl Soft Comput 10 (2010) 520–528. https://doi.org/10.1016/J.ASOC.2009.08.021.

[226] G. Işıklar, G. Büyüközkan, Using a multi-criteria decision making approach to evaluate mobile phone alternatives, (2006). https://doi.org/10.1016/j.csi.2006.05.002.

[227] M. Song, Q. Zhu, J. Peng, E.D.R. Santibanez Gonzalez, Improving the evaluation of cross efficiencies: A method based on Shannon entropy weight, Comput Ind Eng 112 (2017) 99–106. https://doi.org/10.1016/J.CIE.2017.07.023.

[228] C.E. Shannon, A Mathematical Theory of Communication, Bell System Technical Journal 27 (1948) 379–423. https://doi.org/10.1002/J.1538-7305.1948.TB01338.X.

[229] A. De Luca, S. Termini, A definition of a nonprobabilistic entropy in the setting of fuzzy sets theory, Information and Control 20 (1972) 301–312. https://doi.org/10.1016/S0019-9958(72)90199-4.

[230] S. Seker, IoT based sustainable smart waste management system evaluation using MCDM model under interval-valued q-rung orthopair fuzzy environment, Technol Soc 71 (2022) 102100. https://doi.org/10.1016/J.TECHSOC.2022.102100.

[231] J. Rezaei, Best-worst multi-criteria decision-making method, Omega (United Kingdom) 53 (2015) 49–57. https://doi.org/10.1016/j.omega.2014.11.009.

[232] W. Cao, W. Wei, H. Jin, L. Yi, L. Wang, Optimize hydrogen production from chicken manure gasification in supercritical water by experimental and kinetics study, J Environ Chem Eng 10 (2022) 107591. https://doi.org/10.1016/J.JECE.2022.107591.

[233] D. Hantoko, H. Su, M. Yan, E. Kanchanatip, H. Susanto, G. Wang, S. Zhang, Z. Xu, Thermodynamic study on the integrated supercritical water gasification with reforming process for hydrogen production: Effects of operating parameters, Int J Hydrogen Energy 43 (2018) 17620–17632. https://doi.org/10.1016/J.IJHYDENE.2018.07.198.

[234] M. Puig-Gamero, D.T. Pio, L.A.C. Tarelho, P. Sánchez, L. Sanchez-Silva, Simulation of biomass gasification in bubbling fluidized bed reactor using aspen plus®, Energy Convers Manag 235 (2021) 113981. https://doi.org/10.1016/J.ENCONMAN.2021.113981.

[235] F. Kartal, U. Gur, € Ozveren, A deep learning approach for prediction of syngas lower heating value from CFB gasifier in Aspen plus®, (2020). https://doi.org/10.1016/j.energy.2020.118457.

[236] J.E. Favas, E. Monteiro, A. Rouboa, Hydrogen production using plasma gasification with steam injection, (2017). https://doi.org/10.1016/j.ijhydene.2017.03.109.

[237] R.A. Waltz, J.L. Morales, J. Nocedal, D. Orban, An interior algorithm for nonlinear optimization that combines line search and trust region steps, Math Program 107 (2006) 391–408. https://doi.org/10.1007/S10107-004-0560-5.

[238] L.T. Biegler, A.M. Cervantes, A. Ww, Advances in simultaneous strategies for dynamic process optimization, Chem Eng Sci 57 (2002) 575–593. www.elsevier.com/locate/ces (accessed March 25, 2023).

[239] J. Dong, Y. Chen, B. Yao, X. Zhang, N. Zeng, A neural network boosting regression model based on XGBoost, Appl Soft Comput 125 (2022) 109067. https://doi.org/10.24433/CO.9795.

[240] A. Yener Mutlu, O. Yucel, An artificial intelligence based approach to predicting syngas composition for downdraft biomass gasification, (2018). https://doi.org/10.1016/j.energy.2018.09.131.

[241] F. Elmaz, O. Yücel, A.Y. Mutlu, Predictive modeling of biomass gasification with machine learning-based regression methods, (2019). https://doi.org/10.1016/j.energy.2019.116541.

[242] E. Elmaslar Ozbas, D. Aksu, A. Ongen, M. Ali Aydin, H. Kurtulus Ozcan, Hydrogen production via biomass gasification, and modeling by supervised machine learning algorithms, (2019). https://doi.org/10.1016/j.ijhydene.2019.02.108.

[243] Advanced Manufacturing Office, Benchmark the Fuel Cost of Steam Generation, U.S. Department of Energy (2012).

[244] Natural gas - Price - Chart - Historical Data - News, (n.d.). https://tradingeconomics.com/commodity/natural-gas (accessed September 9, 2024).

[245] M.A.J. Huijbregts, Z.J.N. Steinmann, P.M.F. Elshout, G. Stam, F. Verones, M. Vieira, M. Zijp, A. Hollander, R. van Zelm, ReCiPe2016: a harmonised life cycle impact assessment method at midpoint and endpoint level, Int J Life Cycle Assess 22 (2016) 138–147. https://doi.org/10.1007/s11367-016-1246-y.

[246] Y. Ayub, Y. Hu, J. Ren, Estimation of syngas yield in hydrothermal gasification process by application of artificial intelligence models, Renew Energy 215 (2023) 118953. https://doi.org/10.1016/j.renene.2023.118953.

[247] N. Striugas, K. Zakarauskas, A. Džiugys, R. Navakas, R. Paulauskas, An evaluation of performance of automatically operated multi-fuel downdraft gasifier for energy production, Appl Therm Eng 73 (2014) 1151–1159. https://doi.org/10.1016/j.applthermaleng.2014.09.007.

[248] P. Mojaver, S. Jafarmadar, S. Khalilarya, A. Chitsaz, Investigation and optimization of a Co-Generation plant integrated of gasifier, gas turbine and heat pipes using minimization of Gibbs free energy, Lagrange method and response surface methodology, Int J Hydrogen Energy 45 (2020) 19027–19044. https://doi.org/10.1016/J.IJHYDENE.2020.04.278.

[249] S. Jarungthammachote, A. Dutta, Equilibrium modeling of gasification: Gibbs free energy minimization approach and its application to spouted bed and spout-fluid bed gasifiers, (2008). https://doi.org/10.1016/j.enconman.2008.01.006.

[250] D.K. Singh, J. V Tirkey, Process modelling and thermodynamic performance optimization of biomass air gasification fuelled with waste poultry litter pellet by integrating Aspen plus with RSM, Biomass Bioenergy 158 (2022) 106370. https://doi.org/10.1016/j.biombioe.2022.106370.

[251] M. Hauck, S. Herrmann, H. Spliethoff, Simulation of a reversible SOFC with Aspen Plus, (2017). https://doi.org/10.1016/j.ijhydene.2017.01.189.

[252] T. Anderson, P. Vijay, M.O. Tade, An adaptable steady state Aspen Hysys model for the methane fuelled solid oxide fuel cell, Chemical Engineering Research and Design 92 (2014) 295–307. https://doi.org/10.1016/j.cherd.2013.07.025.

[253] E. Achenbach, Three-dimensional and time-dependent simulation of a planar solid oxide fuel cell stack, J Power Sources 49 (1994) 333–348.

[254] F.B. O'Hayre, R. Cha, S. W. Colella, W. G. Prinz, Fuel cell fundamentals.pdf, (2005). https://www.wiley.com/en-hk/Fuel+Cell+Fundamentals%2C+3rd+Edition-p-9781119114154 (accessed March 25, 2023).

[255] W. Doherty, Modelling of Biomass Gasification Integrated with a Solid Oxide Fuel Cell System, (2014). https://doi.org/10.21427/D76P5V.

[256] N. Ramzan, A. Ashraf, S. Naveed, A. Malik, Simulation of hybrid biomass gasification using Aspen plus: A comparative performance analysis for food, municipal solid and poultry waste, Biomass Bioenergy 35 (2011) 3962–3969. https://doi.org/10.1016/j.biombioe.2011.06.005.

[257] J.F. Pérez, A. Melgar, P.N. Benjumea, Effect of operating and design parameters on the gasification/combustion process of waste biomass in fixed bed downdraft reactors: An experimental study, Fuel 96 (2012) 487–496. https://doi.org/10.1016/j.fuel.2012.01.064.

[258] F. Emun, M. Gadalla, T. Majozi, D. Boer, Integrated gasification combined cycle (IGCC) process simulation and optimization, Comput Chem Eng 34 (2010) 331–338. https://doi.org/10.1016/j.compchemeng.2009.04.007.

[259] A.M. Parvez, I.M. Mujtaba, P. Hall, E.H. Lester, T. Wu, Synthesis of Bio-Dimethyl Ether Based on Carbon Dioxide-Enhanced Gasification of Biomass: Process Simulation Using Aspen Plus, Energy Technology 4 (2016) 526–535. https://doi.org/10.1002/ente.201500349.

[260] K. Krim, A. Sachse, A. Le Valant, Y. Pouilloux, S. Hocine, One Step Dimethyl Ether (DME) Synthesis from CO2 Hydrogenation over Hybrid Catalysts Containing Cu/ZnO/Al2O3 and Nano-Sized Hollow ZSM-5 Zeolites, Catal Letters (2022). https://doi.org/10.1007/s10562-022-03949-w.

[261] T. Wang, Y. Li, L. Ma, C. Wu, Biomass to dimethyl ether by gasification/synthesis technology-an alternative biofuel production route, Frontiers of Energy and Power Engineering in China 5 (2011) 330–339. https://doi.org/10.1007/s11708-010-0121-y.

[262] J. Chang, Y. Fu, Z. Luo, Experimental study for dimethyl ether production from biomass gasification and simulation on dimethyl ether production, Biomass Bioenergy 39 (2012) 67–72. https://doi.org/10.1016/j.biombioe.2011.01.044.

[263] Y. Xiang, L. Cai, Y. Guan, W. Liu, Z. Cheng, Z. Liu, Study on the effect of gasification agents on the integrated system of biomass gasification combined cycle and oxy-fuel combustion, Energy (2020) 118–131. https://doi.org/10.1016/j.energy.2020.118131.

[264] K. Wang, Q. Yu, Q. Qin, L. Hou, W. Duan, Thermodynamic analysis of syngas generation from biomass using chemical looping gasification method, Int J Hydrogen Energy 41 (2015) 10346–10353. https://doi.org/10.1016/j.ijhydene.2015.09.155.

[265] M. Materazzi, P. Lettieri, L. Mazzei, R. Taylor, C. Chapman, Tar evolution in a two stage fluid bed-plasma gasification process for waste valorization, Fuel Processing Technology 128 (2014) 146–157. https://doi.org/10.1016/j.fuproc.2014.06.028.

[266] Y. Zhao, J. Yao, G. Chen, J. Liu, Z. Cheng, L. Wang, W. Yi, S. Xu, Energy, efficiency, and environmental analysis of hydrogen generation via plasma co-gasification of biomass and plastics based on parameter simulation using Aspen plus, Energy Convers Manag 295 (2023) 117623. https://doi.org/10.1016/J.ENCONMAN.2023.117623.

[267] T.H. Jayah, L. Aye, R.J. Fuller, D.F. Stewart, Computer simulation of a downdraft wood gasiÿer for tea drying, Biomass Bioenergy 25 (2003) 459–469. https://doi.org/10.1016/S0961-9534(03)00037-0.

[268] G. Lopez, A. Erkiaga, M. Amutio, J. Bilbao, M. Olazar, Effect of polyethylene co-feeding in the steam gasification of biomass in a conical spouted bed reactor, Fuel 153 (2015) 393–401. https://doi.org/10.1016/J.FUEL.2015.03.006.

[269] L.A. Jolaoso, J. Asadi, C. Duan, P. Kazempoor, A novel green hydrogen production using water-energy nexus framework, Energy Convers Manag 276 (2023) 116344. https://doi.org/10.1016/J.ENCONMAN.2022.116344.

[270] S. Sezer, F. Kartal, U. Özveren, Artificial Intelligence Approach in Gasification Integrated Solid Oxide Fuel Cell Cycle, Fuel 311 (2022) 122591. https://doi.org/10.1016/J.FUEL.2021.122591.

[271] I. Ulleberg, Modeling of advanced alkaline electrolyzers: a system simulation approach, 2003. www.elsevier.com/locate/ijhydene.

[272] M. Sánchez, E. Amores, D. Abad, L. Rodríguez, C. Clemente-Jul, Aspen Plus model of an alkaline electrolysis system for hydrogen production, Int J Hydrogen Energy 45 (2020) 3916–3929. https://doi.org/10.1016/j.ijhydene.2019.12.027.

[273] A. Rashad, · Ali Elmaihy, A. Elmaihy, Theoretical and Experimental Performance of Oxy-hydrogen Generators, Arab J Sci Eng 43 (2018) 1279–1289. https://doi.org/10.1007/s13369-017-2821-7.

[274] T. Chai, R.R. Draxler, Root mean square error (RMSE) or mean absolute error (MAE)? -Arguments against avoiding RMSE in the literature, Geosci Model Dev 7 (2014) 1247–1250. https://doi.org/10.5194/GMD-7-1247-2014.

[275] Inc. Aspen Technology, Aspen Plus ® Aspen Plus User Guide, 10.2, Cambridge, 2000. http://www.aspentech.com.

[276] U. Environmental Protection Agency, C. Heat, P. Partnership, Catalog of CHP Technologies, Section 4. Technology Characterization – Steam Turbines, 2015.

[277] A. Habibollahzade, E. Gholamian, A. Behzadi, Multi-objective optimization and comparative performance analysis of hybrid biomass-based solid oxide fuel cell/solid oxide electrolyzer cell/gas turbine using different gasification agents, (2018). https://doi.org/10.1016/j.apenergy.2018.10.075.

[278] U. Environmental Protection Agency, C. Heat, P. Partnership, Catalog of CHP Technologies, Section 4. Technology Characterization – Steam Turbines, (2015).

[279] Y. Ayub, J. Zhou, J. Ren, W. Shen, C. He, S. Toniolo, Tri-generation for sustainable poultry litter valorization: Process design, simulation, optimization, and sustainability assessment for waste-to-wealth, J Clean Prod 418 (2023). https://doi.org/10.1016/j.jclepro.2023.138139.

[280] baoyuan machine, Low Cost Wood Chips Drying Machine Biomass Waste Straw Drier for Fuels Processing - China Biomass Dryer and Biomass Rotary Dryer, (2023). https://baoyuanmachine.en.made-in-china.com/product/gdXGIHfublRj/China-Low-

Cost-Wood-Chips-Drying-Machine-Biomass-Waste-Straw-Drier-for-Fuels-Processing.html (accessed April 10, 2023).

[281] High Performance Biomass Gasifier/Gasification with Biomass Generator - China Biomass Gasification Reactions and Biomass Gasification Review, (2023). https://zcxnypower.en.made-in-china.com/product/FdHxmzouCIhk/China-High-Performance-Biomass-Gasifier-Gasification-with-Biomass-Generator.html (accessed October 5, 2023).

[282] China High Pressure Steam Boiler Feedwater Pump - China High Pressure Pump and High-Pressure Pump, (2023). https://bruce7723.en.made-in-china.com/product/WBiJDKNHLyrb/China-China-High-Pressure-Steam-Boiler-Feedwater-Pump.html (accessed October 5, 2023).

[283] Large 1600 Type Pet Plastic Bottles Plastic Pallet Crushing Machine - China Crusher and Plastic Crusher, (2023). https://plastic-crusher.en.made-in-china.com/product/nxZRkiaoYDVq/China-Large-1600-Type-Pet-Plastic-Bottles-Plastic-Pallet-Crushing-Machine.html (accessed October 5, 2023).

[284] Shell and Plate Welded Heat Exchanger for High Temperature and High Pressure - China Condenser and Cooler, (2023). https://sdwintech.en.made-in-china.com/product/SjyENbfxrMhW/China-Shell-and-Plate-Welded-Heat-Exchanger-for-High-Temperature-and-High-Pressure.html (accessed October 5, 2023).

[285] Dust Trapping Cyclone Separator for Grain Steel Silo - China Cyclone and Cyclone Separator for Grain Steel Silo, (2023). https://tsesilo.en.made-in-china.com/product/yOEfFqJPXbrz/China-Dust-Trapping-Cyclone-Separator-for-Grain-Steel-Silo.html (accessed October 5, 2023).

[286] Azbel 100nm3/H 300nm3/H 500nm3/H 1000nm3/H Nitrogen Air Separator Plant Liquid Nitrogen Equipment Cost - China Liquid Nitrogen Plant and Liquid Nitrogen Air Separation Plant, (2023). https://hzazbel.en.made-in-china.com/product/rnNpkTRGaeVF/China-Azbel-100nm3-H-300nm3-H-500nm3-H-1000nm3-H-Nitrogen-Air-Separator-Plant-Liquid-Nitrogen-Equipment-Cost.html (accessed October 5, 2023).

[287] Ductile Iron Automatic Single Ball Air Valve - China Air Release Valve and Ball Valve, (2023). https://cnsitg.en.made-in-china.com/product/OMnQFohzrwAq/China-Ductile-Iron-Automatic-Single-Ball-Air-Valve.html (accessed October 5, 2023).

[288] Factory Direct Supply D-Type 250 Bar High Pressure H2 Hydrogen CO2 Natural Gas Piston Reciprocating Air Booster Compressor - China Reciprocating Piston Compressor and Hydrogen Compressor, (2023). https://xzhuayan.en.made-in-china.com/product/sFrAKkOHQSWV/China-Factory-Direct-Supply-D-Type-250-Bar-High-Pressure-H2-Hydrogen-CO2-Natural-Gas-Piston-Reciprocating-Air-Booster-Compressor.html (accessed October 5, 2023).

[289] SMA Series Industrial Horizontal End Suction Bare Shaft Industry Centrifugal Water Motor Pump for Water Supply System - China End Suction Centrifugal Pump and End Suction Pump, (2023). https://aikonchina.en.made-in-china.com/product/mFbAMrzKZkpN/China-SMA-Series-Industrial-Horizontal-End-Suction-Bare-Shaft-Industry-Centrifugal-Water-Motor-Pump-for-Water-Supply-System.html (accessed October 5, 2023).

[290] Jtl Low Temperature Rise Steam Compressor for Sugar Plant - China Centrifugal Compressor and Turbo Compressor, (2023). https://jintonglingtech.en.made-in-

china.com/product/InFRZlUVXAkq/China-Jtl-Low-Temperature-Rise-Steam-Compressor-for-Sugar-Plant.html (accessed October 5, 2023).

[291] Suction Type 24t/H Steam Turbine Electric Generator 3000kw - China Generator and Small Steam Turbine, (2023). https://citiczt.en.made-in-china.com/product/pFOtGEgdHnry/China-Suction-Type-24t-H-Steam-Turbine-Electric-Generator-3000kw.html (accessed October 5, 2023).

[292] 100kw Hydraulic Electric Generator 1 MW Generator Free Energy - China 1 Kw Pelton Turbine and 1 Kw River Generator, (2023). https://cdforster.en.made-in-china.com/product/JFaEWrOxVzcG/China-100kw-Hydraulic-Electric-Generator-1-MW-Generator-Free-Energy.html (accessed October 5, 2023).

[293] 10m3 Horizontal Cryogenic Liquid Oxygen CO2 LNG Tank - China Oxygen Storage Tank and Liquid Nitrogen Storage Tank, (2023). https://ckgasequipment.en.made-in-china.com/product/YXHJFOtDndkn/China-10m3-Horizontal-Cryogenic-Liquid-Oxygen-CO2-LNG-Tank.html (accessed October 5, 2023).

[294] J. Steinar Garðarsson, P. Vang, S. Højgaard, R. Nielsen, General rights Predicting the price of solid oxide electrolysers (SOECs), Downloaded from Orbit.Dtu.Dk On (2023).

[295] Fast Install Practical Designed Prefab Light Steel Structure Industrial Workshop Plant Shed - China Prefab Workshop Plant Shed and Steel Structure Workshop, (2023). https://steelstructuredfx.en.made-in-china.com/product/yXBneIAJYHYP/China-Fast-Install-Practical-Designed-Prefab-Light-Steel-Structure-Industrial-Workshop-Plant-Shed.html (accessed October 5, 2023).

[296] Bag Organic Poultry Manure, solid, Packaging Type: Plastic Bags at Rs 3/kilogram in Kasaragod, (2023). https://www.indiamart.com/proddetail/organic-poultry-manure-22262829055.html?pos=8&pla=n (accessed October 5, 2023).

[297] MLP Plastic at Rs 10/kg | Plastic kabadi in Indore | ID: 24980149533, (2023). https://www.indiamart.com/proddetail/mlp-plastic-24980149533.html (accessed October 5, 2023).

[298] Y.K. Salkuyeh, B.A. Saville, H.L. MacLean, Techno-economic analysis and life cycle assessment of hydrogen production from different biomass gasification processes, Int J Hydrogen Energy 43 (2018) 9514–9528. https://doi.org/10.1016/J.IJHYDENE.2018.04.024.

[299] Water Rates | ENWIN, (2023). https://enwin.com/water-rates-wuc/ (accessed October 5, 2023).

[300] Polly Martin, Blue hydrogen cheaper than green H2 in all markets except China amid falling gas prices: BNEF | Hydrogen news and intelligence, DN Media Group (2023). https://www.hydrogeninsight.com/production/blue-hydrogen-cheaper-than-green-h2-in-all-markets-except-china-amid-falling-gas-prices-bnef/2-1-1486049 (accessed October 5, 2023).

[301] Global Petrol Pricess, Methane prices around the world, 02-Oct-2023 | GlobalPetrolPrices.com, (2023). https://www.globalpetrolprices.com/methane_prices/ (accessed October 5, 2023).

[302] Indiamart, Carbon Dioxide Gas, (2023). https://www.indiamart.com/proddetail/carbon-dioxide-gas-18701560748.html?pos=3&kwd=industrial%20carbon%20dioxide%20gas&tags=BA|||8457.428|Price|product|TS|type=attr=1|attrS (accessed October 5, 2023).

[303] Y. Ayub, J. Ren, T. Shi, W. Shen, C. He, Poultry litter valorization: Development and optimization of an electro-chemical and thermal tri-generation process using an extreme

gradient boosting algorithm, Energy 263 (2023). https://doi.org/10.1016/j.energy.2022.125839.

[304] Y. Ayub, J. Ren, C. He, C. Azzaro-Pantel, Co-gasification of biomass and plastic waste for green and blue hydrogen Production: Novel process development, economic, exergy, advanced exergy, and exergoeconomics analysis, Chemical Engineering Journal 480 (2024) 148080. https://doi.org/10.1016/J.CEJ.2023.148080.

[305] N. Striūgas, V. Valinčius, N. Pedišius, R. Poškas, K. Zakarauskas, Investigation of sewage sludge treatment using air plasma assisted gasification, Waste Management 64 (2017) 149–160. https://doi.org/10.1016/j.wasman.2017.03.024.

[306] A.A. Erdogan, M.Z. Yilmazoglu, Plasma gasification of the medical waste, Int J Hydrogen Energy 46 (2021) 29108–29125. https://doi.org/10.1016/j.ijhydene.2020.12.069.

[307] H. Qi, P. Cui, Z. Liu, Z. Xu, D. Yao, Y. Wang, Z. Zhu, S. Yang, Conceptual design and comprehensive analysis for novel municipal sludge gasification-based hydrogen production via plasma gasifier, Energy Convers Manag 245 (2021). https://doi.org/10.1016/j.enconman.2021.114635.

[308] A. Giuliano, E. Catizzone, C. Freda, Process simulation and environmental aspects of dimethyl ether production from digestate-derived syngas, Int J Environ Res Public Health 18 (2021) 1–21. https://doi.org/10.3390/ijerph18020807.

[309] P. Basinas, J. Rusín, K. Chamrádová, S.P. Kaldis, Pyrolysis of the anaerobic digestion solid by-product: Characterization of digestate decomposition and screening of the biochar use as soil amendment and as additive in anaerobic digestion, Energy Convers Manag 277 (2023). https://doi.org/10.1016/j.enconman.2023.116658.

[310] Y. Ayub, J. Zhou, J. Ren, T. Shi, W. Shen, C. He, High-Dimensional Model Representation-Based Surrogate Model for Optimization and Prediction of Biomass Gasification Process, Int J Energy Res 2023 (2023) 1–14. https://doi.org/10.1155/2023/7787947.

[311] K.L. Ng, D. Chadwick, B.A. Toseland, Kinetics and modelling of dimethyl ether synthesis from synthesis gas, 1999.

[312] M. Mollavali, F. Yaripour, H. Atashi, S. Sahebdelfar, Intrinsic kinetics study of dimethyl ether synthesis from methanol on γ-Al2O3 catalysts, Ind Eng Chem Res 47 (2008) 3265–3273. https://doi.org/10.1021/ie800051h.

[313] C. Polsen, P. Narataruksa, P. Hunpinyo, C. Prapainainar, Simulation of single-step dimethyl ether synthesis from syngas, in: Energy Reports, Elsevier Ltd, 2020: pp. 516–520. https://doi.org/10.1016/j.egyr.2019.11.112.

[314] Zibo Zichai New Energy Ltd., 1MW Plasma Gasification 2MW Biomass Gasification Power Plant, (n.d.). https://zcxnypower.en.made-in-china.com/product/dQkpGUaTvLWs/China-1MW-Plasma-Gasification-2MW-Biomass-Gasification-Power-Plant.html (accessed January 4, 2023).

[315] A. Choudhury, G. Felton, J. Moyle, S. Lansing, Fluidized bed combustion of poultry litter at farm-scale: Environmental impacts using a life cycle approach, J Clean Prod 276 (2020). https://doi.org/10.1016/j.jclepro.2020.124231.

[316] M. Baniasadi, A. Tugnoli, R. Conti, C. Torri, D. Fabbri, V. Cozzani, Waste to energy valorization of poultry litter by slow pyrolysis, Renew Energy 90 (2016) 458–468. https://doi.org/10.1016/j.renene.2016.01.018.

[317] Y. Liu, X. Yang, J. Zhang, Z. Zhu, Process Simulation of Preparing Biochar by Biomass Pyrolysis Via Aspen Plus and Its Economic Evaluation, Waste Biomass Valorization 13 (2022) 2609–2622. https://doi.org/10.1007/s12649-021-01671-z.

[318] W. Song, M. Guo, Quality variations of poultry litter biochar generated at different pyrolysis temperatures, J Anal Appl Pyrolysis 94 (2012) 138–145. https://doi.org/10.1016/j.jaap.2011.11.018.

[319] Y. Ayub, J. Ren, T. Shi, W. Shen, C. He, Poultry litter valorization: Development and optimization of an electro-chemical and thermal tri-generation process using an extreme gradient boosting algorithm, Energy 263 (2023). https://doi.org/10.1016/j.energy.2022.125839.

[320] Worldometer, World Population Clock: 8.1 Billion People (LIVE, 2023) - Worldometer, (2023). https://www.worldometers.info/world-population/ (accessed November 22, 2023).

[321] Roisin Greene, Nilachal Mishra, India needs collaborative solutions to tackle its growing waste problem | Mint, Mint (2023). https://www.livemint.com/opinion/first-person/india-needs-collaborative-solutions-to-tackle-its-growing-waste-problem-11690186479560.html (accessed November 22, 2023).

[322] Dr. Muhammad Khurshid, Solid waste: a challenge as well as opportunity, The Express Tribune (2023). https://tribune.com.pk/story/2403472/solid-waste-a-challenge-as-well-as-opportunity (accessed November 22, 2023).

[323] ECDS BBS, Strengthening Environment, Climate Change and Disaster Statistics (ECDS) Project 1 | P a g e, 2022.

[324] Y. Ayub, A. Mehmood, J. Ren, C.K.M. Lee, Sustainable recycling of poultry litter to value-added products in developing countries of South Asia, J Clean Prod 357 (2022). https://doi.org/10.1016/j.jclepro.2022.132029.

[325] S. Jain, S. Jain, I.T. Wolf, J. Lee, Y.W. Tong, A comprehensive review on operating parameters and different pretreatment methodologies for anaerobic digestion of municipal solid waste, Renewable and Sustainable Energy Reviews 52 (2015) 142–154. https://doi.org/10.1016/J.RSER.2015.07.091.

[326] I. Velghe, R. Carleer, J. Yperman, S. Schreurs, Study of the pyrolysis of municipal solid waste for the production of valuable products, J Anal Appl Pyrolysis 92 (2011) 366–375. https://doi.org/10.1016/J.JAAP.2011.07.011.

[327] Y. Ayub, S. Tao, J. Ren, C.K.M. Lee, C. He, A. Manzardo, Poultry litter valorization by application of hydrothermal gasification: Process simulation, Economic, Energic, and Environmental analysis, Int J Energy Res 46 (2022) 23095–23109. https://doi.org/10.1002/er.8610.

[328] C.-N. Wang, V.T. Nguyen, D.H. Duong, H. Tuyet, N. Thai, A Hybrid Fuzzy Analysis Network Process (FANP) and the Technique for Order of Preference by Similarity to Ideal Solution (TOPSIS) Approaches for Solid Waste to Energy Plant Location Selection in Vietnam, Applied Sciences 8 (2018). https://doi.org/10.3390/app8071100.

[329] P. Behrend, B. Krishnamoorthy, Considerations for waste gasification as an alternative to landfilling in Washington state using decision analysis and optimization, Sustain Prod Consum 12 (2017) 170–179. https://doi.org/10.1016/J.SPC.2017.07.004.

[330] Z. Wang, J. Ren, M.E. Goodsite, G. Xu, Waste-to-energy, municipal solid waste treatment, and best available technology: Comprehensive evaluation by an interval-

valued fuzzy multi-criteria decision making method, J Clean Prod 172 (2018) 887–899. https://doi.org/10.1016/J.JCLEPRO.2017.10.184.

[331] M. Eghtesadifard, P. Afkhami, A. Bazyar, An integrated approach to the selection of municipal solid waste landfills through GIS, K-Means and multi-criteria decision analysis, Environ Res 185 (2020) 109348. https://doi.org/10.1016/J.ENVRES.2020.109348.

[332] V.R. Sumathi, U. Natesan, C. Sarkar, GIS-based approach for optimized siting of municipal solid waste landfill, Waste Management 28 (2008) 2146–2160. https://doi.org/10.1016/J.WASMAN.2007.09.032.

[333] Ş. Şener, E. Şener, B. Nas, R. Karagüzel, Combining AHP with GIS for landfill site selection: A case study in the Lake Beyşehir catchment area (Konya, Turkey), Waste Management 30 (2010) 2037–2046. https://doi.org/10.1016/J.WASMAN.2010.05.024.

[334] Y. Ayub, J. Zhou, J. Ren, Y. Wang, W. Shen, C. He, L. Dong, S. Toniolo, Plasma gasification based monetization of poultry litter: System optimization and comprehensive 5E (Energy, Exergy, Emergy, Economic, and Environmental) analysis, Energy Convers Manag 282 (2023). https://doi.org/10.1016/j.enconman.2023.116878.

[335] Y. Ayub, J. Zhou, W. Shen, J. Ren, Innovative valorization of biomass waste through integration of pyrolysis and gasification: Process design, optimization, and multi-scenario sustainability analysis, Energy 282 (2023). https://doi.org/10.1016/j.energy.2023.128417.

[336] S. Jovanovic, S. Savic, N. Jovicic, G. Boskovic, Z. Djordjevic, Using multi-criteria decision making for selection of the optimal strategy for municipal solid waste management, Waste Management and Research 34 (2016) 884–895.

https://doi.org/10.1177/0734242X16654753/ASSET/IMAGES/LARGE/10.1177_0734242X16654753-FIG13.JPEG.

[337] Y. Ayub, J. Zhou, T. Shi, J. Ren, Process safety assessment of thermal technologies for biomass valorization by numerical descriptive approach, Process Safety and Environmental Protection 171 (2023) 803–811. https://doi.org/10.1016/j.psep.2023.01.075.

[338] S. O'Connor, E. Ehimen, S.C. Pillai, G. Lyons, J. Bartlett, Economic and Environmental Analysis of Small-Scale Anaerobic Digestion Plants on Irish Dairy Farms, Energies 2020, Vol. 13, Page 637 13 (2020) 637. https://doi.org/10.3390/EN13030637.

[339] Y. Ayub, Md.A. Moktadir, J. Ren, Sustainable waste valorization process selection through AHP and advanced Interval Valued Fermatean Fuzzy with integrated CODAS, Process Safety and Environmental Protection 185 (2024) 408–422. https://doi.org/10.1016/j.psep.2024.03.019.

[340] G. Weber, Q. Fu, H. Wu, Energy Efficiency of an Integrated Process Based on Gasification for Hydrogen Production from Biomass, Developments in Chemical Engineering and Mineral Processing 14 (2006) 33–48. https://doi.org/10.1002/APJ.5500140104.

[341] Y. Ayub, J. Ren, C. He, Unlocking waste potential: A neural network approach to forecasting sustainable acetaldehyde production from ethanol upcycling in biomass waste gasification, Energy 299 (2024) 131482. https://doi.org/10.1016/J.ENERGY.2024.131482.

[342] Y. Ayub, J. Zhou, T. Shi, J. Ren, Process safety assessment of thermal technologies for biomass valorization by numerical descriptive approach, Process Safety and

Environmental Protection 171 (2023) 803–811. https://doi.org/10.1016/j.psep.2023.01.075.

[343] Biomass Gasifier at Rs 3000000/piece | Thane West | Thane | ID: 15437772230, (n.d.). https://www.indiamart.com/proddetail/biomass-gasifier-15437772230.html?pos=2&kwd=biomass%20gasifier%20plant&tags=||||7546.6187|Price|product (accessed December 1, 2022).

[344] Cryogenic Air Separation Process with Flash Separator - China Oxygen Plant and Liquid Gas Air Separation Process, (n.d.). https://hznuzhuo.en.made-in-china.com/product/BFofOASvEGtz/China-Cryogenic-Air-Separation-Process-with-Flash-Separator.html (accessed December 1, 2022).

[345] Jz Series High-Efficiency Centrifugal Air Compressor Steam Compressor - China High Efficiency Centrifugal Air Compressor and High-Efficiency Centrifugal Air Compressor, (n.d.). https://jintonglingtech.en.made-in-china.com/product/TwGfdxVAsMcn/China-Jz-Series-High-Efficiency-Centrifugal-Air-Compressor-Steam-Compressor.html (accessed December 1, 2022).

[346] Ae-Type Enamel Reactor Used for Chemical Production - China Glass-Lined and Reactor, (n.d.). https://head-graphite.en.made-in-china.com/product/eZzfhFqGALpo/China-Ae-Type-Enamel-Reactor-Used-for-Chemical-Production.html (accessed December 1, 2022).

[347] Stainless Steel Industrial Shell Tube Heat Exchanger for Papermaking Wastewater Treatment - China Shell Tube Heat Exchanger and Air Exchanger, (n.d.). https://shandongpuruipule.en.made-in-china.com/product/COETMxrubSRy/China-Stainless-Steel-Industrial-Shell-Tube-Heat-Exchanger-for-Papermaking-Wastewater-Treatment.html (accessed December 1, 2022).

[348] Lp LPG Gas Storage Tanks Price for Sale in Zimbabwe - China LPG Underground Tanks and LPG Tank, (n.d.). https://cimchonto.en.made-in-china.com/product/HOmJFdAPZkcl/China-Lp-LPG-Gas-Storage-Tanks-Price-for-Sale-in-Zimbabwe.html (accessed December 1, 2022).

[349] High Quality 20 FT30 FT Steel Tank Container Custom Steel Liquid Storage Tank Container - China Container Aluminium Tank and ISO Tank Container, (n.d.). https://hbhuate.en.made-in-china.com/product/fdlAFQUcHKpD/China-High-Quality-20-FT30-FT-Steel-Tank-Container-Custom-Steel-Liquid-Storage-Tank-Container.html (accessed December 1, 2022).

[350] Well-Designed Stainless Steel Industrial Alcohol Distillation Equipment Column - China Alcohol Distillation Column and Ethanol Distillation Column, (n.d.). https://wxty2019.en.made-in-china.com/product/nStJhjsDCKrM/China-Well-Designed-Stainless-Steel-Industrial-Alcohol-Distillation-Equipment-Column.html (accessed December 1, 2022).

[351] 100kw Hydraulic Electric Generator 1 MW Generator Free Energy - China 1 Kw Pelton Turbine and 1 Kw River Generator, (n.d.). https://cdforster.en.made-in-china.com/product/JFaEWrOxVzcG/China-100kw-Hydraulic-Electric-Generator-1-MW-Generator-Free-Energy.html (accessed December 1, 2022).

[352] C. Mevawala, Y. Jiang, D. Bhattacharyya, Techno-economic optimization of shale gas to dimethyl ether production processes via direct and indirect synthesis routes, Appl Energy 238 (2019) 119–134. https://doi.org/10.1016/j.apenergy.2019.01.044.

[353] Lp LPG Gas Storage Tanks Price for Sale in Zimbabwe - China LPG Underground Tanks and LPG Tank, (n.d.). https://cimchonto.en.made-in-

china.com/product/HOmJFdAPZkcl/China-Lp-LPG-Gas-Storage-Tanks-Price-for-Sale-in-Zimbabwe.html (accessed January 4, 2023).

[354] Mysd196-100 Hot Air Blower for Crushing Starch and Gluten - China Backward Centrifugal Fan and Backward Centrifugal Fan Catalogue, (n.d.). https://xinfan.en.made-in-china.com/product/lmSYznjusUki/China-Mysd196-100-Hot-Air-Blower-for-Crushing-Starch-and-Gluten.html (accessed January 4, 2023).

[355] CTI Certificate Industrial Air Cooler/ Finned Tube Bundle Heat Exchanger/ Air Cooled Gas Cooler - China Dry Cooling Tower and Dry Industry Cooler, (n.d.). https://china-coolingtower.en.made-in-china.com/product/MwETqvpUhaRF/China-CTI-Certificate-Industrial-Air-Cooler-Finned-Tube-Bundle-Heat-Exchanger-Air-Cooled-Gas-Cooler.html (accessed January 4, 2023).

[356] L. Qingdao Director Steel Structure Co., Fast Install Practical Designed Prefab Light Steel Structure Industrial Workshop Plant Shed, (2023). https://steelstructuredfx.en.made-in-china.com/product/yXBneIAJYHYP/China-Fast-Install-Practical-Designed-Prefab-Light-Steel-Structure-Industrial-Workshop-Plant-Shed.html (accessed January 4, 2023).

[357] Zibo Zichai, 100kw to 5MW Cotton Stems Cotton Stalks Biomass Gasification Power Plant - China Gas Generator and Power Generator, (2022). https://zcxnypower.en.made-in-china.com/product/uXdxqgRrZSYN/China-100kw-to-5MW-Cotton-Stems-Cotton-Stalks-Biomass-Gasification-Power-Plant.html (accessed December 3, 2022).

Appendix

A1. Description of 1-9 Likert scale for AHP

Likert scale	Meaning of the number
1	Equal importance
2	Somewhat between equal and moderate importance
3	Moderately more important than
4	Somewhat between moderate and strong importance
5	Strongly more important than
6	Somewhat between strong and very strong importance level
7	Very strongly more important than
8	Somewhat between the very strongly and absolute level of higher importance
9	Absolutely more important than

A2. Aspen Plus process simulation for waste co-gasification to produce green H_2

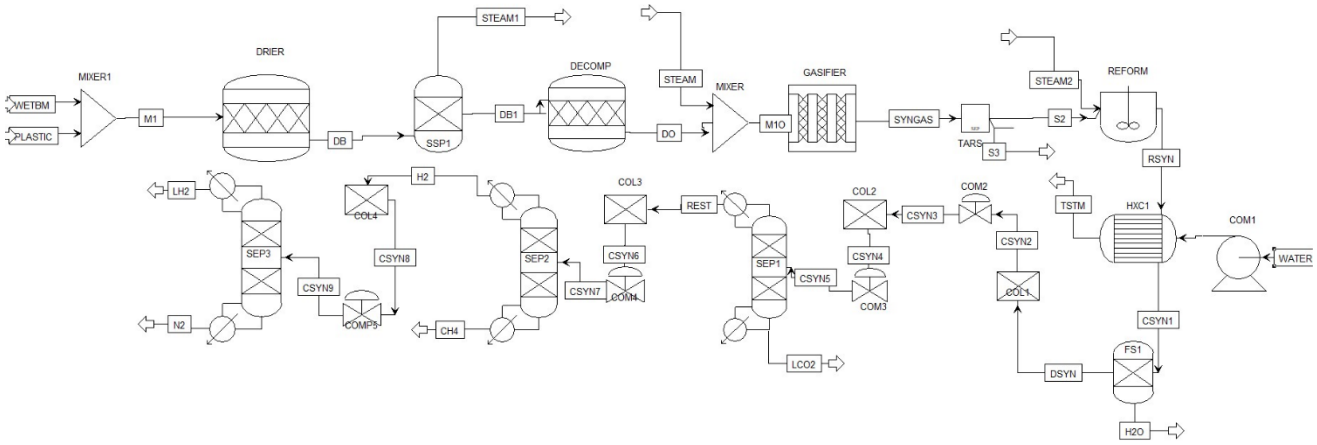

A3. Aspen Plus process simulation for alkaline electrolysis cell to produce green H_2

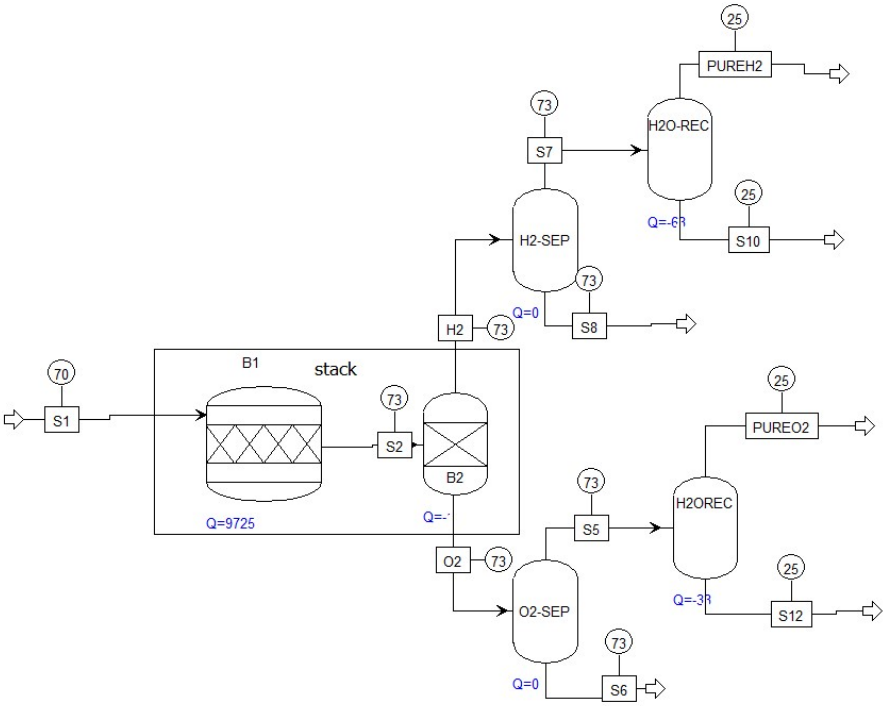

A4. Aspen Plus process simulation for Gasification, SOFC, and CHP based process

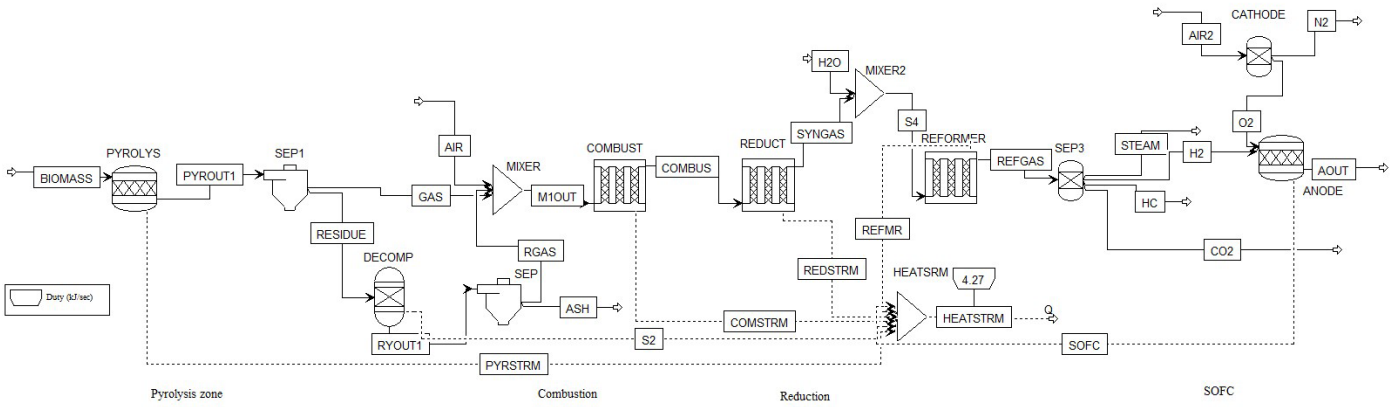

A5. Solid Oxide Fuel Cell Voltage and Current Calculations

Voltage and Current Calculations for SOFC [98,252,270]											
Voltage Losses	**$R_{A,A}$**	**F** (C/mol)	**R** (J/mol.K)	**T_{OP}** (K)	**K_{AN}**	**P_{H2} (bar)**	**P_{O2} (bar)**	**E_{AN}**	**$m_{(slope)}$**		
Anode	4.91628E-05	96485	8.314	1073	2.13E+08	1	1	110000	0.25		
	$R_{A,C}$	**F** (C/mol)	**R** (J/mol.K)	**T_{OP}** (K)	**K_{CA}**	**P_{O2} (bar)**	**P^{O} (bar)**	**E_{CA}** (J/mol)	**$m_{(slope)}$**		
Cathode	9.54848E-05	96485	8.314	1073	1.49E+10	1	1	160000	0.25		
Ohmic	**V_{OA}**		**P_{AN} (mΩ)**	**J**	**t_{A} (m)**	**D_{ma} (m)**	**A**				
Anode	0.000596263		8.14343E-06	18.98908	0.0001	0.022	0.804				
	V_{OC}		**P_{CA} (mΩ)**	**J**	**t_{C} (m)**	**D_{ma} (m)**	**B**	**A**			
Cathode	0.000549935		0.000141933	18.98908	0.0022	0.022	0.13	0.804			
	$V_{O,INT}$		**P_{INT} (mΩ)**	**J**	**T_{INT} (m)**	**D_{ma} (m)**	**W_{int}**				
Interconnection	0.000309722		0.025	18.98908	0.000085	0.022	0.009				
	$V_{O,E}$		**P_{E} (mΩ)**	**J**	**t_{E} (m)**						
Electrolyte	3.90625E-08		5.14276E-05	18.98908	0.00004						
Concentration	**$V_{C,A}$**	**F** (C/mol)	**R** (J/mol.K)	**T_{OP}** (K)	**t_{A} (m)**	**$D_{A,eff}$ (m)**	**Y_{H2} (moles)**	**Y_{H2O} (mole)**	**P_{sofc}**	**J**	
Anode	0.0076	96485	8.314	1073	0.0001	0.022	0.04862	0.048622	1	18.989	
	$V_{C,C}$	**F** (C/mol)	**R** (J/mol.K)	**Psofc**	**d_{O2}** (kg/m3)	**Y_{O2} (moles)**	**T_{OP}** (K)	**$D_{c,eff}$ (m)**	**J**	**t_{c}**	**P_{sofc}**
Cathode	0.000645	96485	8.314	1	1.429	0.0243	1073	0.022	18.989	0.0022	1
Ideal Voltage V_{id}	**V_{id}**	**F** (C/mol)	**Gibb $_{Dgf}$** (J/mol)								
	1.115	96485	-215210								
Nernst Voltage V_{Nr}	**V_{Nr}**	**V_{id}**	**V_{id}**	**R** (J/mol.K)	**$T_{(K)}$**	**P_{H2} (bar)**	**P_{H2O} (bar)**	**P_{O2} (bar)**			
	1.115	96485	1.115	8.314	1073	1	1	1			
Current (I)	**I** (A/m2)	**F**	**$H_{2,cons}$**								
	1824.409751	96485	0.034035731								
Current Density (J)	**J**	**I** (A)	**A** (m2)	**mA/cm^2**							
	18.989	1824.41	96.077	189.891							
Diffusion Coefficient D_{ik}	**D_{ik}**	**T_{OP}** (K)	**M_{i}** (molc. wt. at anode)	**M_{k}** (molc. wt. at cathode)	**$P_{(bar)}$**	**V_{i}**	**V_{k}**				
	1.61E-01	1073	2.016	32	1	0.0098	0.00055				
Actual Voltage	**V_{act} (V)**	**V_{nr} (V)**	**V_{o} (V)**	**V_{a} (V)**	**V_{c} (V)**						
	0.775	1.115	0.00031	0.0070	0.000645						

DC Power	DCP	V_{act}	I								
	1414.11	0.775107153	1824.41								

where $\check{R}_{A,A}$ is the specific resistance of anode, F= Faraday's constant, K_{AN} are the pre-exponential factor of anode, P_o is the reference pressure (1 bar), P_i is the partial pressure of each species, E_{AN} is the activation energy of anode, $\check{R}_g$is the general gas constant, T_{op} is the operating temperature, and m is slope, $\check{R}_{A,C}$ is the specific resistance of cathode, K_{CA} are the pre-exponential factor of cathode, $E_{CA}$is the activation energy of cathode, $V_{O,A}$ is the ohmic loss of anode, j is current density, ρ_{AN} is the anode resistance, A ohmic loss, D_{mA} is cell average diameter (m), t_A anode thickness (m), $V_{O,C}$ is the ohmic loss of cathode, j is current density, ρ_{CA} is the cathode resistance, A and B ohmic loss, D_{mA} is cell average diameter (m), t_C cathode thickness (m), $V_{O,Int}$ is the ohmic loss of interconnection, j is current density, ρ_{Int} is the interconnection resistance, D_{mA} is cell average diameter (m), t_{Int} interconnection thickness (m), $W_{Int}$is the width of *Int.*, $V_{O,E}$ is the ohmic loss of electrolyte, j is current density, ρ_E is the electrolyte resistance, t_E electrolyte thickness (m), $\check{R}_g$is the general gas constant, F is Faraday's constant, P_{SOFC} is the pressure in SOFC, T_{op} is the operating temperature, $D_{A,eff}$ is the diffusion co-efficient of anode, $t_A$is anode thickness, $y^0_{H_2}$ is average H_2 molar fractions, $y^0_{H_2O}$ is average H_2O molar fractions, $D_{C,eff}$ is the diffusion co-efficient of cathode, $t_C$is cathode thickness, $y^0_{H_2}$ is average H_2 molar fractions, δ_{O_2} is oxygen density, V_{id} is ideal voltage, $P_{H_2O}$is the pressure of H_2O, P_{O_2} is the partial pressure of oxygen, $-\triangle g_f$ Gibbs free energy formation, current generated by SOFC (I) and A is the SOFC active area, V_{act}actual voltage of the SOFC, $V_o$ohmic voltage lose, $V_o$activation voltage losses, and V_c concentrate voltage losses.

A6. Aspen Plus simulation model for DME and Methanol (Process G2)

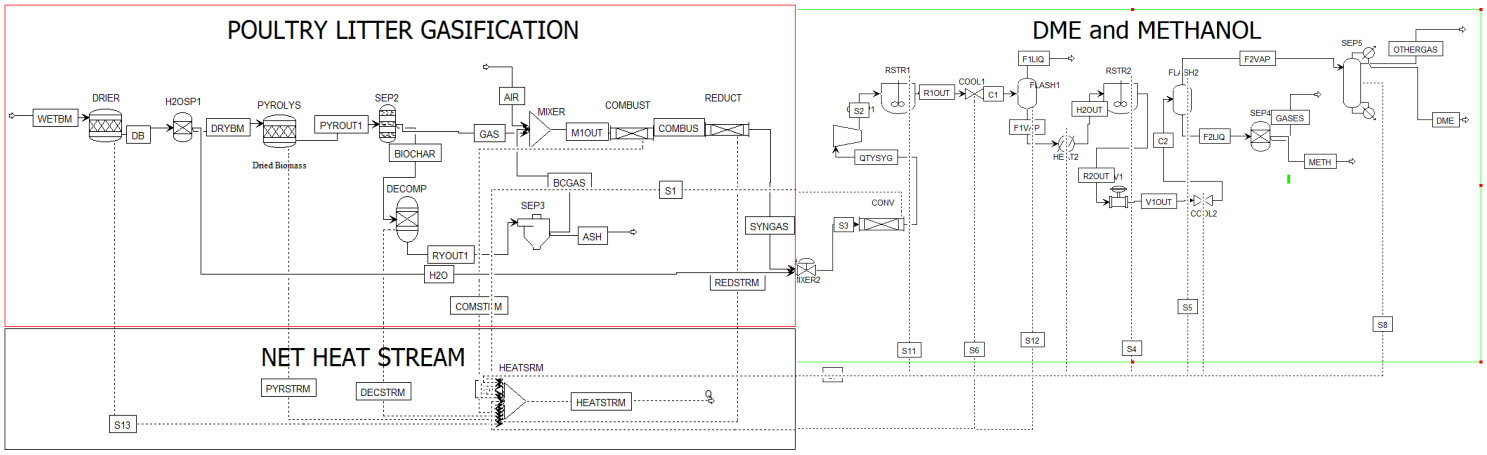

A7. Advanced exergy and exergoeconomics analysis (Process G3)

Exergy Analysis	Exergy (Drier)	Exergy (Gasifier)	Exergy (Comp. 1)	Exergy (Heat XC)	Exergy (Turbine)	Exergy (AEC)	Exergy (Flash Sep)	Exergy (Cool 1)	Exergy (Comp. 2)	Exergy (Comp. 3)	Exergy (Sep. 1)	Exergy (Cool 3)	Exergy (Sep. 2)	Exergy (Cool 4)	Exergy (Sep. 3)
Destructive Exergy	4280	9979.540724	7	9245	13684	1917	580	797	5	516	439	567	144	522	147
Exergy In	23345	26407	44340	25808	35088	7100	25808	26025	26025	26536	26536	2478	2622	1540	1687
Exergy Out	19065	16427.45928	44333	16563	21404	5183	25228	25228	26020	26020	26097	1911	2478	1018	1540
Chemical Exergy	2144.881124	0	0	0	0	0	0	0	0	0	0	0	0	0	0
Physical Exergy	7.664	syngas	0	0	0	0	0	0	0	0	0	0	0	0	0
Product Exergy	19065	5512	44333	4018	21404	4018	25228	25228	26020	26020	26097	1911	2478	1018	1540
Fuel product exergy	9380.386989	20895	7	21790	13684	3082	580	797	5	516	439	567	144	522	147
Fuel exergy	28445.38699	26407	44340	25808	35088	7100	25808	26025	26025	26536	26536	2478	2622	1540	1687
Product exergy	19065	5512	44333	4018	21404	4018	25228	25228	26020	26020	26097	1911	2478	1018	1540
endogenous irreversibility	3495.318055	6208.145523	6.998894903	5933.235237	8347.364797	1399.41	566.9652821	772.5924	4.999039	505.9662	431.7374	437.2627	136.0915	345.0623	134.1909
exogenous irreversibility	784.6819447	3771.3952	0.001105097	3311.764763	5336.635203	517.59	13.03471792	24.40765	0.000961	10.03377	7.262624	129.7373	7.908467	176.9377	12.80913
irreversibility at real condition	4280	9979.540724	7	9245	13684	1917	580	797	5	516	439	567	144	522	147
unavoidable irreversibility	428	498.9770362	0.7	92.45	1368.4	785.97	58	318.8	0.5	30.96	43.9	28.35	5.76	26.1	5.88
unavoidable	0.183336903	0.377912702	0.000157871	0.358222257	0.38999088	0.27	0.022473652	0.030624	0.000192	0.019445	0.016544	0.228814	0.05492	0.338961	0.087137
avoidable irreversibility	3852	9480.563688	6.3	9152.55	12315.6	1131.03	522	478.2	4.5	485.04	395.1	538.65	138.24	495.9	141.12
unavoidable endogenous irreversibility	2.216311361	9820.922854	6.998895077	9455.289751	10121.99848	1731.907295	567.2549771	773.3286	4.99904	506.1595	431.8565	464.0469	136.5144	397.0394	135.2612
endogenous irreversibility product	0.34	6208.145523	6.998894903	5933.235237	8347.364797	1399.41	566.9652821	772.5924	4.999039	505.9662	431.7374	437.2627	136.0915	345.0623	134.1909
unavoidable exogenous irreversibility	425.7836886	-9321.945818	-6.298895077	-9362.839751	-8753.598482	-945.9372952	-509.2549771	-454.529	-4.49904	-475.199	-387.957	-435.697	-130.754	-370.939	-129.381
avoidable endogenous irreversibility	3493.101744	-3612.777331	-1.74449E-07	-3522.054513	-1774.633685	-332.4972952	-0.289695065	-0.73626	-1.8E-07	-0.19324	-0.11917	-26.7842	-0.42284	-51.977	-1.07029
avoidable exogenous irreversibility	358.8982561	13093.34102	6.300000174	12674.60451	14090.23369	1463.527295	522.2896951	478.9363	4.5	485.2332	395.2192	565.4342	138.6628	547.877	142.1903
irreversibility rate of mexogenous	784.6819447	3771.3952	0.001105097	3311.764763	5336.635203	517.59	13.03471792	24.40765	0.000961	10.03377	7.262624	129.7373	7.908467	176.9377	12.80913
Exergoeconomic analysis	**Exergy (Drier)**	**Exergy (Gasifier)**	**Exergy (Compressor 1)**	**Exergy (Heat XC)**	**Exergy (Steam Turbine)**	**Exergy (AEC)**	**Exergy (Flash Separator)**	**Exergy (Cooler 1)**	**Exergy (Compressor 2)**	**Exergy (Compressor 3)**	**Exergy (Separator 1)**	**Exergy (Cooler 3)**	**Exergy (Separator 2)**	**Exergy (Cooler 4)**	**Exergy (Separator 3)**

endogenous exergy destruction cost	22765720.92	40733.38925	45551.77679	38814.35124	54340115.66	9301.872119	3689240.598	5029.462	32.55729	329.5211	282.1402	2846.516	889.3576	2246.305	876.9368
cost per unit	6513.204396	6561.281319	6508.424176	6541.852747	6509.852747	6646.995604	6506.995604	6509.853	6512.71	6512.71	6534.996	6509.853	6534.996	6509.853	6534.996
endogenous irreversibility	3495.318055	6208.145523	6.998894903	5933.235237	8347.364797	1399.41	566.9652821	772.5924	4.999039	505.9662	431.7374	437.2627	136.0915	345.0623	134.1909
exogenous exergy destruction cost	-22759207.72	-34172.10793	-39043.35262	-32272.49849	-54333605.8	-2654.876514	-3682733.603	1480.39	6480.153	6183.189	6252.855	3663.337	5645.638	4263.548	5658.059
endogenous investment cost	3.737949121	425289.5046	30.40595399	457175.1193	77062.1979	235998.0627	4216.057037	6051.381	39.88473	4036.841	4724.842	45213.56	15685.13	66978.7	24886.31
endogenous irreversibility product	0.34	6208.145523	6.998894903	5933.235237	8347.364797	1399.41	566.9652821	772.5924	4.999039	505.9662	431.7374	437.2627	136.0915	345.0623	134.1909
Total investment	209600	377600	192600	309600	197600	677600	187600	197600	207600	207600	285600	197600	285600	197600	285600
Product exergy	19065	5512	44333	4018	21404	4018	25228	25228	26020	26020	26097	1911	2478	1018	1540
endogenous investment cost flow	209596.2621	-47689.50465	192569.594	-147575.1193	120537.8021	441601.9373	183383.943	191548.6	207560.1	203563.2	280875.2	152386.4	269914.9	130621.3	260713.7
avoidable exergy destruction cost	25088.86333	62204.64541	41.00307231	59874.63436	80172.74249	7517.951438	3396.651705	3113.012	29.30719	3158.925	2581.977	3506.532	903.3978	3228.236	922.2186
avoidable irreversibility	3852	9480.563688	6.3	9152.55	12315.6	1131.03	522	478.2	4.5	485.04	395.1	538.65	138.24	495.9	141.12
unavoidable exergy destruction cost	14.4352889	64437.83766	45.55177793	61855.11323	65892.71963	11511.98018	3691.125643	5034.255	32.55729	3296.47	2822.181	3020.877	892.1208	2584.668	883.9311
unavoidable endogenous irreversibility	2.216311361	9820.922854	6.998895077	9455.289751	10121.99848	1731.907295	567.2549771	773.3286	4.99904	506.1595	431.8565	464.0469	136.5144	397.0394	135.2612
unavoidable investment cost	29588.22042	27230.28355	44343.28177	19050.24079	50927.22568	16043.16566	26391.57075	26869.41	26030.38	27092.27	27150.77	5523.465	3216.083	6071.611	2427.549
Product Exergy	19065	5512	44333	4018	21404	4018	25228	25228	26020	26020	26097	1911	2478	1018	1540
avoidable investment cost	180011.7796	350369.7164	148256.7182	290549.7592	146672.7743	661556.8343	161208.4293	170730.6	181569.6	180507.7	258449.2	192076.5	282383.9	191528.4	283172.5
cost of unavoidable endogenous	14.4352889	64437.83766	45.55177793	61855.11323	65892.71963	11511.98018	3691.125643	5034.255	32.55729	3296.47	2822.181	3020.877	892.1208	2584.668	883.9311
unavoidable endogenous irreversibility	2.216311361	9820.922854	6.998895077	9455.289751	10121.99848	1731.907295	567.2549771	773.3286	4.99904	506.1595	431.8565	464.0469	136.5144	397.0394	135.2612
avoidable endogenous	22751.28563	-23704.44841	-1.13539E-06	-23040.76199	-11552.60397	-2210.10806	-1.885044514	-4.79292	-1.2E-06	-1.2585	-0.77875	-174.361	-2.76323	-338.363	-6.99432
avoidable endogenous irreversibility	3493.101744	-3612.777331	-1.74449E-07	-3522.054513	-1774.633685	-332.4972952	-0.289695065	-0.73626	-1.8E-07	-0.19324	-0.11917	-26.7842	-0.42284	-51.977	-1.07029
unavoidable exogenous	2773.216192	-61163.90895	-40.995881	-61250.31894	-56984.63713	-6287.641043	-3313.719898	-2958.91	-29.3009	-3094.84	-2535.29	-2836.32	-854.479	-2414.76	-845.505

unavoidable exogenous irreversibility	425.7836886	-9321.945818	-6.298895077	-9362.839751	-8753.598482	-945.9372952	-509.2549771	-454.529	-4.49904	-475.199	-387.957	-435.697	-130.754	-370.939	-129.381
avoidable exogenous	2337.577699	85909.09382	41.00307344	82915.39636	91725.34647	9728.059498	3398.53675	3117.805	29.3072	3160.183	2582.756	3680.894	906.161	3566.599	929.2129
avoidable exogenous irreversibility	358.8982561	13093.34102	6.300000174	12674.60451	14090.23369	1463.527295	522.2896951	478.9363	4.5	485.2332	395.2192	565.4342	138.6628	547.877	142.1903
unavoidable endogenous investment	1.273458602	134.0143891	1.000539218	106.5534601	80.50513359	28.228336	1.206326547	1.305621	1.000708	1.175224	1.150237	11.61953	1.69987	43.23192	2.415742
endogenous irreversibility product	0.34	6208.145523	6.998894903	5933.235237	8347.364797	1399.41	566.9652821	772.5924	4.999039	505.9662	431.7374	437.2627	136.0915	345.0623	134.1909
unavoidable exogenous investment	29586.94697	27096.26916	44342.28123	18943.68733	50846.72054	16014.93732	26390.36442	26868.1	26029.38	27091.09	27149.62	5511.846	3214.384	6028.379	2425.133
unavoidable investment cost	29588.22042	27230.28355	44343.28177	19050.24079	50927.22568	16043.16566	26391.57075	26869.41	26030.38	27092.27	27150.77	5523.465	3216.083	6071.611	2427.549
avoidable endogenous investment	2.464490519	425155.4903	29.40541477	457068.5659	76981.69277	235969.8344	4214.85071	6050.076	38.88402	4035.665	4723.691	45201.94	15683.43	66935.47	24883.89
avoidable exogenous investment	180009.3151	-74785.77381	148227.3128	-166518.8066	69691.08155	425587	156993.5785	164680.5	181530.7	176472.1	253725.5	146874.6	266700.5	124592.9	258288.6

A8. Process G2: DME economic analysis

Dimethyl Ether Economic Analysis				
Capital Cost				
Items	**QTY**	**Cost ($)**	**Cost (%)**	**Ref.**
Equipment			63%	
Gasifier	1	120000	28%	[343]
Separator	4	12000	3%	[344]
Compressor (200 m3/min)	2	12000	3%	[345]
Stirrer Reactor	2	40000	9%	[346]
Heat Exchanger	2	10000	2%	[347]
Gas Storage	1	10000	2%	[348]
Liquid Storage	1	10000	2%	[349]
Column Separator	1	30000	7%	[350]
Supplementary Equipment	1	21400	5%	
Civil Work/Building				
Shed Area (10000 sq. ft)	10000	29000	7%	
Electrical Installations				
Steam Turbine	1	10000	2%	[351]

Generator	1	120000	28%	[351]
Total (CAP)		***424400***		
Operational Cost				
Items	**QTY**	**Cost ($/d)**	**Cost (%)**	**Ref**
Raw Material ($/d)	23	690	29%	[343]
Labor ($/d)	-	500	21%	[352]
Overhead ($/d)	1	424	18%	[352]
Maintenance/Engineering ($/d)	1	424	18%	[352]
Plant Depreciation ($/d)		116	5%	
Transportation ($/d)		230	10%	
Total (OPR/d)		***2385***		
Revenue				
Items	**QTY (ton)**	**Market Value ($)**	**Market Price $/ton**	
DME (Normal) at 0.1908 kg/kg	4.3884	2861	652	[23]
DME (Optimum) at 0.2426 kg/kg	5.5798	3638		
DME Price /kg			**$ Price/kg**	
DME (Normal)	4388.4	4388.4/2861 =	0.54	
DME (Optimum)	5579.8	5579.8/3638 =	0.43	

A9. Process G2: DME Sustainability Index calculation

Sustainability index calculation for IRR			
Efficiency	**Base**	**Optimized**	**Remarks**
100% (Without Subsidy)	15.1%	26.8%	Below 80% efficiency not included because IRR <0 in base process
90% (Without Subsidy)	5.0%	22.6%	
100% (With subsidy)	30.2%	35.4%	
90% (With subsidy)	27.7%	33.2%	
80% (With subsidy)	24.7%	30.6%	
70% (With subsidy)	20.8%	27.4%	
60% (With subsidy)	15.3%	23.3%	
50% (With subsidy)	5.3%	17.5%	
Average	18.01%	27.10%	
x1	0.180	0.271	

Sustainability index calculation for environment		
LCA	**LCA scores mean**	
Midpoint (average) DME	64.03%	
Endpoint (average) DME	56.86%	
Average	**60.45%**	
	Base	**Optimized**
Yield of DME	19.08%	24.26%
	11.53%	14.66%
	8.670	6.819
Environment Factor x2	0.087	0.068

Sustainability index without weightage		
	Base	**Optimized**
Economic	0.180	0.271
Environment	0.087	0.068
Energy	0.570	0.530
	0.837	***0.869***

A10. Process G2: DME Sustainability Index sensitivity analysis

Sustainability index equal weightage			
	Weightage	**Base**	**Optimized**
Economic	0.333	0.060	0.090
Environment	0.333	0.029	0.023
Energy	0.333	0.190	0.177
		0.279	***0.290***
Sustainability index different weightage			
	Weightage	**Base**	**Optimized**
Economic	0.450	0.081	0.122
Environment	0.275	0.024	0.019
Energy	0.275	0.157	0.146
		0.262	***0.286***
Sustainability index different weightage			
	Weightage	**Base**	**Optimized**
Economic	0.275	0.050	0.075
Environment	0.450	0.039	0.031
Energy	0.275	0.157	0.146
		0.245	***0.251***
Sustainability index equal weightage			
	Weightage	**Base**	**Optimized**
Economic	0.275	0.050	0.075
Environment	0.275	0.024	0.019
Energy	0.45	0.257	0.239
		0.330	***0.332***

A11. Plasma gasification to DME simulation model

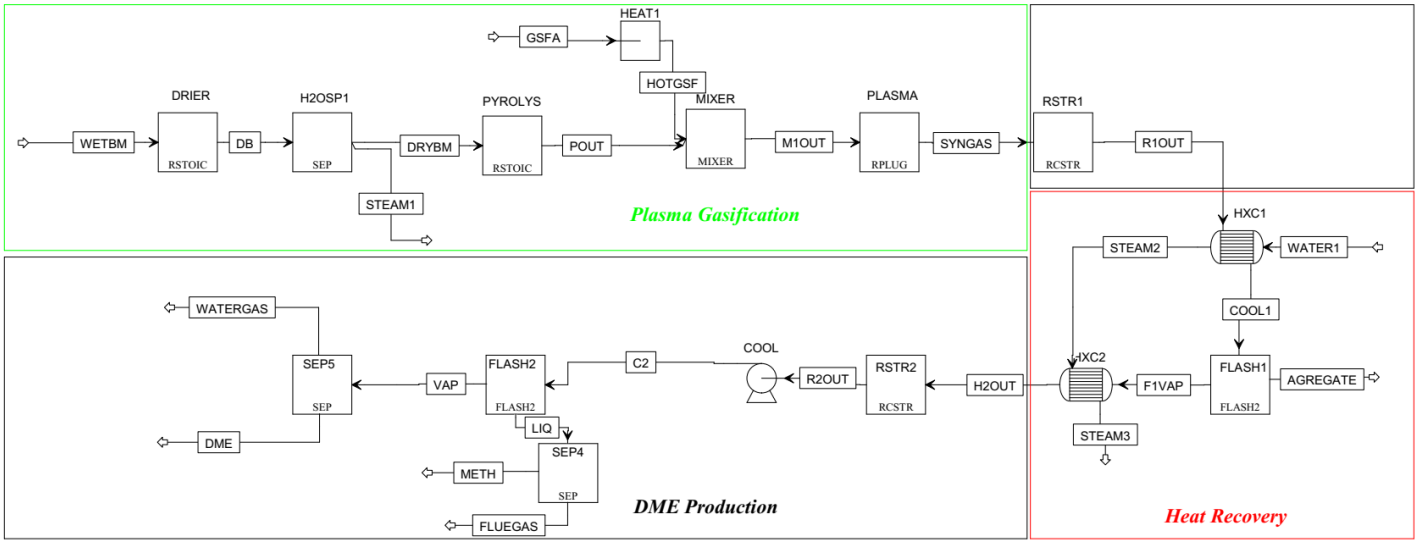

A12. Plasma gasification surrogate model pseudocode

```
Procedure Optimization
Initial
Set process=Aspen Plus model, x0=[1000,1000,227,300], x.lo= [1000,200,150,100]
    x.lo= [3000,1000,350,2000], maxFun=1500
Defined function ObjFun (input, process)
   Let values of selection operations of process=input,
         S=running sate of process,
         output=Flowrate of DME in Aspen Plus result
      Run process
   If S = 'error'
    output=0
   else
    output=-output
   end
   Return output
end
Configure surrogate optimization problem by using x0, x.lo, x.up, maxFun,
ObjFun
Do surrogate optimization by calling MATLAB function 'surrogateopt'
Return optimum solution and objective value
```

A13. Plasma gasification to DME economic analysis

Capital Cost (10 ton/h capacity)				
Items	**QTY**	**Cost ($)**	**Cost (%)**	**Ref.**
Equipment			63%	
Gasifier	1	65000	15%	[314]
Separator	5	25000	6%	[344]
Compressor (200 m^3/min)	2	12000	3%	[345]
Stirrer Reactor	2	30000	7%	[346]
Heat Exchanger	2	20000	5%	[347]
Gas Storage Bowser	1	10000	2%	[353]
Column Separator	1	30000	7%	[350]
Heater	1	20000	5%	[354]
Gas Cooler (condenser)	1	20000	5%	[355]
Supplementary Equipment	1	38400	9%	
Civil Work/Building				
Shed Area (10000 sq. ft)	10000	29000	7%	[356]
Electrical Installations				
Steam Turbine	1	20000	5%	[203]
Generator	1	120000	27%	[357]
Total (CAP)		***439400***		
Operational Cost				
Items	**QTY**	**Cost ($/d)**	**Cost (%)**	

Raw Material ($/d)	230	9200	64%	
Labor ($/d)	-	1500	10%	
Overhead ($/d)	1	220	2%	
Maintenance/Engineering ($/d)	1	439	3%	
Utility ($/d)		3000	21%	
Plant Depreciation ($/d)		120	1%	
Total (OPR/d)		***14479***		
Revenue				
Items	**QTY**	**Market Value ($)**	**Cost $/ton**	
DME (Normal) @ 0.15 kg/t	34.5	17975	521	
DME (Optimum) @ 0.18 kg/t	41.4	21569		
Total (REV)				

A14. Pyrolysis-gasification process simulation model

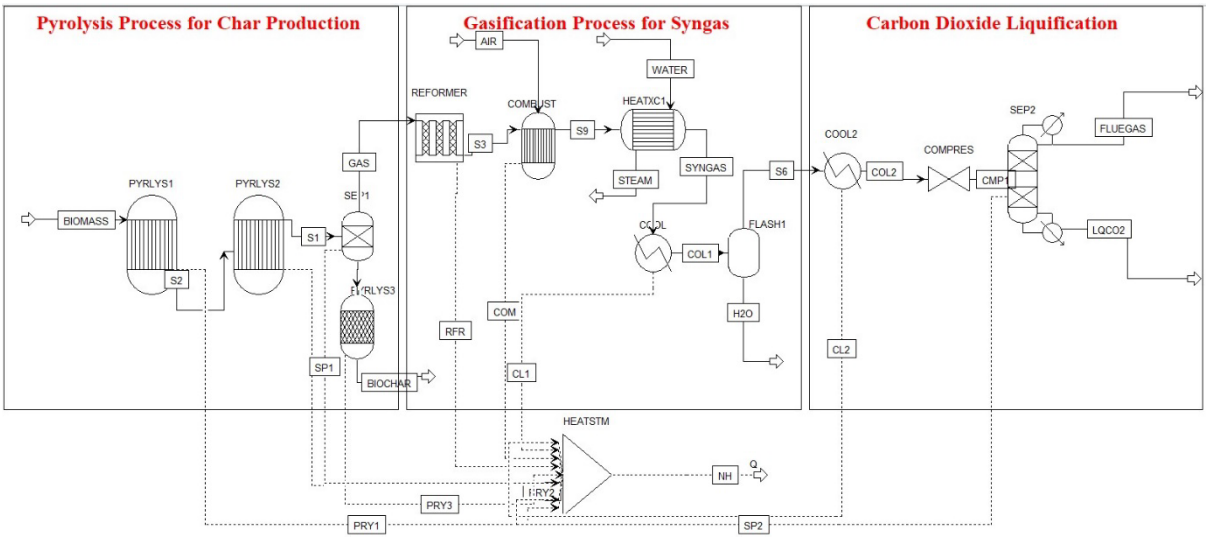

A15. Pyrolysis-gasification process electric power potential

Assumption: Inlet and outlet mass flow is equal				
	Base Process	**Scenario 1**	**Scenario 2**	**Scenario 3**
	Inlet Stream	**Inlet Stream**	**Inlet Stream**	**Inlet Stream**
Turbine Efficiency	60-62	60-62	60-62	60-62
Generator efficiency	89-90	89-90	89-90	89-90
Inlet Pressure	25 bars	25 bars	25 bars	25 bars
Inlet Temperature	540 C	605 C	579 C	532 C
Mass Flow	18000 kg/hr	20000 kg/hr	30000 kg/hr	30000 kg/hr
Isentropic Efficiency	61	61	61	61
Generator efficiency	89-90	89-90	89-90	89-90
	Outlet Stream	**Outlet Stream**	**Outlet Stream**	**Outlet Stream**
Outlet Pressure	1.04	1.0	1.0	1.0
Outlet Temperature	283 C	332 C	312 C	277 C
Phase	Gas	Gas	Gas	Gas
Mass Flow	18000 kg/hr	20000 kg/hr	30000 kg/hr	30000 kg/hr
Energy Flow				
Power Out	**2302 *kW***	**2788 *kW***	**4044 *kW***	**3796 *kW***

A16. Pyrolysis-gasification process sustainability Index Score

Scenarios	**Basic**	**Scenario 1**	**Scenario 2**	**Scenario 3**	**Weightage**		**Weightage 1**	**Weightage 2**
Energy	0.59	0.66	0.47	0.46	0.25		0.4	0.2
Safety	0.19	0.19	0.12	0.12	0.25		0.2	0.4
Power	0.57	0.69	1.00	0.94	0.25		0.2	0.2
Economic	0.36	0.37	0.44	0.43	0.25		0.2	0.2
Sustainability Index (Equal Wt.)	***0.428***	***0.477***	***0.507***	***0.488***	**Weightage 3**		**Weightage 4**	**BWM**
Sustainability Index (W1)	***0.460***	***0.514***	***0.499***	***0.482***	Energy	0.2	0.2	0.507
Sustainability Index (W2)	***0.380***	***0.420***	***0.429***	***0.414***	Safety	0.2	0.2	0.081
Sustainability Index (W3)	***0.456***	***0.520***	***0.605***	***0.578***	Power	0.4	0.2	0.189
Sustainability Index (W4)	***0.415***	***0.455***	***0.493***	***0.477***	Economic	0.2	0.4	0.223
Sustainability Index (BWM)	***0.503***	***0.563***	***0.534***	***0.517***				

Best criterion: $E_{2\ (economic)}$ and worst criterion: $E_{3\ (power)}$

Criteria Number = 4	Criterion 1	Criterion 2	Criterion 3	Criterion 4
Names of Criteria	Economic	Energy	Power	Safety
Select the Best	Economic			
Select the Worst	Power			

Best to Others	Economic	Energy	Power	Safety
Economic	1	2	5	3
Others to the Worst	Power			
Economic	5			
Energy	3			
Power	1			
Safety	2			
Weights	Economic	Energy	Power	Safety
	0.22297297	0.50675676	0.18918919	0.08108108
Input-Based CR	0.05			
Associated Threshold	0.1994			

A17. Pyrolysis-gasification process Scenario 2 optimization results

Pyrolysis °C	**Reformer °C**	**Air flowrate (kg/h)**	**CO_2 (kg/h)**	**Steam Temp. °C**
800	478.2	3559.5	6285.1	573.5
800	478.2	3559.5	6285.1	573.5
800	478.2	3559.5	6285.1	573.5
800	478.2	3559.5	6285.1	573.5
800	478.2	3559.5	6285.1	573.5
800	478.3	3559.5	6285.1	573.5
800	479.3	3560.5	6284.6	573.6
800	481.3	3562.5	6283.6	574.0
800	**512.5**	**3125.0**	**6268.5**	**579.5**
800	437.5	4875.0	6304.1	566.3
800	543.8	2187.5	6253.0	584.9
800	450.0	2500.0	6298.3	568.5
800	418.8	1937.5	6312.8	563.0
800	575.0	1250.0	6237.0	590.4
800	556.3	4312.5	6246.7	587.1
800	606.3	2812.5	6220.7	595.8
800	625.0	3750.0	6210.6	599.0

A18. Pyrolysis-gasification process Scenario 3 optimization results

Pyrolysis °C	Reformer °C	Air Flowrate (kg/h)	CO_2 (kg/h)	Steam Temp. °C	Biochar (kg/h)
706.3	481.3	3562.5	5366.8	323.5	3774.3
706.3	800.0	3562.5	5253.4	386.4	3774.3
706.3	400.0	3562.5	5388.1	307.2	3774.3
712.5	800.0	1625.0	5328.5	407.8	3742.4
712.5	662.5	1625.0	5385.8	381.3	3742.4
712.5	400.0	1625.0	5470.4	329.4	3742.4
718.8	800.0	2187.5	5401.9	428.7	3711.0
718.8	400.0	2187.5	5550.7	351.1	3711.0
718.8	543.8	2187.5	5505.9	379.4	3711.0
725.0	575.0	1250.0	5570.0	406.3	3680.2
725.0	800.0	1250.0	5473.4	449.0	3680.2
725.0	400.0	1250.0	5628.8	372.2	3680.2
731.3	800.0	2812.5	5542.5	468.6	3650.2
731.3	400.0	2812.5	5704.3	392.6	3650.2
731.3	606.3	2812.5	5630.2	432.3	3650.2
737.5	800.0	4875.0	5609.2	487.4	3621.2
737.5	437.5	4875.0	5764.3	419.5	3621.2
737.5	400.0	4875.0	5776.9	412.2	3621.2
740.6	715.6	1000.0	5683.6	481.1	3607.0
743.8	400.0	3437.5	5846.5	431.0	3593.2
743.8	800.0	3437.5	5673.0	505.4	3593.2
743.8	768.8	3437.5	5689.2	499.8	3593.2
750.0	450.0	2500.0	5894.4	458.4	3566.3
750.0	800.0	2500.0	5734.0	522.6	3566.3
750.0	400.0	2500.0	5912.8	449.0	3566.3
756.3	800.0	1062.5	5791.9	539.0	3540.6
756.3	400.0	1062.5	5975.8	466.0	3540.6
756.3	731.3	1062.5	5828.6	526.7	3540.6
762.5	800.0	3125.0	5846.7	554.4	3516.2
762.5	400.0	3125.0	6035.3	482.1	3516.2
762.5	512.5	3125.0	5989.5	502.8	3516.2
768.8	800.0	4687.5	5898.3	569.0	3493.0
768.8	400.0	4687.5	6091.4	497.2	3493.0
768.8	468.8	5000.0	6063.2	509.9	3493.0
768.8	693.8	4687.5	5956.4	550.3	3493.0
775.0	**800.0**	**3562.5**	**5946.9**	**582.6**	**3471.2**
775.0	400.0	1862.5	6144.0	511.5	3471.2
775.0	625.0	3750.0	6041.6	552.0	3471.2
775.0	400.0	3750.0	6144.0	511.5	3471.2
775.0	800.0	3750.0	5946.9	582.6	3471.2
781.3	800.0	4312.5	5992.2	595.4	3450.6
781.3	400.0	4312.5	6193.1	524.8	3450.6
781.3	556.3	4312.5	6122.9	552.9	3450.6
793.8	400.0	1937.5	6281.6	548.8	3413.4
793.8	418.8	1937.5	6273.3	552.2	3413.4

800.0	418.8	1937.5	6312.8	563.0	3396.7
800.0	625.0	2512.5	6210.6	599.0	3396.7
800.0	481.3	3562.5	6283.6	574.0	3396.7
800.0	606.3	2812.5	6220.7	595.8	3396.7
800.0	543.8	2187.5	6253.0	584.9	3396.7
800.0	500.0	2700.0	6274.6	577.3	3396.7
800.0	575.0	1250.0	6237.0	590.4	3396.7
800.0	437.5	4875.0	6304.1	566.3	3396.7
800.0	450.0	2500.0	6298.3	568.5	3396.7
800.0	512.5	3125.0	6268.5	579.5	3396.7
800.0	425.0	1962.5	6309.8	564.1	3396.7
800.0	550.0	3275.0	6249.8	586.0	3396.7
800.0	556.3	4312.5	6246.7	587.1	3396.7
800.0	575.0	3937.5	6237.0	590.4	3396.7
800.0	575.0	4387.5	6237.0	590.4	3396.7

A19. Survey sample for biomass waste valorization processes

Criteria <Process Name i.e., HTG, AND>	AL	VL	L	ML	EE	MH	H	VH	AH
The capital cost and operational cost of the process (-)									
Marketability (demand) of the final products (+)									
Rate of return on investment (+)									
Process maintenance and personnel cost (-)									
GHG/Particulate matter emissions (-)									
Soil/Land/Aquatic pollution (-)									
Land use for the process (-)									
Product emission throughout product life cycle (-)									
Process energy and exergy recovery (+)									
Access and technology adaptability (+)									
Waste treatment effectiveness and vol. reduction (+)									
Diversification of material handling (+)									
Process occupational safety hazards (-)									
Public acceptance and employment generation (+)									
Political support through existing policies (+)									
Promoting social responsibility (+)									
Absolutely low (AL), Very low (VL), Low (L), Medium low (ML), Exactly equal (EE), Medium high (MH), High (H), Very high (VH), Absolutely high (AH)									

A20. Fuzzy score based on experts' opinions for waste valorization process selection

		Economic				Environment				Technology				Social Governance			
		C1	**C2**	**C3**	**C4**	**C5**	**C6**	**C7**	**C8**	**C9**	**C10**	**C11**	**C12**	**C13**	**C14**	**C15**	**C16**
Gasification	α^-	0.35	0.75	0.6	0.25	0.35	0.25	0.25	0.35	0.45	0.6	0.45	0.6	0.35	0.45	0.45	0.5
Expert 1	α^+	0.45	0.85	0.75	0.35	0.45	0.35	0.35	0.45	0.6	0.75	0.6	0.75	0.45	0.6	0.6	0.5
	β^-	0.4	0.05	0.1	0.5	0.4	0.5	0.5	0.4	0.15	0.1	0.15	0.1	0.4	0.15	0.15	0.5
	β^+	0.55	0.15	0.2	0.6	0.55	0.6	0.6	0.55	0.25	0.2	0.25	0.2	0.55	0.25	0.25	0.5
Pyrolysis	α^-	0.45	0.5	0.45	0.45	0.45	0.45	0.5	0.45	0.45	0.35	0.45	0.45	0.6	0.5	0.5	0.45
Expert 1	α^+	0.6	0.5	0.6	0.6	0.6	0.6	0.5	0.6	0.6	0.45	0.6	0.6	0.75	0.5	0.5	0.6
	β^-	0.15	0.5	0.15	0.15	0.15	0.15	0.5	0.15	0.15	0.4	0.15	0.15	0.1	0.5	0.5	0.15
	β^+	0.25	0.5	0.25	0.25	0.25	0.25	0.5	0.25	0.25	0.55	0.25	0.25	0.2	0.5	0.5	0.25
HTG	α^-	0.45	0.45	0.25	0.45	0.35	0.5	0.5	0.5	0.35	0.15	0.5	0.25	0.6	0.25	0.25	0.35
Expert 1	α^+	0.6	0.6	0.35	0.6	0.45	0.5	0.5	0.5	0.45	0.2	0.5	0.35	0.75	0.35	0.35	0.45
	β^-	0.15	0.15	0.5	0.15	0.4	0.5	0.5	0.5	0.4	0.6	0.5	0.5	0.1	0.5	0.5	0.4
	β^+	0.25	0.25	0.6	0.25	0.55	0.5	0.5	0.5	0.55	0.75	0.5	0.6	0.2	0.6	0.6	0.55
AND	α^-	0.35	0.5	0.35	0.5	0.45	0.45	0.45	0.45	0.45	0.45	0.35	0.25	0.5	0.45	0.35	0.45
Expert 1	α^+	0.45	0.5	0.45	0.5	0.6	0.6	0.6	0.6	0.6	0.6	0.45	0.35	0.5	0.6	0.45	0.6
	β^-	0.4	0.5	0.4	0.5	0.15	0.15	0.15	0.15	0.15	0.15	0.4	0.5	0.5	0.15	0.4	0.15
	β^+	0.55	0.5	0.55	0.5	0.25	0.25	0.25	0.25	0.25	0.25	0.55	0.6	0.5	0.25	0.55	0.25
Gasification	α^-	0.6	0.6	0.35	0.45	0.15	0.25	0.45	0.25	0.6	0.35	0.45	0.5	0.6	0.45	0.35	0.35
Expert 2	α^+	0.75	0.75	0.45	0.6	0.2	0.35	0.6	0.35	0.75	0.45	0.6	0.5	0.75	0.6	0.45	0.45
	β^-	0.1	0.1	0.4	0.15	0.6	0.5	0.15	0.5	0.1	0.4	0.15	0.5	0.1	0.15	0.4	0.4
	β^+	0.2	0.2	0.55	0.25	0.75	0.6	0.25	0.6	0.2	0.55	0.25	0.5	0.2	0.25	0.55	0.55
Pyrolysis	α^-	0.5	0.45	0.45	0.5	0.45	0.45	0.25	0.45	0.6	0.75	0.5	0.35	0.6	0.6	0.5	0.35
Expert 2	α^+	0.5	0.6	0.6	0.5	0.6	0.6	0.35	0.6	0.75	0.85	0.5	0.45	0.75	0.75	0.5	0.45
	β^-	0.5	0.15	0.15	0.5	0.15	0.15	0.5	0.15	0.1	0.05	0.5	0.4	0.1	0.1	0.5	0.4
	β^+	0.5	0.25	0.25	0.5	0.25	0.25	0.6	0.25	0.2	0.15	0.5	0.55	0.2	0.2	0.5	0.55
HTG	α^-	0.75	0.45	0.75	0.6	0.45	0.5	0.45	0.35	0.45	0.25	0.75	0.6	0.45	0.5	0.45	0.25
Expert 2	α^+	0.85	0.6	0.85	0.75	0.6	0.5	0.6	0.45	0.6	0.35	0.85	0.75	0.6	0.5	0.6	0.35
	β^-	0.05	0.15	0.05	0.1	0.15	0.5	0.15	0.4	0.15	0.5	0.05	0.1	0.15	0.5	0.15	0.5
	β^+	0.15	0.25	0.15	0.2	0.25	0.5	0.25	0.55	0.25	0.6	0.15	0.2	0.25	0.5	0.25	0.6

AND	α^-	0.35	0.5	0.45	0.6	0.6	0.45	0.45	0.75	0.5	0.75	0.5	0.35	0.25	0.75	0.6	0.5
Expert 2	α^+	0.45	0.5	0.6	0.75	0.75	0.6	0.6	0.85	0.5	0.85	0.5	0.45	0.35	0.85	0.75	0.5
	β^-	0.4	0.5	0.15	0.1	0.1	0.15	0.15	0.05	0.5	0.05	0.5	0.4	0.5	0.05	0.1	0.5
	β^+	0.55	0.5	0.25	0.2	0.2	0.25	0.25	0.15	0.5	0.15	0.5	0.55	0.6	0.15	0.2	0.5
Gasification	α^-	0.75	0.15	0.25	0.5	0.35	0.25	0.25	0.35	0.35	0.35	0.6	0.6	0.5	0.35	0.35	0.6
Expert 3	α^+	0.85	0.2	0.35	0.5	0.45	0.35	0.35	0.45	0.45	0.45	0.75	0.75	0.5	0.45	0.45	0.75
	β^-	0.05	0.6	0.5	0.5	0.4	0.5	0.5	0.4	0.4	0.4	0.1	0.1	0.5	0.4	0.4	0.1
	β^+	0.15	0.75	0.6	0.5	0.55	0.6	0.6	0.55	0.55	0.55	0.2	0.2	0.5	0.55	0.55	0.2
Pyrolysis	α^-	0.6	0.35	0.35	0.45	0.35	0.25	0.5	0.35	0.25	0.15	0.25	0.25	0.45	0.6	0.25	0.25
Expert 3	α^+	0.75	0.45	0.45	0.6	0.45	0.35	0.5	0.45	0.35	0.2	0.35	0.35	0.6	0.75	0.35	0.35
	β^-	0.1	0.4	0.4	0.15	0.4	0.5	0.5	0.4	0.5	0.6	0.5	0.5	0.15	0.1	0.5	0.5
	β^+	0.2	0.55	0.55	0.25	0.55	0.6	0.5	0.55	0.6	0.75	0.6	0.6	0.25	0.2	0.6	0.6
HTG	α^-	0.45	0.35	0.75	0.75	0.25	0.15	0.45	0.25	0.45	0.15	0.6	0.6	0.75	0.45	0.5	0.25
Expert 3	α^+	0.6	0.45	0.85	0.85	0.35	0.2	0.6	0.35	0.6	0.2	0.75	0.75	0.85	0.6	0.5	0.35
	β^-	0.15	0.4	0.05	0.05	0.5	0.6	0.15	0.5	0.15	0.6	0.1	0.1	0.05	0.15	0.5	0.5
	β^+	0.25	0.55	0.15	0.15	0.6	0.75	0.25	0.6	0.25	0.75	0.2	0.2	0.15	0.25	0.5	0.6
AND	α^-	0.15	0.6	0.25	0.35	0.6	0.45	0.35	0.5	0.35	0.35	0.6	0.5	0.75	0.75	0.6	0.6
Expert 3	α^+	0.2	0.75	0.35	0.45	0.75	0.6	0.45	0.5	0.45	0.45	0.75	0.5	0.85	0.85	0.75	0.75
	β^-	0.6	0.1	0.5	0.4	0.1	0.15	0.4	0.5	0.4	0.4	0.1	0.5	0.05	0.05	0.1	0.1
	β^+	0.75	0.2	0.6	0.55	0.2	0.25	0.55	0.5	0.55	0.55	0.2	0.5	0.15	0.15	0.2	0.2
Gasification	α^-	0.75	0.6	0.45	0.45	0.25	0.25	0.6	0.25	0.35	0.15	0.75	0.5	0.25	0.45	0.5	0.35
Expert 4	α^+	0.85	0.75	0.6	0.6	0.35	0.35	0.75	0.35	0.45	0.2	0.85	0.5	0.35	0.6	0.5	0.45
	β^-	0.05	0.1	0.15	0.15	0.5	0.5	0.1	0.5	0.4	0.6	0.05	0.5	0.5	0.15	0.5	0.4
	β^+	0.15	0.2	0.25	0.25	0.6	0.6	0.2	0.6	0.55	0.75	0.15	0.5	0.6	0.25	0.5	0.55
Pyrolysis	α^-	0.45	0.45	0.6	0.45	0.45	0.5	0.35	0.35	0.45	0.75	0.5	0.5	0.6	0.6	0.45	0.5
Expert 4	α^+	0.6	0.6	0.75	0.6	0.6	0.5	0.45	0.45	0.6	0.85	0.5	0.5	0.75	0.75	0.6	0.5
	β^-	0.15	0.15	0.1	0.15	0.15	0.5	0.4	0.4	0.15	0.05	0.5	0.5	0.1	0.1	0.15	0.5
	β^+	0.25	0.25	0.2	0.25	0.25	0.5	0.55	0.55	0.25	0.15	0.5	0.5	0.2	0.2	0.25	0.5
HTG	α^-	0.9	0.6	0.5	0.6	0.45	0.15	0.25	0.25	0.45	0.25	0.45	0.75	0.75	0.5	0.35	0.6
Expert 4	α^+	0.9	0.75	0.5	0.75	0.6	0.2	0.35	0.35	0.6	0.35	0.6	0.85	0.85	0.5	0.45	0.75
	β^-	0.1	0.1	0.5	0.1	0.15	0.6	0.5	0.5	0.15	0.5	0.15	0.05	0.05	0.5	0.4	0.1

	β^+	0.1	0.2	0.5	0.2	0.25	0.75	0.6	0.6	0.25	0.6	0.25	0.15	0.15	0.5	0.55	0.2
AND	α^-	0.45	0.5	0.45	0.6	0.5	0.6	0.6	0.6	0.35	0.75	0.5	0.25	0.5	0.35	0.45	0.75
Expert 4	α^+	0.6	0.5	0.6	0.75	0.5	0.75	0.75	0.75	0.45	0.85	0.5	0.35	0.5	0.45	0.6	0.85
	β^-	0.15	0.5	0.15	0.1	0.5	0.1	0.1	0.1	0.4	0.05	0.5	0.5	0.5	0.4	0.15	0.05
	β^+	0.25	0.5	0.25	0.2	0.5	0.2	0.2	0.2	0.55	0.15	0.5	0.6	0.5	0.55	0.25	0.15
Gasification	α^-	0.45	0.5	0.45	0.5	0.25	0.5	0.35	0.45	0.35	0.5	0.5	0.5	0.35	0.45	0.35	0.35
Expert 5	α^+	0.6	0.5	0.6	0.5	0.35	0.5	0.45	0.6	0.45	0.5	0.5	0.5	0.45	0.6	0.45	0.45
	β^-	0.15	0.5	0.15	0.5	0.5	0.5	0.4	0.15	0.4	0.5	0.5	0.5	0.4	0.15	0.4	0.4
	β^+	0.25	0.5	0.25	0.5	0.6	0.5	0.55	0.25	0.55	0.5	0.5	0.5	0.55	0.25	0.55	0.55
Pyrolysis	α^-	0.5	0.15	0.5	0.45	0.35	0.6	0.35	0.5	0.35	0.6	0.5	0.35	0.35	0.25	0.45	0.35
Expert 5	α^+	0.5	0.2	0.5	0.6	0.45	0.75	0.45	0.5	0.45	0.75	0.5	0.45	0.45	0.35	0.6	0.45
	β^-	0.5	0.6	0.5	0.15	0.4	0.1	0.4	0.5	0.4	0.1	0.5	0.4	0.4	0.5	0.15	0.4
	β^+	0.5	0.75	0.5	0.25	0.55	0.2	0.55	0.5	0.55	0.2	0.5	0.55	0.55	0.6	0.25	0.55
HTG	α^-	0.25	0.45	0.45	0.45	0.45	0.35	0.5	0.5	0.45	0.25	0.5	0.45	0.35	0.35	0.45	0.35
Expert 5	α^+	0.35	0.6	0.6	0.6	0.6	0.45	0.5	0.5	0.6	0.35	0.5	0.6	0.45	0.45	0.6	0.45
	β^-	0.5	0.15	0.15	0.15	0.15	0.4	0.5	0.5	0.15	0.5	0.5	0.15	0.4	0.4	0.15	0.4
	β^+	0.6	0.25	0.25	0.25	0.25	0.55	0.5	0.5	0.25	0.6	0.5	0.25	0.55	0.55	0.25	0.55
AND	α^-	0.45	0.45	0.35	0.45	0.45	0.25	0.35	0.35	0.25	0.35	0.35	0.25	0.5	0.5	0.5	0.5
Expert 5	α^+	0.6	0.6	0.45	0.6	0.6	0.35	0.45	0.45	0.35	0.45	0.45	0.35	0.5	0.5	0.5	0.5
	β^-	0.15	0.15	0.4	0.15	0.15	0.5	0.4	0.4	0.5	0.4	0.4	0.5	0.5	0.5	0.5	0.5
	β^+	0.25	0.25	0.55	0.25	0.25	0.6	0.55	0.55	0.6	0.55	0.55	0.6	0.5	0.5	0.5	0.5
Gasification	α^-	0.6	0.6	0.25	0.45	0.45	0.25	0.25	0.45	0.6	0.25	0.6	0.45	0.45	0.45	0.15	0.45
Expert 6	α^+	0.75	0.75	0.35	0.6	0.6	0.35	0.35	0.6	0.75	0.35	0.75	0.6	0.6	0.6	0.2	0.6
	β^-	0.1	0.1	0.5	0.15	0.15	0.5	0.5	0.15	0.1	0.5	0.1	0.15	0.15	0.15	0.6	0.15
	β^+	0.2	0.2	0.6	0.25	0.25	0.6	0.6	0.25	0.2	0.6	0.2	0.25	0.25	0.25	0.75	0.25
Pyrolysis	α^-	0.75	0.45	0.25	0.6	0.6	0.25	0.25	0.6	0.45	0.1	0.6	0.45	0.6	0.35	0.1	0.45
Expert 6	α^+	0.85	0.6	0.35	0.75	0.75	0.35	0.35	0.75	0.6	0.1	0.75	0.6	0.75	0.45	0.1	0.6
	β^-	0.05	0.15	0.5	0.1	0.1	0.5	0.5	0.1	0.15	0.9	0.1	0.15	0.1	0.4	0.9	0.15
	β^+	0.15	0.25	0.6	0.2	0.2	0.6	0.6	0.2	0.25	0.9	0.2	0.25	0.2	0.55	0.9	0.25
HTG	α^-	0.45	0.6	0.45	0.45	0.25	0.25	0.25	0.45	0.6	0.25	0.15	0.45	0.45	0.6	0.15	0.6
Expert 6	α^+	0.6	0.75	0.6	0.6	0.35	0.35	0.35	0.6	0.75	0.35	0.2	0.6	0.6	0.75	0.2	0.75

	β^-	0.15	0.1	0.15	0.15	0.5	0.5	0.5	0.15	0.1	0.5	0.6	0.15	0.15	0.1	0.6	0.1
	β^+	0.25	0.2	0.25	0.25	0.6	0.6	0.6	0.25	0.2	0.6	0.75	0.25	0.25	0.2	0.75	0.2
AND	α^-	0.45	0.75	0.6	0.45	0.15	0.15	0.45	0.25	0.45	0.6	0.5	0.35	0.35	0.45	0.6	0.6
Expert 6	α^+	0.6	0.85	0.75	0.6	0.2	0.2	0.6	0.35	0.6	0.75	0.5	0.45	0.45	0.6	0.75	0.75
	β^-	0.15	0.05	0.1	0.15	0.6	0.6	0.15	0.5	0.15	0.1	0.5	0.4	0.4	0.15	0.1	0.1
	β^+	0.25	0.15	0.2	0.25	0.75	0.75	0.25	0.6	0.25	0.2	0.5	0.55	0.55	0.25	0.2	0.2
Gasification	α^-	0.6	0.45	0.5	0.6	0.5	0.25	0.25	0.45	0.45	0.45	0.45	0.6	0.45	0.5	0.45	0.5
Expert 7	α^+	0.75	0.6	0.5	0.75	0.5	0.35	0.35	0.6	0.6	0.6	0.6	0.75	0.6	0.5	0.6	0.5
	β^-	0.1	0.15	0.5	0.1	0.5	0.5	0.5	0.15	0.15	0.15	0.15	0.1	0.15	0.5	0.15	0.5
	β^+	0.2	0.25	0.5	0.2	0.5	0.6	0.6	0.25	0.25	0.25	0.25	0.2	0.25	0.5	0.25	0.5
Pyrolysis	α^-	0.75	0.6	0.35	0.45	0.5	0.5	0.35	0.35	0.5	0.45	0.6	0.5	0.45	0.5	0.45	0.5
Expert 7	α^+	0.85	0.75	0.45	0.6	0.5	0.5	0.45	0.45	0.5	0.6	0.75	0.5	0.6	0.5	0.6	0.5
	β^-	0.05	0.1	0.4	0.15	0.5	0.5	0.4	0.4	0.5	0.15	0.1	0.5	0.15	0.5	0.15	0.5
	β^+	0.15	0.2	0.55	0.25	0.5	0.5	0.55	0.55	0.5	0.25	0.2	0.5	0.25	0.5	0.25	0.5
HTG	α^-	0.5	0.5	0.5	0.5	0.35	0.5	0.35	0.35	0.5	0.45	0.5	0.5	0.5	0.45	0.5	0.5
Expert 7	α^+	0.5	0.5	0.5	0.5	0.45	0.5	0.45	0.45	0.5	0.6	0.5	0.5	0.5	0.6	0.5	0.5
	β^-	0.5	0.5	0.5	0.5	0.4	0.5	0.4	0.4	0.5	0.15	0.5	0.5	0.5	0.15	0.5	0.5
	β^+	0.5	0.5	0.5	0.5	0.55	0.5	0.55	0.55	0.5	0.25	0.5	0.5	0.5	0.25	0.5	0.5
AND	α^-	0.35	0.35	0.35	0.35	0.45	0.45	0.5	0.6	0.25	0.45	0.35	0.35	0.35	0.45	0.45	0.5
Expert 7	α^+	0.45	0.45	0.45	0.45	0.6	0.6	0.5	0.75	0.35	0.6	0.45	0.45	0.45	0.6	0.6	0.5
	β^-	0.4	0.4	0.4	0.4	0.15	0.15	0.5	0.1	0.5	0.15	0.4	0.4	0.4	0.15	0.15	0.5
	β^+	0.55	0.55	0.55	0.55	0.25	0.25	0.5	0.2	0.6	0.25	0.55	0.55	0.55	0.25	0.25	0.5

A21. Weights calculation for biomass waste valorization processes

AHP Weights Calculations for main criteria and sub-criteria (One expert sample)									
	Economic	**Environment**	**Technological**	**Social Governance**		**Normalize Weights**	**Consistency Check**	**NW/CC**	**CI**
Economic	1.00	3.00	5.00	3.00	2.59	0.5112	2.1116	4.1305	**0.0382**
Environment	0.33	1.00	5.00	1.00	1.14	0.2243	0.9274	4.1351	
Technological	0.20	0.20	1.00	0.33	0.34	0.0670	0.2799	4.1741	**CR**
Social Governance	0.33	1.00	3.00	1.00	1.00	0.1974	0.79349	4.0189	**0.043**
					5.067		***Lambda_max***	***4.1147***	
Subjective and Objective Weights									
		Equal		**Entropy**		**CRITIC**		**AHP**	

	Main Criteria Weights			
Economic	0.2500	0.3794	0.4597	0.4426
Environment	0.2500	0.1972	0.2698	0.2242
Social	0.2500	0.1335	0.0885	0.1264
Technology	0.2500	0.2898	0.1820	0.2068